AWARD NUMBER: W81XWH-15-1-0574

TITLE: Long Term Follow-up of the Late Effects of Acute Radiation Exposure in Primates

PRINCIPAL INVESTIGATOR: J. Mark Cline, DVM, PhD

CONTRACTING ORGANIZATION: Wake Forest University Health Sciences
Winston-Salem, NC 27157-0001

REPORT DATE: OCTOBER 2019

TYPE OF REPORT: Annual

PREPARED FOR: U.S. Army Medical Research and Materiel Command
Fort Detrick, Maryland 21702-5012

DISTRIBUTION STATEMENT: Approved for Public Release;
Distribution Unlimited

The views, opinions and/or findings contained in this report are those of the author(s) and should not be construed as an official Department of the Army position, policy or decision unless so designated by other documentation.

REPORT DOCUMENTATION PAGE

Form Approved
OMB No. 0704-0188

Public reporting burden for this collection of information is estimated to average 1 hour per response, including the time for reviewing instructions, searching existing data sources, gathering and maintaining the data needed, and completing and reviewing this collection of information. Send comments regarding this burden estimate or any other aspect of this collection of information, including suggestions for reducing this burden to Department of Defense, Washington Headquarters Services, Directorate for Information Operations and Reports (0704-0188), 1215 Jefferson Davis Highway, Suite 1204, Arlington, VA 22202-4302. Respondents should be aware that notwithstanding any other provision of law, no person shall be subject to any penalty for failing to comply with a collection of information if it does not display a currently valid OMB control number. **PLEASE DO NOT RETURN YOUR FORM TO THE ABOVE ADDRESS.**

1. REPORT DATE *(DD-MM-YYYY)*	**2. REPORT TYPE**	**3. DATES COVERED** *(From -To)*
OCTOBER 2019	Annual	30SEP2018-29SEP2019

4. TITLE AND SUBTITLE
Long Term Follow-up of the Late Effects of Acute Radiation Exposure in Primates

5a. CONTRACT NUMBER
PR141508

5b. GRANT NUMBER
W81XWH-15-1-0574

5c. PROGRAM ELEMENT NUMBER

6. AUTHOR(S)
J Mark Cline, DVM, PhD, DACVP
Professor
Pathology/Comparative Medicine
Radiation Oncology
EMAIL: jmcline@wfubmc.edu

5d. PROJECT NUMBER

5e. TASK NUMBER

5f. WORK UNIT NUMBER

7. PERFORMING ORGANIZATION NAME(S) AND ADDRESS(ES)
Wake Forest School of Medicine
Medical Center Boulevard
Winston-Salem, NC 27157

8. PERFORMING ORGANIZATION REPORT NUMBER

9. SPONSORING / MONITORING AGENCY NAME(S) AND ADDRESS(ES)
U.S. Army Medical Research and
Materiel Command
Fort Detrick, Maryland 21702-5012

10. SPONSOR/MONITOR'S ACRONYM(S)

11. SPONSOR/MONITOR'S REPORT NUMBER(S)

12. DISTRIBUTION / AVAILABILITY STATEMENT
Approved for Public Release; Distribution Unlimited

13. SUPPLEMENTARY NOTES

14. ABSTRACT This program studies the mechanisms and consequences of delayed effects of acute radiation exposure (DEARE) in non-human primates (NHP), with complementary mechanistic and therapeutic studies in mice. The program consists of 4 projects, focused on: 1. Type 2 diabetes mellitus (T2DM); 2. Radiation-induced heart disease (RIHD); 3. Chronic immune impairment; and 4. Genomics and transcriptomics. Major findings include peripheral microvascular and bioenergetic abnormalities in NHP with T2DM; restrictive myocardial fibrosis in RIHD; dose and age-dependent immuen impairment; and ongoing sequencing work which will inform us regarding the molecular pathogenesis of T2DM,

15. SUBJECT TERMS Radiation; delayed effects; late effects; heart; immune system; type 2 diabetes mellitus; genomics; transcriptomics; *Mus musculus*; *Macaca mulatta*.

16. SECURITY CLASSIFICATION OF:			**17. LIMITATION OF ABSTRACT**	**18. NUMBER OF PAGES**	**19a. NAME OF RESPONSIBLE PERSON**
a. REPORT	**b. ABSTRACT**	**c. THIS PAGE**			**19b. TELEPHONE NUMBER** *(include area code)*
U	**U**	**U**	**UU**	**144**	USAMRMC

Standard Form 298 (Rev. 8-98)
Prescribed by ANSI Std. Z39.18

TABLE OF CONTENTS

		Page
1.	**Introduction**	**4**
2.	**Keywords**	**4**
3.	**Accomplishments**	**5**
4.	**Impact**	**81**
5.	**Changes/Problems**	**81**
6.	**Products**	**88**
7.	**Participants & Other Collaborating Organizations**	**94**
8.	**Special Reporting Requirements**	**99**
9.	**Appendices**	**99**

Attachments:

Quad Chart

Manuscripts

Caudell et al., 2019

Hale et al., 2019

Michalson et al, 2019

1. INTRODUCTION: Narrative that briefly (one paragraph) describes the subject, purpose and scope of the research.

The **subject** of this research is the phenomenon of Delayed Effects of Acute Radiation Exposure (DEARE). The **purpose** and overarching goal of this program is to explore our recent clinically relevant observations of DEARE in a unique cohort of non-human primates (NHP), termed the Radiation Survivor Cohort (RSC), and a smaller more controlled group of NHP exposed to radiation prospectively, termed the Prospective Radiation Cohort (PRC), with complementary studies in mouse models to explore growth factor therapeutics and genomic consequences. The **scope** of this work consists of 4 projects making use of these unique NHP resources: 1. Studies of type 2 diabetes mellitus (T2DM); 2. Radiation-induced heart disease (RIHD); 3. Chronic immune impairment with restriction of the antigenic response repertoire; and 4. Genomic and transcriptomic studies which will inform us regarding the molecular pathogenesis of T2DM, RIHD, and immune impairment in the context of DEARE. Work during the first four years of this program has proceeded as planned, with slight logistical modifications but no major changes or delays.

2. KEYWORDS: Provide a brief list of keywords (limit to 20 words).

Radiation; delayed effects; late effects; heart; immune system; type 2 diabetes mellitus; genomics; transcriptomics; *Mus musculus*; *Macaca mulatta*.

3. ACCOMPLISHMENTS:

What were the major goals of the project?

Major goals are listed below by project, including relevant dates and percentage completion as indicated.

Core Primate Studies (Cline)

SA1: Provide NHP Investigative Platform

Major Task 1:	Regulatory Approval (months 1-6)
Milestone:	Local Institutional Animal Care and Use Committee (IACUC) and DOD Animal Care and Use Review Office (ACURO) approvals in place (100%)
Major Task 2:	Access to Long Term Radiation Survivor Cohort (months 1-6)
Milestone:	Scheduling and meetings in progress (80%)
	Sample collections have begun, in support of all projects (planned for months 6-60; 85% complete)
Major Task 3:	Acquisition of Prospective Cohort (months 1-6)
Milestone:	Animals arrived at Wake Forest 2/9/16 (100% completed).
Major Task 4:	Irradiation and Study of Prospective Cohort
Milestone:	Irradiations in Y2Q1 (100% completed)

SA2: Promote Synergy and Productivity

Major Task 5:	Data management/tracking, group interactions (months 1-6)
Milestones:	Data management (100% completed for years 1-4)
	Establish monthly web meetings (100% complete)
	Annual strategic retreat to be scheduled (100% complete for years 1-4)
	Publications (months 6-60; 60% complete in the context of 5 year plan, cardiac, metabolic and genomic papers submitted and accepted; abstracts presented at the annual Radiation Research Society Meeting and other meetings)

SA3: Facilitate Translation and Therapeutic/Preventive approaches

Major Task 6:	Strategize towards clinical implementation and future funding
Milestones:	Promote new grant submissions (months 36-60; 60% complete)
	Progress update at end of year 2 (100% complete)

Project 1: Diabetes (Kavanagh)

SA1: Document the time course of IR-mediated reduced insulin sensitivity

Major Task 1: PRC - Prospective Cohort
Milestones: Create a longitudinal clinical profile of diabetes mellitus (DM) risk with irradiation (70% achieved in context of 5 year plan)
Local IACUC approval (100% achieved)
ACURO Approval (100% Achieved)
Baseline CT imaging (100% achieved)
Characterize changes in skeletal muscle structure & function (50% achieved)
Characterize changes in adipose structure and function (70% achieved)

Major Task 2: RSC - Radiation Survivor Cohort
Milestones: Generate comparable clinical data in monkeys with DM as DEARE to compare with the earlier prospectively irradiated monkeys (90% achieved)
Insulin sensitivity data collection (100% achieved)

SA2: Examine IR-related increases in oxidation of tissue proteins over time

Major Task 3: Redox Proteomics of prospective and long-term irradiated tissue
Milestones: Compare and contrast early and late changes in redox proteomics following irradiation in mice and monkeys. Verify the role of Akt protein in DM. Identify individual or protein clusters with long-term modifications following irradiation. (90% achieved)

SA3: Track extracellular matrix (ECM) remodeling, including fibrosis, in muscle and adipose depots after irradiation

Major Task 4: ECM characterization and magnetic resonance imaging (MRI).
Milestones: Characterize tissue changes in both prospective and long-term IR monkeys and relate these to in vivo insulin sensitivity assessments.
Validate the utility of MR imaging to detect qualitative tissue changes (85% achieved)

SA4: Evaluate therapeutic agents that reduce fibrosis and restore fat expansion to mitigate metabolic changes with IR.

Major Task 5: Mouse intervention study
Milestones: Prevent metabolic disease development in IR mice with interventions.
Demonstrate reductions in protein modifications and/or tissue remodeling with treatment (90% achieved).

Project 2 – Radiation-Induced Heart Disease (Register)

We proposed 3 inter-related Specific Aims across the 5 Year Grant Period.

SA 1: Determine the Effects of Total Body Irradiation on NHP Cardiac Structure and Function.

Major Task 1: Novel cardiac MRI approaches will be used to evaluate myocardial tissue fibrosis, a key component of RIHD, in order to follow changes in myocardial phenotypes in animals across time. Additional structural and functional cardiac phenotypes to be assessed by echocardiography/MRI include left ventricular (LV) mass, posterior and interventricular wall thickness, right ventricular thickness, and aortic wall thickness. Functional parameters will include systolic and diastolic function, ejection fraction, aortic stiffness/pulse wave velocity, wall motion, and electrocardiography. Grid tag mapping will be also used to assess strain and LV volume.
Scheduled Dates: Months 6-48
Milestones: Percent completion: 75% in the context of 5 year plan
Detailed cardiac ultrasound (US) evaluations have been conducted and images acquired on the RSC (year 01, year 02, year 03, GE instrument) and on the PRC (baseline, 20 weeks (March 2017), 1 year (October 2017), 2 years (October 2019) and will be obtained at the 3 year timepoint in coming weeks (October 2018). Echocardiographic image analysis was conducted using the scanner for images collected in the PRC at Baseline, and at other timepoints using US image analysis software (TOMTEC) which we purchased for the project. Drs. Register, Michalson, and staff were trained in its use. Data from baseline which was collected and measured on the GE instrument were validated for reproducibility by repeat reads using the TOMTEC software. M Mode measurements were assessed on the GE US instrument with plans to move analyses to the TOMTEC. Cardiac MRI image analysis is underway and extensive MR phenotype data has been collected in the PRC. Tissue collections from subjects going to necropsy continue. Over the past year we have been carefully evaluating characteristics of hearts from RSC monkeys that have come to necropsy, including assessments of 1) coronary artery atherosclerosis, 2) myocardial fibrosis (Trichrome), myocardial cell populations (endothelial cells, fibroblasts, and macrophage subpopulations, 3) myocardial gene expression using RNAseq (global) and Nanostring technology (immune targeted); 4) myocardial small RNA levels using miRNAseq (global) and Nanostring miRNA (targeted) profling (underway). Ongoing studies are further characterizing myocardium.

SA 2: Identify Novel Molecular Biomarkers of Cardiovascular Injury and RIHD

Major Task 2: Identify and evaluate emerging serum markers of cardiac damage implicated in cardiomyocyte death (microRNAs such as miR133a) and extracellular matrix remodeling (type I and III collagen propeptides and degradation products). Circulating miRNA levels and serum extracellular matrix turnover biomarkers will be evaluated in relation to structural and functional phenotypes and histologic and biomolecular features of myocardial tissues and differentially expressed myocardial mRNA and miRNA which will be identified through expression profiling of heart tissues obtained at necropsy.
Scheduled Dates: Months 6-48
Milestones: Percent completion: 40%
RSC: blood samples obtained and processed; PRC: baseline and immediate post-radiation blood samples were collected, processed, and archived for future biochemical analyses. Ongoing blood collections are underway.

SA 3: Determine the Efficacy of Candidate Mitigating Agents on RIHD.

Major Task 3: Assessment of Mitigating Agents. We propose to retrospectively and prospectively assess cardiac and coronary artery injury in NHP in studies of mitigating agents, using animals in the de novo cohort, the long-term cohort, and from prospective studies of growth factors (e.g. HGH), superoxide dismutase mimetics, and novel therapeutics (e.g. platelet analogs). We will use the pathologic and biomarker approaches noted above, including in vivo assessments. These results will be critical to our understanding of RIHD. The preliminary data suggests that the changes in the heart based on the radiation dose are significantly greater that would have been predicted from prior murine studies.
Scheduled Dates: Months 6-48
Milestones: Percent completion: 45% complete in the context of a 5 year plan plan (assessed effects of a mitigating agent (superoxide dismutase analogue, hexyl MnSOD) on myocardial gene expression, (manuscript in development), performed histologic staining of coronary arteries in available hearts and completed assessments of atherosclerotic lesion size, collected cardiac tissues from a Project 1 mouse study and cardiac tissue from rhesus monkeys, planning for ECM and other biomarkers in the radiation survivor cohort; other evaluations are under way). Myocardium from the RSC has been phenotyped for atherosclerosis and is being organized for preparation for RNAseq.

Goals for the past year related to analyzing the 36-month post-radiation cardiac MRI and echocardiographic imaging in the PRC, conducting RNAseq and miRNAseq on RNA isolated of myocardium from deceased RSC subjects, additional immunohistochemical analysis of individual cell types and macrophage polarization in myocardium from deceased RSC and Control rhesus monkeys, characterizing blood samples from the PRC and the RSC, continuing plans for analysis of ECM and other biomarkers, planning for MR assessments of the RSC, ongoing molecular and cellular phenotyping of the monocytes in the PRC and the RSC, submission of manuscript containing comprehensive echocardiographic phenotyping of the RSC describing the effects of radiation on the heart. One manuscript related to the PRC and a second related to the RSC have been published in the past year, another is to be submitted in the near future. Presentations are scheduled for the Radiation Research Society and the American Heart Association.

Project 3 – Immune Recovery (Duke Consortium – Chen & Sempowski)

SA 1: Define the roles of thymopoiesis and peripheral expansion in overall T cell reconstitution after radiation-induced injury based on radiation dose.

Major Task 1: NHP Studies (5% complete in context of 5 year plan, first analysis in progress)
Milestones:

1.1. Phenotypic analyses in long-term cohort (60 months, 75% complete)
1.2. sjTREC in long-term cohort (60 months, 60% complete)
1.3. Phenotypic analyses in prospective cohort (60 months, 95% complete)
1.4. sjTREC in prospective cohort (60 months, 80% complete)
1.5. Determine primary immune response to influenza vaccine (36 months, 70% complete)
1.6. Determine primary and recall immune response to influenza vaccines (60 months, 50% complete)

Major Task 2: Murine Studies
Milestones:

2.1. Local IACUC Approval (3 months, 100% complete)
2.2. Determine the roles of thymopoiesis and peripheral expansion in overall T cell recovery in the classic radiation injury model (18 months, 100% complete)
2.3. Determine the roles of thymopoiesis and peripheral expansion in overall T cell recovery in the second radiation injury model (7-24 months, 100% complete)

SA 2: Determine if therapeutic agents identified in our previous studies are able to promote or accelerate overall T cell immunity after radiation injury.

Major Task 3: HGH Mouse Studies
Milestones:

3.1. Determine the effect of HGH on phenotypic T cell reconstitution (25-36 months, 0% complete)
3.2. Determine the effect of HGH on functional T cell recovery (37-48 months, 0% complete)
3.3. Determine the mechanism by which HGH promote T cell reconstitution (49-60 months, 0% complete)

Major Task 4: IGF-1 Mouse Studies
Milestones:

4.1. Determine the effect of IGF-1 on phenotypic T cell reconstitution (25-36 months, 80% complete)
4.2. Determine the effect of IGF-1 on functional T cell recovery (37-48 months, 0% complete)
4.3. Determine the mechanism by which IGF-1 promote T cell reconstitution (49-60 months, 0% complete)

Project 4 - Genomic Sequencing and Stem Cell Lines (Duke Consortium – Dave)

Aim1: Define the genetic mutations and gene expression signatures induced by DEARE

Major Task 1: Exome Sequencing
Milestones:
DNA Sample extraction (months 1-36) - 100% complete
Exome analyisis (months 13-60) - 40% complete
Major Task 2: Transcriptome Sequencing
RNAseq (months 6-48) - 80% complete
RANseq analysis (months 12-60) - 70% complete

Aim 2: Determine the molecular basis of lymphoid immunodeficiency induced by DEARE.

Major Task 1: Generate iPSCs
Milestones: iPSC from controls complete 100% complete
Milestones: iPSC from genetic variants 30% complete

Major Task 2: Differentiate iPSCs into lymphoid lineages
Milestone(s) Achieved: B cell characterization 50% complete
Milestone(s) Achieved: T cell characterization 50% complete

What was accomplished under these goals?

Core Primate Studies (Cline)

1) Major activities:

Protocol approvals for all animal studies; establishment of subcontracts and accounts; development of a meeting schedule; review of goals and plans with all investigators; hiring/allocation of effort for personnel; acquisition of NHP subjects for the prospective cohort; pre-irradiation physical examinations, imaging, and blood sampling for all projects; total body irradiation.
Characteristics of our animal populations are briefly described below.

2) Specific objectives:

As per SOW. Regulatory approvals, establishment of meeting schedule, hiring, planning, animal acquisition, irradiation.

3) Results/key outcomes:

- All animal protocol approvals complete at local and ACURO level
- Subcontracts and accounts established
- Goals and plans reviewed with all investigators
- Monthly web conferences established and continuing
- Hiring/effort allocations made as planned
- Secure server folders established for data exchange
- NHP subjects acquired for PRC, irradiations completed and studies in progress
- Sampling and data acquisition on schedule

4) Other achievements:

Data presented at local and national meetings each year.

A brief overview and synopsis of major findings is presented below.

The Radiation Survivor Cohort (RSC)

The population of the RSC is shown graphically in Figure 1. Briefly, this cohort consists of rhesus macaques (*Macaca mulatta*) irradiated as juveniles or adults, in the range of 3-8.5 Gy via single total body exposure, at a dose delivery of 60-80 cGy/min. The cohort is supported by the National Institute of Allergy and Infectious Disease (NIAID), which is leveraged by this DOD Focused Program award. Animals were acquired between 2007 and 2019 through an “adoption” strategy from multiple sites. The RSC currently consists of 141 irradiated animals and 36 controls. The population has a 4:1 male:female ratio. Animals are housed socially whenever possible, primarily in pens, and fed a custom-formulated “Typical American Diet”. All animals receive daily environmental enrichment and are part of a behavioral management program. Approximately one-third of the animals were given mitigating agents (e.g. antibiotics or growth factors) during the acute period of hematopoietic injury. This cohort is studied using a multidisciplinary approach to long-term morbidity/mortality. Notably, some animals are now 15 years out from irradiation (1/2 of their lifespan), providing a unique long-term view of DEARE.

Animals in the RSC undergo a regular schedule of medical care and assessment, including but not limited to:

Daily
- Twice-daily clinical observations
- Environmental enrichment

Monthly
- Physical exam
- Blood collection for experimental measures and archive
- Urine collection for experimental measures and archive
- Body weight

Semiannually
- Complete blood counts
- Clinical chemistry panels
- Testing for diabetes mellitus (hemoglobin A1c, glucose, with glucose tolerance testing and mimimal model testing on a subset)
- Anthropometrics (trunk length, waist diameter)

Annually
- Flow cytometry
- Bone marrow aspirate
- Echocardiography
- Computed tomography scan (whole body)
- Renal ultrasound
- Gastrointestinal endoscopy and biopsy
- Bronchoalveolar lavage
- Cranial MRI (subset, 3 year rotation)
- Ocular exam

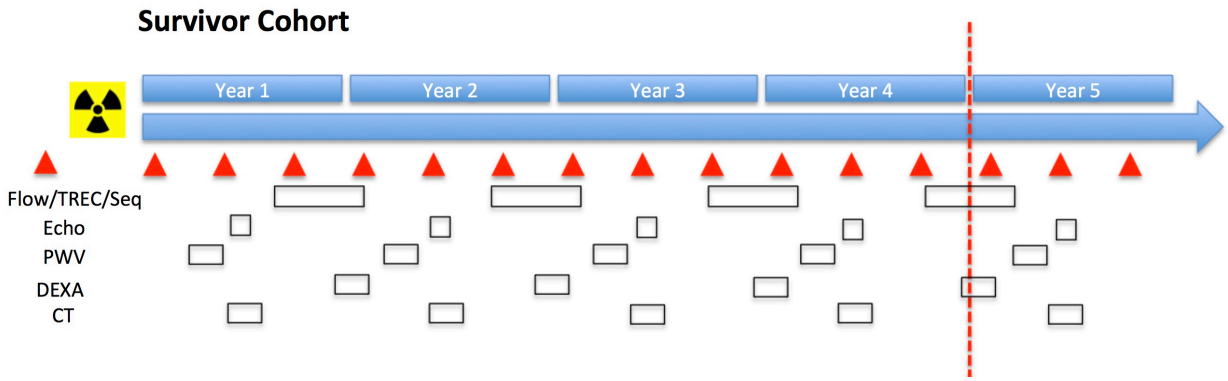


Figure 1: Diagram representing the annual schedule of clinical assessments in the RSC. The vertical red line indicates the current date. Red triangles indicate blood collection dates. Abbreviations: Flow = flow cytometric measurement of lymphocyte subets; TREC = T cell receptor excision circles; Seq = DNA and RNA sequencing collections from peripheral blood; Echo = echocardiography; PWV pulse wave velocity; DEXA = dual energy x-ray absorptiometry; CT = computed tomography.

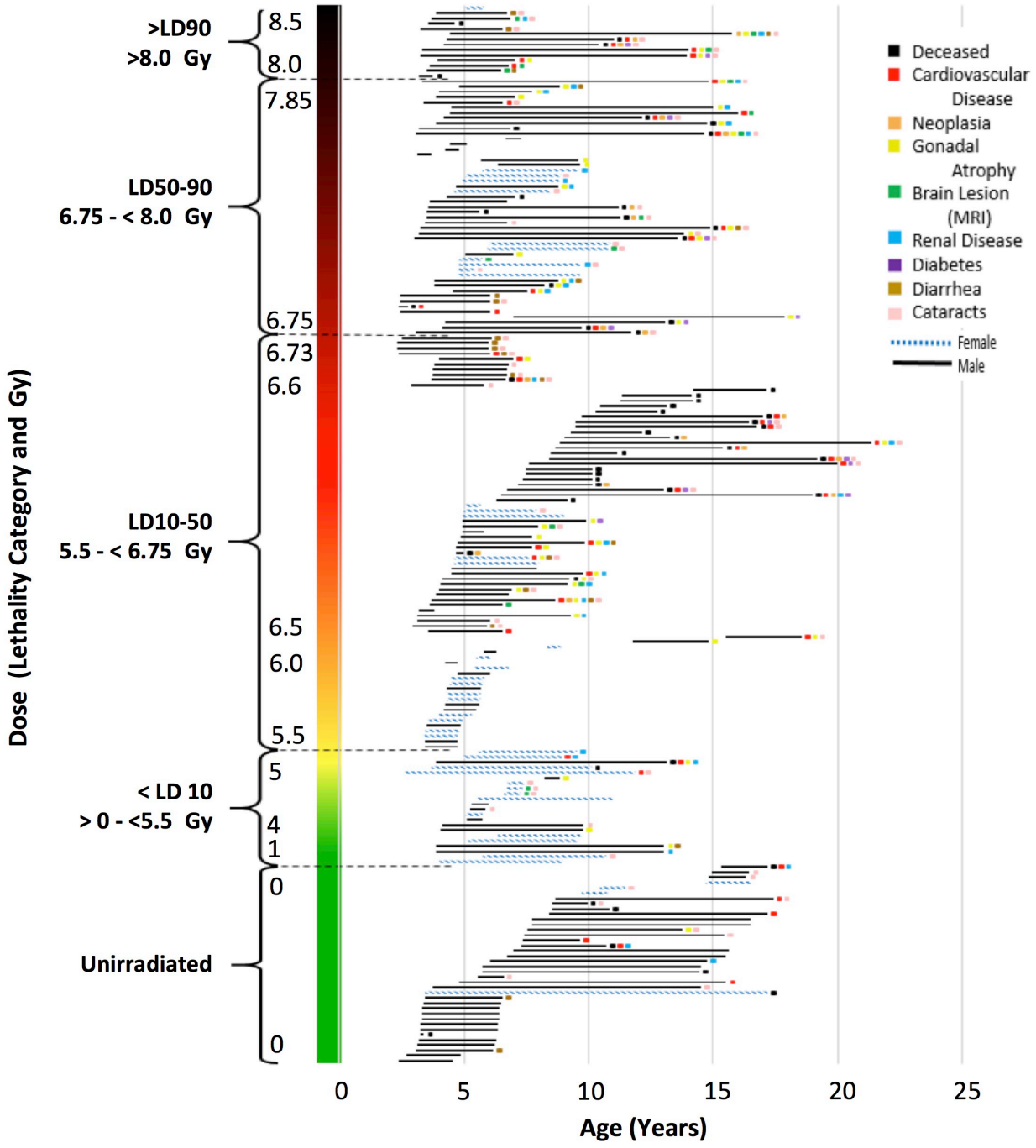


Figure 2: Age and dose distribution of the Radiation Survivor Cohort *(updated 10/19) Each horizontal bar represents a single animal; the left end of the bar is the age at which the animal was irradiated, and the right end of the bar is the animal's current age or age at time of death. Green circles represent the current age of non-irradiated controls. For rhesus monkeys, the typical age a puberty is 3.5 years; typical lifespan is 30 years.*

Morbidity

All animals are given routine veterinary care, and we have established clinical criteria for identification and management of animals with health abnormalities. Major patterns of morbidity in the RSC are summarized in Table 1, below.

Table 1: Threshold-based determinations of morbidity in the long-term Radiation Survivor Cohort (updated 2019).

Organ/ Disease	Irradiated	Control	Criteria for Diagnosis	Criteria for Euthanasia or Removal
Diabetes	9.2% (13/141)	0% (0/36)	Hemoglobin A1c (HbA1c) >6.5% Three fasting blood glucose measurements > 100 mg/dL Any non-fasted blood glucose > 200 mg/dL Long term treatment	Long term Insulin Treatment
Kidney	19.1% (27/141)	8.3% (3/36)	BUN > 30 mg/dl or Cr > 1.1 mg/dl Loss of renal volume >50% Urolithiasis	Clinical Renal Failure/Uremia
Lung	6.3% (9/141)	5.6% (2/36)	Pulmonary consolidation on CT scan Bullous emphysema >25% Hypoxia (SPO2 < 80%) Respiratory rate >80 breaths per minute	Respiratory distress
GI	14.9% (21/141)	5.6% (2/36)	Any lesion on endoscopy Diarrhea (severity code >2 for >5 days)	Chronic diarrhea with weight loss
Skin	13.5% (19/141)	2.6% (1/38)	Persistent dermatitis, alopecia or loss of pigmentation	Severe extensive dermatitis
Heart/CV	27.7% (39/141)	16.7% (6/36)	Murmur detected on auscultation or echocardiography Mean arterial pressure >120 Adult stroke volume <5 mls & Cardiac output <0.5 L/min at >7 y	Congestive heart failure or substantial dysfunction
Brain (any lesion)	12% (17/141)	0% (0/36)	Y/N MRI lesions visible on SWI Neurologic abnormality on clinical exam	Clinical neurologic abnormality, large infarct or edema on MRI
Eyes (cataracts)	39.0% (55/141)	25.0% (9/36)	Any lens opacity on annual slit-lamp exam	n/a
Behavior	17.7% (25/141)	33.3% (12/36)	Any behavioral abnormality requiring individual management plan	Unmanageable self-injurious behavior or depression
Neoplasia	16% (23/141)	0% (0/36)	Any neoplastic disease (imaging or biopsy)	Malignancy
Testicular atrophy	48.6% (36/74)	0% (0/20)	Testis volume <10 ml each after 7 years of age; Vol = (p/6)(LxW^2)	n/a
Bone	41.8% (59/141)	2.8% (1/36)	Adult bone mineral content (BMC) < 274g or density (BMD) < 0.373 g/cc	Fracture
Obese **Underweight**	11.3% (16/141) 33.3% (47/141)	33.3% (12/36) 16.7% (6/36)	Obesity: Waist Circumference > 45 cm or DEXA Body Fat > 30% Underweight: Waist Circumference < 25 cm or DEXA Adult Body Fat < 12.3%	Unintended weight loss >25% in non-obese animal

Abbreviations: BMC = bone mineral content; BMD = bone mineral density; BUN = blood urea nitrogen; Cr = serum creatinine; CT = computed tomography scan; CV = cardiovascular; DEXA = dual emission x-ray absorptiometry; HbA1c = hemoglobin A1c; MRI = magnetic resonance imaging; NSD = no significan difference; SP02 = oxygen saturation.

Pathology

As the project progresses, animals age out of the cohort. In the event that animals die or must be euthanized due to illness, a complete necropsy is done including samples from all major organ systems. Gross lesions are photographed. Major organs are weighed and collected both snap-frozen in liquid nitrogen and fixed in 4% paraformaldehyde (or investigator's method of choice). Histopathologic interpretation of pathologic findings is done by veterinary pathologists. The tissue collection checklist includes over 100 samples, including:

Adrenal glands	Fat (visceral and	Mammary glands	Skin
Arteries (aorta,	subcutaneous)	Muscle	Small intestine
coronary, iliac, carotid)	Gonads	Nerves (sciatic, sural)	Spleen
Bone (humerus, femur,	Hair	Oral mucosa	Stomach
vertebrae)	Heart	Ovaries (F)	Teeth
Bone marrow	Kidney	Pancreas	Testis (M)
Brain (multiple levels)	Large intestine	Pituitary	Thymus
Cervix	Liver	Prostate (M)	Tongue
Esophagus	Lung	Salivary gland	Trachea
Eyes	Lymph nodes		Uterus (F)

The Prospective Radiation Cohort (PRC)

The study design for the PRC is shown below. These specific-pathogen-free animals were acquired and quarantined in year 1 and irradiated in October 2016. Imaging and sample collections are proceeding as per the program statement of work and the needs of the individual projects.

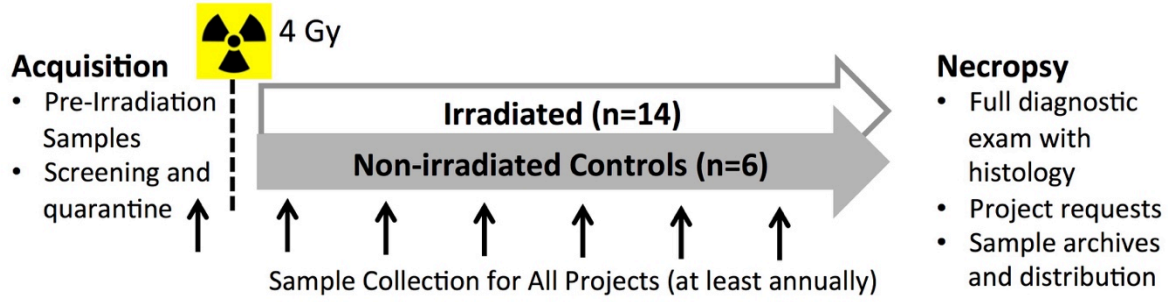


Figure 3: Study design for the Prospective Radiation Cohort (PRC).

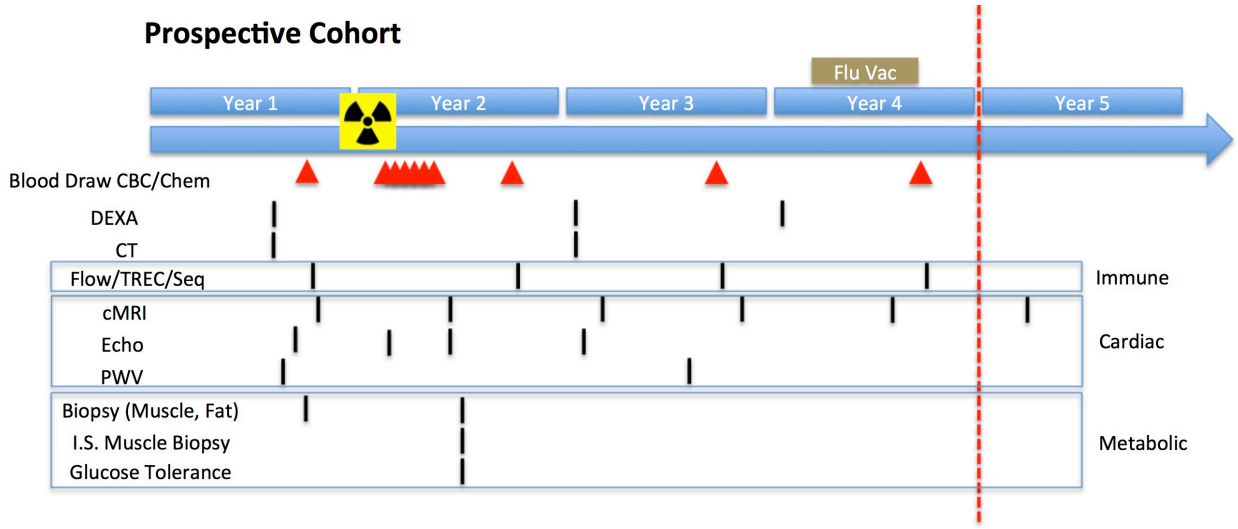


Figure 4: Diagram showing clinical assessments in the Prospective Cohort. The vertical red line indicates the current date. Red triangles indicate blood collection dates. Abbreviations: CBC = complete blood count; Chem = serum chemistry measurements; cMRI = cardiac magnetic resonance imaging; Echo = echocardiography; PWV = pulse wave velocity; I.S. = insulin stimulated.

Acute radiation effects have been reported previously and are now published (e.g. Michalson et al., 2019). New delayed-effects data are presented in the individual project reports below.

Necropsy Plans for the Prospective Cohort

The original plan for the Prospective Cohort included euthanasia and necropsy examination of all major organ systems, with an emphasis on cardiovascular outcomes. This was scheduled for Year 5 Quarter 1. Due to delays at the beginning of the Program have revised this timeline to extend in-life studies through February 2020, with necropsies occurring in March 2020. The tissue collection protocol will be similar to that described above for the RSC.

Project 1. Diabetes (Kavanagh)

The overall goal of Project 1 is to identify pathways that track some radiation survivors on a path that results in dysregulated metabolism and increased risk for diabetes. Our studies (**Figures 1.1 and 1.2**) utilize a unique reverse translational flow whereby diabetes has been reported in survivors of radiation exposures, including our nonhuman primates, and we have designed studies to identify the time course, tissue targets, and interventional strategies that will combat diabetogenesis in at-risk individuals. In accordance with this continuum, this annual report is divided into sections that address major accomplishments within the sub-studies named the Radiation Survivor Cohort (RSC), the Prospective Radiation Cohort (PRC), and the Interventional Rodent Studies.

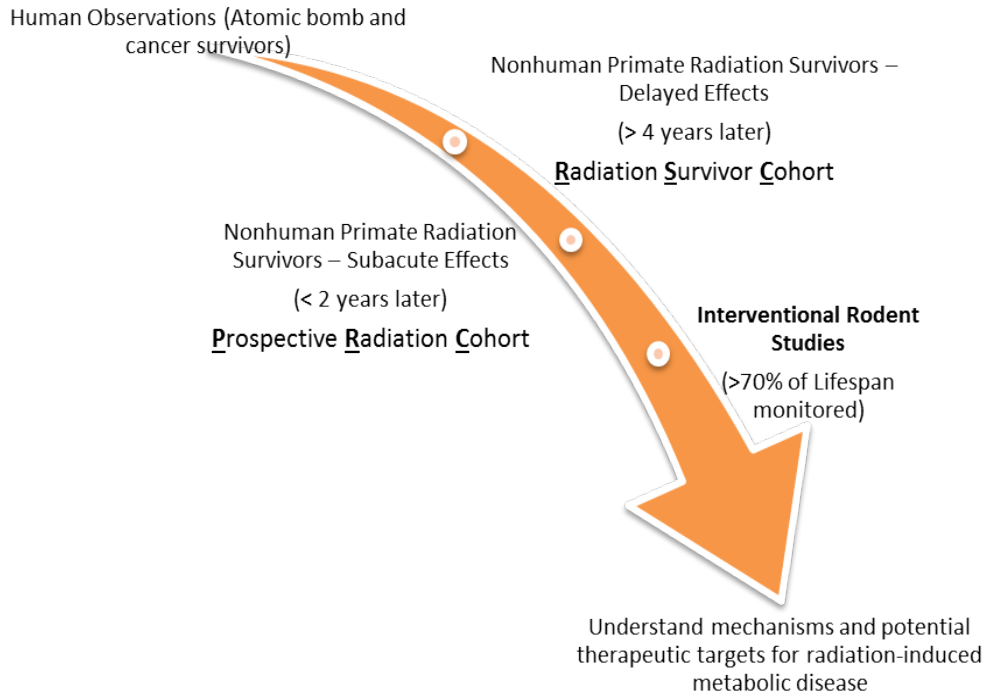


Figure 1.1: Studies reported on for Project 1.

A diagram of the monkey cohorts (RSC and PRC) and the assessment points are shown in **Figure 1.2**. We are halfway through the assessment period.

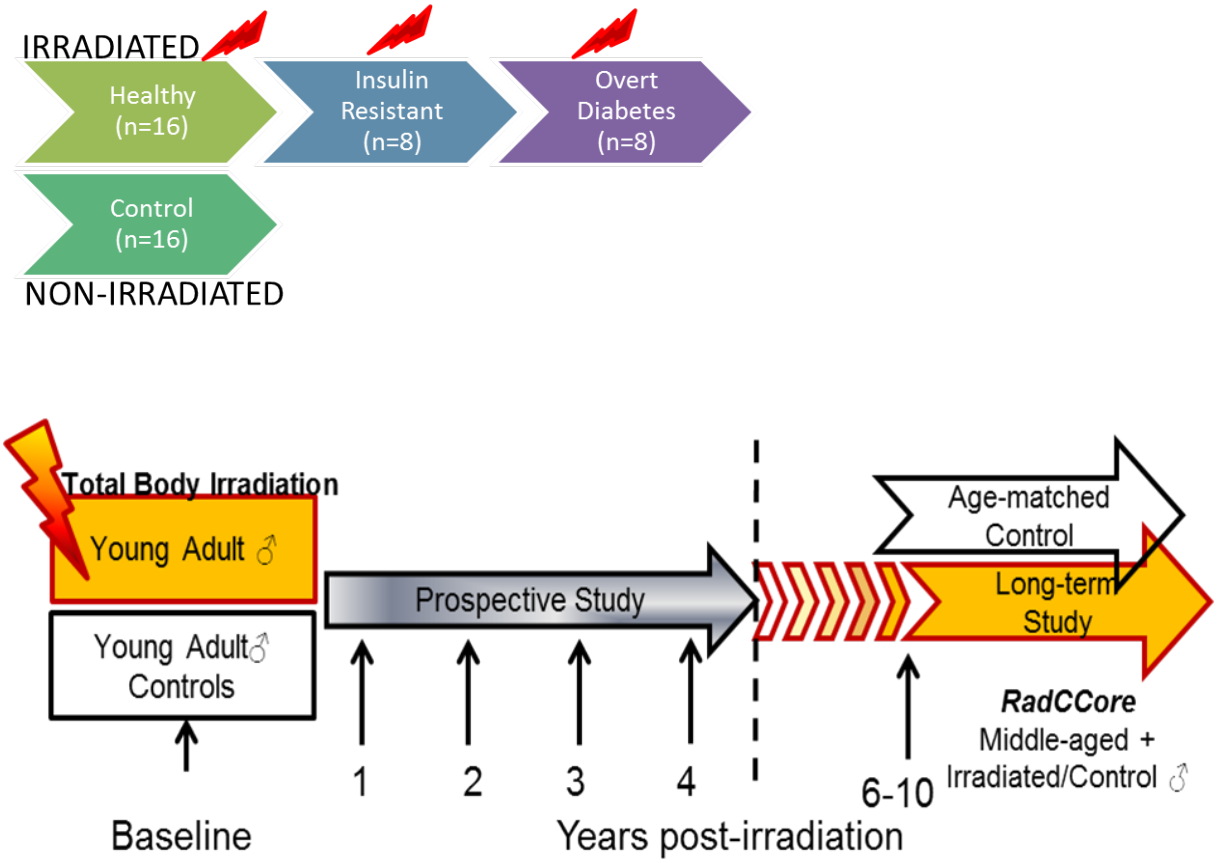


Figure 1.2. RSC monkey groups evaluated within Project 1 (top) and the overlap/continuum achieved with the PRC and RSC

1. **Radiation Survivor Cohort (RSC)**

Our prior published studies identified that skeletal muscle maintains an insulin resistant state years after radiation exposure, but animals exhibiting indicators of enhanced capillary perfusion were able to maintain normal overall glucose metabolism and prevent diabetes from developing.

During the current year, we have completed four large milestones, which are listed below and are then expanded on separately.

1) We have re-analyzed skeletal muscle proteomics and confirmed differences with immunodetection methods for selected top hits.
2) We have looked for circulatory cytokine profiling in collaboration with Duke in survivor monkeys
3) We have looked at proteomic and histological changes associated with an intervention that improves proteostasis.
4) We have followed up from prior data regarding intestinal barrier dysfunction to demonstrate the validity of our biomarker, but find dysfunction is not a consistent delayed effect of radiation.

1. Survivor cohort Proteomics

The non-targeted skeletal muscle proteomics outcomes were re-analyzed. We identify S100 proteins (3 isoforms) as specifically upregulated in irradiated skeletal muscle. These proteins are regulatory and have a variety of actions that may be relevant to the insulin resistance and structural changes observed in skeletal muscle. S100-A13 is the most distinctly upregulated. Elevations of S100-A13 was confirmed by protein analysis and is graphed below. The significance of this could lie in S100-A13's action to move fibroblast-growth-factor 1 to be extracellularly located and facilitate signaling fibrosis through extracellularly facing TGFb receptors. Importantly, this finding is synergy between Projects 1 and 2, as the S100-A13 protein isoform is most highly expressed in skeletal and cardiac muscle tissues, and could be a molecular link between the fibrosis and dysfunction seen in both tissues. Fibrosis assessment of muscle tissue will be re-assessed and we expect levels to be higher, as trends were apparent at 6 months post-exposure.

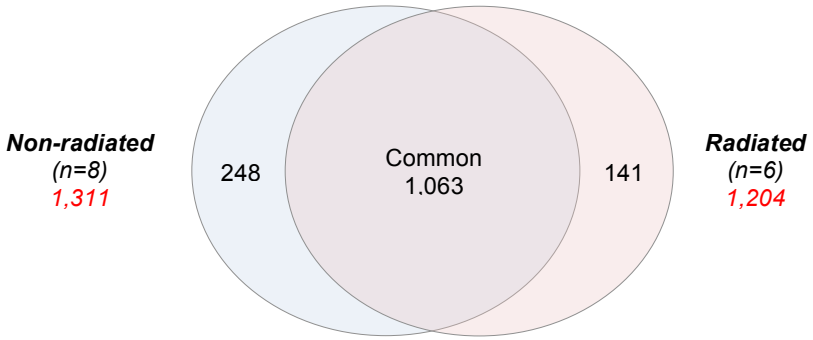


Figure 1.3. Patterns of protein expression in skeletal muscle of NHP.

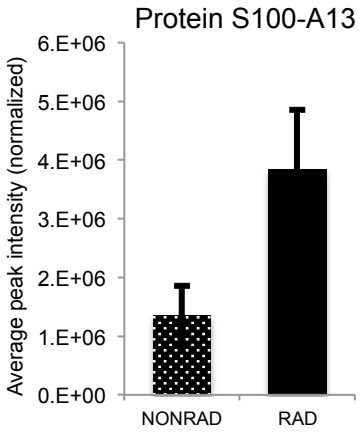


Figure 1.4. Protein S100-A13 is differentially up-regulated in the skeletal muscle of irradiated NHP.

Table 1.1. Top differentially irradiated proteins in irradiated animals.

			RAD/NONRAD	
Description	*Accession*	*MW [kDa]*	*Fold ratio*	*p-Value*
Glyoxylate reductase/hydroxypyruvate reductase	Q9UBQ7	35.6	12.000	0.00120
Protein S100-A13	Q99584	11.5	6.667	0.00458
Sodium/potassium-transporting ATPase subunit beta-1	P05026	35.0	5.333	0.03752
Proline-rich basic protein 1	E7EW31	106.9	5.333	0.03752
Myosin light chain 5	Q02045	19.5	4.667	0.00231
39S ribosomal protein L12, mitochondrial	P52815	21.3	4.444	0.00345
Succinate dehydrogenase [ubiquinone] cytochrome b small subunit, mitochondrial	O14521	17.0	2.667	0.02850
Electron transfer flavoprotein-ubiquinone oxidoreductase, mitochondrial	Q16134	68.5	2.237	0.01880
60S ribosomal protein L35	P42766	14.5	2.000	0.02244

We also completed proteomics profiling of skeletal muscle before and after intervention with proteostasis mediator, geranylgeranlyacetone (GGA). In this study, we observed in the intervention animals, there were general decrease in proteins over the course of study, whereas control animals generally were unchanged or increased. The significant different proteins between groups (proteins expressed as within individual change over baseline) demonstrate that a few important changes occurred. Notably, a reduction in peroxiredoxin-5 indicates reduced oxidative stress was present. Further, reduced Ras and Rho proteins are positives and indicate a lessening of intercellular interactions. In other studies of skeletal muscle and diabetes, we know that there is strong upregulation of extracellular and intercellular interactions are present.

Table 1.2. Protein expression in skeletal muscle. The listed proteins were reduced after treatment with GGA.

Description	*Accession*	*MW [kDa]*	*p-Value*
Cathepsin B	P07858	37.8	0.01123
Cell division control protein 42 homolog	P60953	21.2	0.00893
Ferrochelatase, mitochondrial	P22830	47.8	0.01611
Galectin-1	P09382	14.7	0.0031
Heterogeneous nuclear ribonucleoprotein A3	P51991	39.6	0.01096
Myomesin-3	Q5VTT5	162.1	0.00553
Peroxiredoxin-5, mitochondrial	P30044	22.1	0.01855
Ras-related C3 botulinum toxin substrate 1	P63000	21.4	0.01066
Ras-related protein Rab-14	P61106	23.9	0.00454
Transforming protein RhoA	P61586	21.8	0.01066

2. Cytokine profiling

Circulatory cytokine shifts in response to GGA/proteostasis improvement were not observed. Measurements were made using the 32-plex panel optimized for NHPs by our Duke collaborators. Of all 32 analytes, only 11 were detected reliably in NHP circulation, and the values are reported below. Only IL-7 had a suggestion it may change in response to treatment. There was a 46% reduction in IL-7 with GGA treatment, compared to a 35% increase in IL-7 measured in control animals.

Table 1.2. Blood cytokine concentrations in NHPs treated with GGA.

	IL-1b	IL-23	BLC	EOTAXIN	IL-8	MCP-1	SDF-1a	G-CSF/CSF-3	IL-7	VEGF-A	VEGF-D
Group	**(pg/mL)**	**(pg/mL)**	**(pg/mL)**	**(pg/mL)**	**(pg/mL)**	**(pg/mL)**	**(pg/mL)**	**(pg/mL)**	**(pg/mL)**	**(pg/mL)**	**(pg/mL)**
BL CTL	13.39	32.93	74.11	80.25	44.13	194.71	453.05	92.84	5.51	21.21	10.10
	7.67	9.10	24.47	28.43	15.52	59.21	68.62	78.32	2.96	10.71	6.92
BL GGA	16.46	63.78	69.22	139.85	106.65	190.25	476.72	96.86	5.22	24.83	12.93
	7.196	35.46	25.43	49.59	55.80	48.81	106.62	35.78	2.50	5.86	2.86
TX CTL	19.866	44.61	102.69	133.40	46.33	334.10	563.27	106.11	7.45	21.97	9.44
	16.33	31.96	42.65	59.84	14.58	79.80	127.88	30.90	4.38	7.73	4.81
TX GGA	18.10	104.8	92.61	213.16	96.90	334.52	569.42	131.48	2.81	19.03	7.66
	5.87	56.61	35.85	85.07	46.99	168.87	125.14	51.92	1.13	8.89	4.53
P-value	0.89	0.51	0.85	0.50	0.38	1.00	0.97	0.64	0.17	0.81	0.78

3. Intervention results: Tissue remodeling in radiation survivors

The overall goal of our studies is to prevent the development of diabetes and our strategy aims at tissue remodeling through reducing stimulus for fibrosis, and directly fibrosis pathways. In this intervention study of radiation survivor monkeys, we evaluated skeletal muscle collagens, capillarization, and perfusion using penetrance of tissue by albumin-bound dyes. Companion studies of irradiated mice have been completed and reported in prior years. Our intervention increased our proteostasis mediator heat shock protein 70 (HSP70) in skeletal muscle (Figure X). We saw a non-significant reduction in pSMAD2/3 signaling, which is the primary intracellular mediator for fibrosis signaling and a key read-out for our TGFb inhibition studies described more fully below.

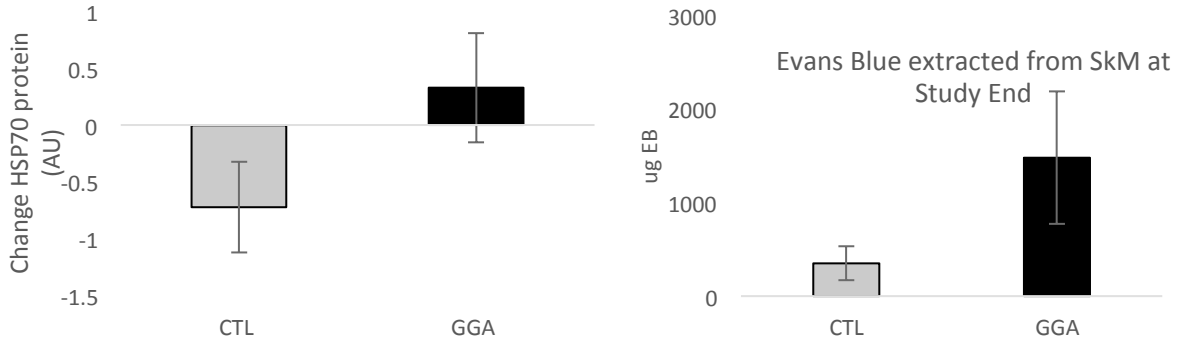


Figure 1.5. GGA treatment increased HSP70 and perfusion (Evans blue) in skeletal muscle of NHPs.

In the graphs above, we can appreciate that change in the proteostasis effector molecule HSP70 co-occurred with improved delivery of Evan's blue dye to musculature. This is indicative of better perfusion. To support tissue remodeling, protein ubiquination (a process that occurs with HSP70-mediation and the ligase, parkin) was increased in treated tissue (8.5 vs 4.1% of proteins, p=0.05).

Gene expressions by PCR reflects a global reduction in the need to upregulate HSP70 transcription. This is consistent with less need for cytosolic protein chaperoning, and the mechanism of GGA, which is to stabilize and extend the half-life of existing HSP70.

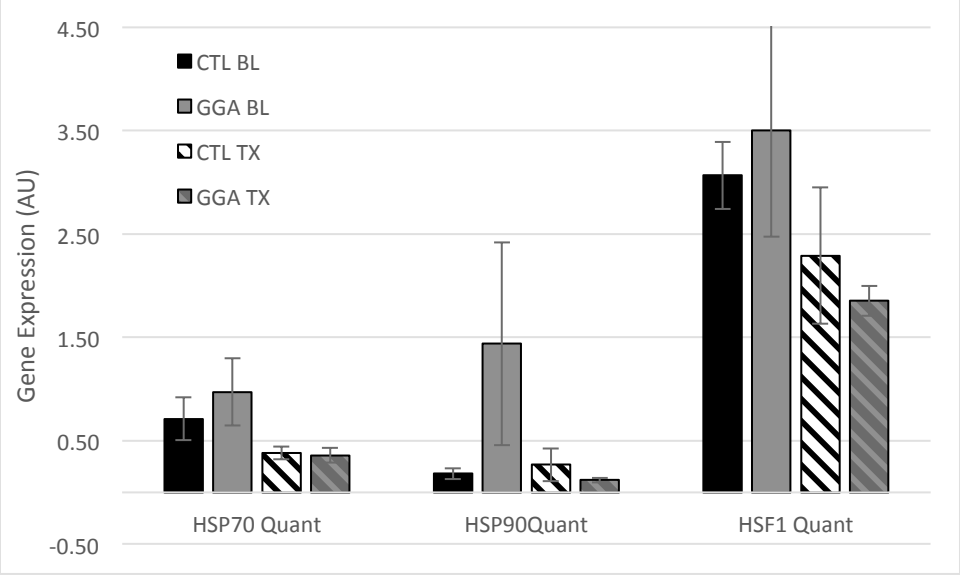


Figure 1.6. GGA treatment (TX) increased skeletal muscle RNA expression of HSP70, HSP90, and HSF1 in treated NHPs relative to baseline (BL).

Skeletal muscle showed signs of being able to effectively remodel over the course of 11 weeks of GGA treatment to increase HSP70. We saw a significant decrease in endothelial cell area measured by histology (CD31 positive cell number; p=0.05). While this may appear inconsistent with perfusion measures being increased, this is consistent with what we have observed with age-related skeletal tissue remodeling. We see skeletal muscle fibrosis tends to increase with normal aging, and is significantly related to increases in CD31 positive staining area. So this coordinated reduction in fibrosis and capillarization is evidence of an anti-aging effect. Enhanced proteostasis is a feature of extra-ordinarily long-lived mammals and thus this study has achieved a number of outcomes:

1) We know remodeling can occur in a radiation survivor with just months of intervention
2) Proteostasis reverses an age-related change in skeletal musculature
3) Capillary density as measured by histology is not a reliable measure of functional tissue perfusion.

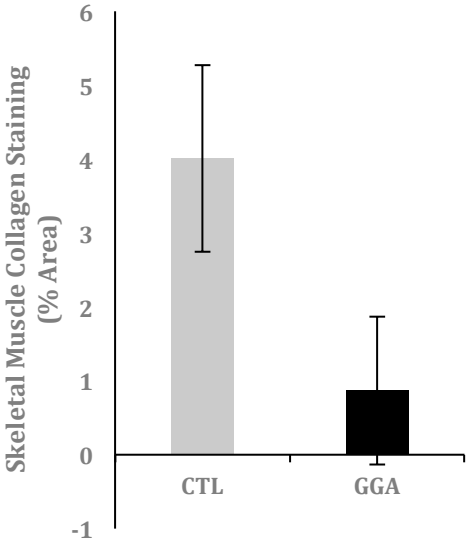


Figure 1.7. GGA treatment (TX) reduced collagen deposition in skeletal muscle in NHPs.

4. Intestinal Barrier Dysfunction.

Prior publication on this cohort of radiation survivor monkeys (DeBo et al, Rad Res 2017) identified lipopolysaccharide-binding protein (LBP1) as elevated in circulation. This biomarker is primarily produced in the liver. LBP1 is a response to translocated bacteria and bacterial antigens that travel within the portal circulation that drain the intestines. As radiation survivors have ongoing evidence of both inflammation and immune dysregulation, we hypothesized that intestinal barrier dysfunction was a source for pro-inflammatory stimuli. We evaluated in a separate subset of the survivor cohort primates the biomarker levels of LBP1 and intestinal tissue bacterial gene abundance. We evaluated the duodenum, jejunum, ileum and colon from 19-22 individuals with concurrent plasma measures of LBP1. 16s gene abundance measures by PCR of DNA extracted is a method to identify prokaryotic genome levels in mammalian tissue or biospecimens. We find that bacteria are detectable in the gastrointestinal tissues, and

significantly more 16s bacterial genes were amplified from colonic tissue. This relates to the bacterial content of the colon being vastly greater than other levels of the intestine.

We did not see differences in bacterial tissue abundance relating to sex or radiation status. However, these data did validate the use of LBP1 as a biomarker as a significant association was observed between tissue bacteria and circulating LBP1.

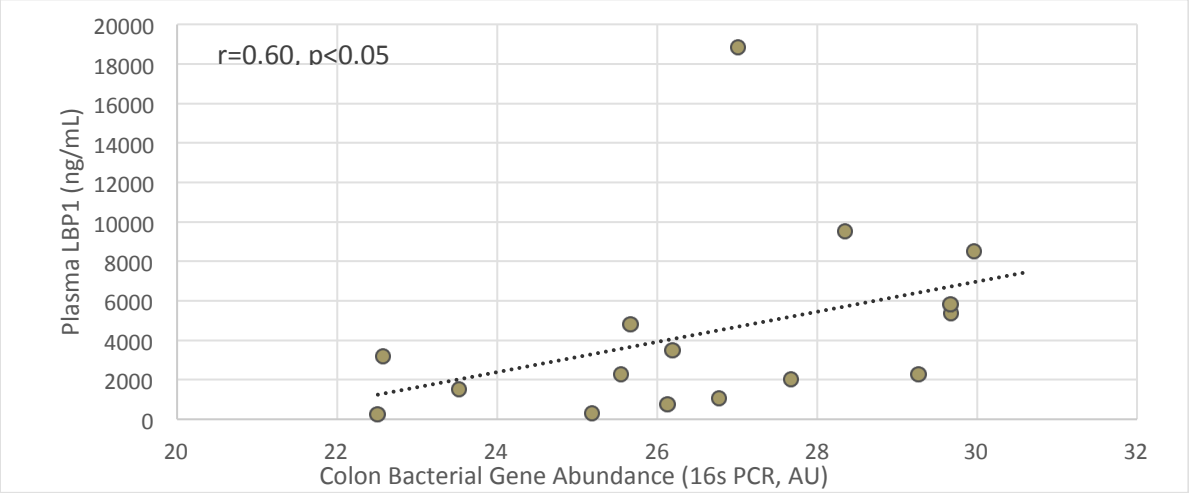


Figure 1.8. Plasma LBP1 correlated with colonic bacterial abundance.

2. Prospective Radiation Cohort

Twenty monkeys were stratified into a radiation exposed (RAD) and control (CTL) based on bodyweight and cardiovascular risk factors. This year we completed assessments at 2 years post total body irradiation, and our primary work has centered on describing the changes in body composition and metabolism. We have confirmed the observation that whole body irradiation increases the incidence and prevalence of diabetes in a prospective study that is truly one of a kind. We link the metabolic derangement with changes in adipose distribution and structure. This work is under review at the “Red Journal”, the leading publication for radiation physics and biology, and has been presented at Obesity Week which the leading scientific meeting for the study of adipose distribution and related biology.

Abstract taken from our submitted manuscript:

Purpose: Diabetes mellitus (DM) is a delayed effect of radiation exposure in human and non-human primates. DM is characterized by peripheral tissue insulin resistance, thus irradiation exposure may cause important changes in insulin-sensitive tissues like muscle and adipose.
Methods and Materials: We prospectively investigated changes in response to irradiation (4Gy whole body exposure) in 16 male rhesus macaques. We evaluated changes in body composition and glycemic control over two years, and insulin responsiveness, lipolysis, inflammation, and fibrosis at study end.
Results: Irradiated animals accumulate less fat and significantly increased percent glycation of hemoglobin A1c over time, such that 40% of irradiated monkeys had values that define them as diabetic at two years. Subcutaneous (SQ) adipose tissue was insulin resistant as evidenced by reduced phosphorylation of the insulin receptor substrate-1 in response to insulin challenge, and

had increased basal lipolysis despite comparable insulin exposures to control animals. Irradiated SQ adipose tissue had more macrophage infiltration and adipocytes were larger. The observed hypertrophy was associated with decreased glycemic control and macrophage infiltration correlated with decreased adiponectin, signifying that inflammation is associated with worsening health. No evidence of SQ adipose fibrosis was detected.
Conclusions: Our study is the first to prospectively illustrate that sub-lethal irradiation exposures directly propagate metabolic disease in the absence of obesity in non-human primates and implicate SQ adipose dysfunction as a target tissue.

Below is the graph depicting the key finding of our NHP study. Glycosylated A1c percentages is the key monitoring metric for long term glucose concentrations in the circulation. It is clear that from 18 months onwards, glucose dysregulation occurs in the irradiated monkeys and is significant. At 2 years, 40% of irradiated monkeys had diabetes versus 0% prevalence in the control monkeys ($p<0.05$).

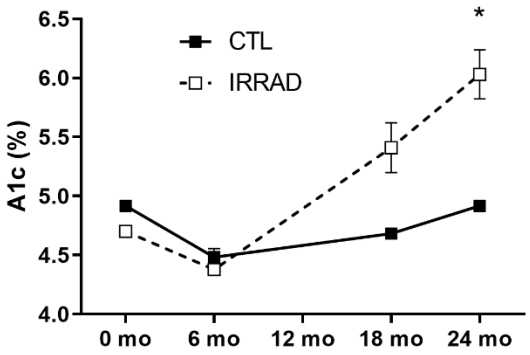


Figure 1.9. Hemoglobin A1c is increased in irradiated NHPs, indicating a propsensity to develop diabetes.

Unlike typical diabetes development, which commonly develops after obesity, irradiation leads to relative fat deficiency and stunted growth over time. The graphs below indicate weight and fat mass by two imaging methodologies was lower post-exposure.

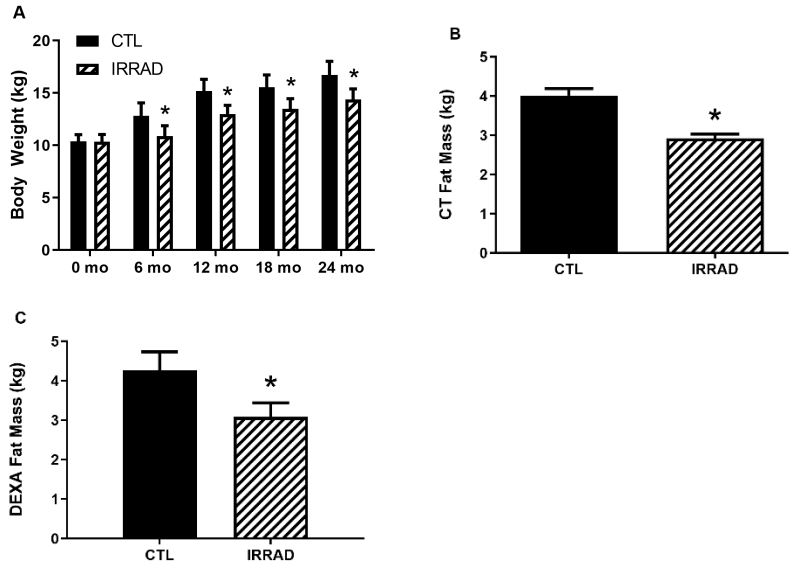


Figure 1.10. Despite the increase in the diabetes marker HbA1c (Figure 1.8), irradiated NHPs have lower fat mass, as measured by (A) body weight, (B) computed tomography, and (C) dual energy x-ray absorptiometery.

The table below gives more details about their phenotype, which is unremarkable aside from the changes in body composition and size. The fat appears to be lost from multiple storage sites (subcutaneous, visceral, hepatic) and there is a tendency for the fat to be lipolytic in the basal state, as measured by release of free fatty acids (and glycerol, data not shown) which infers insulin resistance. These body compositional changes and increased diabetes prevalence mirror our findings in the NHP radiation survivor cohort (Kavanagh et al 2015 Rad Res).

Table 1.3. Anthropometric and clinical chemistry values in irradiated NHP indicate a reduction in stature and lean body mass relative to controls.

	CTL	IRRAD	p-value
Crown-Rump (m)	0.59 (0.01)	0.56 (0.01)	0.05
Body Mass Index (kg/m^2)	47.55 (3.99)	45.71 (2.94)	0.35
Arm Circumference	23.02 (0.68)	21.55 (0.68)	0.08
Leg Circumference	33.31 (1.42)	30.03 (1.24)	0.05
Waist Circumference (cm)	52.67 (3.77)	47.62 (3.05)	0.15
Systolic Blood Pressure (mmHg)	135.43 (3.14)	133.61 (7.08)	0.44
Diastolic Blood Pressure (mmHg)	81.38 (6.54)	79.53 (6.16)	0.42
HOMA (AU)	10.87 (2.01)	15.33 (4.63)	0.53
Fasting Insulin (µIU/mL)	59.48 (12.54)	80.53 (24.07)	0.56
Fasting Glucose (mg/dL)	75.88 (5.80)	77.08 (14.09	0.53
Total Cholesterol	173 (20.9)	203 (15.6)	0.29
Triglycerides	31.7 (18.3)	58.8 (14.0)	0.28
Basal Non-Esterified Free Fatty Acids* (FFA/mg adipose)	0.191 (0.189)	0.5212 (0.145)	0.10
CT Liver Attenuation (HU)	58.2 (1.93)	54.9 (1.47)	0.21
CT Psoas Muscle Attenuation (HU)	62.2 (0.90)	61.2 (0.70)	0.42
CT Abdominal SQ Fat Area (cm^2)	28.9 (4.40)	21.7 (3.41)	0.11
CT Abdominal VIS Fat Area (cm^2)	67.7 (11.2)	47.9 (8.63)	0.09
SQ:VIS Fat Area	0.48 (0.13)	0.54 (0.10)	0.72
DEXA Lean Mass (kg)	11.0 (0.43)	9.47 (0.33)	0.02
CT Lean Mass (kg)	10.1 (0.45)	9.47 (0.35)	0.14

We further confirmed insulin resistance by doing in vivo dynamic testing, whereby adipose was collected before and after insulin infusion. Adipose tissue fails to adequately respond to insulin. Consistent with this, we have repeatedly measured reduced insulin signaling in irradiated NHP skeletal muscle. In the series of graphs below, irradiated subcutaneous adipose tissue has less insulin receptor substrate 1 activation with insulin infusion (A), larger average fat cell diameter (B), and more macrophages infiltrating the fat tissue (C). All of these features are profiles of an unhealthy adipose depot.

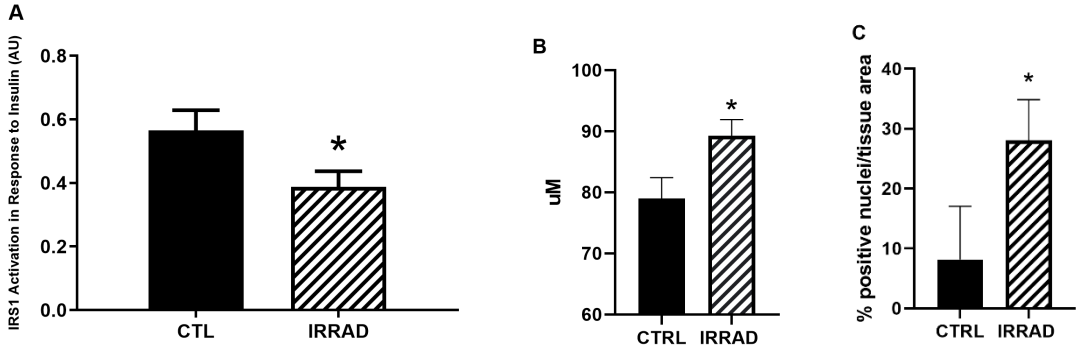


Figure 1.11. Reduced insulin responsiveness (A), increased adipocyte size (B) and increased macrophage infiltration of fat (C) in irradiated NHP.

Adiponectin is an adipocyte-secreted hormone that is a powerful insulin sensitizer. It did not differ in circulation, but was related to macrophage density ($r=-0.56$, $p=0.02$). Glycemic control was significantly related to fat cell size and lipolysis rates ($r=0.61$ and 0.69, $p<0.01$ for both associations). These clinical measures and tissue characteristics are supportive evidence of how important normal adipose function is for whole body metabolism.

As with the radiation survivor monkeys, circulatory inflammatory profiles were unremarkable in the 2 year post-exposure monkeys (data not shown). We also looked for evidence of fibrosis and fibrosis signaling in adipose, and found no evidence of fibrotic remodeling. Data regarding capillary density (CD31), extracellular matrix components, and TGFb signaling is tabulated below. Analyses were covaried by body weight, as weight differed between the groups.

Table 1.4. Adipose tissue. Markers of vascularity (CD31) fibrosis, and TGFb signaling (pSMAD2/3) show no difference with irradiation.

	CTL	IRRAD	ANCOVA p-value
$CD31^{+ve}$ cell density (cell/um)	0.0000434 (0.00011)	0.0000341 (0.000013)	0.58
MTC fibrosis (% area)	2.23 (0.89)	2.46 (0.67)	0.81
Collagen 1 (% area)	17.7 (1.53)	18.9 (1.17)	0.55
Collagen 3 (% area)	14.5 (1.37)	15.0 (1.05)	0.77
Collagen 4 (% area)	11.5 (1.25)	11.7 (0.95)	0.92
Fibronectin (% area)	8.69 (0.77)	9.21 (0.62)	0.61
pSMAD2/3 (AU)	0.369 (0.031)	0.481 (0.084)	0.35

Collectively, these data show for the first time that whole body irradiation leads to diabetes and persistent changes in adipose amount and function. These changes in adipose tissue contribute to disease development. We know skeletal muscle is also insulin resistant, and irradiated skeletal muscle shows negative remodeling of capillarization and extracellular matrix. We believe the combination of adipose and skeletal muscle remodeling and dysfunction causes insulin to be ineffective in removing glucose from the circulation, for muscle metabolism or adipose uptake and storage as triglycerides.

Other work planned for the final grant year will center on following up the important diabetogenesis finding. We have developed methods for culturing pre-adipocytes from primary tissue explants. We expect irradiation to reduce proliferative capacity, hypothesized to be the result of higher senescent cell burdens. Radiation exposure is a well-known inducer of senescence in cells, and their presence in adipose has significant ramifications as a driver of health in both animal models and people. The image series below shows differentiation of pre-adipocyte cells collected from an irradiated NHP at days 1, 4, 9 and 11. The growth and differentiation of these cells, to become adipocytes capable of accumulating triglycerides, is visually apparent.

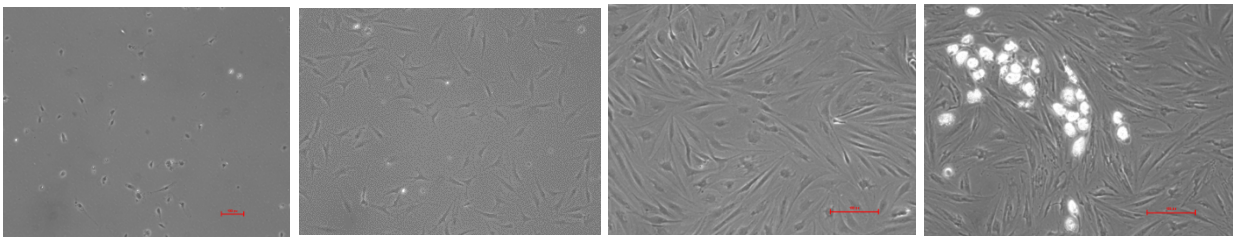


Figure 1.12. Images from left to rigth show cultured pre-adipocytes from NHPs; at 11 days of culture lipid droplets (white) are abundant.

In the final year, we plan to finish the assessment of skeletal muscle structure, function, and proteomics change over the 2-year period and relate these findings to the radiation-induced diabetogenesis.

As part of our longitudinal assessments, we have collaborated with Jenny Ting of the University of North Carolina to evaluate the microbiome over time and have unearthed an important translational story; however, a radiation signature was not present. In repeated assessments of the fecal microbiome, shifts did occur post-exposure (12 months), however these group effects did not persist at 2 years post-exposure.

We have noted a phenotype that is not radiation-related. Animals that were hypertensive at the beginning of the study, stayed hypertensive (group effect p=0.008). All NHPs are consuming a western-like diet, and even individuals with low blood pressure, increase over the course of study but do remain normotensive (time effect p=0.08). We see hypertension is associated with exponential increases in LBP1, the marker of microbial translocation from a leaky intestine.

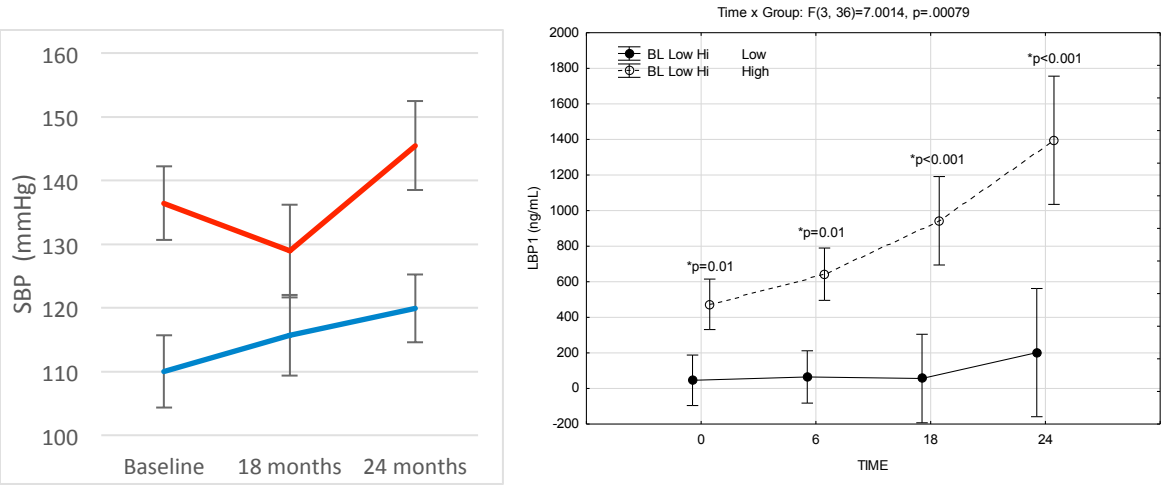


Figure 1.13. Non-radiation related finding; grouping of animals by blood pressure reveals an association between serum lipopolysaccharide binding protein 1 (LBP1) and systolic blood pressure (SBP).

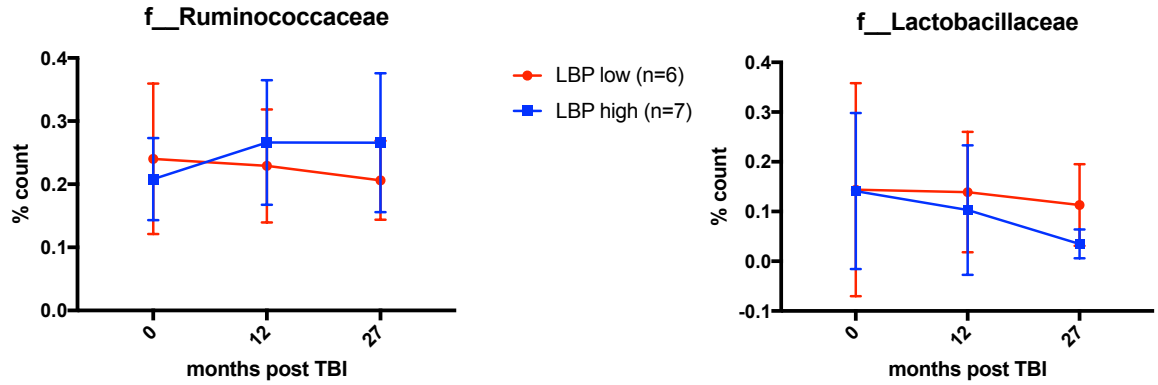


Figure 1.14. Microbiome shift from “healthy” lactobacullus predominance to ruminococcal predominance in animals with higher serum LBP.

When the microbiome was assessed by these groupings (low and high LBP1), the hypertensive “host” develops a less healthy microbiome with significant reductions in lactobacillaceae and significantly increased ruminococcaceae at both 12 and 27 month time points.

Few studies to date have good repeated intra-individual microbiome sampling, so these data are novel and of interest. We have checked that effects are present when irradiated animals are removed from the grouped analyses, and outcomes were consistent.

The final grant year also will include euthanasia of the animals in this cohort to facilitate collection of tissues and samples that are not readily available. We will add data regarding microbiomes (niche microbiomes, metabolomes, gastrointestinal and related immune tissue profiling).

3. Interventional Rodent Studies

We have taken our whole body irradiation + high fat, high sugar diet rodent model and have completed a 12-month interventional study designed to evaluate potential countermeasures to abrogate radiation-induced insulin resistance. In last year's annual report, we described the initial findings of improvements in fatty liver, which is a metabolic epidemic in the U.S and one without any therapeutic options. Our data was selected for an oral presentation at Digestive Diseases Week in San Diego (May 2019), which is the largest U.S. based meeting for the American Association of Liver Diseases.

Last years' reported findings are summarized as:

- Pharmacokinetics of IPW-5371 in tissue and plasma
- Liver non-alcoholic steatohepatitis scores
- Liver triglyceride content
- Liver fibrosis
- Lung fibrosis signaling (pSMAD2/3)

Our work in the current year has focused on solidifying the anti-fibrotic effects of IPW-5371 (a Transforming Growth Factor beta [TGFb] receptor 1 inhibition; IPW-5371 by Innovation Pathways). In all these outcomes, IPW-5371 significantly improved the phenotypes at 6 months, and at 12 months. We confirm that TGFb signaling is reduced in liver, as we had previously demonstrated in lung tissue. Both IPW-5371 groups have a significant difference in post-hoc testing using a factorial ANOVA model. WD=western diet; IRRAD=sub-lethal total body irradiation; IPW=IPW-5371; TAD=tadalafil.

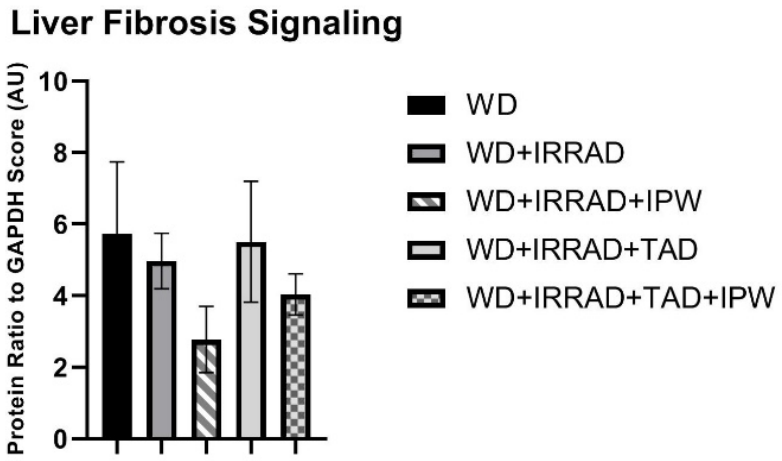


Figure 1.15. Treatment of mice with the TGFb inhibitor IPW-5371 (IPW) reduces expression of pro-fibrotic TGFbeta in liver.

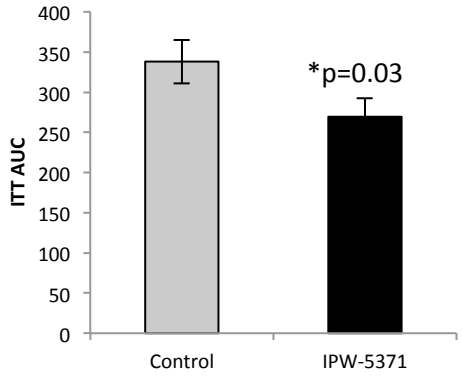


Figure 1.16. Treatment of mice with the TGFb inhibitor IPW-5371 (IPW) reduces the area under the curve for glucose.

We evaluated responses to insulin, as fatty liver determines insulin sensitivity of both lean and overweight people. The group of mice exposed to IPW-5371 as a sole agent had the best response to insulin tolerance testing (ITT), represented by a significantly smaller area under the curve (AUC) for glucose which is graphed above.

As the data generated from the prospective radiation cohort demonstrates, adipose tissue needs to be able to expand. Adipose tissue expansion allows for excess calories consumed to be stored as triglycerides in appropriate tissues. Lack of ectopic fat, particularly liver fat, is a key clinical feature of overweight and obese people protected from diabetes and related metabolic disturbances. This rodent data supports the need for reduced TGFb signaling and suggests that this pathway would be an effective intervention in the irradiated non-human primates, which consistently demonstrate less adipose and worsened metabolic function. We did not see differences in fat masses measured from irradiated rodents with our pharmacological exposures. However, as liver adipose was reduced we hypothesized that IPW-5371 exposed mice would have lower TGFb signaling, and possibly better ability to remodel and expand fat.

We estimated adipose tissue expansion and cellular density by measuring DNA and triglyceride content, normalized by the wet weight of tissue examined. Adipose expansion in response to TGFb receptor inhibition was clearly present. This expansion was discernable also when tissue total protein content, rather than DNA content, was the cellular normalization factor.

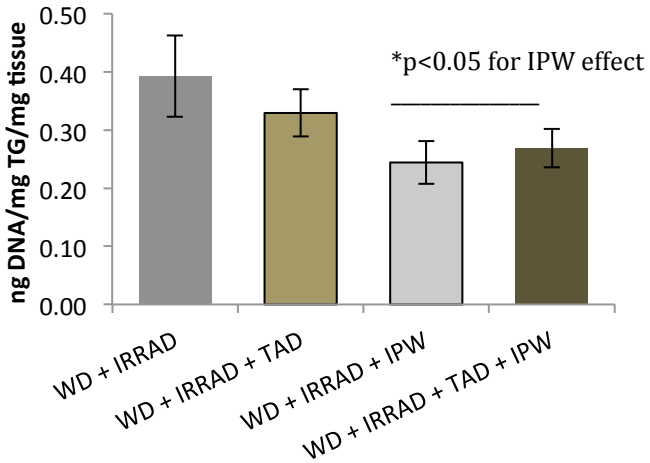


Figure 1.17. Treatment of mice with the TGFb inhibitor IPW-5371 (IPW) reduces the DNA to triglyceride ratio in tissue homogenates.

A model for our proposed adipose response to TGFb receptor 1 inhibition is below, and will be the framework for future proposals. IPW-5371 has had pharmacokinetic evaluations in NHPs, and an oral formulation ready for efficacy testing in vivo planned to be complete by 2020.

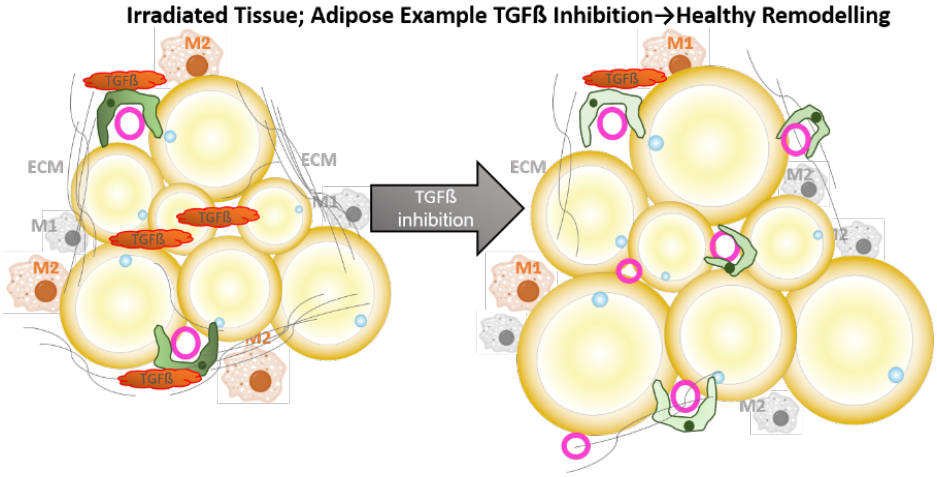


Figure 1.18. Model for TGFb inhibition effects; reduction in M2 profibrotic macrophages, and improved perfusion.

We have continued to investigate the pharmacological interaction observed between tadalafil and IPW-5371, and have found consistent cardiovascular lesions in exposed male mice only. Last year we reported the significant death rates from combined exposures, and this year we confirm the presence of inflammatory and necrotic lesions. Thirteen male mice exposed to the drug combination IPW-5371 and tadalafil had heart histology assessed by a blinded reviewer. Twenty three percent of mice had died from acute hemorrhage and hypovolemia and served as positive cases for lesion review. All 13 samples had lesions noted in the heart. Two aortic sections evaluated also had evidence of inflammation. The general description of the lesions is below:

> *The left ventricular outflow track was infiltrated by mesenchymal cell proliferation beginning at the base and extending along the walls. Elastin fibers within the outflow track were separated and disorganized, primarily adjacent to the mesenchymal cell proliferation. Mild to moderate hemorrhage and mixed lymphocytic infiltration were present within the walls of the outflow track primarily in areas adjacent to mesenchymal cell proliferation. Acellular fibrinoid change was present in four samples. Rare foci of nuclear debris were seen in the walls of the outflow track in three samples. Single foci of cartilaginous metaplasia were present in three samples. Mild to moderate external hemorrhage was present in two samples. Myxomatous degeneration was present in one or more valves in two samples. Lesions were even present in mice that were euthanized without clinical signs.*

We suspect tadalafil is driving the negative interaction. Adipose expansion was inhibited by tadalafil, when male mice were dose with tadalafil alone or in combination with IPW-5371. No differences in female mice were observed.

Our plan for the final grant year will be to publish 3 papers that focus on these studies that directly address changes in insulin sensitivity as a result of radiation exposure; 1. Mouse model, 2. IPW-5371 benefits to metabolism and adipose distribution, 3. Tadalafil sex-specific

interactions with TGFb inhibition. Remaining data to be generated includes macrophage quantitation in adipose tissues, and general pathology review of tissues exposed to the investigational new drug, IPW-5371.

We have a fourth paper in preparation that uses the control NHP skeletal muscle histology, and the microbiome interactions with hypertension will likely be the fifth.

4) Other Achievements:

Nothing to Report

Project 2 – Radiation/Heart Disease (Register)

1) Major Activities

a) Collection and processing of blood samples in the prospective cohort during the subacute post-radiation phase for planned serum and plasma biomarker analyses.

b) Monitoring and surveillance of animals in the prospective cohort

c) Continued discussions with Duke investigators on cross-project technical collaboration on cell collections, processing, and data analysis, manuscript development, and future grant applications.

d) Analysis of gene expression in iliac arteries obtained from RSC cohort subjects which had gone to necropsy. Key target genes being investigators include collagen, macrophage and T cell markers, as well as selected cytokines and chemokines.

e) Biomarkers: Cardiac biomarkers: Assessed plasma NT-proBNP and multiplex cytokines/chemokines/biomarkers in samples from a previous study in which we have cardiac phenotypes including fibrosis and global gene expression. Shipped plasma samples from a prior study to an outside collaborating miRNA analytical group (*Chromologic LLC*, Monrovia CA) for miRNA analysis.

f) Cardiac tissue analyses: Processing of myocardial and coronary artery tissue blocks (RSC, & past Project with mitigator) for assessment of coronary artery atherosclerosis (CAA) and cell types using immunohistochemical analyses, stained sections for which we developed new protocols for semi-automated atherosclerosis assessments. Manuscript about to be submitted to AHA journal.

g) Cardiac Ultrasound Analysis Software: Ongoing discussions with the vendors of our cardiac Image Analysis software system (TOMTEC). We upgraded the computer and software for customized output to accommodate the smaller NHP heart sizes.

h) Cardiac Ultrasound Data collected from the PRC studies have been collected and evaluated from the 1st 3 years. Ultrasound images from the past 3 years in the RSC are 100% completed and a new manuscript about to be submitted.

j) Cardiac MRI studies on the 16 PRC monkeys were scheduled and are ½ way completed for the 2 year timepoint. Analyses of the images from have been partially completed. We are working to have specialized image analyses completed in the coming months.

k) Monthly DOD Conference calls

l) Newly funded grant *"Effects of Ionizing Radiation (IR) on Myocardial DNA Methylation Profiles in Relation to Cardiomyopathy in a Nonhuman Primate Model"* from the 2018 Peer Reviewed Medical Research Program for a Discovery Award to expand this work into a new area (epigenetic regulation through DNA methylation) has been initiated.

m) Publication of manuscript describing the effects of radiation on lymphoid organ systems in *Radiation Research.*

2) Specific objectives

Collections of samples, US, and cMRI images from the prospective cohort as described above. Planning for next cardiac imaging and biomarker assessments. Analysis of myocardium from RSC.

3) Results/key outcomes

3.1) Effects of TBI on Monocyte Polarization in the PRC: A Potential Mediator of Cardiac and Systemic Radiation Induced Fibrosis: Manuscript published in Radiation Research.

Background: Radiation induced fibrosis (RIF) is a delayed effect of acute ionizing radiation exposure (DEARE) affecting not only the heart, but other tissues including the lungs, liver and skin, and resulting in reduced tissue function and increased morbidity. Monocytes may be classified into classical (CD14++, CD16-), intermediate (CD14++, CD16+), and non-classical ($CD14+^{low}$, CD16++) subtypes in humans and non-human primates (NHPs), and it is likely one or more subpopulations of monocytes may play an integral role in the pathogenesis of RIF. We explored the hypothesis that moderate to high levels of total body irradiation (TBI) can alter monocyte polarization and produce phenotypes which could promote multi-organ fibrosis.

Summary of monocyte paper findings: The manuscript reports that monocyte phenotypes shifted towards intermediate and non-classical phenotypes at 6 months post-irradiation, accompanied by gene expression changes in intermediate monocytes, but not classical monocytes. The pathways identified from available algorithms are associated with pro-fibrotic and anti-inflammatory signaling pathways which could function to push intermediate monocytes towards M2 macrophage polarization upon extravasation. These findings support the notion that monocyte programming may present a novel target opportunity for therapies to inhibit or prevent radiation induced fibrosis in the heart and elsewhere.

3.2) Cardiac Functional, Structural, and Cellular Alterations in Rhesus Macaque Survivors of Ionizing Radiation Exposure (manuscript to be submitted)
Abstract:
Rationale: Radiation induced heart disease (RIHD) is a significant concern for survivors of ionizing radiation exposures through accidental, malicious, or medical means.
Objective: The purpose of this study was to investigate the effects of total body irradiation (TBI) on the heart in male rhesus macaques, a translational non-human primate (NHP) model.
Methods and Results: Echocardiography was performed on survivors of a single dose (6.4-8.5 Gy) of TBI (n=34) and non-irradiated controls (n=26) divided into longer (LT IRR) and shorter term (ST IRR) survivors and controls. LT IRR had increased transmitral early filling velocities (E), decreased early mitral annular descent velocities (e'), higher E/e' ratios and decreased early (e') to late (a') mitral annular descent velocity ratios (e'/a') compared to LT CTL (all $p \leq 0.05$), indicating diastolic dysfunction. Apical 4 chamber-derived stroke volume, cardiac output, and end-diastolic volume were also lower in LT IRR than controls (all $p \leq 0.05$). ST IRR animals had similar alterations in LV diastolic function but not in cardiac volumetric measures. Histochemical and immunohistochemical analyses of sections of LV, IVS, and RV from deceased irradiated animals (n=17) exposed to a single dose (6.9-8.05) Gy TBI and deceased non-irradiated controls (n=12) demonstrated that IRR animals had increased LV fibrosis decreased LV and IVS capillary density, increased pan-cardiac fibroblast staining area, increased pan-cardiac macrophage staining, increased LV and IVS M2 macrophages, and increased pan-cardiac M1 macrophages (all $p<0.05$).

Conclusions: LV diastolic dysfunction due to radiation exposure may be a physiological consequence of decreased capillary density, activation and expansion of fibroblasts, and increased accumulation of pro-fibrotic and pro-inflammatory macrophages, all of which lead to increased myocardial stiffness due to fibrosis. Collectively, these findings provide insight on the delayed effects of acute ionizing radiation exposure and indicate that therapies targeting macrophage regulation of fibrosis may mitigate radiation induced heart disease.

RESULTS

Echocardiographic phenotyping

Two groups of animals were chosen from our available dataset of 60 NHP for the current study of echocardiographic phenotypes, 1) an older, longer term survivor group of 14 mature adult (12.6 to 20.3 year old) long-term survivors (LT IRR) exposed to a single TBI dose of 6.5 to 8.4 Gy approximately 9.7 to 11.6 years earlier, which were compared to 15 age-matched, nonirradiated controls (LT CTL)(Table 1), and younger, shorter term survivor group (ST IRR) of 20 young adult (4.7 to 6.0 year old) exposed to a single TBI dose of 6.4-8.5 Gy approximately 2.16 to 2.96 years earlier, which were compared to 10 age-matched, nonirradiated controls (ST CTL)(**Table 2.1**).

Table 3.1: Animal Demographics of Previously Irradiated Long Term, Short Term, and Deceased Male Rhesus Macaque Survivors (LT IRR, ST IRR, Deceased IRR) and Controls (LT CTL, ST CTL, Deceased CTL)

	LT IRR (N=14)	LT CTL (N=15)	P	ST IRR (N=20)	ST CTL (N=10)	P	Deceased IRR (N=17)	Deceased CTL (N=12)	P
Age (Years)	14.96 (0.63)	14.15 (0.28)	0.25	5.47 (0.08)	5.25 (0.33)	0.40	12.14 (0.96)	9.33 (0.92)	0.47
Years Since Irradiation	10.48 (0.18)	---	---	2.51 (0.07)	---	---	5.80 (0.55)	---	---
Dose (Gy)	7.40 (0.16)	---	---	7.01 (0.14)	---	---	6.93 (0.13)	---	---
Body Weight (kg)	11.31 (1.11)	14.62 (1.25)	0.06	9.22 (0.56)	8.77 (0.35)	0.86	13.25 (0.85)	10.90 (0.54)	**0.04**[a]
Body Surface Area (m^2)	0.48 (0.03)	0.55 (0.03)	0.16	0.42 (0.29)	0.41 (0.01)	0.97	0.54 (0.02)	0.47 (0.02)	0.06

Data presented as mean (SEM)

Echocardiographic Phenotypes of Long Term Survivors

Structural and functional differences between LT IRR and LT CTL animals were assessed using B mode, M mode, and pulsed wave and tissue Doppler echocardiography. LT IRR animals differed from LT CTL in several diastolic function measures including increased transmitral early filling velocities (E) and E wave deceleration slope and decreased early mitral annular descent velocities (e') that resulted in higher E/e' ratios and decreased early (e') to late (a') mitral annular descent velocity ratios (e'/a') (all p≤0.05) (**Figure 2.1**). The remaining diastolic function measures of transmitral late filling velocity (A), a', and E/A ratio were not different between groups. Stroke volume (biplane and apical 4 chamber views), cardiac output (apical 4 chamber view), and end diastolic volume (apical 4 chamber views), were lower in LT IRR than LT CTLs (all p ≤ 0.05) and biplane measures of cardiac output and end diastolic volume tended to be lower as well (both p=0.07) (**Figure 2.2**). M mode measures of cardiac structure corroborated our previous findings of decreased left ventricular diameters at end systole (LVIDs) and diastole (LVIDd) in LT IRR animals compared to LT CTLs, and also showed tendencies for decreased LV posterior wall thickness at end systole (LVPWs) (p=0.07) and diastole (LVPWd) (p=0.06). No differences were observed in interventricular septal thicknesses at end systole (IVSs) or end diastole (IVSd) (both p> 0.5). Parasternal long axis measurement of the LV outflow tract

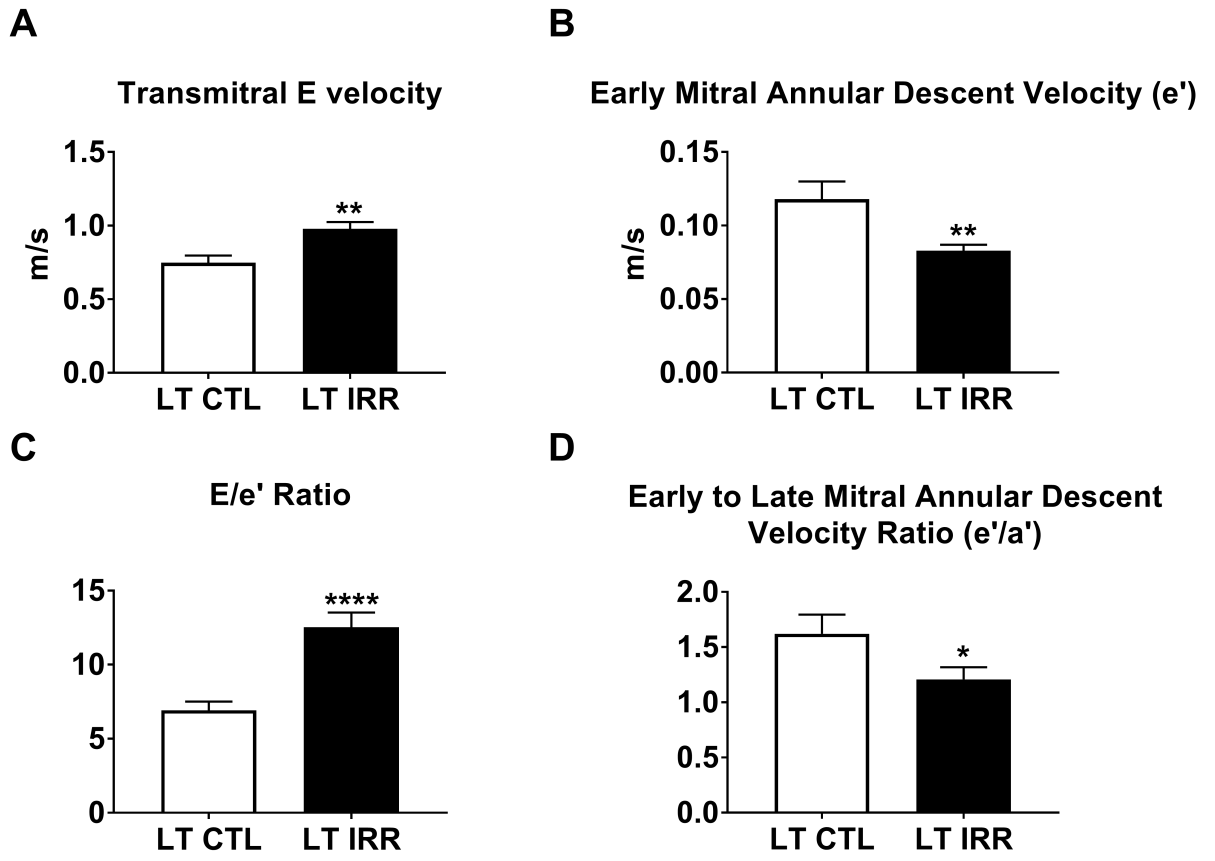


Figure 2.1 Echocardiographic Diastolic Function in Long Term Irradiated (LT IRR) and Long Term Controls (LT CTL): LT IRR animals had significantly increased transmitral early filling peak velocity (E) (Panel A), decreased early mitral annular descent velocity (e') (Panel B), increased E/e' ratio (Panel C) and decreased early to late mitral annular descent velocity ratio (e'/a') (Panel D) compared to LT CTL animals. Data are mean ± SEM. *p<0.05, **p<0.01, ****p<0.0001

diameter (LVOT) showed that LT IRR animals had significantly narrower outflow tract diameters compared to LT CTL (p=0.01) (Table 4). No differences in heart rate, blood pressures (systolic, diastolic, and mean), ejection fraction, fractional shortening, or left atrium volume and size measures; aortic root to left atrium ratio (AO/LA) and left atrial end systolic volume (biplane) (LA Vol BP) were found.

Echocardiographic Phenotypes of Short Term Survivors

Structural and functional differences between ST IRR and ST CTL animals were evaluated similarly as LT IRR vs LT CTLs. Like LT IRR animals, ST IRR animals also had increased E/e' ratios and decreased e' and e'/a' ratios compared to ST CTLs (all p≤0.05) (**Figure 2.3**), while E, A, E/A ratio, and a' were not significantly different between groups. ST IRR and ST CTL did not differ in cardiac output, stroke volume, end diastolic volumes, heart rate, blood pressures (systolic diastolic, and mean), ejection fraction, fractional shortening, IVSd, ESV, LVIDs, LVIDd, AO/LA, or LA Vol BP.

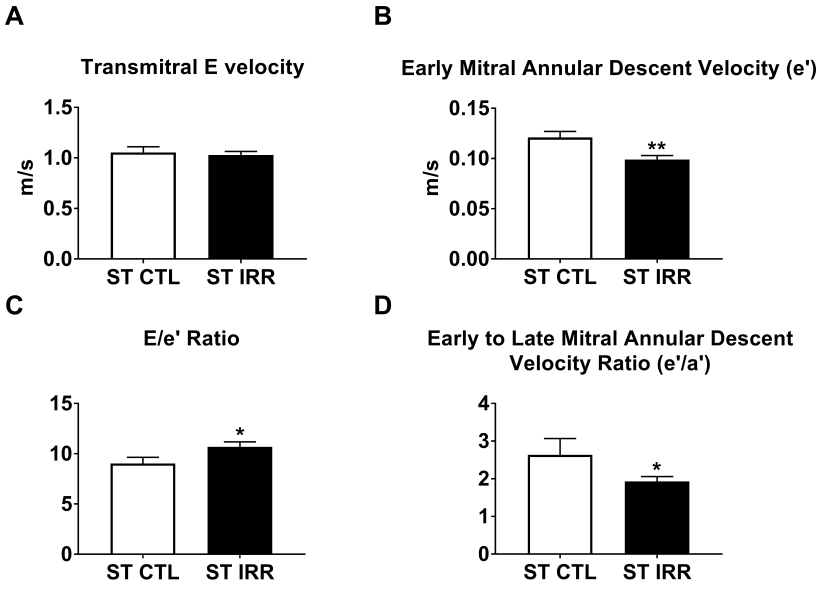


Figure 2.2 Echocardiographic Cardiac Volume Measures in Long Term Irradiated (LT IRR) and Long Term Controls (LT CTL): LT IRR animals tended to have decreased cardiac output calculated by method of disks measurements using the perpendicularly oriented apical 2 chamber (A2C) and apical 4 chamber (A4C) views resulting biplane measurement (BP)(Panel A). LT IRR animals did have significantly lower cardiac output when only the A4C chamber view was used (Panel B). Additionally, LT IRR animals had decreased stroke volume (BP measurement) and a tendency for decreased end diastolic volume (BP measurement). Data are mean ± SEM. *p<0.05

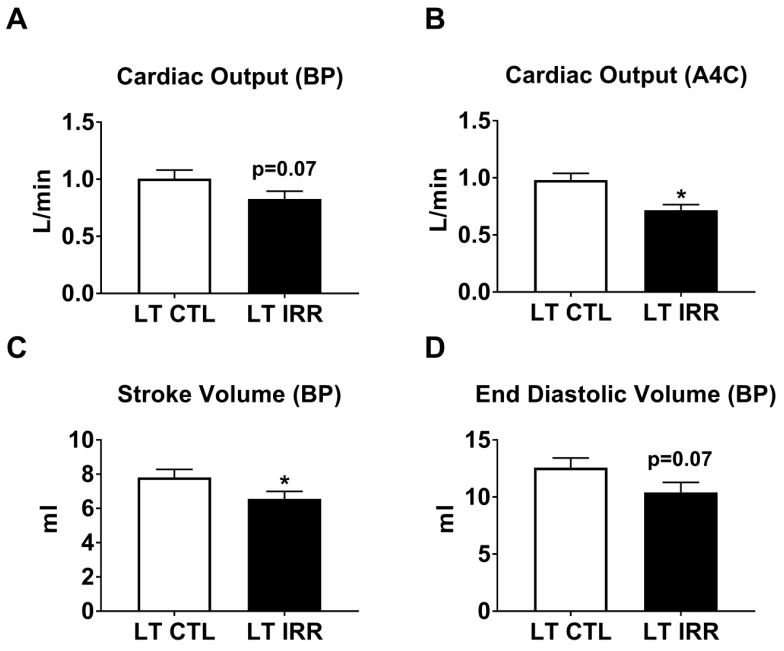


Figure 2.3 Echocardiographic Diastolic Function in Short Term Irradiated (ST IRR) and Short Term Controls (ST CTL): ST IRR animals had no differences in transmitral early filling peak velocity (E) (Panel A), but decreased early mitral annular descent velocity (e') (Panel B), increased E/e' ratio (Panel C) and decreased early to late mitral annular descent velocity ratio (e'/a') (Panel D) compared to ST CTL animals. Data are mean ± SEM. *p<0.05, **p<0.01

Histological and Immunohistochemical Staining of the Left Ventricular, Interventricular Septal, and Right Ventricular Myocardium

Sections of LV, IVS, and RV from 17 deceased previously irradiated animals (Deceased IRR) and 12 deceased controls (Deceased CTL) were evaluated for structural and cellular components using histochemical and immunohistochemical stains for fibrosis (Masson's trichrome), capillary density (CD31), fibroblasts (S100A4), macrophages (CD68 and CD163) and M1 or M2 macrophages (pSTAT1/CD163 and c-Maf/CD163 respectively). IRR animals had

significantly greater positive trichrome staining of the LV ($p<0.05$), and no significant difference in the RV or IVS compared to CTL animals. (**Figure 2.4**) Capillary density was reduced in the IRR group in the LV ($p<0.05$) and IVS ($p<0.01$), but not the RV. (**Figure 2.4**).

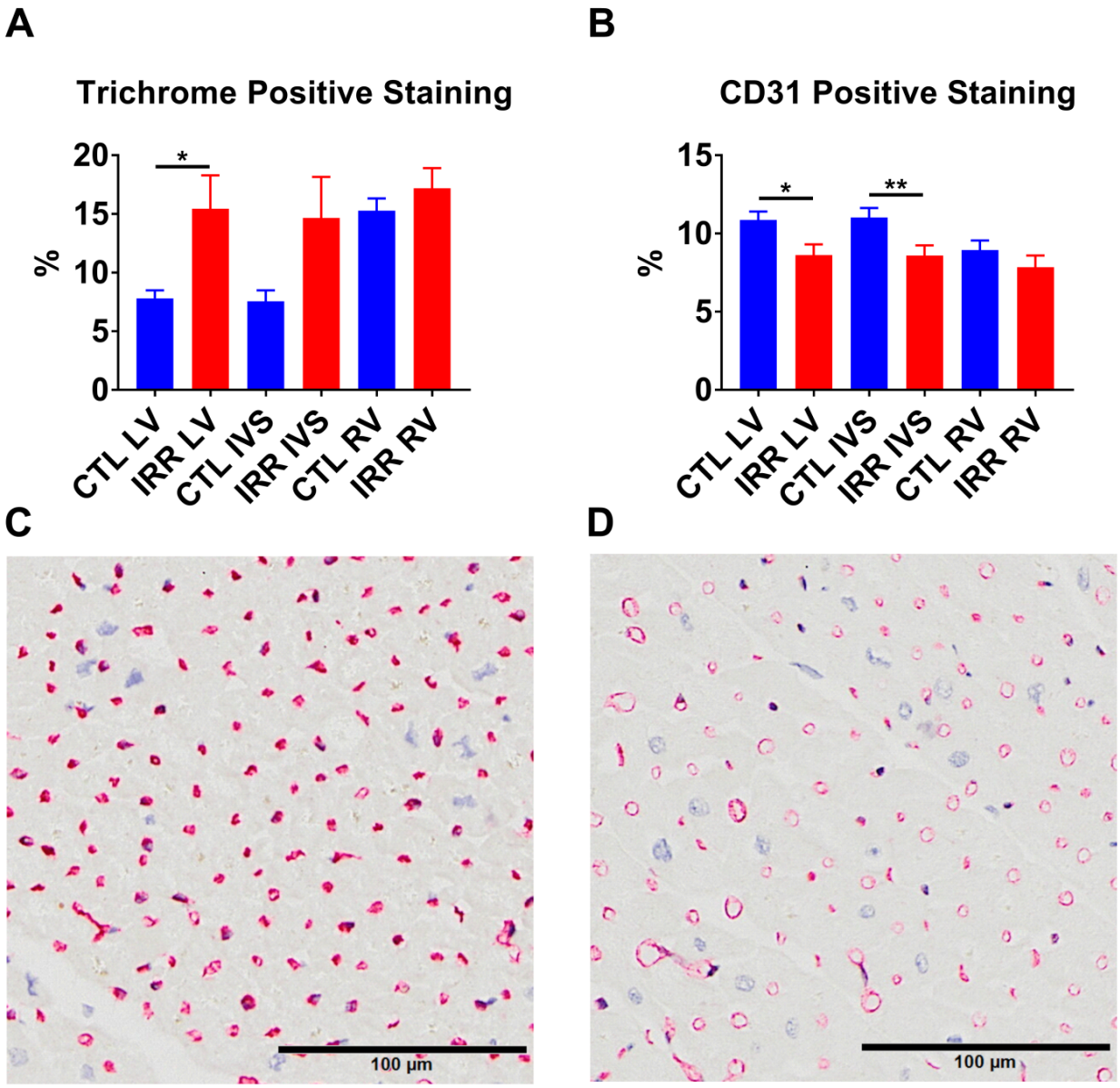


Figure 2.4 Fibrosis and Capillary Density Immunostaining in Deceased Irradiated (IRR) and Control (CTL) Animals: IRR animals had significantly increased percent positive trichrome staining of the left ventricle (LV) but not the interventricular septum (IVS) or right ventricle (RV) compared to CTL. IRR animals also had significantly decreased CD31 percent positive staining in the LV and IVS, but not RV compared to CTL (Panel B). Panels C and D are representative CD31 stained sections of LV mid-myocardium from a CTL and IRR animal respectively, demonstrating increased CD31 staining in CTLs. *$p<0.05$, **$p<0.01$

IRR myocardium exhibited increased S100A4^{+} area in all cardiac sections (LV p<0.01, IVS p<0.001, and RV p<0.05) compared to CTL (**Figure 2.5**). In addition, approximately 100 fold less CD68^{+} macrophage staining area (LV mean= 8900 um^2, IVS mean=6134 um^2, RV =3484 um^2) was observed relative to CD163^{+} macrophage staining area (LV mean= 905232 um^2, IVS mean= 720474 um^2, RV mean= 339053 um^2) across all animals, and CD163 staining frequently co-localized with CD68 staining (**Figure 2.6**). Based on these findings we subsequently used CD163 as a pan-macrophage marker and used nuclear staining pSTAT1 or c-Maf to indicate M1 or M2 like macrophages respectively. Deceased IRR animals had increased CD163^{+} macrophage staining in the LV (p<0.05), IVS (p<0.01), and RV (p<0.05), increased c-Maf^{+}/CD163^{+} macrophages in the LV (p<0.05) and IVS (p<0.01), but not RV, and increased pSTAT1^{+}/CD163^{+} macrophages in the LV (p<0.01), IVS (p<0.01), and RV (p<0.05).(Figure 8) Finally, we compared the c-Maf^{+}/CD163^{+} (M2) to pSTAT1^{+}/CD163^{+} (M1) ratio and found that IRR animals had a significant decrease in the M2/M1 ratio across all assessed regions of the heart (all p<0.05).(**Figure 2.7**)

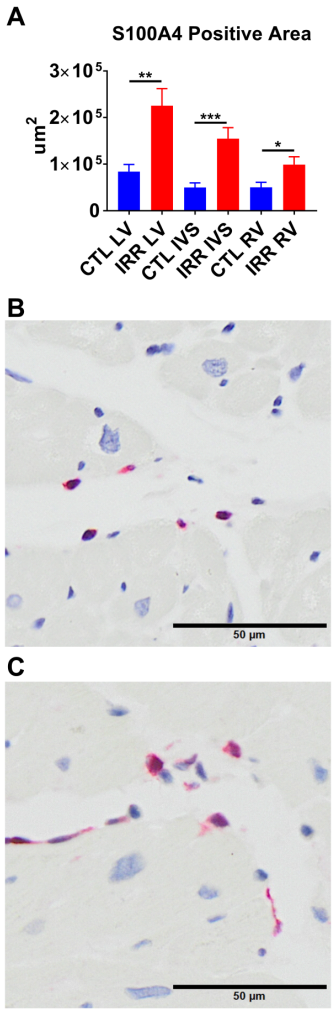


Figure 2.5 Fibroblast Immunostaining in Deceased Irradiated (IRR) and Control (CTL) Animals: IRR animals had greater S100A4 staining in all evaluated sections of myocardium compared to CTL animals (Panel A). Panels B and C are representative mid-myocardial S100A4 stained sections from a CTL and IRR animal respectively illustrating typical positive

staining increases in IRR animals. *p<0.05, **p<0.01, ***p<0.001

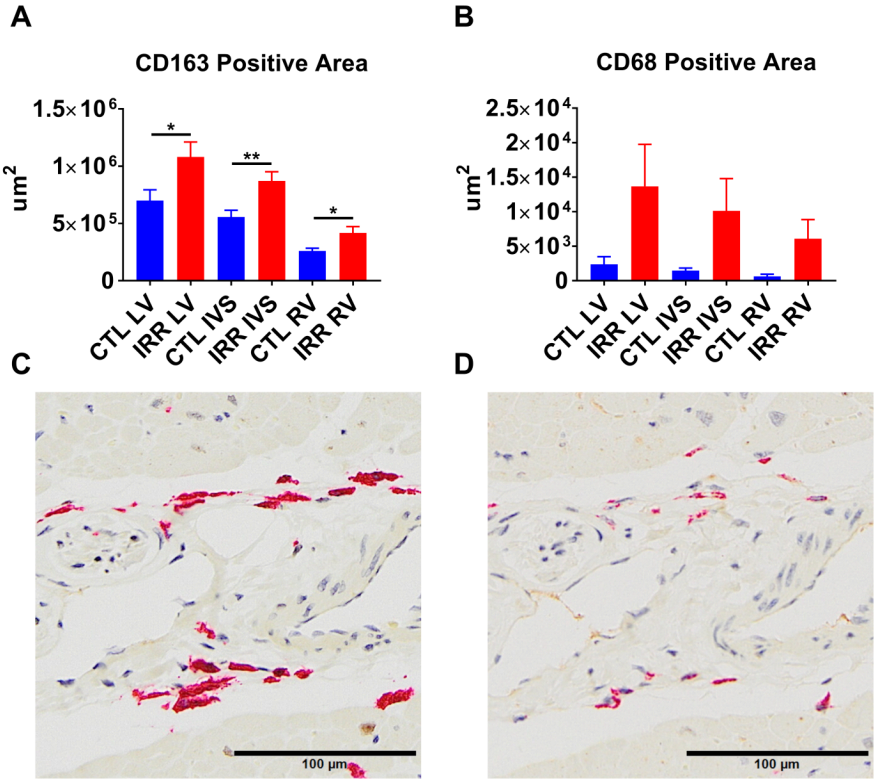


Figure 2.6 Macrophage Immunostaining in Deceased Irradiated (IRR) and Control (CTL) Animals: IRR animals had increased normalized CD163 positive staining area in the left ventricle (LV), interventricular septum (IVS), and right ventricle (RV) compared to controls (CTL)(Panel A). In contrast no differences were observed in CD68 staining which was highly variable across both groups (Panel B). Panels C and D are CD163 and CD68 stains respectively from the same animal in the same location illustrating that $CD68^{+}$ macrophages were also often $CD163^{+}$.*p<0.05, **p<0.01

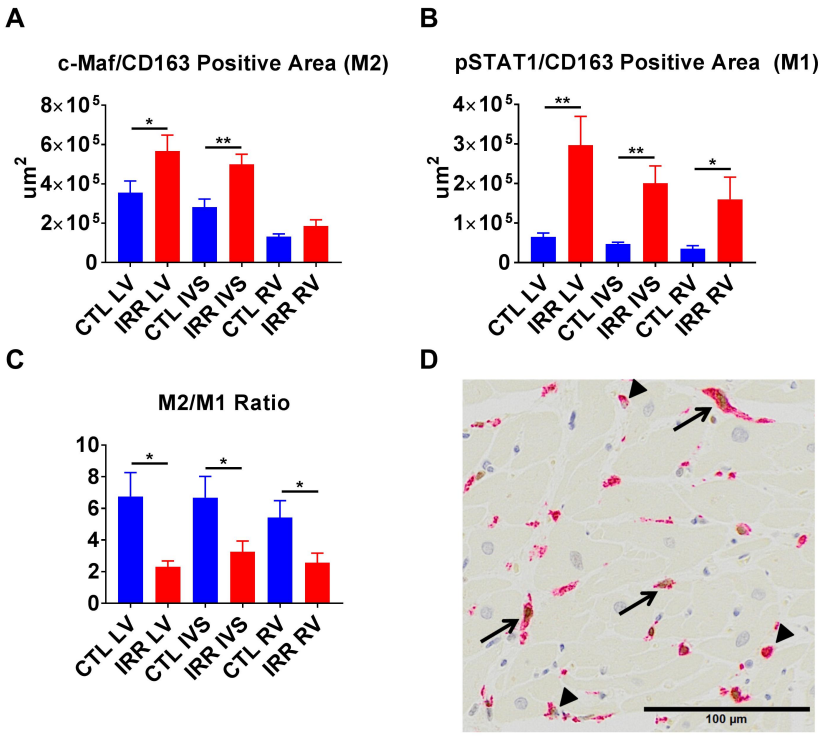


Figure 2.7 Macrophage Polarization in Irradiated (IRR) and Control (CTL) Myocardium: IRR animals had increased c-Maf$^+$/CD163$^+$ staining (M2 polarization) in the left ventricle (LV), interventricular septum (IVS), but not right ventricle (RV) compared to controls (CTL)(Panel A). Increased pSTAT1$^+$/CD163$^+$ staining (M1 polarization) was noted in all sections (LV, IVS, and RV) in IRR animals compared to CTL (Panel B). This translated to a decrease in the M2/M1 macrophage ratio across all sections in IRR animals (Panel C). Panel D is a representative dual stained image indicating dual stained c-Maf$^+$/CD163$^+$macrophages (arrows) and single stained CD163$^+$ macrophages (arrowheads) from the LV of an irradiated animal. *p<0.05, **p<0.01

Conclusions: LV diastolic dysfunction due to radiation exposure may be a physiological consequence of decreased capillary density, activation and expansion of fibroblasts, and increased accumulation of pro-fibrotic and pro-inflammatory macrophages, all of which lead to increased myocardial stiffness due to fibrosis. Collectively, these findings provide insight on the delayed effects of acute ionizing radiation exposure and indicate that therapies targeting macrophage regulation of fibrosis may mitigate radiation induced heart disease.

3.3 Molecular Characterization of Myocardium from Deceased RSC Subjects

Subjects

Male rhesus macaques (n=41) were obtained from the Armed Forces Radiobiology Research Institute, the University of Maryland, the University of Illinois at Chicago, the Lovelace Respiratory Research Institute, and the Michael E. Keeling Center for Comparative Medicine and Research. Irradiated macaques were ~3-10 years of age at time of irradiation and received 5.0-8.5 Gy total body gamma irradiation.

Sample Preparation

Sections of left ventricle were obtained from animals that had died or were euthanized due to morbidity. At necropsy, subjects were flushed with saline, and sections of myocardium were removed and flash frozen for later analysis. Tissue was partially pulverized under liquid N2 and further homogenized with a bead mill. Total RNA was isolated and purified using a Zymo Quick DNA/RNA Miniprep Plus Kit to retain miRNAs. RNA integrity numbers (RIM) were determined for each sample and only samples above RIN=6.4 were used in the present analyses.

RNAseq Methods
cDNA Library Preparation and Sequencing Methods Total RNA was used to prepare cDNA libraries with the SMARTert Stranded Total RNA-Seq Kit v2 - Pico Input Mammalian (TaKaRa Bio USA Inc., Mountain View, CA). Briefly, 8 ng of total RNA was subjected to fragmentation followed by reverse-transcription. Illumina sequencing adaptors were attached during PCR amplification and the double-stranded cDNA was purified using AMPure XP magnetic beads. Finally, the cDNA was subjected to rRNA depletion and the stranded libraries were pre-amplified with PCR. The library size distribution was validated and quality inspected on an Agilent 2100 Bioanalyzer using a High Sensitivity DNA chip (Agilent Technologies). The quantity of each cDNA library was measured using a Qubitt 3.0 Fluorometer (Thermo Fisher Scientific). Libraries were sequenced to a read depth of .35M reads per sample using 1 x 75 bp single-end (SE) sequencing (Illumina, San Diego, CA) on the Illumina NextSeq 500.

miRNAseq Methods
miRNAseq libraries were generated using a Trilink Biotechnologies CleanTag® Small RNA Library Prep Kit. Data analysis will proceed soon.

Preliminary Analysis of RNAseq dataset: RNAseq data was evaluated using MultiQC v0.7 (Phil Ewels, available on GitHub). Alignment was conducted with STAR using the rhesus genome (Macaca mulatta v 8.0.1). Cutadapt was used to find and remove primer adapter sequences, primers, poly-A tails and other unwanted sequence high-throughput sequencing reads. Analyses were carried out using R, Bioconductor, and custom codes. Quality control for high throughput sequence data was assessed using FastQC (Simon Andrews at the Babraham Institute in Cambridge). The Adjusted P, is the genomic adjusted raw p value, FDR_Genomic_Adjusted_P is Benjamini & Hockberg. The genomic adjustment is evidenced by the pp plots, which takes the raw p value and removes inflation typically found in data analyzed with DESeq2.

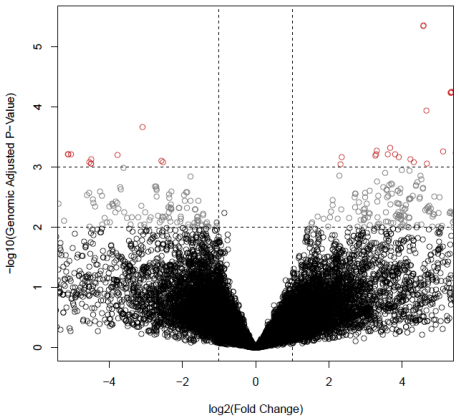


Figure 2.8 Volcano Plot of RNAseq Data from Male Rhesus RSC Subjects:
Plot shows adjusted p values for different up and down regulated genes in TBI (n=22) vs Control subjects (n=16).

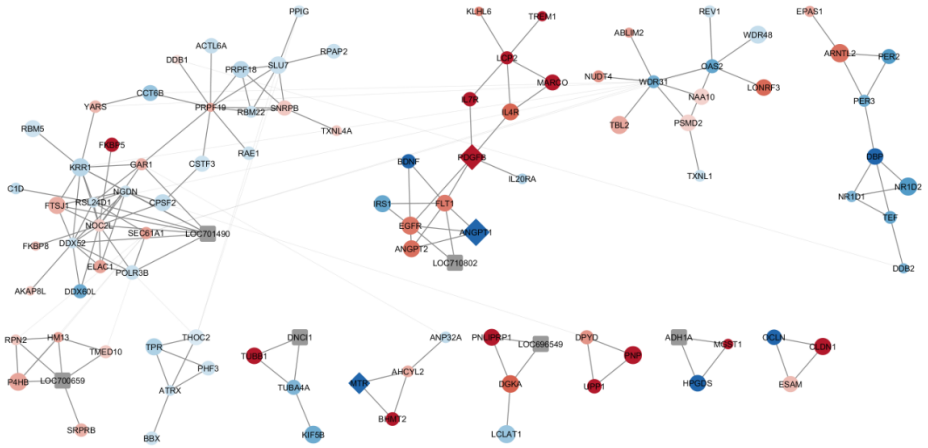


Figure 2.9: MCODE Pathways identified from DEGs illustrated in Figure 2.8.

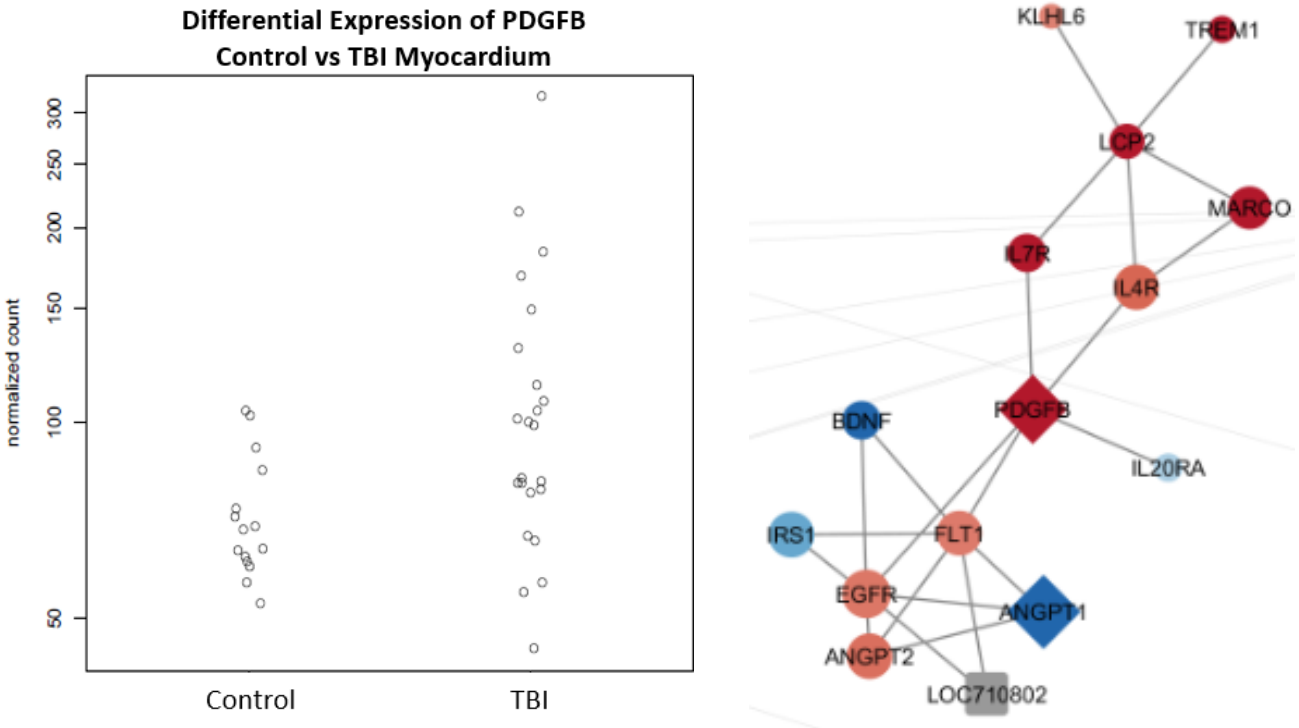


Figure 2.10: Differential expression of PDFGB in Control vs TBI Subjects. (left panel) PDGFB related pathway illustrated with DEGs noted by red (upregulated) or blue (downregulated genes). PDGF gene itself. (right panel)

Preliminary analyses have identified PDGFB and PDGFB related pathways as a potential key mediator of radiation effects in the heart (Figure 2.10). PDGFB overexpression in mouse models leads to moderate cardiac fibrosis (Gallini et al. PMID: 27816607). Interestingly, stem cell antigen expressing (Sca-1) positive cells have been shown to overexpress PDGFB in addition to being able to home to injured heart (Samal et al. PMID: 22749858).

nCounter XT Gene Expression Assay
Purified RNA samples were diluted with RNase free water to a final concentration of 10 ng/μL. Samples were hybridized with a Nanostring NHP Immunology Reporter CodeSet Panel and incubated at 65°C for 16 hours after which temperature ramped down to 4°C until analyses. Hybridized samples were read using an nCounter SPRINT Profiler Instrument.

Statistical Analysis
Statistical analyses were preformed using nCounter Advanced Analysis Software (version 2.0.115) and Statistica (version 13.1).

Preliminary Results:

At p=0.05, 125 transcripts were higher and 23 genes were lower in TBI myocardium relative to control (**Figure 2.11A**). The top ten upregulated transcripts were: S100A8, S100A9, C6, SOCS3, MASP1, CD209, FOS, CD163, ITGAM, and CCL2. Numerous transcripts for macrophage markers were significantly higher in the TBI heart, including CD14, CD68, CD163. Upregulated genes associated with M1 (classically activated, proinflammatory) macrophage phenotype included MAPK3, TLR1 and FKBP5. Upregulated genes associated with the M2 (alternatively activated, profibrotic) phenotype included CD209, C1QB, SMAD7, MASP1, MRC1, CYBB, IL13RA1, CEBPB and CSF1. Amongst all upregulated genes, S100A8 and S100A9 showed the greatest increases in TBI (**Figure 2.11A,C**). The top ten downregulated transcripts were: CD38, KIT, CCL24, THY1, DPP4, DEFb1, CD3EAP, MYL2, MAP2K6, and OAS2. **Figure 2.11B** shows relative differences in markers associated with specific immune cell types between control and TBI. Genes related to macrophages were the showed the greatest increase in TBI myocardium, followed by signatures representative of cytotoxic cells, CD45+ cells (lymphocyte common antigen (LCA) expressed on all leucocytes) and dendritic cells. Differential content of transcripts for the monocyte marker CD14 and key macrophage markers CD68, CD163 are shown in **Figure 2.11C.**

Figure 3.11 Targeted Analysis of Inflammation & Cell Type Gene Expression in Myocardium

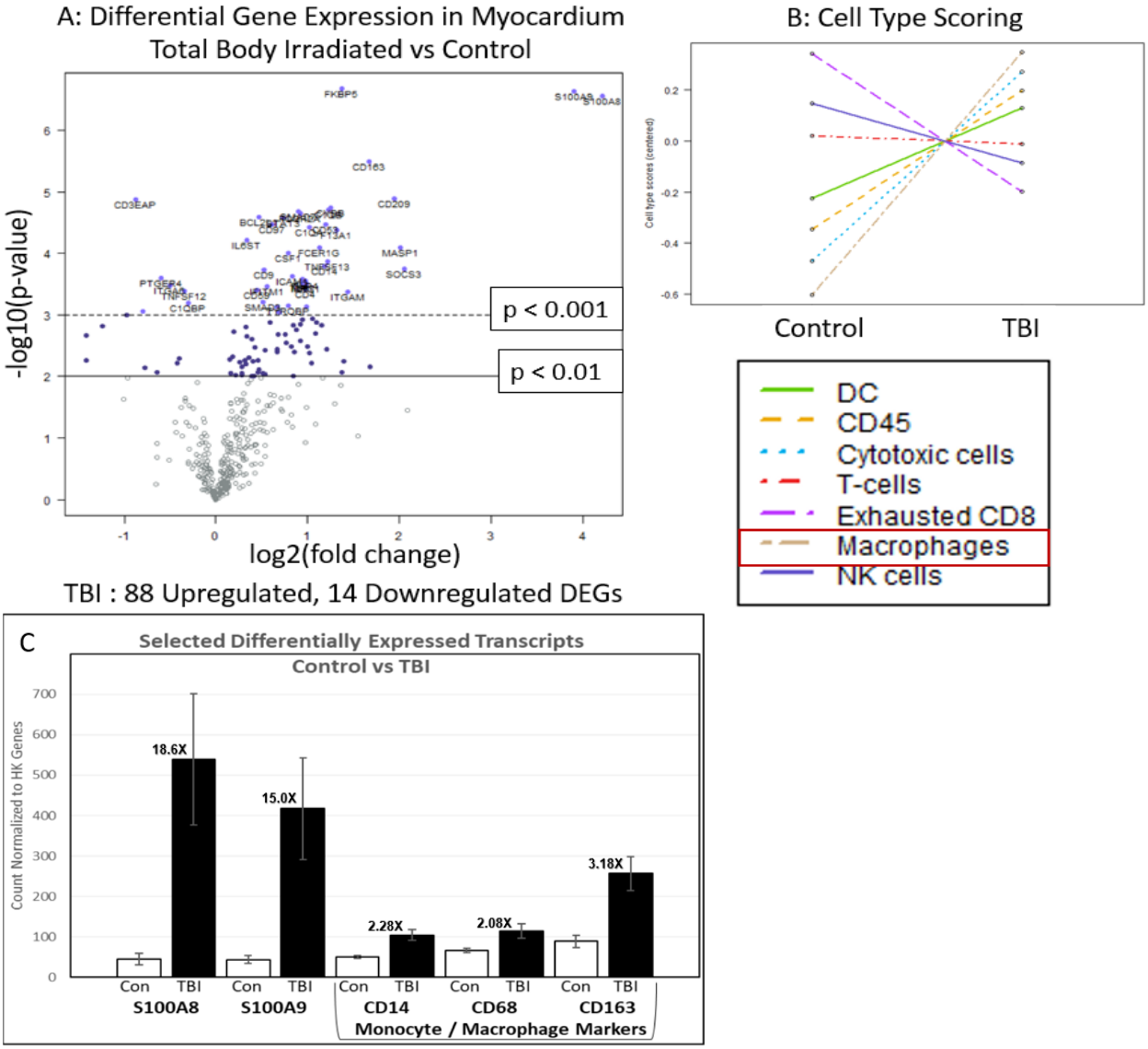
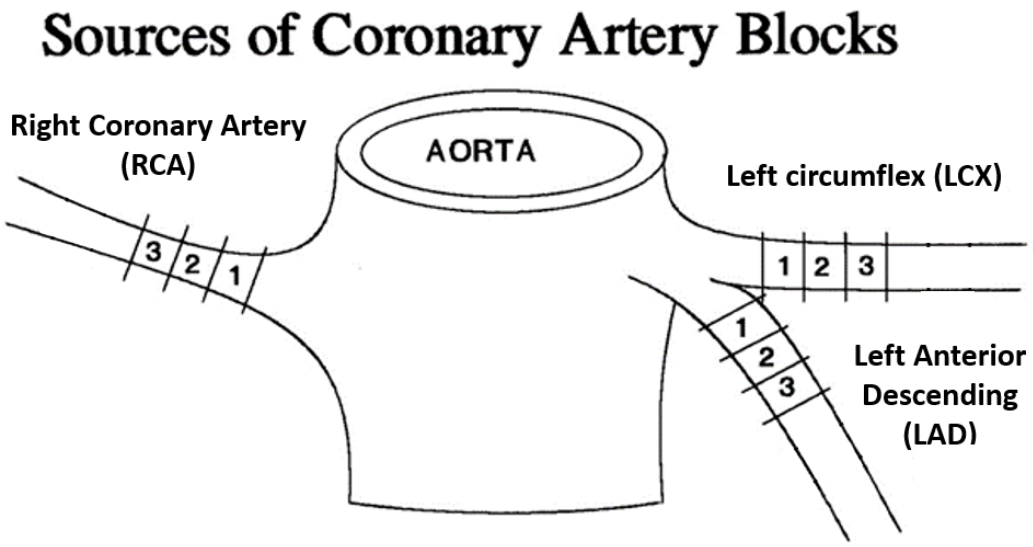


Figure 2.11: Immunology Related Targeted Myocardial G ene Expression Analyses
A: Volcano plot of the statistical significance vs. fold difference between control and TBI myocardial genes. **B:** Plot showing relative differences in cell type specific gene expression signatures between control and TBI groups. **C:** Selected differentially expressed transcripts in control vs TBI.

Other Achievements:

Kris Michalson, DVM, PhD, who successfully defended his PhD dissertation in December 2018, This body of work was largely based upon the study of Radiation Induced Heart Disease and supported by this program. Earlier this year Dr. Michalson accepted a position as Director of Translational Veterinary Medicine at the Gene Therapy Program within the Perelman School of Medicine at the University of Pennsylvania.

Coronary Artery Atherosclerosis in RSC:
Hearts obtained from RSC and control rhesus monkeys which have gone to necropsy were evaluated for atherosclerosis extent using standard methods and approaches developed at Wake Forest. Briefly, three blocks from each of the main epicardial coronary arteries (left circumflex, left anterior descending and right epicardial arteries (shown in **Figure 2.12**) were sectioned and then stained with Verhoeff-van Gieson stain in order to facilitate identification of the internal and external elastic lamella (stained black), cell nuclei (stained black), and collagen (stained red) and the measurement of atherosclerosis (intimal area). Intimal area and other parameters (maximal intimal thickness, maximal medial thickness, internal elastic lamella length) were measured using algorithms and protocols developed in the Register lab for Visiopharm. Images of the unfiltered raw data from each of the coronary blocks are shown in **Figure 2.13**. Statistical analysis of these data are underway, and will require correction for amount of time while consuming the moderately atherogenic diet, age, and other key parameters. Note: controls are animals that have been euthanized due to illness and are not true age and time matched healthy controls.



Adapted from Register, Appt, Clarkson Methods Mol Biol. 2016;1366:517-532.

Figure 2.12: Illustration of the sources of the coronary arteries evaluated in the RSC.

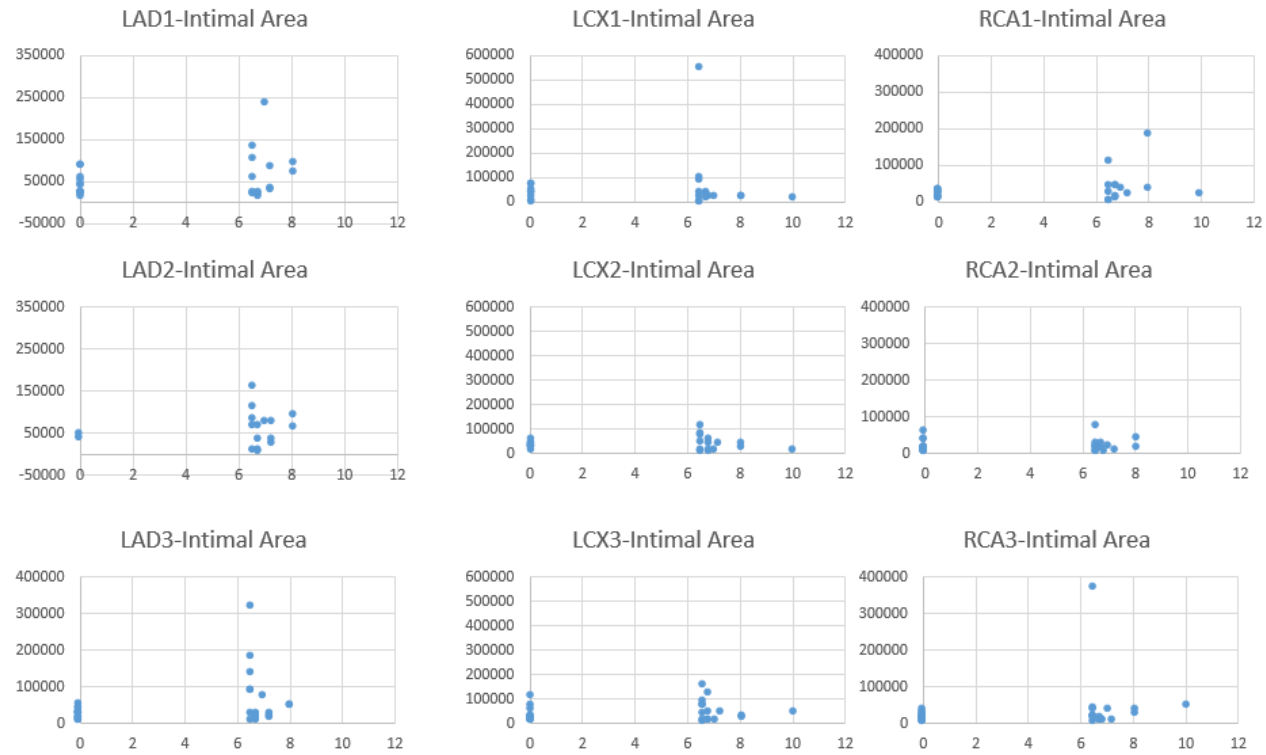


Figure 2.13: Raw data of atherosclerosis (intimal area in um^2) from the 9 blocks of coronary arteries illustrated in Figure 2.12.

Monocyte Polarization in the PRC as a Potential Mediator of Cardiac and Systemic Radiation Induced Fibrosis:

Radiation induced fibrosis (RIF) is a delayed effect of acute ionizing radiation exposure (DEARE) affecting not only the heart, but other tissues including the lungs, liver and skin, and resulting in reduced tissue function and increased morbidity. Monocytes may be classified into classical (CD14++, CD16-), intermediate (CD14++, CD16+), and non-classical ($CD14+^{low}$, CD16++) subtypes in humans and non-human primates (NHPs), and it is likely one or more subpopulations of monocytes may play an integral role in the pathogenesis of RIF. We are exploring the hypothesis that moderate to high levels of total body irradiation (TBI) can alter monocyte polarization and produce phenotypes which could promote multi-organ fibrosis. To date we have evaluated the PRC subjects (16 young adult male rhesus macaques, 10 with TBI with 4 Gy high-energy X-rays (IRR) vs 6 non-irradiated controls (CTL, n=6). Total monocyte counts were obtained from CBCs that were collected before irradiation, then weekly after irradiation for two months and monthly thereafter. Total monocytes were acutely depleted in IRR animals ($p<0.05$), but recovered by day 30 post-irradiation and did not differ from CTL levels thereafter (**Figure 2.14**).

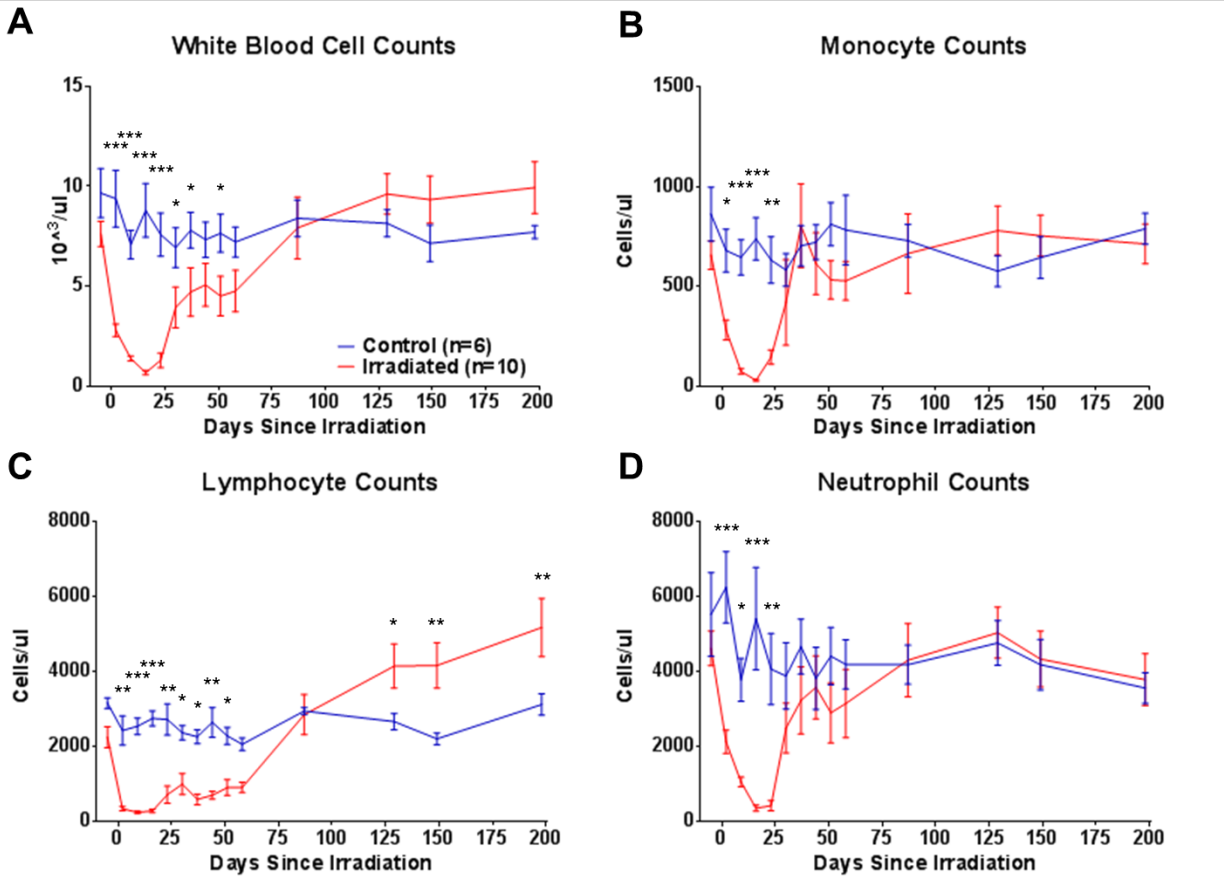


Figure 2.14: **Peripheral Immune Cell Recovery after Total Body Irradiation.** Total white blood cells (A), monocyte (B), lymphocyte (C), and neutrophil counts (D) were all acutely depleted by TBI. Monocytes and neutrophils recovered by 30 days post-irradiation while total white blood cells and lymphocytes remained significantly decreased until days 51 and 58 post-irradiation respectively. After recovery, total white blood cells, monocytes, and neutrophils in IRR animals did not differ from CTL but lymphocytes increased above CTL animals at day 129 post irradiation and remained elevated thereafter. *p<0.05, **p<0.01, ***p<0.001

Monocytes were isolated from peripheral blood mononuclear cells (PBMCs) by a positive selection strategy using anti-CD14+ magnetic beads. The monocyte fraction was then sorted into classical, intermediate, and non-classical monocyte subsets using fluorescence-activated cell sorting (FACS) prior to and 6 months after TBI. At 6 months post irradiation, monocyte polarization shifted towards lower classical (92% ↓ 86%) and higher intermediate (7% ↑ 12%) and non-classical monocyte subsets (0.6% ↑ 2%) (all p<0.05) in IRR animals compared to baseline (**Figure 2.15**). No change in monocyte subsets was observed in CTL animals.

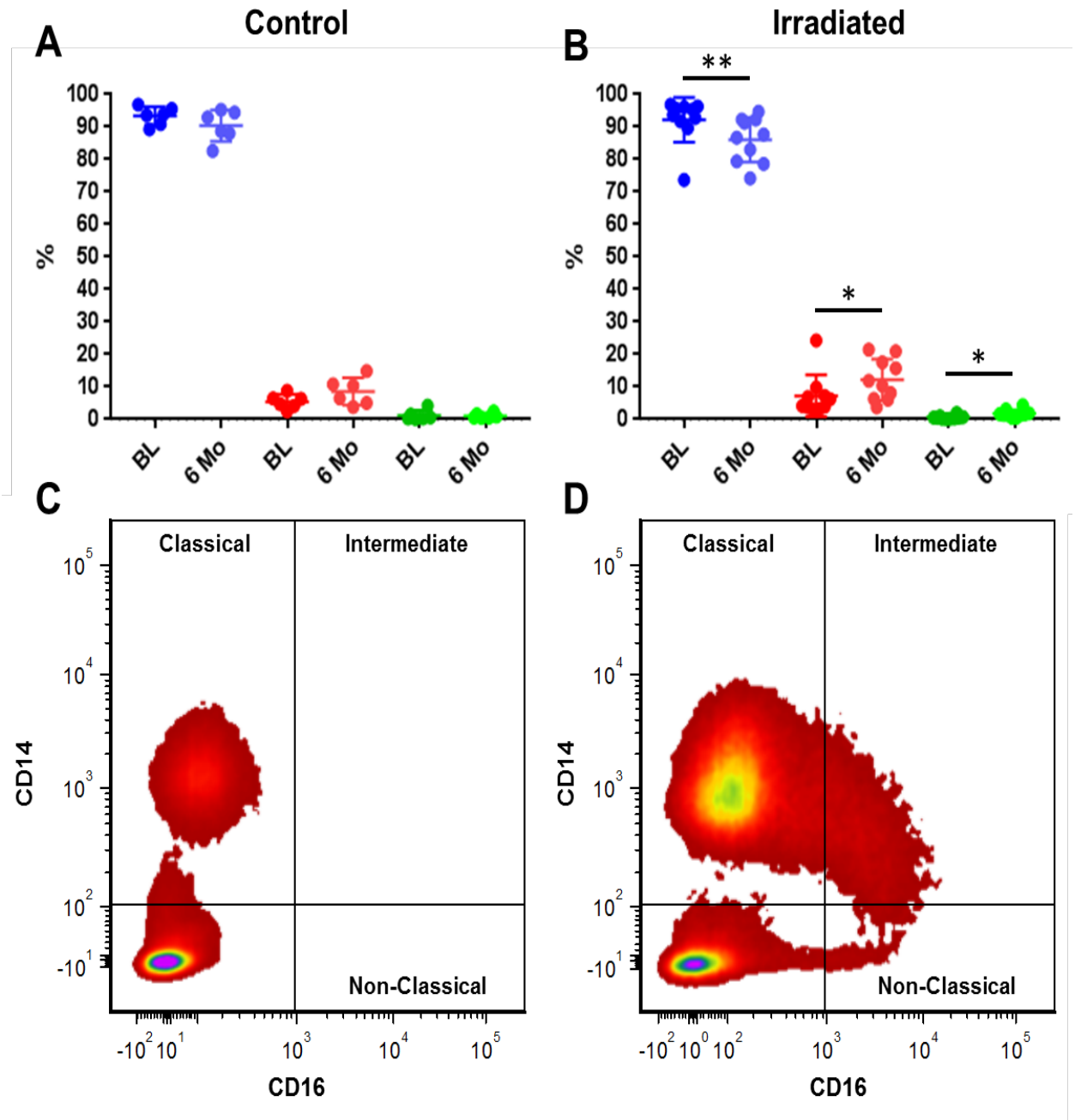


Figure 2.15: **Alterations in Distribution of Monocyte Subtypes after Total Body Irradiation.** Monocyte polarization was unaltered in control animals at 6 months post sham-irradiation (A). In contrast in irradiated animals has significant shifts shifted towards lower classical and higher intermediate and non-classical monocyte subsets compared to baseline (B). Flow cytometry density plots from a representative control (C) and irradiated (D) animal are shown at 6 months post-irradiation. (*p<0.05, **p<0.01)

Monocyte Subtypes Exhibit Distinct Transcriptional Profiles Which Differentially Respond to TBI

Transcriptional profiles in classical and intermediate monocyte subsets were assessed using RNAseq. Classical monocyte gene expression did not change significantly over time or cross-sectionally between IRR or CTL groups. In contrast, significant numbers of differentially

expressed genes (DEGs) were detected in intermediate monocyte comparisons between IRR vs. all animals at baseline (BL) (304 DEGs), and in IRR vs. CTL animals 6 months after irradiation (67 DEGs). Intermediate monocytes also differed between baseline and 6 months in CTL animals (147 DEGs). Pathway analysis was used to identify genes within significant canonical pathways, yielding 60 DEGs that were specific to IRR intermediate monocytes (data not shown). These DEGs and significant canonical pathways were associated with pro-fibrotic and anti-inflammatory signaling pathways that have been noted to induce M2 macrophage polarization upon extravasation. These findings support the hypothesis that TBI may alter monocyte programming and polarization towards a profibrotic phenotype, providing a novel target opportunity for therapies to inhibit or prevent RIF..

This work has been published.
Michalson KT, Macintyre AN, Sempowski GD, Bourland JD, Howard TD, Hawkins GA, Dugan GO, Cline JM, Register TC. Monocyte Polarization is Altered Post-Irradiation in Male Rhesus Macaques: Implications for Delayed Effects of Acute Radiation Exposure. Radiat Res. 2019 Aug;192(2):121-134. doi: 10.1667/RR15310.1).

Grants:

CDMRP Discovery Award 12662528 Register (PI) 05/01/19-04/30/21
Effects of Ionizing Radiation (IR) on Myocardial DNA Methylation Profiles in Relation to Cardiomyopathy in a Nonhuman Primate Model
The goal of this project is to determine 1) the effects of radiation exposure on myocardial DNA methylation profiles, 2) relationships between myocardial methylation profiles, myocardial fibrosis, and cardiac function, and myocardial transcriptional profiles.

Abstracts: An abstract was submitted and accepted for the 2019 Radiation Research Meeting in San DIego, describing the effects of radiation on cardiac structure and function from the RSC. A related abstract was selected for oral presentation at the 2019 AHA meeting in Philadelphia. Abstracts, presentations, and manuscripts are listed in section 6.

Program Project Planning: Studies supported by the current program have led to plans to develop a P01 application to NIAID which was recently presented to NIAID staff and is pending approval for submission.

Project 3: Immune Recovery (Chen/Sempowski - Duke)

1) Major Activities (Year 3)

a) Collaborated with the Primate Core at WFU to design and perform a vaccine response study in the prospective cohort (X-150-3). All 16 animals were dosed with 2018/9 quadrivalent seasonal flu vaccine and 23-valent pneumococcal polysaccharide vaccine approved for human use. Serum was collected before and at multiple timepoints after vaccination. These sera are in the process of being assayed for antibodies against the relevant flu strains and pneumococcus serotypes.
b) Received and processed blood from all NHP in the X-10-12 long-term survivor cohort. Performed immunophenotyping and froze viable PBMC and plasma for future batch molecular analysis and multiplex cytokine profiling, respectively.
c) Collaborated with the Primate Core and Wake Forest Data Services to develop a standardized data import table for transmission of data from Duke to a central database at Wake Forest University. Re-gated all NHP flow cytometry data collected from 2016-2019 to ensure gating consistency (450 samples). Transmitted data to WFU for database import and provided project biostatistician with list of biologically important questions to test using the imported flow cytometry data in conjunction with existing demographic and Complete Blood Count and white blood cell differential data already present in the database.
d) Collaborated with Project 2 (Register) to publish paper on monocyte phenotypes in X-10-12.
e) TCRalpha and beta sequencing library preparation was optimized and paired baseline and 9-month post-irradiation PBMC from the X-15-03 prospective cohort were sequenced.
f) We studied phenotypic immune recovery in different lymphoid organs after irradiation. Functional immune recovery was also studied.
g) The experiment using a second model to study the contribution of thymopoiesis and peripheral expansion to overall T cell reconstitution was completed.
h) We studied T cell repertoire recovery in mice using T cell receptor deep sequencing.

2) Specific Objectives (Year 4)

SA 1: Define the roles of thymopoiesis and peripheral expansion in overall T cell reconstitution after radiation-induced injury based on radiation dose.

Major Task 1: NHP Studies

Phenotypic analyses in prospective and long-term cohorts

Major Task 2: Murine Studies

Determine the roles of thymopoiesis and peripheral expansion in overall T cell recovery in two mouse radiation injury models

SA 2: Determine if therapeutic agents identified in our previous studies are able to promote or accelerate overall T cell immunity after radiation injury.

Major Task 3: HGH Mouse Studies

Determine the effect of HGH on phenotypic T cell reconstitution

Major Task 4: IGF-1 Mouse Studies

Determine the effect of IGF-1 on phenotypic T cell reconstitution

3) Results/Key Outcomes (Year 4)

SA1 Major Task 1: NHP Studies (Sempowski, Duke)

Long-term cohort (X-10-12):
At intervals throughout year 4, PBMC and plasma from 114 animals in the long-term survivor cohort (X-10-12) were isolated and stored. Fresh PBMC from all 114 animals were immunophenotyped via flow cytometry using previously described panels for B cells, T cells, NK, NK-T, and dendritic cells. These data represent the third annual round of immunophenotyping for this cohort. We have started the fourth annual round of immunophenotyping, and this round is expected to be complete by January 2020.

Cell isolation and sjTREC quantification from frozen PBMCs collected during Y3 was completed (Figure 3.1). The trends in sjTREC number observed in the samples collected during Y3 are similar to those previously reported from the same cohort using samples collected during Y2. i.e. both CD4 and CD8 sjTRECs trend highest for animals who received a mid-range (6-8 Gy) dose, and decrease as the age at analysis increases.

Cell isolation and sjTREC quantification from frozen PBMC collected during Years 4 and 5 is planned for Y5Q2 and Y5Q3 respectively.

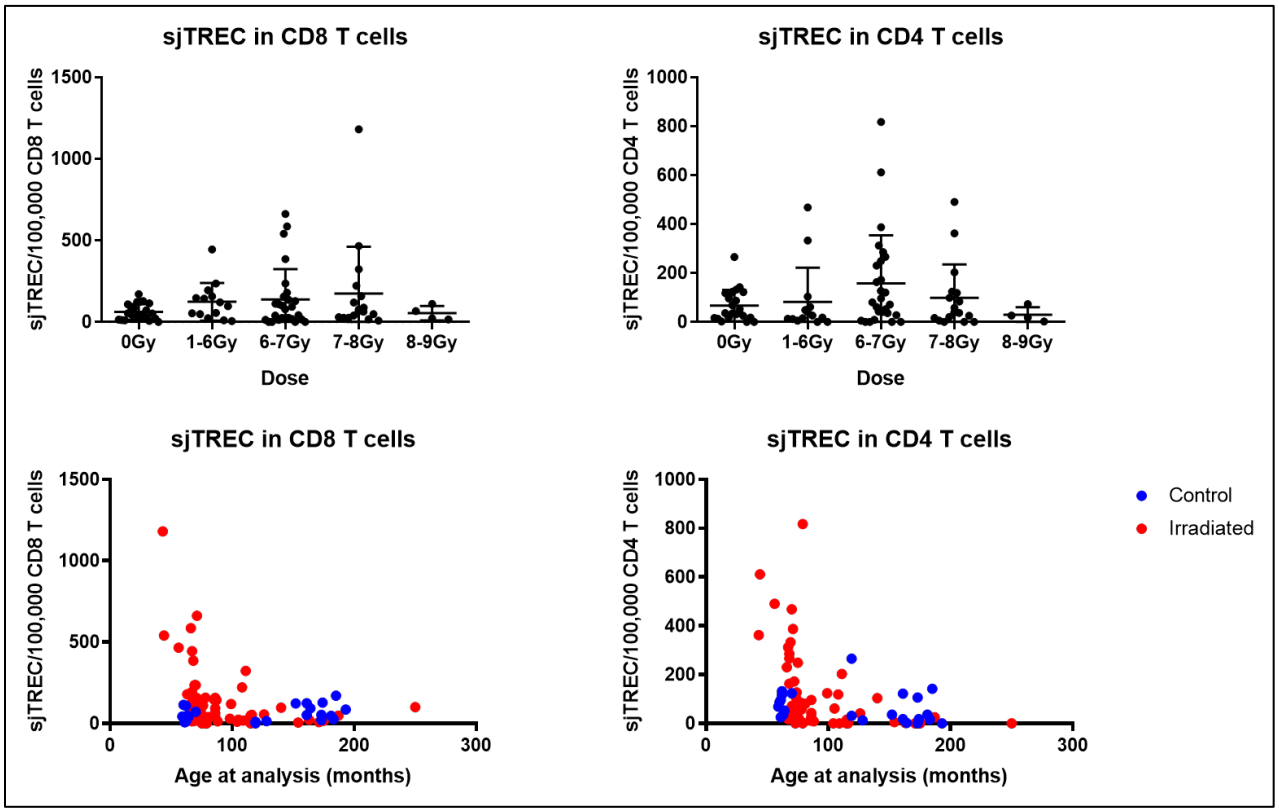


Figure 3.1. sjTREC quantification in CD4 and CD8 T cells collected from long-term cohort animals in Year 3. Data are expressed relative to dose (upper) and age at analysis (lower).

Statistical analysis of the immunological data obtained from this cohort requires consideration of multiple demographic factors (e.g. age, sex, dose, age at irradiation, morbidities) that are stored in a database at Wake Forest University. To streamline the analysis and prevent duplication of data sources, we collaborated with Wake Forest Data Services and the Primate Core to create new forms in the existing database for storage of all flow cytometry, sjTREC, ELISA and

Luminex data collected from the survivor and prospective cohorts. We then re-analyzed the flow data from all 450 samples collected from Y2-Y4 to ensure gating consistency. These re-analyzed data were submitted to the Data Services team for database import. In parallel, we worked with the Primate Core biostatistician (Janet Tooze), to develop a list of biologically important questions to test against the complete dataset. These analyses are ongoing. During Y5, all data collected will be submitted to WFU using the gating and data transfer approaches developed during Y4.

Prospective Cohort (X-15-03)
Molecular analysis of samples from Prospective Cohort
We initially proposed to work with Adaptive Biotechnologies to develop a T cell receptor (TCR) deep sequencing assay. As this assay was not available by the end of Y3, we instead worked with the Duke Human Vaccine Institute Sequencing Core to develop an in-house pipeline for NHP TCRalpha and beta sequencing using primer libraries developed by Takara Bioscience. In Y4 we demonstrated that we could use this pipeline to successfully obtain T cell Receptor (TCR) alpha and beta variable region sequences using RNA extracted from cryopreserved Rhesus macaques PBMC (Table 3.1) and Figure 3.2.

Table 3.1. Summary of TCR sequencing reads from two Rhesus macaques.

	NHP TCR-alpha Chain Sequencing			NHP TCR-beta Chain Sequencing		
Animal	Total TCR-α chains sequenced	Unique TCR-α chain clones	Frequency of 3 most common TCR-α clones	Total TCR-β chains sequenced	Unique TCR-β chain sequences identified	Frequency of 3 most common TCR-β clones
A	5,953,218	6,043	1.5%, 1.3%, 1.0%	3,409,458	5,287	12.1%, 2.6%, 2.0%
B	4,915202	9,262	2.4%, 1.8%, 1.3%	1,601,043	11,271	6.2%, 5.6%, 5.3%

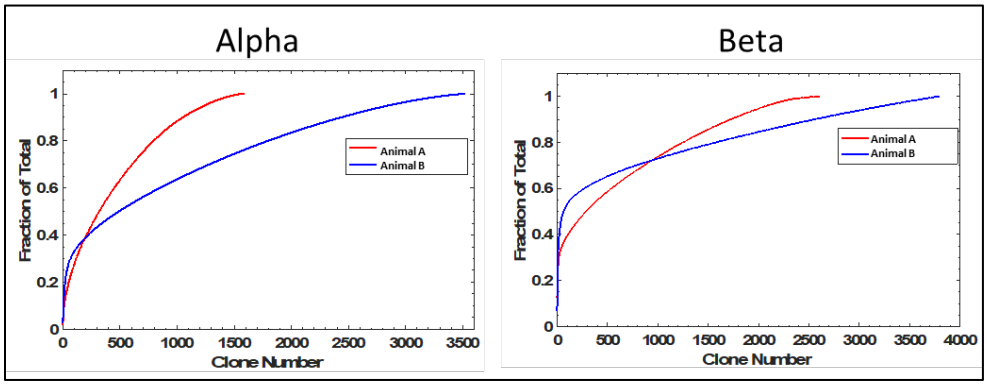


Figure 3.2. Clone distribution of TCR alpha and beta chains in sequence libraries generated using PBMC from two Rhesus macaques.

After confirming we could obtain NHP TCR alpha and beta sequences, we sequenced the TCRalpha and beta chains in six duplicate cryopreserved NHP PBMC samples to determine the appropriate sequence variability constraints to use for analysis. We then sequenced the TCRalpha and beta chains in cryopreserved PBMC from paired baseline and 9-month post irradiation animals in the X-15-03 cohort. Leftover RNA was stored for future use (rtPCR / RNA-seq). Some samples did not yield sufficient RNA for effective sequencing; however, all samples with sufficient RNA yielded sequence data that passed quality control. Example sequence

distributions and preliminary numbers of unique TCRalpha/beta clones identified as of this report are show in Figures 3.3 and 3.4. The sequence data are currently being analyzed for radiation-induced changes in clonality, clonal frequency, etc. Results are expected Y5Q1.

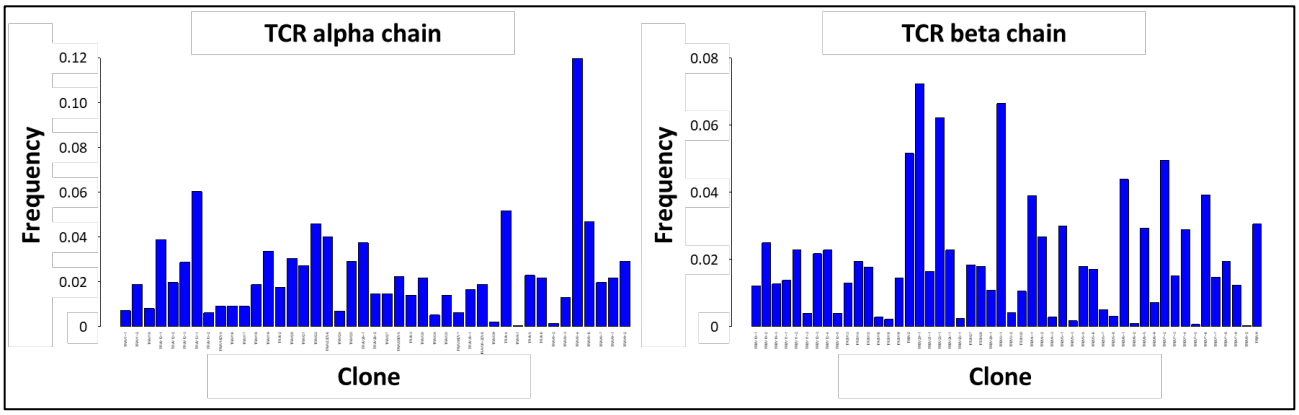


Figure 3.3. Representative alpha and beta clone distribution plots for a single prospective cohort subject prior to irradiation.

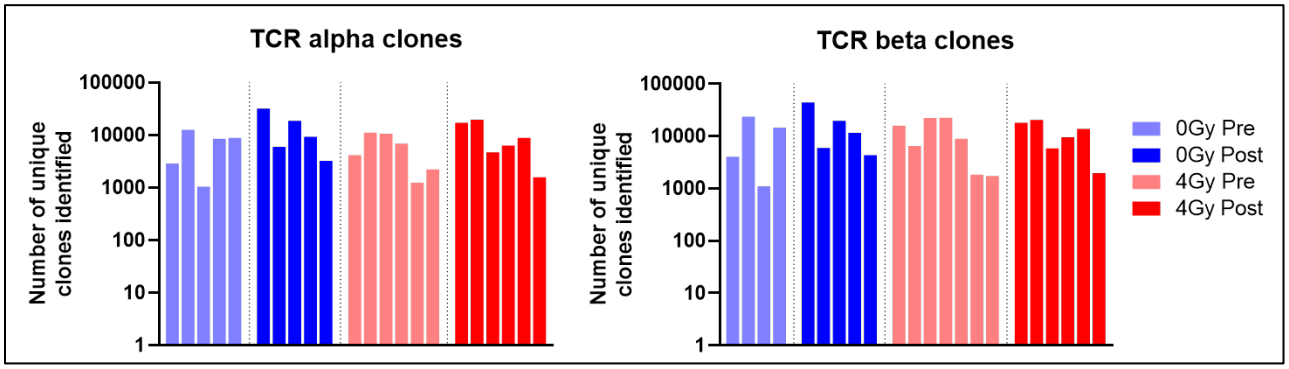


Figure 3.4. Preliminary numbers of unique TCR alpha (left) and TCR beta (right) clones identified in prospective cohort PBMC collected from the 0 Gy mock control (blue) and 4 Gy irradiated (red) NHP before (faint) and 9 months after (bold) exposure. Each bar represents a sample from a different animal in a given group.

Immunophenotyping of Prospective Cohort

Flow cytometry data collected in Y1-Y3 was re-gated to ensure consistency of approach, as described above. The data were then assembled into draft figures in preparation for a manuscript submission (target submission date: January 2020). The data support findings reported in Y2 from analysis of the X-10-12 long-term survivor cohort, namely that the gross adaptive immune cell populations return to close to normal distributions several months after irradiation, but that the repopulation process shifts the T cell naïve/central and effector memory populations. In particular, there is a delayed recover of naïve CD4 T cells whether these defined as either CD45RA+ or $CD28^{mid}Cd95^{low}$ (Figures 3.5 and 3.6).

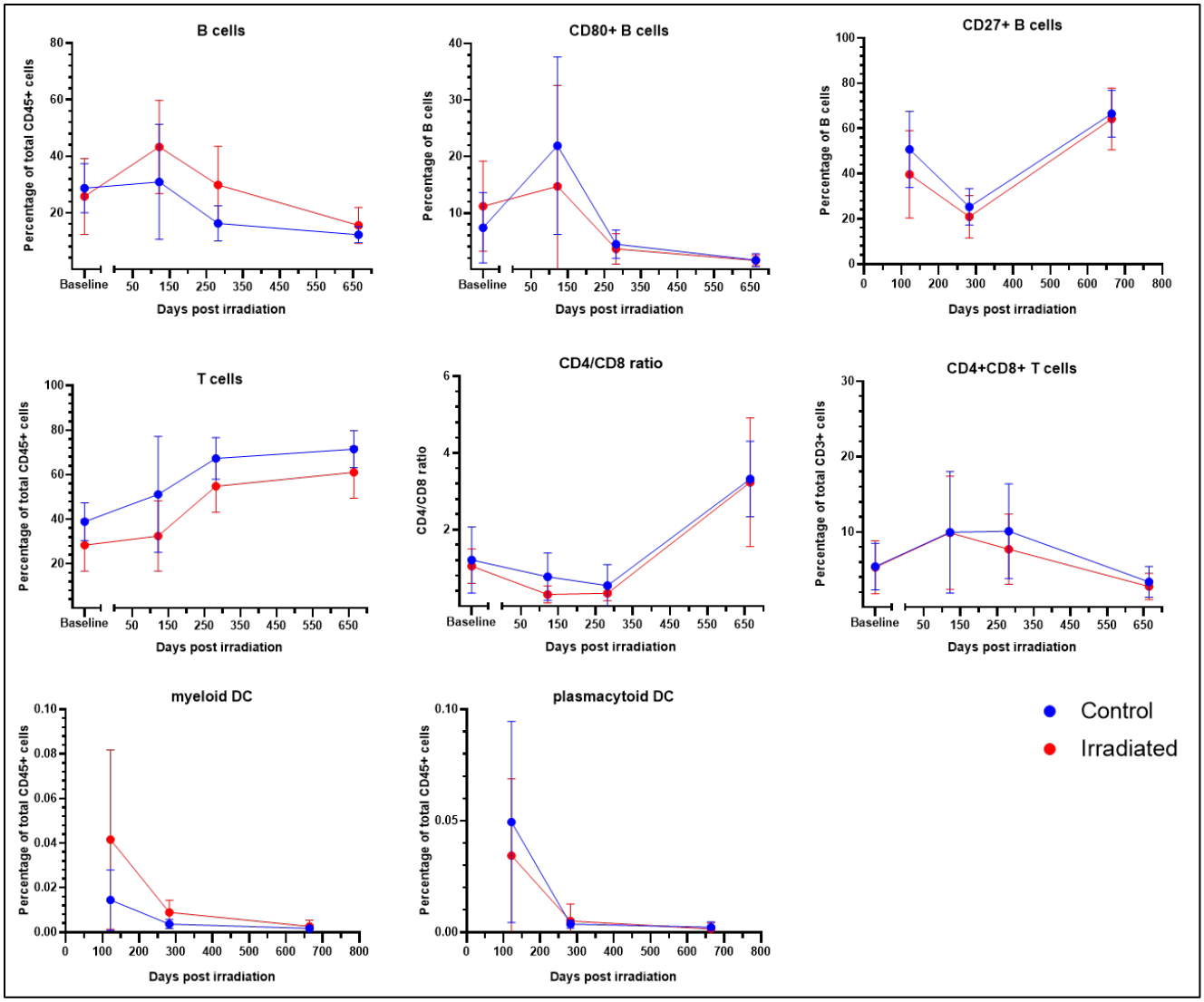


Figure 3.5. Flow cytometry analysis of B cells, T cells, and dendritic cells in mock and 4Gy irradiated animals from the prospective study at up to 21 months post-irradiation. Data show mean ± standard deviation. B cells are defined as $CD45^+$ $CD20^+$, T cells as $CD45^+CD3^+$, and myeloid and plasmacytoid dendritic cells (DC) as described in Autissier *et al.* (2010) *J Immunol Methods*, 360:119.

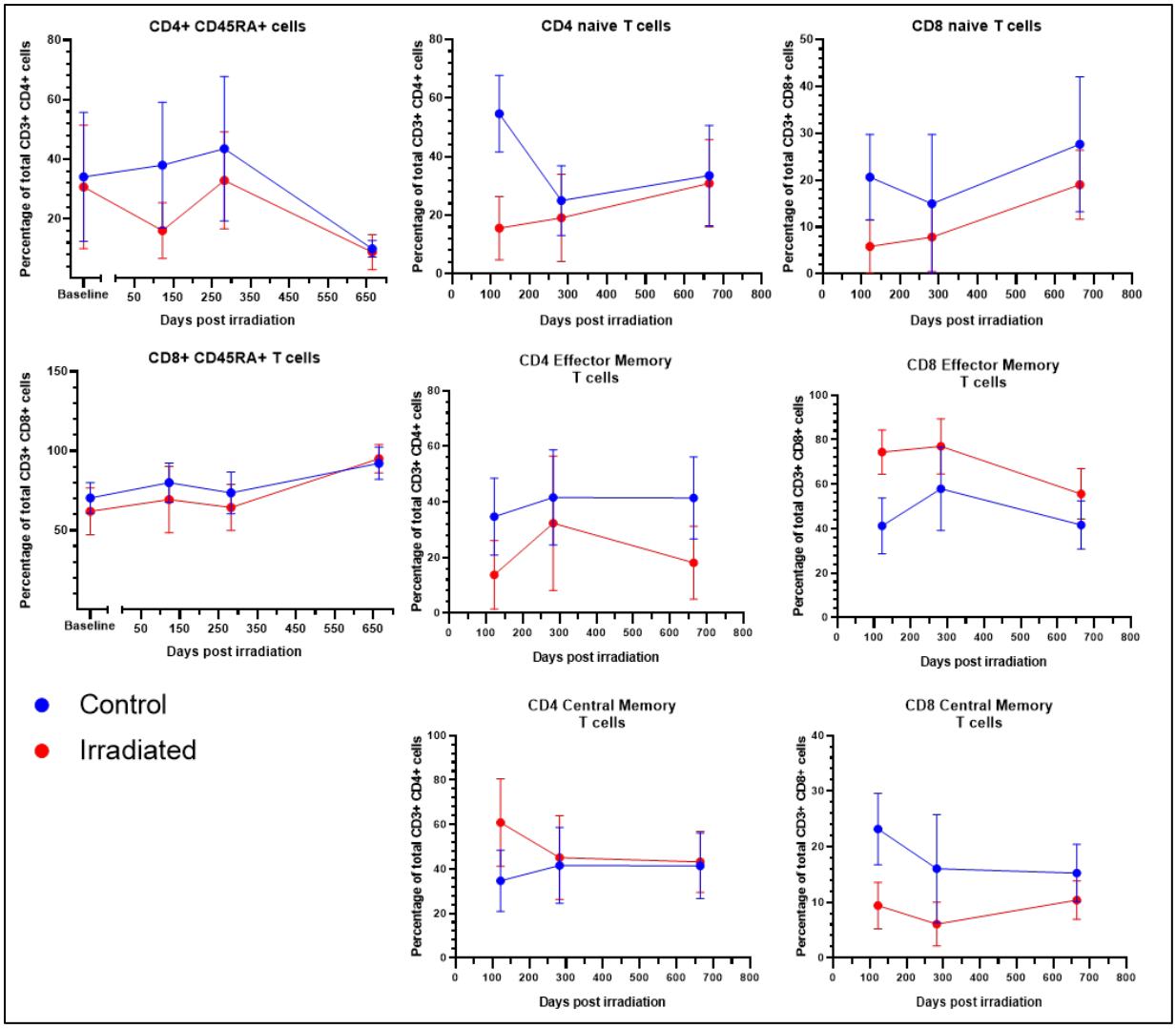


Figure 3.6. Flow cytometry analysis of naïve and memory T cells in mock and 4Gy irradiated animals from the prospective study at up to 21 months post-irradiation. T cells are defined as $CD45^{+}CD3^{+}$. Subpopulations are defined as: naïve $CD28^{mid}CD95^{low}$, central memory $CD28^{high}$, $CD95^{high}$, effector memory $CD28^{low/-}$,$CD95^{mid/high}$. Data show mean ± standard deviation.

Immune Response Evaluation using Prospective Cohort

We worked with the Wake Forest Primate Core and the other project teams to design and run a vaccination study using the prospective cohort. The 16 animals in the cohort (6 mock irradiated, 10 irradiated) were vaccinated with a quadrivalent 2018/19 seasonal flu vaccine approved for human use (FluLaval tetra containing hemagglutinin (HA) proteins from two A influenza strains: A/Michigan/45/2015(H1N1) A/Singapore/INFIMH-16-0019/2016(H3N2), and two B strains: B/Phuket/3073/2013 B/Colorado/06/2017). The vaccine was administered using the recommended pediatric dose of two 0.5 mL IM doses 4 weeks apart (primary and booster). With Science Officer approval, the animals were also vaccinated IM with a 23-valent pneumococcal polysaccharide vaccine approved for human use (Pneumovax-23).

Serum samples were collected at various timepoints along the study for humoral (antibody) analysis. Plasma and PBMC were collected at baseline and 112 days after the initial FluLaval

injection for future studies (Figure 3.7). Pneumovax-23 was selected as a second vaccine for this study as collaborative pilot studies by members of the Primate Core and Project 3 suggested that irradiated primates receiving this vaccine exhibited poor antibody responses to select serotypes (Hale *et al. PLoSOne* (2019):14(2):e0210663). The pilot study only evaluated responses to 11 of the 23 serotypes in the vaccine and the time between irradiation and vaccination varied between animals; the current study will build on this work to confirm if TBI does indeed lead to epitope-specific holes in adaptive immunity.

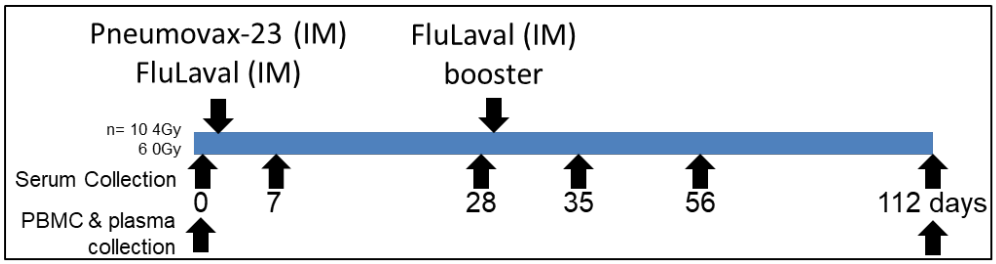


Figure 3.7. Timeline of Pneumovax-23 and FluLaval vaccination study.

Serum samples from this study are currently being evaluated for antibody responses to each influenza HA via microneutralization assay and all 23 pneumococcal serotypes via multiplex bead array. Data are expected Y5Q1.

Additional Collaborative Effort
In collaboration with Project 1 (Kavanagh), the Project 3 group (Sempowski *et al.*) ran a 32-plex bead array assay to quantify 32 immunological biomarkers in mouse plasma collected from 41 mice irradiated and treated with potential mitigators IPW-5371 (an anti-fibrotic TGFβ1R inhibitor) and/or Tadalafil (an angiogenic PDE5 inhibitor). D ata from this experiment are discussed in the report from Project 1.

SA1 Major Task 2: Murine Studies (Chen, Duke)

Splenic T cells remained low at high dose TBI while T cell subset composition underwent dose-specific changes
To determine whether T cells at other peripheral sites exhibit recovery trend similar to that in the peripheral blood, we first investigated T cells in the spleen. To address this question, mice were either nonirradiated (0 Gy), sublethally irradiated at low dose (2 Gy), intermediate dose (5 Gy), high dose (7 Gy), or irradiated at 7 Gy and transplanted with 5 x 10^5/mouse Lin^- bone marrow from donors. Splenocytes were collected and assessed by flow cytometry at 14 weeks. While total splenic CD4 and CD8 T cells increased moderately at low and intermediated doses (2 Gy and 5 Gy), the numbers were significantly lower at 7 Gy compared to nonirradiated control (Figure 3.8A and B). As expected, the BMT control group underwent significant T cell recovery, with T cell numbers higher (CD4 T cells) or comparable (CD8 T cells) to nonirradiated control. We further assessed the relative abundance of distinct T cell subsets using well-established markers, including $CD44^-CD62L^+$ T_N (naïve T cells), $CD44^+CD62L^+$ T_{CM} (central memory T cells), $CD44^+CD62L^-$ T_{EM} (effector memory T cells). The composition of T cell subsets was altered by TBI, and varied with the treatment dose (Figure 3.8C and D). As expected, the restoration of T cell number in the BMT group was accompanied by an increase in the naïve T cell compartment, likely due to an increase in thymic output following reconstitution by donor cells. Unexpectedly, TBI groups at all doses showed increased percentage of naïve T cells in both the CD4 and CD8 T cell compartments. In particular, low dose group demonstrated a much more prominent increase in the naïve T cell composition. Therefore, the increase in total T cells

at low and intermediate doses was primarily contributed by increased naïve T cell numbers (Figures 3.8C and D, Fig. 3.9A and D). In contrast, the lower T cell recovery at high dose TBI was primarily reflected by a prominent defect in effector memory T cell recovery (Figure 3.9C and F). In addition, the percentage of CD4 T_{CM} remained relatively uniform across all groups, while CD8 T_{CM} was increased in all TBI groups. These data reflect that following high dose TBI, splenic T cells were unable to recover to the level comparable to nonirradiated controls as shown in peripheral blood T cells, indicating the requirements for long-term T cell reconstitution in the spleen may differ from those for peripheral blood. Furthermore, varying TBI doses have distinct effects on the composition of T cell subsets. This may reflect the effect of TBI doses on T cell homeostatic proliferation specifically in the spleen.

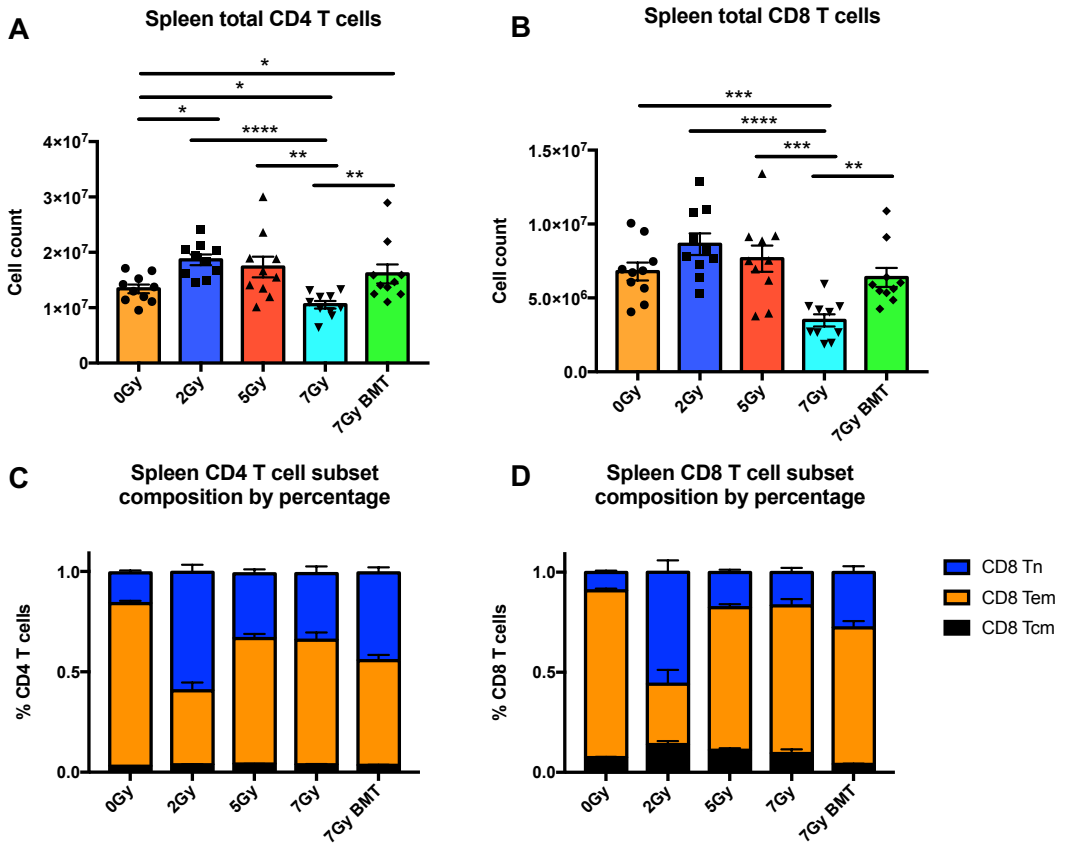


Figure 3.8. T cell subset reconstitution by frequency in the spleen. C57BL/6 mice were sublethally irradiated at indicated doses. Splenocytes were isolated at week 14 and analyzed for $CD4^+$ (A) and $CD8^+$ (B) T cell numbers and corresponding T cell subset composition (C) and (D) by flow cytometry.

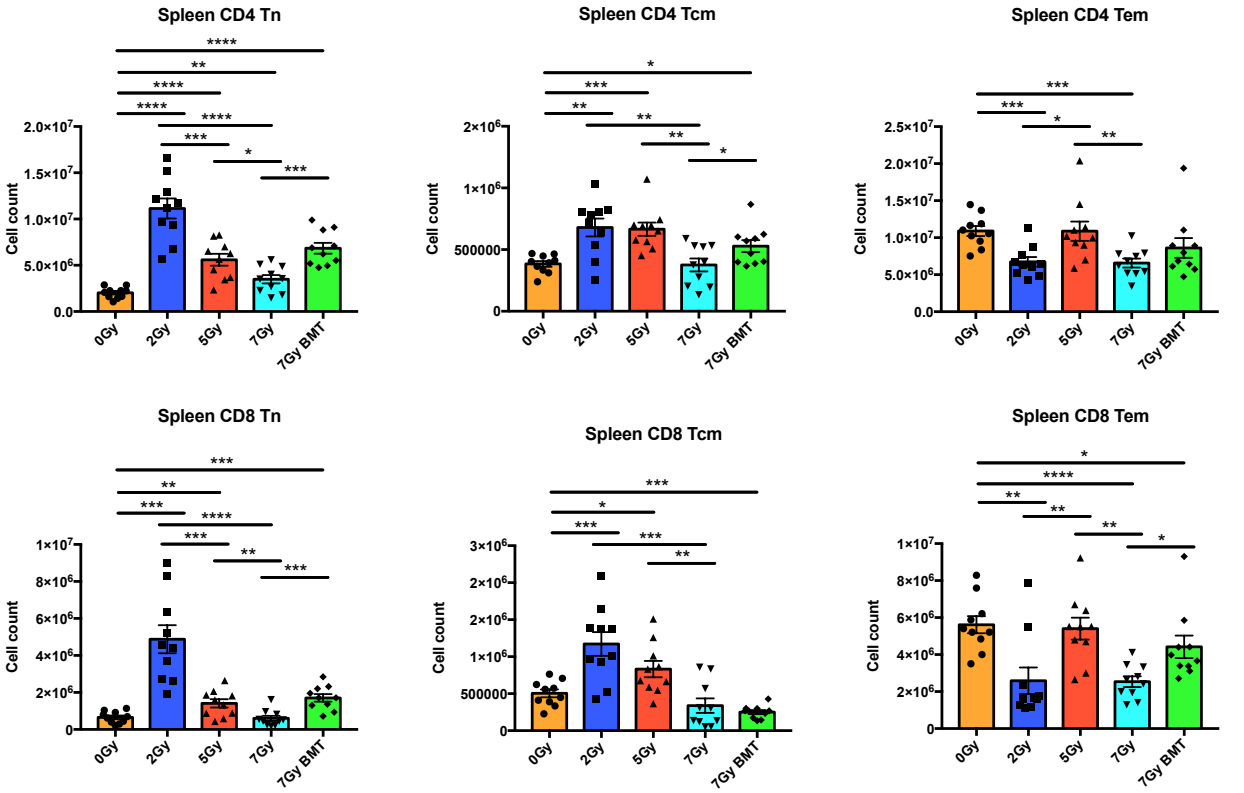


Figure 3.9. T cell subset reconstitution by cell number in the spleen. C57BL/6 mice were sublethally irradiated at indicated doses. Splenocytes were isolated at week 14 and analyzed for $CD4^+$ (A-C) and $CD8^+$ (D-F) for each subset population.

Bone marrow and lymph node T cell recovery was differentially affected by TBI
The differences in T cell recovery in the spleen and peripheral blood raised the question whether the T cell reconstitution profile following TBI is tissue-specific. We further assessed T cell numbers at other lymphoid sites, including the bone marrow and lymph nodes.

Although commonly known for its ability to house HSCs, bone marrow also serves as an important reservoir for mature T cells. Memory T cells, in particular, were shown to preferentially colonize in the bone marrow, serving as a source for protection against blood-borne pathogens. We first investigated the effect of TBI on bone marrow CD4 T cells. In contrast to peripheral blood and the spleen, TBI did not appear to impact total CD4 T cells numbers with high dose treatment (Figure 3.10A). However, the percentage (Figure 3.10C) and number (Figure 3.11C) of T_{EM} cells were progressively decreased at 2 Gy, 5 Gy, and 7 Gy, suggesting a defect in CD4 T_{EM} recovery. In contrast, CD4 T_N and T_{CM} numbers were not drastically impacted by TBI treatment, except a slight increase observed at 7 Gy for CD4 T_N cells (Figure 3.11A). In contrast, CD8 T_N cells were significantly decreased at 7 Gy compared to nonirradiated (Figure 3.11D), while also reflected by the percentage composition (Figure 3.10C). As expected, both CD4 and CD8 T_N cells were significantly increased in the BMT group compared other groups, likely due to increased thymic output from donor cells. In terms of memory T cells, the numbers of CD8 T_{EM} remained relatively comparable across all TBI groups, while CD8 T_{CM} increased at higher doses of TBI (Figure 3.11E), likely contributing to the increase in total CD8 T cells at high dose TBI (Figure 3.10B and D).

For assessment of T cell recovery in the lymph nodes, we collected and analyzed pooled lymph nodes consisting of superficial cervical, axillary, brachial, and inguinal. Similar to previous analysis, subset frequencies were calculated. However, cell counts were not included in the analysis due to decreased size and ability to identify corresponding lymph nodes in groups with TBI treatments. Similar to bone marrow CD4 T cells, the percentage of lymph node T_N cells remained relatively constant across all TBI groups, with a slight increase with high dose treatment. Consequently, the percentage of T_{EM} at high dose was lower than the rest of the TBI groups (Figure 3.10E). In contrast, T_{CM} remained negligible across all groups. Furthermore, the percentage of CD8 T_N and T_{EM} remained relatively stable across all TBI groups. However, similar to bone marrow T_{CM}, lymph node T_{CM} percentage increased in a dose-dependent trend (Figure 3.10F).

In summary, we showed that T cell subsets were differentially affected in the bone marrow and lymph nodes compared to other peripheral sites. Although CD4 T_N cell number remained relatively stable, CD8 T_N cell number was significantly decreased at high dose TBI. In the memory T cell compartment, CD4 T_{EM} cell count decreased with increasing TBI dose while CD8 T_{EM} cell count remained relatively stable. The T cell recovery profile in pooled lymph nodes also differed from those observed at other sites. While the frequency of CD4 Tem exhibited a moderate decrease at high dose TBI, other subsets, including CD8 T_N and T_{EM}, remained relatively stable in frequency.

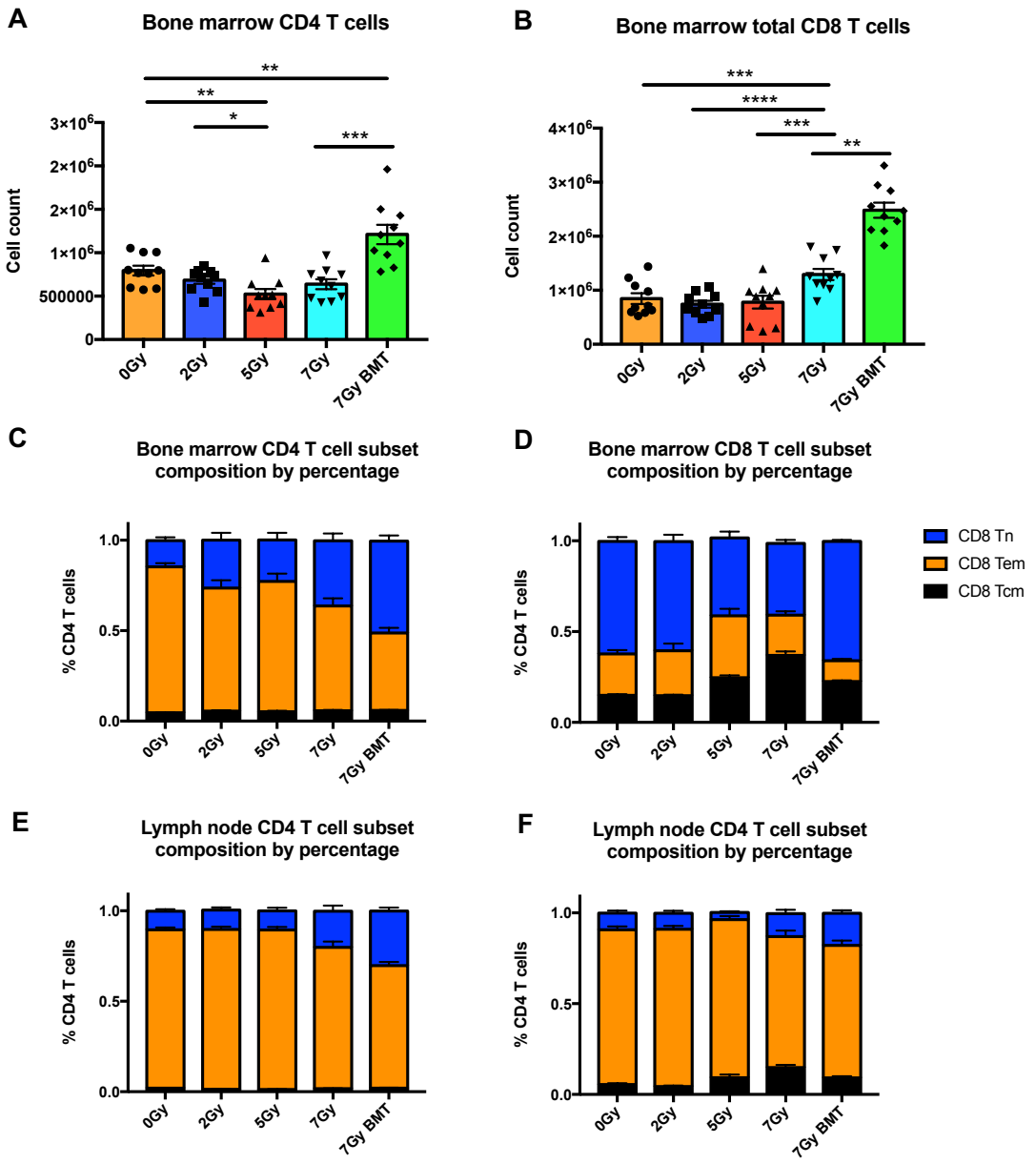


Figure 3.10. Long-term T cell reconstitution was differentially affected in bone marrow and lymph nodes. C57BL/6 mice were nonirradiated (0 Gy), sublethally irradiated or irradiated at 7 Gy and transplanted with 5 x 10^5/mouse Lin^- bone marrow from C57BL/6 mice. At week 14, bone marrow cells were collected for $CD4^+$ (A) and $CD8^+$ (B) and T cell subset frequencies (C) and (D). Lymph node cells were isolated for T cell subset frequencies (E) and (F).

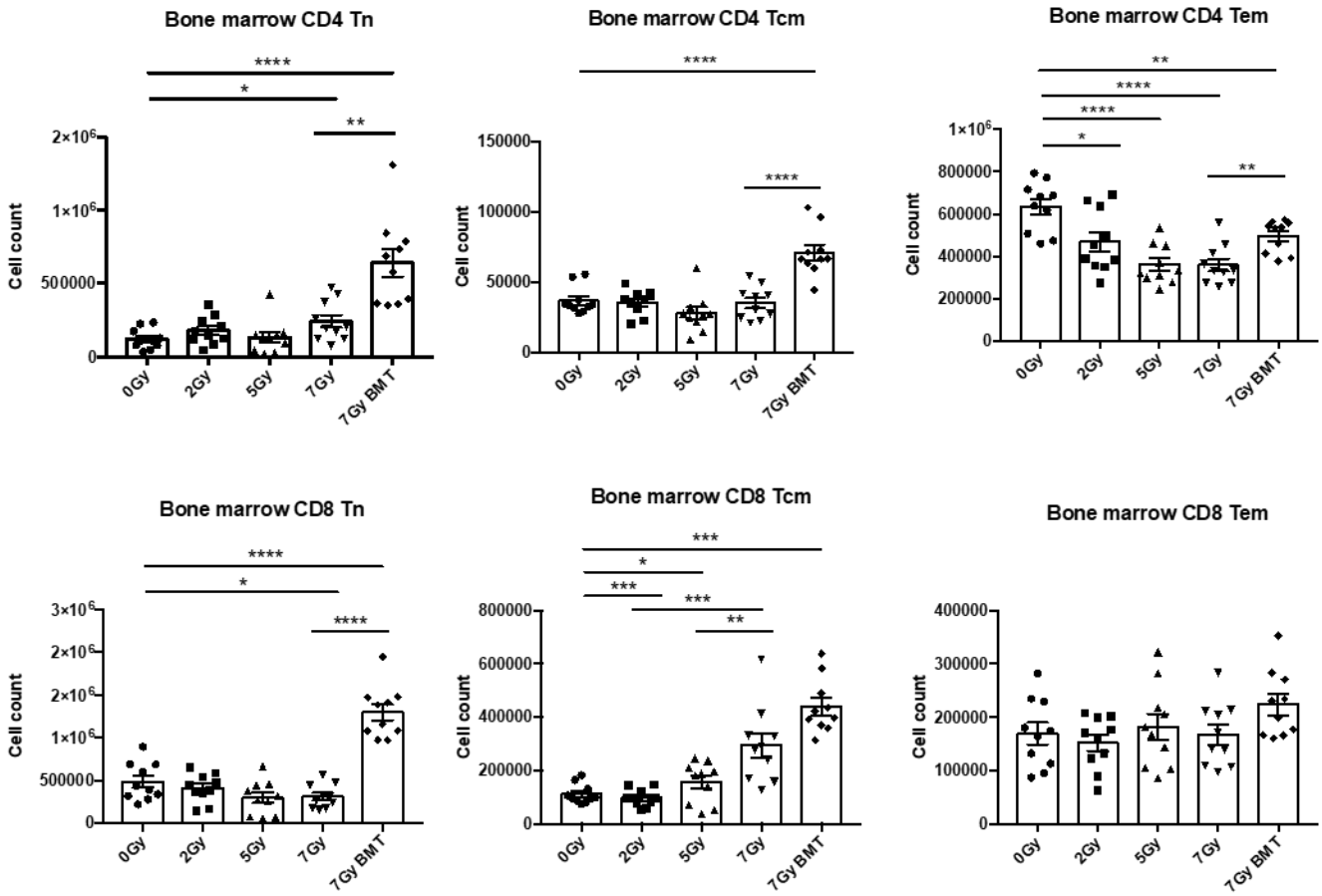


Figure 3.11. T cell subset reconstitution by cell number in the bone marrow. C57BL/6 mice were sublethally irradiated at indicated doses. Bone marrow cells were isolated at week 14 and analyzed for $CD4^+$ (A-C) and $CD8^+$ (D-F) for each subset population.

T cells retained capacity to respond to TCR stimulation ex vivo

Functionally, T cells recovered after TBI may be able to undergo effective clonal expansion and mediate protective response against pathogens, which can be reflected by their ability to rapidly proliferate in response to TCR stimulation. To assess whether T cells maintain the functionality to respond to TCR receptor stimulation following long-term TBI, we utilized ex vivo assays to measure the proliferative response. Splenocytes were isolated at 14 weeks following TBI treatment, followed by ex vivo activation using anti-CD3 and anti-CD28 antibodies for 48h, pulsed with BrdU for cell cycle analysis (Figure 3.12A). Following stimulation, CD4 T cells from TBI groups uniformly underwent rapid proliferation at rates comparable to that of the nonirradiated group (S phase: 0 Gy, 91.88 ± 0.61%; 2 Gy, 92.60 ± 0.96%; 5 Gy, 93.60 ± 0.63%; 7Gy, 93.60 ± 0.69%) (Fig. 6B). Similarly, CD8 T cells at varying TBI doses retained the capacity to respond to TCR stimulation (S phase: 0 Gy, 93.17 ± 0.71 %; 2 Gy, 93.89 ± 0.69 %; 5 Gy, 93.23 ± 0.90%; 7Gy, 91.93 ± 1.61%) (Figure 3.12C). Overall, no proliferative defect in response to TCR stimulation ex vivo was detected.

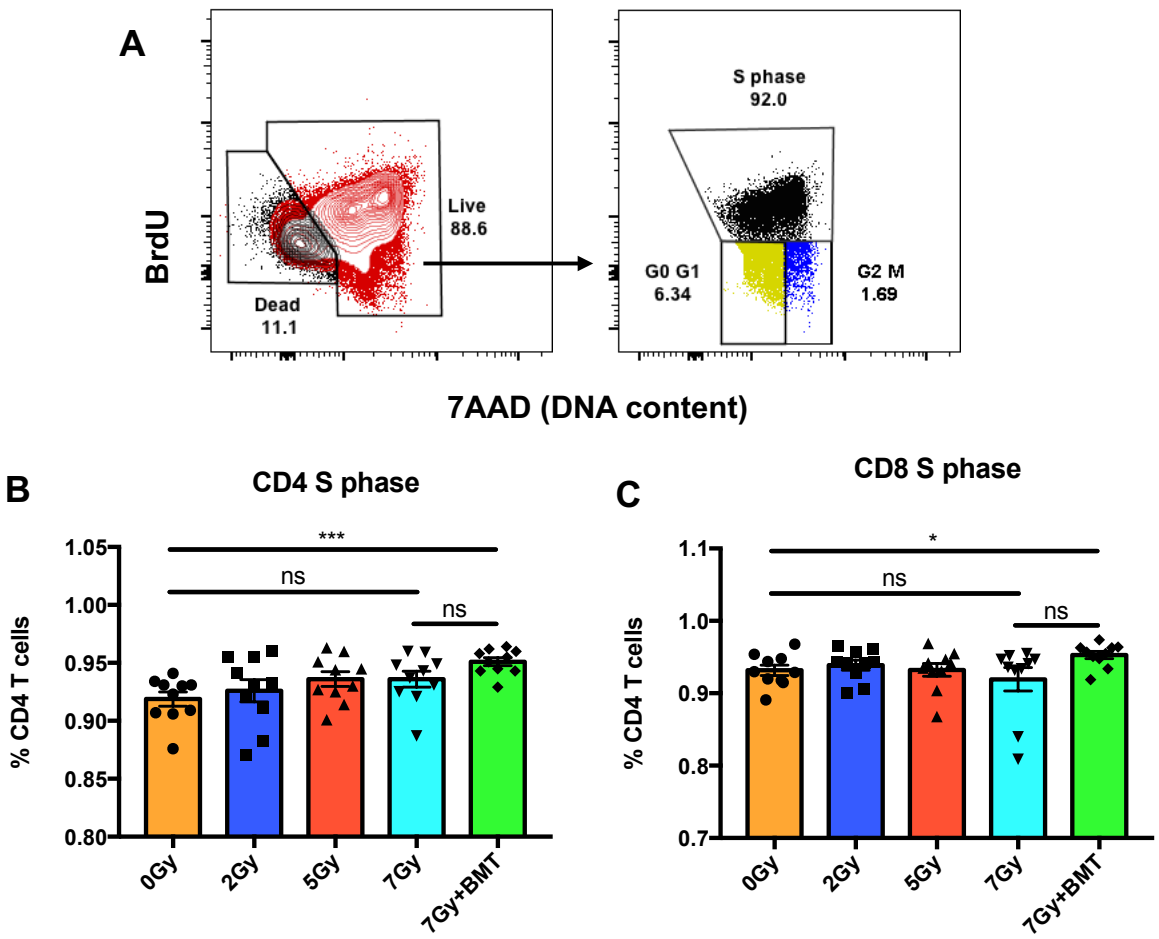


Figure 3.12. T cells retained capacity to respond to TCR stimulation ex vivo following TBI. C57BL/6 mice were nonirradiated (0 Gy), sublethally irradiated or irradiated at 7Gy and transplanted with 5 x 10^5/mouse Lin- bone marrow from C57BL/6 mice. Splenocytes were isolated 14 weeks following treatment for ex vivo activation using anti-CD3 and anti-CD28 antibodies for 48h, pulsed with BrdU for cell cycle analysis (A). Percentage of cells in the S phase of activated CD4 T cells (B) and CD8 T cells (C) were analyzed by flow cytometry.

T cell repertoire diversity exhibited no overt defect after varying doses of TBI

We have shown that splenic T cells did not experience a significant defect in cell count except at high dose TBI, indicating that there may be compensatory mechanisms to restore T cell numbers in irradiation-induced lymphophenia. Moreover, T cell subset analysis revealed that the naïve T cell compartment in TBI-treated groups appeared to undergo expansion particularly at the low dose treatment, possibly contributing to the maintenance of TCR repertoire diversity, which can affect the range of immune response against a variety of pathogens. To determine whether various TBI doses lead to distinct repertoire diversity outcomes, we analyzed the clonal diversity of each group in splenic T cells using clonality as a measurement of the degree of dominance by expanded clones within the entire repertoire (Figure 3.13A). As expected, majority of the clones across all groups underwent minimal clonal expansion due to the lack of need for immunization with specific antigens. Furthermore, we observed an overall effective maintenance of repertoire diversity at low, intermediate, and high dose TBI, with a trend for decreased diversity for intermediate and high doses (higher clonality). We further assessed the Shannon entropy of observed clones assigned to each VJ recombination (Figure 3.13B), with

the curve log_2N representing the maximum diversity (highest possible entropy). The above data demonstrated that intermediate TBI dose significantly reduced the TCR diversity compared to nonirradiated group. As expected, we observed a trend for decreased diversity across all TBI groups when compared to BMT group where thymic output was increased by donor bone marrow progenitors. However, we did not detect a statistical difference between high dose TBI and nonirradiated group, possibly due to limited sample size. To visualize the frequency distribution of individual clones, we analyzed the top 100 clones designated by distinct amino acid sequences of the CDR3 region (Figure 3.13C). Representing the relative frequencies of observed clones, the distributions of specific samples correspond to the degree of clonal expansion (samples 163 and 165 in intermediate dose TBI, sample 174 in high dose TBI). Overall, although there was probably a trend for higher dose TBI groups to have higher clonality, the TCR repertoire diversity across all TBI groups appeared to be effectively restored compared to nonirradiated group, indicating no overt defect and possible underlying compensatory mechanisms to maintain diversity.

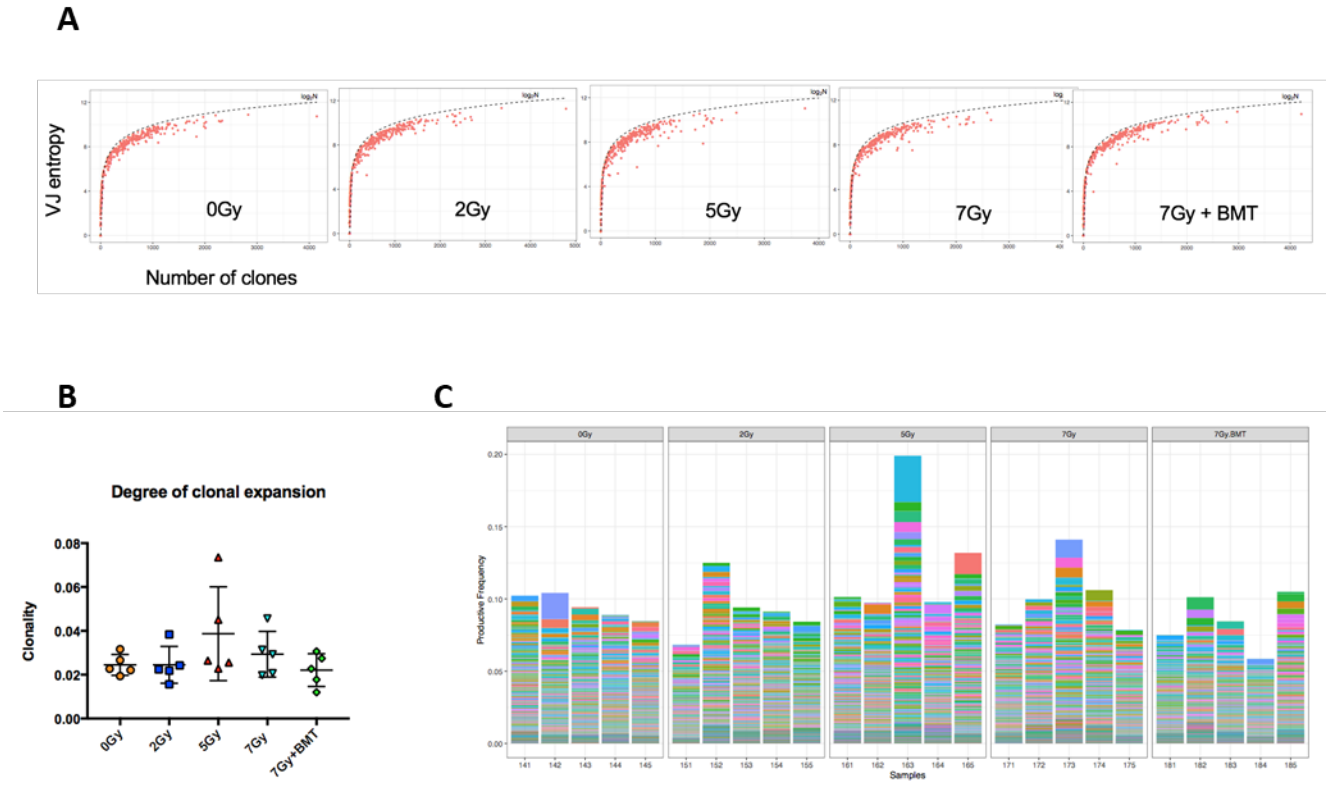


Figure 3.13. T cell repertoire diversity underwent restoration following TBI. C57BL/6 mice were sublethally irradiated at various doses. Splenocytes were isolated at week 14 and analyzed for clonality (A) and Shannon entropy for corresponding VJ cassettes (B) using TCRβ deep sequencing. Splenocytes were further analyzed for the frequency distribution of top 100 clones (C). $p < 0.05$, 0 Gy vs 5 Gy; 2 Gy, 5 Gy, 7 Gy vs. 7 Gy BMT.

TBI induced defects in total thymic output, but no overt developmental blocks
Interestingly, the above data on TCR repertoire analysis demonstrated that TCR diversity in TBI groups were relatively comparable to the nonirradiated group. Moreover, ex vivo stimulation assays showed that T cells from TBI groups retained the capacity to respond to TCR stimulation. Despite these observations, our findings of various lymphoid organs revealed tissue- and T cell lineage-specific changes during T cell reconstitution, including a prominent

defect in splenic Tem and bone marrow T_N cell numbers. Following development and maturation in the thymus, RTEs migrate to various sites and contribute to the peripheral T cell pool. We hypothesize that increasing TBI doses induce waning thymic output. Therefore, we further tested the effect of TBI on thymic output as a potential mechanism for observed defects in T cell reconstitution. Thymocytes were collected at 14 weeks after TBI treatments for total thymocyte numbers (Figure 3.14A). Thymocyte numbers exhibited a trend for dose-dependent decline, with a significant defect at high dose TBI compared to nonirradiated group.

For T cell development assessment, double-negative (DN) thymocyte frequencies were analyzed by CD44 and CD25 expression (Figure 3.14B). Overall, the above data revealed that TBI treatments caused a defect in total thymic output, but did not affect T cell lineage commitment (DN2 to DN3) and β-selection (DN3 to DN4), as the frequencies for each DN stage were comparable across all groups (Figure 3.14C). There was a minor increase in the double-positive (DP) frequency at 2Gy possibly due to the corresponding drop in DN frequency (Figure 3.14D). However, overall it appears that positive selection was not impaired. Similarly, negative selection was unaffected as reflected by comparable SP populations. Importantly, these data are in line with earlier findings that thymic recovery is limited by the number of BM-derived settling progenitorss as the total DN frequency underwent a diminishing trend following increasing doses of TBI (Figure 3.14C). The larger distribution in the 7 Gy group likely reflects biological variations, which could be compensated by increased sample size.

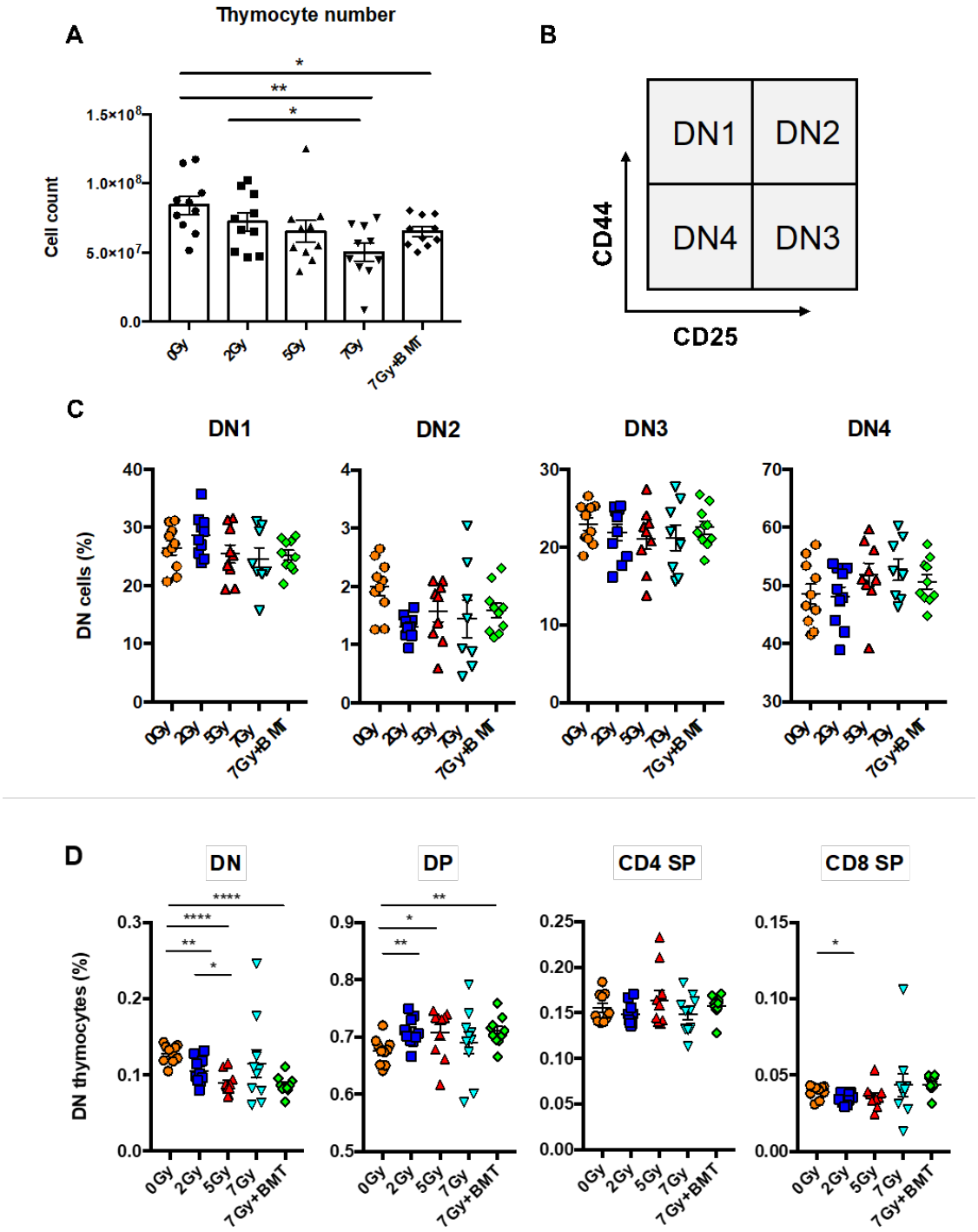


Figure 3.14. TBI induced defects in total thymic output, but not developmental blocks. At week 14, thymocytes were collected for total thymocyte numbers (A). DN thymocyte frequencies were analyzed by CD44 and CD25 expression (B) and shown in (C). CD4 SP, CD8 SP, and DP thymocyte frequencies separated by CD4 and CD8 expression were shown in (D).

Determine the roles of thymopoiesis and peripheral expansion in overall T cell recovery in a second radiation injury model

To study the contribution of thymopoiesis and peripheral expansion to overall T cell reconstitution , C57BL/6 mice (CD45.2+ CD90.2+) were first lethally irradiated (10.5 Gy) and then reconstituted with irradiated (0 Gy, 2 Gy, 5 Gy, and 7 Gy) CD45.1+CD90.1+ Lin- bone marrow cells (5×10^5) and CD45.2+ CD90.1+ splenic T cells (1×10^7). Bone marrow and T cells were irradiated with three different doses (2 Gy, 5 Gy, and 7 Gy). Non-irradiated control (0 Gy) was also included. The experimental design is shown in Figure 3.15. The plan was to monitor T cells and T cell subsets (CD3+, CD4+, and CD8+) derived from Lin- cells (CD45.1+CD90.1+) and splenic T cells (CD45.2+ CD90.1+) in peripheral blood separately over time (e. g., day 7, 14, and weekly until day +98) by flow cytometry. In this model, CD45.1+CD90.1+ T cells represent those generated through thymopoiesis and CD45.2+ CD90.1+ T cells represent those derived from peripheral expansion. Unfortunately, all the mice in both 5 Gy and 7 Gy groups died within two weeks after transplantation. All the mice in the other two groups (0 Gy and 2 Gy) survived and are recovering.

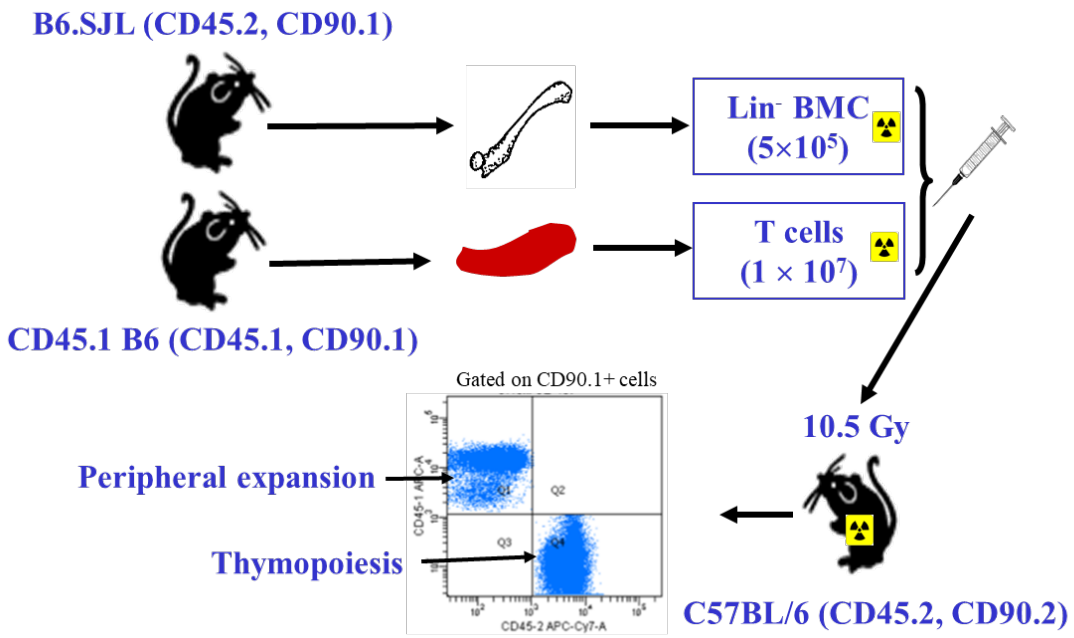


Figure 3.15. A schematic showing the animal model used to study the contribution of thymopoiesis and peripheral expansion to overall T cell reconstitution.

As shown in Figure 3.16, in the mice that received non-irradiated (0 Gy) bone marrow stem cells and T cells, T cells that were derived from transferred peripheral T cells as well as radioresistant T cells comprised the majority of T cell pool at day 36. These T cells were dropped while bone marrow-derived T cells were increased over time. After day +88, the ratios of T cells from different sources became stable at least until day +102. T cell composition showed a similar pattern in the recipients of irradiated (2 Gy) bone marrow stem cells and T cells. Interestingly, T cells derived from bone marrow stem cells (presumably through thymopoiesis) contributed more to the T cell pool after day +88 in the 2 Gy irradiated group compared those in the non-irradiated group.

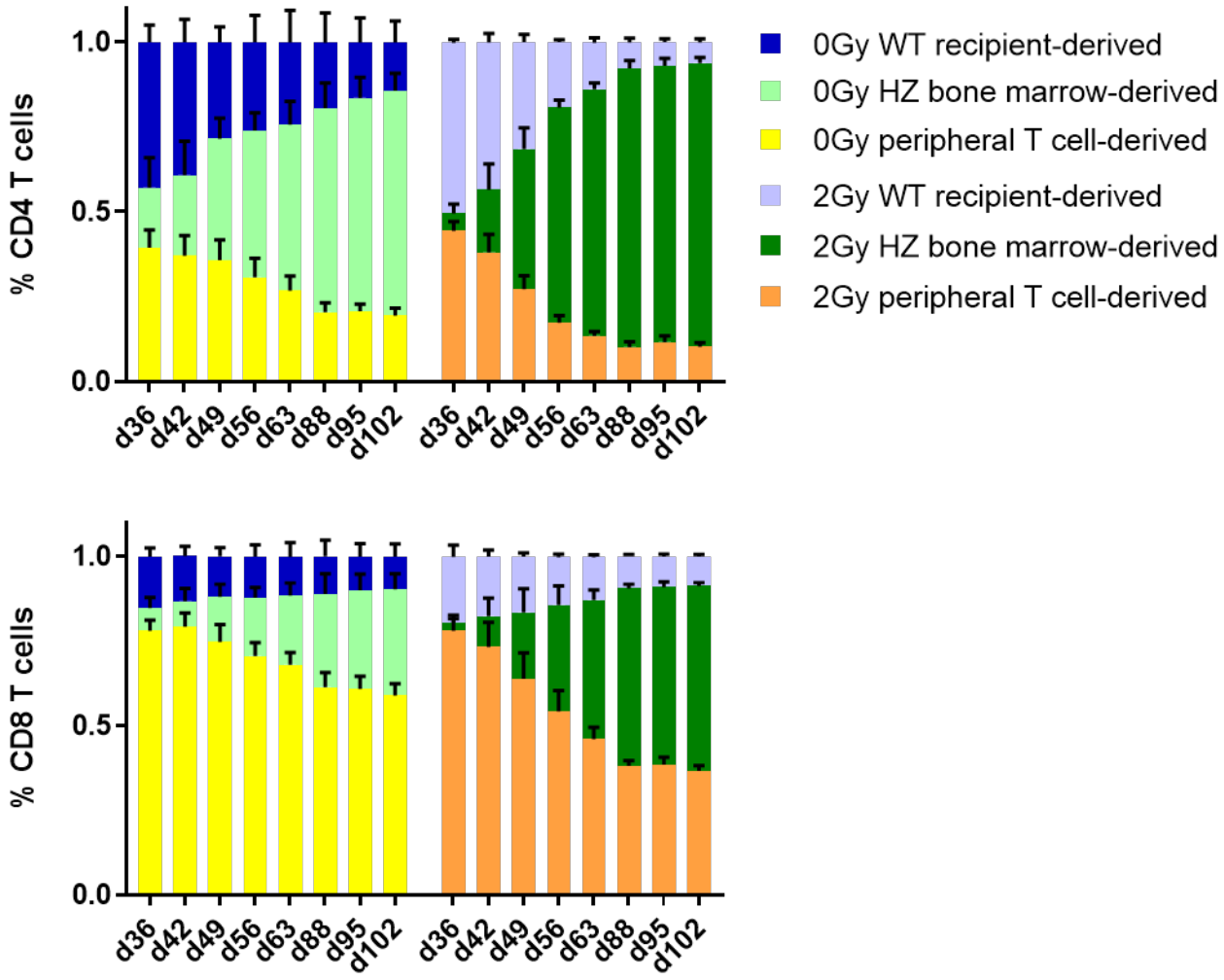


Figure 3.16. Source of CD4 T cells following transplantation

4) Other Achievements:

Nothing to report.

Project 4 - Genomic Sequencing and Stem Cell Lines (Dr. Dave)

1) Major Activities

a) Collection and processing of blood samples in the prospective cohort during the subacute post-radiation phase for planned genomic analyses.
b) Completion of exome sequencing proposed in Aim 1. This include method development for reliable mutation and expression identification from NHPs for which no standard methods currently exist.
c) Continued discussions with Duke and Wake Forest investigators on cross-project technical collaboration on cell collections, processing, and analysis.
d) Generation and analysis of RNAseq data from NHPs: We continue to improve the analytical approaches for gapped alignments in NHPs that is important to measure expression from the RNA sequencing reads while skipping the introns in the NHP reference genomes.
e) Development of deconvolution approaches to resolve different cell types in RNAseq performed on peripheral blood mononuclear cells obtained from NHPs.
f) Development of in vivo stem cell regeneration model that provides a functional approach to validation of genetic alterations. We performed ex vivo studies of iPS differentiation and are now developing in vivo approaches to overcome the limitations of the ex vivo approaches.
g) Monthly DOD Conference calls

2) Specific Objectives

There were two main goals of project 4. First, to define the genetic mutations and gene expression signatures induced by radiation. Second, define the molecular basis of immune deficiency and hematologic malignancies induced by radiation.

3) Results and Key Outcomes

Define genetic mutations induced by radiation (Aim #1)
In the past year, we continued to develop and have now finalized our methodologies for DNA whole exome sequencing n order to define the genetic mutations in rhesus macaques, we had to fully develop the methodologies for next generation sequencing and bioinformatics analysis. In the past year, we completed the development of methodologies for whole exome sequencing from rhesus macaque DNA and developed the methodology for transcriptome sequencing from rhesus macaque RNA.

We have now performed DNA/RNA extraction on a total of 48 cases from 16 individuals before and at two time points after treatment with radiation. Of these, 13 individuals (N=39 cases) yielded sufficient amounts of starting DNA and RNA for sequencing.
All sequencing libraries were carefully quantified using Agilent Bioanalyzer. Representative sequencing library size-distribution plots for whole exome sequencing (Figure 4.1A) and RNA sequencing (Figure 4.1B) are shown. We also preliminarily sequenced on library on the Illumina Miseq and confirmed even distribution of A/C/G/T bases with very few called as unknown (N). These results indicate that our library construction process has worked well.

RNA-seq Preprocessing

RNA sequence reads were trimmed (Bolger et al., 2014) to remove any remaining Illumina adapter sequences and aligned to the hg19 transcriptome using STAR, a spliced read aligner which allows for sequencing reads to span multiple exons. On average, we were able to align 90% of the sequencing reads for each sample to the reference rhesus macaque genome. Transcript quantification at the gene and transcript level was performed (Li et al., 2011) and expression values were then FPKM normalized, to account for differences in library depth across samples.

Principal Components Analysis (PCA) identified major shifts in gene expression across samples after exposure to radiation. We hypothesized that radiation predominantly affected one or more cell types that resulted in changes in observed gene expression arising from an admixture of cell types. To evaluate the effects of radiation on different cell types, we examined (Newman et al., 2015) the proportions of leukocyte subpopulations in each sample from the normalized expression data. We used validated gene expression profiles to define signatures associated with each lymphocyte type and used 100 permutations to estimate the significance of results. ANOVA tests were then used to determine whether the percentage of each cell type differed across treatment groups.

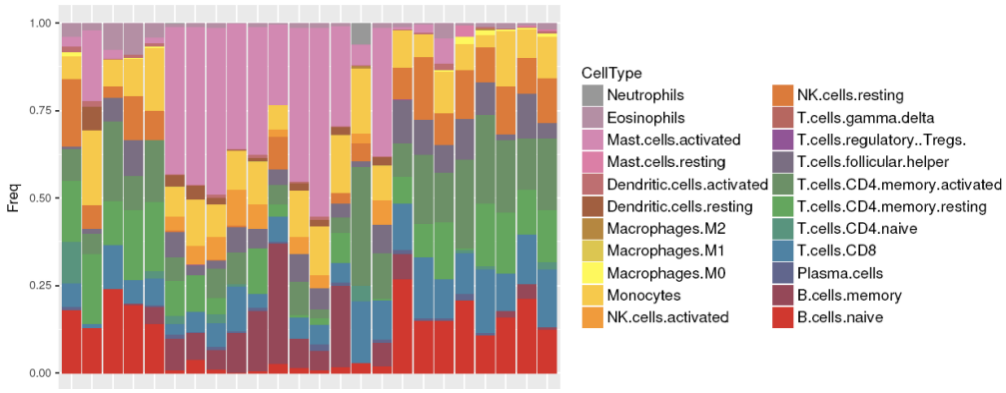


Figure 4.1: Deconvolution analysis of immune populations after exposure to radiation.

Our analysis indicates a large increase ($p < 0.05$) in the proportion of activated mast cells in mid-timepoint samples relative to baseline and late-timepoint samples. We also found that baseline and late-timepoint samples had significantly higher levels of naïve B-cells whereas mid-timepoint samples had significantly higher levels of memory B-cells. There were far fewer significant differences in the proportion of immune cell types between baseline and late-timepoint samples, suggesting the broad effects of radiation on the immune system may be largely reversible in these samples (Figure 4.1).

This analysis is consistent with the observation that memory B cells are best able to withstand the pro-apoptotic effects of radiation. In the memory B cells, we observed two predominant genes that may explain their survival following radiation. The first gene, not surprisingly, is BCL2, which is a known anti-apoptotic factor and is known to be associated with survival of B cells in response to a number of different pro-apoptotic stimuli. The other gene to emerge from this analysis was CRLF2, which is a transcription factor known to be involved in B cell differentiation and lineage development.

Exome sequencing analysis

A critical question in post-radiation exposure and recovery is whether there are clonal effects that guide recovery, i.e. whether radiation leads to the development or selection of clones of

hematopoietic stem cells that disproportionately contribute to hematopoiesis. We examined this question by performing whole exome sequencing on the same individuals subjected to RNAseq. We have DNA sequencing from each of the three time points for each individual. Our results suggest that there are no clonal effects post radiation, i.e. there is no dominant clone being selected by radiation. We are continuing to analyze these data across individuals to examine whether such approaches will increase our power for detecting subclones.

Develop a stem-cell based model to generate immune B cells in vitro (AIM #2)

Given the potential multigenic nature of genetic variation and the emerging role for B cell receptor signaling and other immune functions, we proposed to differentiate stem cells from irradiated macaques (or human stem cells with the genetic modifications present in irradiated macaques) into B cells to better understand their function and the long-term effects of radiation on immune function.

We have previously developed the schema shown in Figure 4.2 below to differentiate B cells from stem cells.

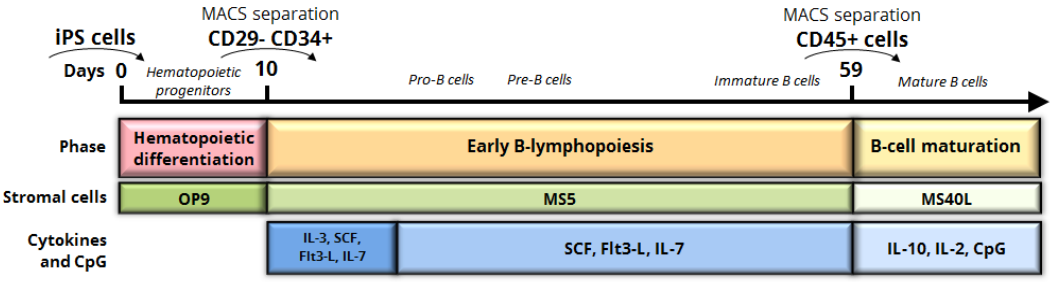


Figure 4.2: Schema for generating B lymphoid cells.

The yields of B cells from three consecutive experiments at at 90 days are shown below, and were on-average, less than 1%. Two additional experiments with new reagents yielded no measurable B cells.

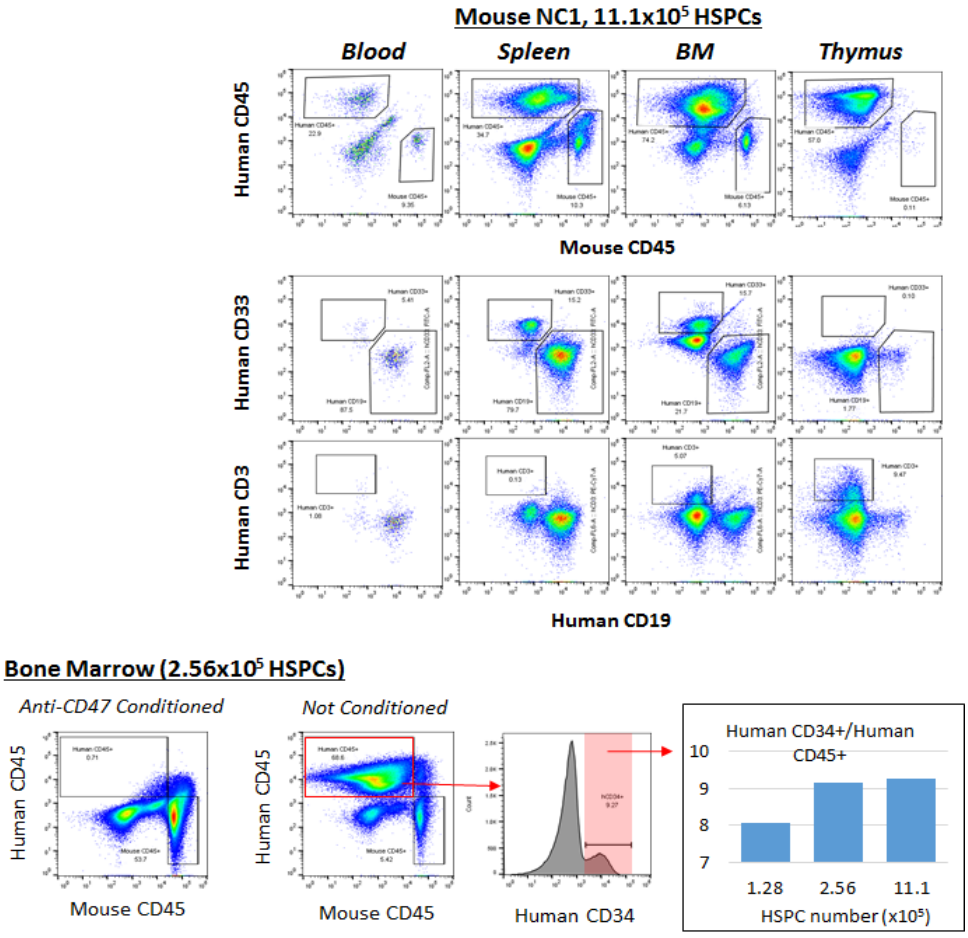


Figure 4.3: Presence of B cells (CD19+), T cells (CD3+), and myeloid cells (CD33+) in blood, spleen, bone marrow, and thymus at 10 weeks post transplantation.

Recognizing these critical limitations, we initiated experiments using a humanized mouse model that transplants human stem cells to regenerate intact and functional human immune cells into an immune compromised mouse to generate the data shown in Figure 4.3.

Generation of humanized mouse model:

We used the NOD,B6.SCIDIl2rγ$^{-/-}$kit$^{W41/W41}$ (NBSGW) mice as the base model to generate a humanized mouse. NBSGW mice are ideal for this type of project as they contain a polymorphism in the *Sirpa* gene providing for phagocytic tolerance of human cells, PRKDC^{scid} mutation and Il2rγ$^{-/-}$ mutations which lead to absence of T, B, and NK cells thus preventing xenoreactivity, and a c-kit mutation resulting in impairment of hematopoiesis of the mouse cells, providing a competitive advantage to transplanted cells.We have comprehensively tested this system in experiments transplanting CD34+ hematopoietic stem cells from anonymized human donors.

Figure 4.3 shows our success with generation complete human lineages in mice by implanting as few as 125,000 human stem cells. As shown, we were able to identify substantial numbers of human derived circulating B cells (CD19+), T cells (CD3+) and myeloid cells (CD33+) in blood,

spleen, bone marrow and thymus of the mice. Importantly, these humanized mice have an essentially unlimited supply of B and T cells for future experiments.
Interestingly, stem cell dosage did not have a large impact on the recovery of mature human immune cells by the time mice were 10 weeks old. Thus, we can reliably generate humanized mouse models by injecting human stem cells. Human embryonic stem cell lines can be used as an alternative starting point for stem cells.
After our initital success in generating these humanized mice, we encountered significant difficulties in altering individual genes. In addition, we transduced these cells with GFP to be able to track the cells containing the CRISPR constructs using their fluourescence. We found that these cells containing the correct CRISPR constructs failed to engraft in the recipient mice, leading to us to test several iterations of the viral vector used to transduce the human stem cells with the appropriate CRISPR constructs. We found that, although the CRISPR elements worked as designed in our prior tests, the process of transplantation somehow resulted in alterations in chromatin to a closed conformation leading to silencing of expression.

We finally tested a CRISPR construct that was coupled to a previously described (Zhang et al, Mol Ther, 2010) ubiquitous chromatin opening element. This resulted in persistence of expression and maintenance of GFP expression (Figure 4.4).

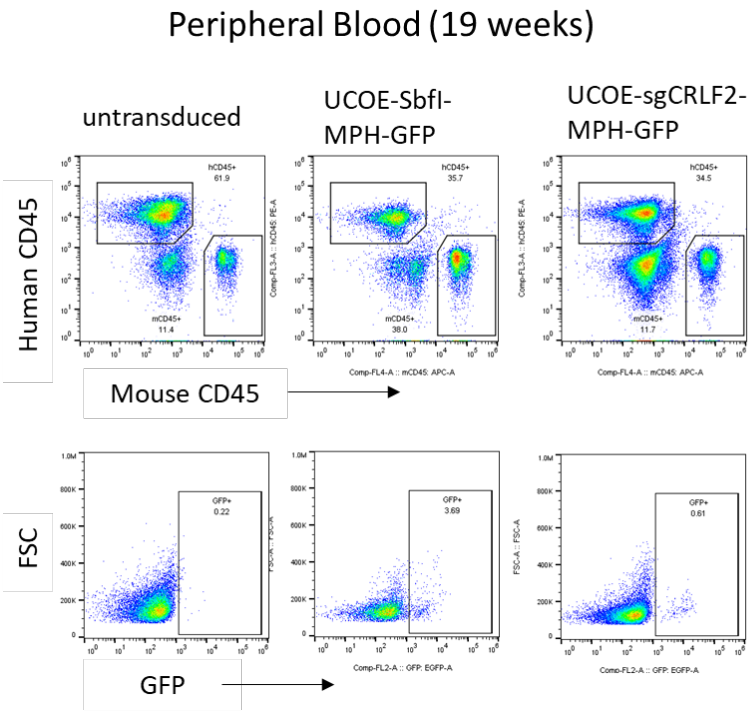


Figure 4.4: Engraftment of B cells occurs successfully in both untransduced and transduced cells, but only the UCOE containing elements have significant numbers of GFP+ cells.

Interestingly, we also found vastly improved engraftment with these modified stem cells with engraftment exceeding an average of 50% at 21 days, which is well within expected time frames.

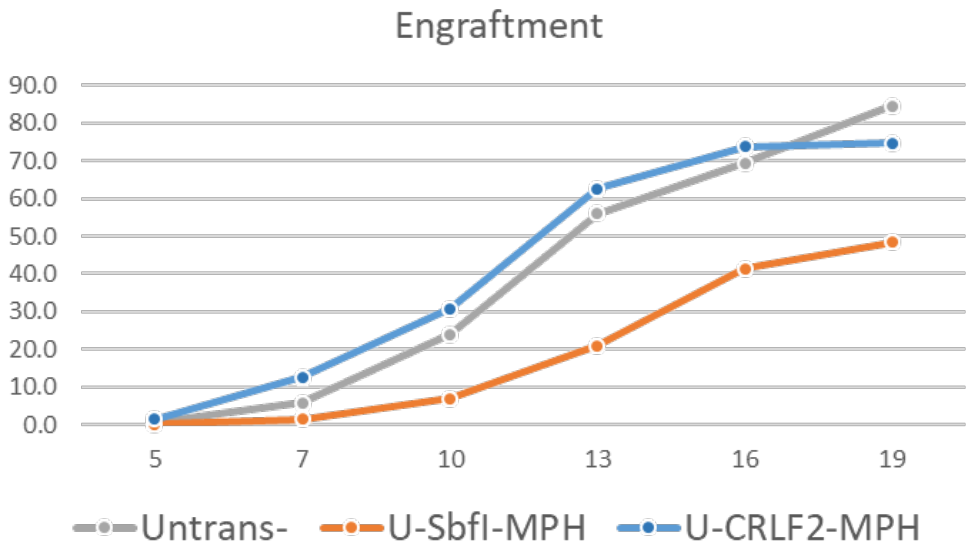


Figure 4.5: Engraftment of B cells occurs successfully in both untransduced and transduced cells and human cells are detectable under all three conditions by 10 days.

These experiments inform our approaches going forward, where we will plan to sample multiple tissues for engraftment and ensure that the cell types being sampled are of human origin.

Expected Outcomes: At the end of this Aim, we will have generated and characterized hematopoietic lineages from genetic alterations observed in DEARE macaques and demonstrated the feasibility of our approach for modeling complex genetic interactions.

4) Other Achievements

Nothing to report.

What opportunities for training and professional development has the project provided?

Overall (PI Cline)

1. All investigators participated in monthly teleconferences, and the project leader for projects 1-3 participated in an in-depth discussion of this program's goals and objectives on October 16, 2019 hosted by the PI's team at Wake Forest School of Medicine (Dr. Dave was absent due to a medical emergency).
2. Investigators (Drs Cline, Dugan, and Register) and Fellows (Drs. Andrews, Michalson and Thakur) attended the 2018 Radiation Research Society meeting, which provided education and professional development.

Project 1 Diabetes (PI Kavanagh).

1. We have two students continuing to work on the project (Alistaire Ruggiero and Dr. Nicole Bacarella).
2. We have recruited a new graduate student to work on senescence cell identification in adipose tissue (Amanda Olivier).
3. A junior faculty member has joined the project (Dr. Chia-Chi Key) to share methods for pre-adipocyte differentiation and learn about radiation effects.

Project 2 RIHD (PI Register)

1. Image Analysis Software, Cardiac Ultrasound, Cardiac MRI, and RNAseq analysis
2. Tissues: VisioPharm, programmable, development of semi-automated programs to assess myocardial, arterial, and other histologic and immunohistochemical phenotypes including fibrosis and atherosclerosis. Some of this work has resulted in training experience for undergraduate students (Ben Williams, University of South Carolina Sophomore), Matthew O'Brien, Wake Forest University Junior-Senior, Abby Anderson, Wake Forest University Junior).
3. Cardiac Ultrasound: CV ultrasound applications and measurements has been optimized through interactions with Cardiology faculty and vendors, establishing new SOPs for prospective cohort.
4. Cardiac MRI: Register and Michalson have ongoing interactive discussion sessions with Clinical Cardiology staff and faculty
5. Gene expression analyses: Ongoing practical experience in the utilization of Bioconductor and R to conduct RNAseq and other genomics analyses and in the the use of Ingenuity Pathways software.

Project 3 (Immune Recovery) PI Sempowski and Chen

1. Yujing Zou is a PhD student who is mentored by Dr. Chen. She was involved in many aspects of this study.

Project 4 (Genomics) PI Dave

Nothing to Report

How were the results disseminated to communities of interest?

Overall Program (Cline)

Study design, public health and strategic relevance, and opportunities for collaboration were presented by Dr. Cline at several venues:

- The NIH/NIAID Centers for Medical Countermeasures Against Radiation (Annual meeting 12/11-12/18, and reports during monthly teleconferences with the CMCR Steering Committee)
- The NIH Radiation/Nuclear Program Polypharmacy Workshop, NIAID, Rockville, MD, Oct 24, 2018 (Invited Speaker)
- The annual Radiation Countermeasures Center of Research Excellence (RadCCORE) meeting at Duke University, Durham, NC
- MD Anderson Cancer Center, Houston, TX, 10/10/19 (Invited Speaker)
- Comparative Medicine Research Strategy Meetings, Wake Forest School of Medicine
- Department of Radiation Oncology, Wake Forest School of Medicine
- Wake Forest Animal Resources Program Continuing Education Seminar

Project 1 - Diabetes (Kavanagh)

- Comparative Medicine Research Strategy Meetings
- Dr. Kavanagh attended a DOD-focused research retreat at Duke University (4th of September 2019) to share research progress and discuss collaborative opportunities.
- Digestive Diseases Week, San Diego 2019; oral presentation and interaction with fatty liver research scientists.
- Data from these studies were presented within invited seminars (“Intestinal Aging and Healthspan”) at The Barshop Institute for Longevity and Aging Studies, University of Texas Health Sciences Center, San Antonio, TX (March 2019), and the University of Tasmania School of Medicine. Hobart Tasmania Australia (May 2019).

Project 2 - Radiation-Induced Heart Disease (Register)

- Comparative Medicine Research Strategy Meetings
- Presentations at the annual Radiation Research meeting, at the annual RADCCORE meeting at Duke University, in Departmental and other seminars at Wake Forest, along with special presentations and discussion with visiting Cardiologists from other institutions.

Project 3 - (Immune Recovery) (Sempowski/Chen)

- Presentations at the annual Radiation Research meeting, and at the annual RADCCORE meeting at Duke University.

Project 4 - Genomics (Dave)

- Nothing to report

What do you plan to do during the next reporting period to accomplish the goals?
If this is the final report, state "Nothing to Report."

Describe briefly what you plan to do during the next reporting period to accomplish the goals and objectives.

Overall (PI Cline):

No Change from Statement of Work.

For all projects we anticipate continued local and national presentations of results at relevant scientific meetings, and publications of results in the peer-reviewed literature.

Project 1 (Diabetes, PI Kavanagh):

No Change from Statement of Work.

Project 2 (RIHD, PI Register):

No Change from Statement of Work.

During the next quarter, we will be

1) Analyzing the post-radiation Cardiac MRI and echocardiographic imaging in the PRC
2) Continuing RNAseq and miRNAseq of myocardium from deceased RSC subjects
3) Additional immunohistochemical analysis of individual cell types and macrophage polarization in myocardium from deceased RSC and Control rhesus monkeys
4) Collecting and characterizing blood samples from the PRC and the RSC
5) Continuing statistical analyses of the effects of radiation exposure on echocardiographic outcomes in the RSC
6) Continuing image analysis of cardiac MR images in the PRC
7) Statistical analysis of data collected to date from the cardiac MRI
8) Continuing plans for analysis of ECM and other biomarkers
9) Planning for MR assessments of the RSC
10) Ongoing molecular and cellular phenotyping of the monocytes in the RSC
11) Submission of manuscript containing comprehensive echocardiographic phenotyping of the RSC describing the effects of radiation on the heart
12) Final necropsy of the PRC with collection of myocardial and other samples to undergo detailed molecular and cellular characterization
13) Statistical analyses of biomarker, functional, structural, and molecular datasets.

Project 3 (Immune Recovery, PI Sempowski/Chen):

Finalize data analysis and submit two NHP-related manuscripts by Y5Q3, the first describing our findings from the prospective cohort and the second describing our findings from the long-term survivor cohort. Presentations, abstracts, meetings and manuscripts as studies mature.

Project 4 (Genomics, PI Dave): Abstracts/meetings and manuscripts as studies mature.

In the coming year, we will scale up the sequencing. We will sequence 30 whole exomes and 30 transcriptomes to preliminarily define the genomic signatures associated with DEARE. For AIM #2, we will repeat our experiments to generate B cells from stem cells. We will increase the exposure to CD40L, which is known to stimulate B cell production and differentiation. We will carefully monitor these experiments for increased efficiency of lymphoid differentiation.

4. **IMPACT:** Describe distinctive contributions, major accomplishments, innovations, successes, or any change in practice or behavior that has come about as a result of the project relative to:

What was the impact on the development of the principal discipline(s) of the project?

Overall (PI Cline):

The findings produced by this program have increased awareness of the multi-systemic nature of late radiation effects, in the domains of radiation biology, radiation mitigation, and medical management of affected individuals post-exposure.

Project 1 (Diabetes, PI Kavanagh):

The work described in this report indicates that radiation exposure produces systemic dysregulation of metabolic functions, leading to altered protein signaling pathways, impaired tissue blood flow and deranged metabolic activity, including overt diabetes mellitus.

Project 2 (Radiation Induced Heart Disease, PI Register):

The project has produced new data on the effects of radiation on myocardial fibrosis and cardiac function, on myocardial fibroblast populations, on myocardial macrophage polarization, on myocardial capillarization, and on monocyte polarization, implicating monocyte and macrophage driven pathways in promoting pro-fibrotic pathways and producing evidence of restrictive cardiomyopathy and diastolic dysfunction.

Project 3 (Immune Recovery, PI Sempowski/Chen):

The results from the murine study reveal for the first time that, even though total body irradiation has long-lasting effect on thymopoiesis, its effects on T cell numbers, individual T cell function, and T cell repertoirs are minimum

Project 4 (Genomics, PI Dave): Abstracts/meetings and manuscripts as studies mature.

Nothing to report. Future elucidation of the underlying genomic, transcriptomic and functional consequences is anticipated as Project 4 (Genomics/Dave) progresses into the analytic phase in year 3.

What was the impact on other disciplines?

The impact of our findings is broad, and spans multiple groups and agencies working to understand and mitigate delayed effects of acute radiation exposure, including the DOD, BARDA, NIH, FDA, and NASA. We anticipate that our data will influence response strategies, biomarker development, and re-adjustment of regulatory assumptions regarding the modeling, prediction and treatment of the long-term consequences described herein.

What was the impact on technology transfer?

Nothing to Report

What was the impact on society beyond science and technology?

Nothing to Report

5. CHANGES/PROBLEMS: The Project Director/Principal Investigator (PD/PI) is reminded that the recipient organization is required to obtain prior written approval from the awarding agency Grants Officer whenever there are significant changes in the project or its direction. If not previously reported in writing, provide the following additional information or state, "Nothing to Report," if applicable:

Changes in approach and reasons for change

Overall (Cline, PI):

As noted previously, delays in the acquisition and irradiation of animals at the beginning of the award in 2015 and 2016 have slightly pushed back terminal necropsy studies. These were initially planned for Year 5 Quarter 1 (December 2019), and have now been pushed back to Year 5 Quarter 2 (March, 2020).

Project 1 (Diabetes, PI Kavanagh):

Nothing to report.

Project 2 (RIHD, PI Register):

Delay in initiating PRC component combined with delays in the final necropsy will make finishing the proposed detailed analytical work in Project 2 by the original end date difficult or impossible to accomplish. Project 2 PI is hopeful for a no cost extension to allow completion of key aims related to the PRC; this possibility has led to preliminary discussions with our Science Officer, and further discussion will be undertaken in the coming quarter.

Project 3 (Immune Recovery, PI Sempowski/Chen):

Nothing to report.

Project 4 (Genomic, PI Dave):

The expected yield of B cells from differentiation experiments was roughly 10%. However, the actual yields that we observed at 90 days was on-average, less than 1%. Repeating these experiments did with new reagents did not improve the yields of B cells. Therefore, we have change the approach to differentiate the stems cells in vivo using a Nod-Scid-gamma (NSG) mouse model. This new approach was scientifically approved in 2017 and received ACURO approval 8/1/18.

Actual or anticipated problems or delays and actions or plans to resolve them

Overall:

As noted previously, delays in the acquisition and irradiation of animals at the beginning of the award in 2015 and 2016 have slightly pushed back terminal necropsy studies. These were initially planned for Year 5 Quarter 1 (December 2019), and have now been pushed back to Year 5 Quarter 2 (March, 2020).

Project 1 (Diabetes, PI Kavanagh):

Nothing to report.

Project 2 (Radiation Induced Heart Disease, PI Register)

Nothing to Report.

Project 3 (Immune Recovery, PI Sempowski/Chen)

Due to the unexpected observations that T cell numbers are able to recover back to normal level around 6 weeks post-irradiation, we do not anticipate that the therapeutic window is wide enough for HGH and IGF-1 to work when given long after irradiation as we initially proposed. In fact, we could not demonstrate that IGF-1 was able to promote immune reconstitution post-irradiation as we reported in the Year 3 report. As an alternative approach detailed in the proposal, we plan to test other new and more potent agents. One of these agents that we are interested in testing is new IL-7, called rhIL-7-hyFc. This product has a long half-life in vivo and is being testing in several human trials. We are currently in the process of obtaining this product with NetImmunotech, who owns this product.

We will obtain prior written approval if significant changes in objectives and scope will need to be made.

Project 4 - Genomic Sequencing and Stem Cell Lines (PI Dave)

Nothing to Report.

Changes that had a significant impact on expenditures

Overall/Primate Core

Nothing to report.

Project 1 (Diabetes, PI Kavanagh)

Nothing to report.

Project 2 (Radiation-Induced Heart Disease, PI Register)

Nothing to report.

Project 3 (Immune Recovery, PI Sempowski/Chen)

The HGH experiments were postponed. The funds allocated for these experiments have been spent slower that originally budgeted

Project 4 (Genomics, PI Dave)

Nothing to report.

Significant changes in use or care of human subjects, vertebrate animals, biohazards, and/or select agents

Significant changes in use or care of human subjects

Not applicable - No human subjects

Significant changes in use or care of vertebrate animals

Overview

1. For the Nonhuman Primate Prospective Cohort Protocol PR141508.01, the Wake Forest Protocol number A15-083 was renewed & replaced by Protocol A18-062, without a major change in scope, as part of institutional policy (all Wake Forest protocols are replaced and renumbered at 3 year intervals)..

2. For PR141508.2 (Project 2 mice): This protocol was replaced with Wake Forest IACUC protocol number #A18-024 (all Wake Forest protocols are replaced and renumbered at 3 year intervals). The ACURO Assigned Number is unchanged as PR141508.02. The protocol remains identical to that of #A15-068 but the animal number is reduced on account of the work that has already been completed.

3. A new protocol PR141508.05 (Duke IACUC protocol number A010-17-01) was instituted in support of mouse studies in Project 4.

4. A variety of minor protocol amendments were made throughout the year, reflecting personnel changes and minor procedural changes.

Specific details are given below.

Core Primate Studies (Cline)

Protocol 1 of 5 total: [ACURO Assigned Number]: PR141508.04

Title: Radiation Countermeasures Long Term Response of Rhesus Macaques

Target required for statistical significance: 120

Target approved for statistical significance: 132

Submitted to and Approved by:

Wake Forest IACUC original approval 9/17/13 as A13-117

Wake Forest IACUC renewed/reapproved 6/23/16 as A16-094

Wake Forest IACUC renewed/reapproved 6/14/19 as A19-028

Current ACURO approval was requested 6/23/19; review is under way.

Amendments since our prior annual report are shown below.

Amendments

Protocol # A16-094 - Radiation Survivor Core

Amendment No.	Reason for amendment	Wake Forest IACUC approval date	ACURO approval date
28	Personnel change; addition of Brianna Sellers	10/11/18	10/5/18
29	Personnel change; updated duties for Ashley Davis; removal of William Carerra	1/23/19	1/31/19
30	Personnel change; addition of Beth Uberseder	2/15/19	2/19/19
31	Personnel change; addition of Dr. Brendan Johnson	3/11/19	3/12/19
32	Personnel change; addition of Dr. Chaudry Adeem Asim	4/4/19	4/11/19
33	Personnel change; addition of Austin Tedder	5/16/19	Not required as per new ACURO policy
34	Personnel change; addition of students John Post, Cecilia Armstrong, Mariah Williams, Daniel Bissinger; removal of Dr. Kris Michalson	6/12/19	Not required

Protocol # A19-028 - Radiation Survivor Core renewal 2019

Amendment No.	Reason for amendment	Wake Forest IACUC approval date	ACURO approval date
1	Personnel added (Daniel Bissinger)	6/25/19	Not required
2	Personnel added (Shane Sills)	7/16/19	Not required
3	Cerebrospinal fluid collection added (not DOD funded)	10/7/19	Pending

Status

This long-term cohort is under study as planned. No changes in DOD-funded work will be done until pending ACURO approval is obtained.

Protocol 2 of 5 total [ACURO Assigned Number]: PR141508.01

Title: Prospective Radiation Cohort: Cardiac and Metabolic Studies

Target required for statistical significance: 20

Target approved for statistical significance: 28

Submitted To And Approved By:

Wake Forest IACUC (Protocol #A15-083, approved 7/6/15)

ACURO approval (9/3/15, ACURO no. PR141508.01)

Replaced by Protocol #A18-062 as part of routine full renewal every 3 years as per IACUC policy

Amendments since last annual progress report.

A18-062

Amendment No.	Reason for amendment	Wake Forest IACUC approval date	ACURO approval date
9	Addition of influenza and Streptococcus vaccines	10/10/18	10/17/18
10	Personnel change; addition of Brianna Sellers	10/11/18	10/17/18
11	Personnel change; addition of Alistaire Ruggiero	11/15/18	11/19/18
12	Addition of a new room location, increased monitoring duration	11/6/18	11/16/18
13	Personnel change; addition of Chrissy Sherrill	1/4/19	1/8/19
14	Personnel change; updated duties for Ashley Davis	1/23/19	1/30/19
15	Personnel change; updated duties for Beth Uberseder	2/15/19	2/19/19
16	Personnel change; addition of Chaudry Adeem Asim	3/11/19	3/12/19
17	Personnel change; addition of Austin Tedder	4/2/19	4/11/19
18	Personnel change; addition of Brendan Johnson	5/16/19	Not required
19	Personnel change; addition of John Post, Cecilia Armstrong, Mariah Williams Daniel Bissenger	6/18/19	Not required
20	Personnel change; addition of Shane Sills	7/16/19	Not required
21	Personnel change; addition of Vincent Yao, removal of Chaudry Adeem, Cecilia Armstrong, Danieal Bissinger, Jacob Cleary, John Post, Austin Tedder, Mariah Williams	Pending	Not required

Status

Studies continue as planned; animals are now 2 years out from irradiation.

Protocol 3 of 5 total: ACURO Assigned Number PR141508.02

Title: **Prospective Evaluation of Diabetogenesis Post-irradiation in Mice (Metabolic Effects of Radiation Exposure)**

Target required for statistical significance: 200

Target approved for statistical significance: 200

Submitted To And Approved By:

Wake Forest IACUC (A15-068, Approved 5/20/15

ACURO (PR141508.02, Approved 10/19/15)

Amendments since prior annual report: None

This protocol was replaced with Wake Forest IACUC protocol number #A18-024 (all Wake Forest protocols are replaced and renumbered at 3 year intervals). The ACURO Assigned Number is unchanged as PR141508.02. The protocol remains identical to that of #A15-068 but the animal number is reduced on account of the work that has already been completed.

Amendments: None

Status: Approved studies are in progress.

Protocol 4 of 5 total:

Protocol [ACURO Assigned Number]: PR141508.03

Title: IMMUNOLOGICAL INJURY AND RECOVERY AFTER RADIATION INJURY

Target required for statistical significance: 4184 mice

Target approved for statistical significance: 4184 mice

Submitted to and approved by:

Duke IACUC (A142-15-05, Approved on 5/28/15)

ACURO (PR141508.03, Approved on 3/3/16)

Amendments: None

Status: Approved, work in progress.

Protocol 5 of 5 total:

Protocol [ACURO Assigned Number]: PR141508.05

Title: HUMANIZED MOUSE MODEL OF LYMPHOMA BY ENGRAFTMENT OF CRISPR-CAS9-EDITED HUMAN HEMATOPOIETIC CELLS

Target required for statistical significance: 4184 mice

Target approved for statistical significance: 4184 mice

Submitted to and approved by:
Duke IACUC (A010-17-01, Approved on 1/27/18)
ACURO (PR141508.05, Approved on 8/1/18)

Amendments: None

Status: Approved, work in progress.

Significant changes in use of biohazards and/or select agents

Nothing to report

6. PRODUCTS: List any products resulting from the project during the reporting period. If there is nothing to report under a particular item, state "Nothing to Report."

- **Publications, conference papers, and presentations**

Report only the major publication(s) resulting from the work under this award.

Journal publications.

Overall (Cline): See below by project.

Project 1 (Diabetes, PI Kavanagh):

Sherrill C and **Kavanagh K**. Fight Club: Using Housing Conditions to Curb Male Cage Aggression. 2019 Laboratory Animal Science Professional; March: 38 – 40.

Bacarella N, Ruggiero A, Davis AT, Uberseder B, Davis MA, Bracy DB, Wasserman DH, Cline JM, Sherrill C, **Kavanagh K**. Whole Body Irradiation Induces Diabetes and Adipose Insulin Resistance in Non-human Primates. Int J Rad Onc Biol Physics 2019 *Under review*

Project 2 (Radiation-Induced Heart Disease, PI Register):

Michalson KT, Macintyre AN, Sempowski GD, Bourland JD, Howard TD, Hawkins GA, Dugan GO, Cline JM, Register TC. Monocyte Polarization is Altered Post-Irradiation in Male Rhesus Macaques: Implications for Delayed Effects of Acute Radiation Exposure. Radiat Res. 2019 Aug;192(2):121-134. doi: 10.1667/RR15310.1

Project 3 (Immune Recovery, PI Sempowski/Chen):

Caudell DL, Michalson KT, Andrews RN, Snow WW, Bourland JD, DeBo RJ, Cline JM, Sempowski GD, Register TC. Transcriptional Profiling of Non-Human Primate Lymphoid Organ Responses to Total-Body Irradiation. Radiat Res. 2019;192:40-52. PMID: 31059377.

Hale LP, Rajam G, Carlone GM, Jiang C, Owzar K, Dugan G, Caudell D, Chao N, Cline JM, Register TC, Sempowski GD. Late effects of total body irradiation on hematopoietic recovery

and immune function in rhesus macaques. PLoS One. 2019;13;14(2):e0210663. PMID: 30759098; PMCID: PMC6373904.

Project 4 (Genomics, PI Dave):

Panea RI, Love CL, Shingleton JR, Reddy A, Bailey JA, Moormann AM, Otieno JA, Ong'echa JM, Oduor CI, Schroeder KMS, Masalu N, Chao NJ, Agajanian M, Major MB, Fedoriw Y, Richards KL, Rymkiewicz G, Miles RR, Alobeid B, Bhagat G, Flowers CR, Ondrejka SL, Hsi ED, Choi WWL, Au-Yeung RKH, Hartmann W, Lenz G, Meyerson H, Lin YY, Zhuang Y, Luftig MA, Waldrop A, Dave T, Thakkar D, Sahay H, Li G, Palus BC, Seshadri V, Kim SY, Gascoyne RD, Levy S, Mukhopadhyay M, Dunson DB, Dave SS. The whole genome landscape of Burkitt lymphoma subtypes. Blood. 2019 Sep 26. pii: Blood.2019001880. doi: 10.1182/blood.2019001880. [Epub ahead of print] PubMed PMID: 31558468.

Note: Attribution to this program is under review (JM Cline)

Books or other non-periodical, one-time publications.

Overall (PI Cline)

Nothing to report.

Note regarding the Radiation Research Society.
2018: The meeting was in September, so abstracts were reported last year

Project 1 (Diabetes, PI Kavanagh)

Digestive Diseases Week, San Diego 2019; oral presentation. “Transforming Growth Factor ß1 Receptor Antagonist Therapy Improves Non-Alcoholic Hepatic Steatosis In A Novel Diet And Irradiated Mouse Model”
Federal Support was acknowledged.

Data from these studies were presented within invited seminars (“Intestinal Aging and Healthspan”) at The Barshop Institute for Longevity and Aging Studies, University of Texas Health Sciences Center, San Antonio, TX (March 2019), and the University of Tasmania School of Medicine. Hobart Tasmania Australia (May 2019).
Federal Support was acknowledged.

Project 2 (Radiation Induced Heart Disease, PI Register):

(PS7-25) Myocardial functional, structural, and cellular alterations in Rhesus Macaque survivors of ionizing radiation exposure Kristofer T. Michalson, DVM PhD; Dalane Kitzman, MD; Gregory O. Dugan, DVM; David L. Caudell, DVM PhD; J Mark. Cline, DVM PhD; Thomas C. Register, PhD Wake Forest School of Medicine, Winston-Salem, NC
Abstract will be presented at The 65th Radiation Research Society Annual Meeting 2019
Federal support acknowledged

Project 3 (Immune Recovery, PI Sempowski/Chen):

(PS7-22) Long-term T cell reconstitution in peripheral blood and lymphoid organs following total body irradiation (TBI) Yujing Zou; Xinhua Chen; Yiqun Jiao; Ying Huang; Xiaoli Nie; Xiaoyan Yang; Suijing Wu; Andrew Macintyre; Nelson Chao; Gregory Sempowski; and Benny Chen Duke University, Durham, NC
Abstract will be presented at The 65th Radiation Research Society Annual Meeting 2019
Federal support acknowledged

Project 4 (Genomics, PI Dave):

Nothing to report.

Other publications, conference papers, and presentations.

Overall: (PI Cline):

Project 1 Presentation, Program Annual Retreat, Wake Forest School of Medicine, October 16th 2019. Federal Support was acknowledged.

Rotating monthly presentations of project progress via WebEx to Progam Team.

Primate Radiation Survivor Core
J Mark Cline; John Olson; Greg Dugan; Rachel Andrews; Kylie Kavanagh; Daniel Bourland; David Hanbury; Ann Peiffer; Thomas Register; Ryne DeBo; David Caudell; Greg Sempowski and Nelson Chao
Centers for Medical Countermeasures against Radiation Annual Meeting, Rockville, MD, December 3-5, 2018
Federal Support was acknowledged.

Project 1 (Diabetes, PI Kavanagh):

Rotating monthly presentations of project progress via WebEx to Program Team.

Project 1 Presentation, Program Annual Retreat, Wake Forest School of Medicine, October 16th, 2019. Federal Support was acknowledged.

Project 2 (Radiation-Induced Heart Disease, PI Register):

Rotating monthly presentations of project progress via WebEx to Progam Team.

Project 3 Presentation, Program Annual Retreat, Wake Forest School of Medicine, October 16th, 2019
Federal Support was acknowledged.

Project 3 (Immune Recovery, PI Sempowski/Chen):

Rotating monthly presentations of project progress via WebEx to Progam Team.

Project 3 Presentation, Program Annual Retreat, Wake Forest School of Medicine, October 16th, 2019
Federal Support was acknowledged.

Project 4 (Genomics, PI Dave):

Rotating monthly presentations of project progress via WebEx to Progam Team.

- **Website(s) or other Internet site(s)**

Nothing to report

- **Technologies or techniques**

Nothing to report

- **Inventions, patent applications, and/or licenses**

Nothing to report

- **Other Products**

Overall (PI Cline):

Nothing to report.

Project 1 (Diabetes, PI Kavanagh):

Nothing to report.

Project 2 (Radiation Induced Heart Disease, PI Register):

Grant applications submitted and funded

Pathology Internal Pilot Grant Application (funded) $25,000 Thomas C. Register, PhD. “In Situ Molecular Profiling of Myocardial Responses to Ionizing Radiation in Rhesus Macaques” July 2017-June 2018

RADCCORE Pilot Grant Application (funded)
5U19AI067773-13 (Register-PI) $100,000 (Year 1) 08/01/17-07/31/18
“Monocyte Polarization in Acute and Delayed Responses to Total Body Irradiation in Nonhuman Primates” This project is designed to determine the effect of total body irradiation on circulating monocyte polarization and transcriptional programming in the acute and chronic phases post irradiation, and to explore relationships of these monocyte phenotypes with radiation induced conditions in male rhesus macaques.

Grant applications submitted and pending

Peer Reviewed Medical Research Program for a Discovery Award ($200,000, pending)
“Effects of Ionizing Radiation (IR) on Myocardial DNA Methylation Profiles in Relation to Cardiomyopathy in a Nonhuman Primate Model”. (Register-PI 2018)

Project 3 (Immune Recovery, PI Sempowski/Chen):

Nothing to report.

Project 4 (Genomics, PI Dave):

Nothing to report.

7. PARTICIPANTS & OTHER COLLABORATING ORGANIZATIONS

What individuals have worked on the project?

Core Primate Studies (Cline)

Name:	J. Mark Cline *No change*
Name:	Michael Benedict *No change*
Name:	Daniel Bourland *No change*
Name:	David Caudell *No change*
Name:	Janet Tooze *No change*
Name:	Jean Gardin *No change*
Name:	Matt Dwyer *No change*
Name:	Russell O'Donnell *No change*
Name:	Chrystal Bragg *Left lab for another position; replaced by McKinley Williams-McDowell*
Name:	McKinley Williams-McDowell *Replacement hire for Chrystal Bragg*
Name:	Renae Hall *No change*
Name:	Patricia Warren *No change*

Project 1 – Diabetes (Kavanagh)

Name:	Kylie Kavanagh *No change*

Name: Ashley Davis
No change

Name: Christina Sherrill
No change

Name: Cristina Furdui
No change

Name: Xiaofei Chen
Left the laboratory

Name Hanzhi Wu
Replacment for Xiaofei Chen

Project 2 – Radiation/Heart Disease (Register)

Name: Thomas Register
No change

Name: Sujethra Vasu
No change

Name: Craig Hamilton
No change

Name: James Bottoms
No change

Name: Maryanne Post
No change

Project 3 – Immune Recovery (Chen & Sempowski)

Name: Benny Chen
No change

Name: Gregory Sempowski
No change

Name: Lesslee Arwood
No change

Name: Xinhua Chen
Project Role: Visiting Scholar
Researcher Identifier (e.g. ORCID ID): N/A
Nearest person month worked: 6
Contribution to Project: Dr. Chen has performed flow cytometry experiments and data analyses

Name:	Laura Hale No change
Name:	Yiqun Jiao No change
Name:	Andrew Macintyre, PhD No Change
Name: Project Role: Researcher Identifier (e.g. ORCID ID): Nearest person month worked: Contribution to Project	Xiaoli Nie Visiting Scholar N/A 1 Dr. Nie has performed flow cytometry experiments and data analyses
Name:	Brittany Sanders, MS No change
Name:	Xiaoyan Yang No change
Name:	Yujing Zou No change

Project 4 - Genomic Sequencing and Stem Cell Lines (Duke Consortium – Dave)

Name:	Sandeep Dave No change
Name:	Anupama Reddy No change
Name:	Cassandra Love No change
Name:	Guojie Li No change
Name: Project Role: Researcher Identifier (e.g. ORCID ID): Nearest person month worked: Contribution to Project:	Qiu Qin Staff scientist N/A 3 (supported through non-DOD sources) Bioinformatics
Name: Project Role: Researcher Identifier (e.g. ORCID ID): Nearest person month worked:	Alexander Waldrop Staff scientist N/A 3 (supported through non-DOD sources)

Contribution to Project: Bioinformatics

Has there been a change in the active other support of the PD/PI(s) or senior/key personnel since the last reporting period?

J. Mark Cline (PI)

Changes in *Current* Support as reported in the original application:

Nothing to report

Daniel Bourland (Co-Investigator)

Changes in *Current* Support as reported since the last reporting period (annual report):

Project Title: Evaluation of a Red Duroc Porcine Model to Address Cutaneous Radiation Injury in Black (Type III/VI) Skin
Change: New award

Project Title: Biodosimetry for Irradiated Blood
Change: New award

David Caudell (Co-Investigator)

Changes in *Current* Support as reported since the last reporting period (annual report):

Project Title: Determining the Effects of Duavee on Pain and Lesion Volume In a Non-human primate Model of Naturally Occurring Endometriosis
Change: Project Complete

Christina Furdui (Co-Investigator)

Changes in *Current* Support as reported since the last reporting period (annual report):

Project: New Oxidation-Sensing Probes to Evaluate Mitochondrial Dysfunction in Lung Injury
Change: New Award

Project: Redox Biology and Medicine Training Program
Change: New Award

Project: Human Peroxiredoxin 3: A Novel Target for the Treatment of Mesothelioma
Change: New Award

Project: Bioenergetic and Epigenetic Reprogramming by Obesity in Sepsis
Change: New Award

Kylie Kavanagh (Co-Investigator)

Changes in *Current* Support as reported since the last reporting period (annual report):

Project Title: Age-Related Changes in Intestinal Function and Sarcopenia in Monkeys
Change: Project Complete

Project Title: Copper is a Host Effector in Protection Against Urinary Tract Infection
Change: New award

Project Title: Assessment of ARCUS Nuclease Driven Gene Editing Following Lipid Nanoparticle
Change: New award

Project Title: Assessment of the Pharmacological Effects of TAK-XXX in Obese Female Cynomolgus Monkeys
Change: New award

Thomas Register (Project 3 PI)

Changes in *Current* Support as reported in the original application:

Project Title: Monocyte Polarization in Acute and Delayed Responses to Totla Body Irradiation
Change: Project Complete

Project Title: Effects of Western & Mediterranean Diets on Metabolic & Neuropathologic Risk Factors for Alzheimer's Disease in Non-human Primates
Change: New award

Janet Tooze (Co-Investigator)

Changes in Current Support as reported since the last reporting period (annual report):

No changes to report

Greg Sempowski (Project 3 Co-PI - Duke)

Changes in Current Support as reported since the last reporting period (annual report):

No changes to report

Benny Chen (Project 3 Co-PI - Duke)

Changes in Current Support as reported since the last reporting period (annual report):

No changes to report

Sandeep Dave (Project 4 PI - Duke)

Changes in Current Support as reported since the last reporting period (annual report):

No changes to report

What other organizations were involved as partners?

Nothing to report

8. SPECIAL REPORTING REQUIREMENTS

COLLABORATIVE AWARDS: For collaborative awards, independent reports are required from BOTH the Initiating PI and the Collaborating/Partnering PI. A duplicative report is acceptable; however, tasks shall be clearly marked with the responsible PI and research site. A report shall be submitted to **https://ers.amedd.army.mil** for each unique award.

Not Applicable

QUAD CHARTS: If applicable, the Quad Chart (available on https://www.usamraa.army.mil) should be updated and submitted with attachments.

Appended

9. APPENDICES:

Attach all appendices that contain information that supplements, clarifies or supports the text. Examples include original copies of journal articles, reprints of manuscripts and abstracts, a curriculum vitae, patent applications, study questionnaires, and surveys, etc.

Three completed manuscripts are attached:

Caudell DL, Michalson KT, Andrews RN, Snow WW, Bourland JD, DeBo RJ, Cline JM, Sempowski GD, Register TC. Transcriptional Profiling of Non-Human Primate Lymphoid Organ Responses to Total-Body Irradiation. Radiat Res. 2019;192:40-52. PMID: 31059377.

Hale LP, Rajam G, Carlone GM, Jiang C, Owzar K, Dugan G, Caudell D, Chao N, Cline JM, Register TC, Sempowski GD. Late effects of total body irradiation on hematopoietic recovery and immune function in rhesus macaques. PLoS One. 2019;13;14(2):e0210663. PMID: 30759098; PMCID: PMC6373904.

Michalson KT, Macintyre AN, Sempowski GD, Bourland JD, Howard TD, Hawkins GA, Dugan GO, Cline JM, Register TC. Monocyte Polarization is Altered Post-Irradiation in Male Rhesus Macaques: Implications for Delayed Effects of Acute Radiation Exposure. Radiat Res. 2019 Aug;192(2):121-134. doi: 10.1667/RR15310.1

Long Term Follow-up of the Late Effects of Acute Radiation Exposure in Primates
Proposal Log Number PR141508

PI: J Mark Cline, DVM, PhD **Org:** Wake Forest Health Sciences **Award Amount:** $9,999,998

Study/Product Aim(s)

To study delayed effects of acute radiation exposure (DEARE) with a focus on our newly-described radiation-induced pathologies, through phenotypic and mechanistic studies, including:

1. Type 2 diabetes mellitus
2. Radiation-induced heart disease (RIHD)
3. Chronic immune impairment with restriction of the antigenic response repertoire; and
4. Radiation-specific genomic signatures underlying 1-3.

Approach

We will use unique nonhuman primate (NHP) resources, including a pre-existing long-term (10+ year) radiation-exposed survivor cohort and development of a prospective cohort allowing baseline pre-exposure assessments and 4 years of follow-up. Complementary immune, metabolic, and interventional studies to be done in mice. Priority will be given to pathways and strategies with high potential for translation to human exposures and outcomes.

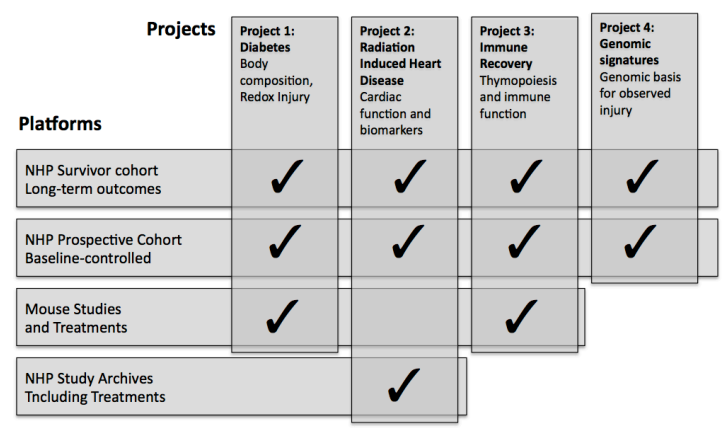


Figure 1. Schematic overview of the matrix relationship between populations of irradiated animals studied and investigative approaches used.

Accomplishments: NHP and mouse irradiation studies under way. Data collection and analysis in progress. Methods development in progress for some novel outcomes, as planned. Initial publications and abstracts, data presented at national meetings.

Timeline and Cost

Activities CY	15	16	17	18	19	20
Oversight/Core Primate Studies						
Proj 1 Diabetes						
Proj 2 Radiation/Heart Disease						
Proj 3 Immune Recovery						
Proj 4 Genomic sequencing and stem cell lines						
Estimated Budget ($K) ***Based on budget period 09/30/15 – 09/29/20. Budget period in ( ) after dollar amounts.***	1	2	3	4	5	

$2,150,541 (1)
$1,975,657 (2)
$2,030,283 (3)
$1,979,721 (4)
$1,863,796 (5)

Updated: October 29, 2019

Goals/Milestones

CY15 Goal – Program/Project "Kickoff"
- ☑ Regulatory approvals, establishment of admin structure, scheduling/ planning
- ☑ Animal acquisition and NHP quarantine & sampling/analysis, both cohorts

CY16 Goals – Prospective NHP studies begin, preliminary results presented nationally
- ☑ Exome sequencing and IPSCs from NHP studies (in progress)
- ☑ Irradiation of NHP prospective cohort and post-irradiation sampling/analysis for cardiac, redox, tissue composition, RNA profiling, and biomarker studies; presentation of early results (in progress)
- ☑ Mouse radiation studies: classic model

CY17 Goal – Continued NHP and mouse studies
- ☑ Mouse radiation studies: secondary model development
- ☑ Continued analysis of NHP composition/biomarkers as above based on preliminary results; presentation of data

CY18 Goal – Continued NHP and mouse studies
- ☐ Mouse intervention study of HGH and IGF-1 (phenotypic)
- ☑ Continued analysis of NHP composition/biomarkers as above; publication
- ☑ Preliminary cell lineage data from NHPs presented nationally

CY19 Goal – Continued NHP and mouse studies
- ☐ Mouse intervention study of HGH and IGF-1 (functional)
- ☑ Primate studies as above continue; publication

CY20 Goal – Analysis and publication of results
- ☐ Mouse intervention study of HGH and IGF-1 (mechanistic)
- ☐ Necropsy of prospective cohort, analysis of terminal outcomes; publication

Comments/Challenges/ Issues/Concerns
- No changes to timeline at this time
- No changes in quarterly expenditures at this time

Budget Expenditure to Date

Projected Expenditure:
$2,150,541
GY 2015/2016
$1,975,657
GY 2017
$2,030,283
GY 2018
$1,979,721
GY 2019

RADIATION RESEARCH **192**, 40–52 (2019)
0033-7587/19 $15.00
©2019 by Radiation Research Society.
All rights of reproduction in any form reserved.
DOI: 10.1667/RR15100.1

Transcriptional Profiling of Non-Human Primate Lymphoid Organ Responses to Total-Body Irradiation

David L. Caudell,[a,1] Kristofer T. Michalson,[a] Rachel N. Andrews,[a] William W. Snow,[a] J. Daniel Bourland,[b] Ryne J. DeBo,[a] J. Mark Cline,[a] Gregory D. Sempowski[c] and Thomas C. Register[a,1]

Departments of [a] Pathology, Section on Comparative Medicine and [b] Radiation Oncology, Wake Forest School of Medicine, Winston Salem, North Carolina; and [c] Department of Medicine, Duke University School of Medicine, Durham, North Carolina

Caudell, D. L., Michalson, K. T., Andrews, R. N., Snow, W. W., Bourland, J. D., DeBo, R. J., Cline, J. M., Sempowski, G. D. and Register, T. C. Transcriptional Profiling of Non-Human Primate Lymphoid Organ Responses to Total-Body Irradiation. *Radiat. Res.* 192, 40–52 (2019).

The global threat of exposure to radiation and its subsequent outcomes require the development of effective strategies to mitigate immune cell injury. In this study we explored transcriptional and immunophenotypic characteristics of lymphoid organs of a non-human primate model after total-body irradiation (TBI). Fifteen middle-aged adult, ovariectomized, female cynomolgus macaques received a single dose of 0, 2 or 5 Gy gamma radiation. Thymus, spleen and lymph node from three controls and 2 Gy (n = 2) and 5 Gy (n = 2) exposed animals were assessed for molecular responses to TBI through microarray-based transcriptional profiling at day 5 postirradiation, and cellular changes through immunohistochemical (IHC) characterization of markers for B and T lymphocytes and macrophages across all 15 animals at time points up to 6 months postirradiation. Irradiated macaques developed acute hematopoietic syndrome. Analysis of array data at day 5 postirradiation identified transcripts with ≥2-fold difference from control and a false discovery rate (FDR) of $P_{adj} < 0.05$ in lymph node (n = 666), spleen (n = 493) and thymus (n = 3,014). Increasing stringency of the FDR to $P < 0.001$ reduced the number of genes to 71 for spleen and 379 for thymus. IHC and gene expression data demonstrated that irradiated animals had reduced numbers of T and B lymphocytes along with relative elevations of macrophages. Transcriptional analysis revealed unique patterns in primary and secondary lymphoid organs of cynomolgus macaques. Among the many differentially regulated transcripts, upregulation of noncoding RNAs [*MIR34A* for spleen and thymus and *NEAT1* (*NCRNA00084*) for thymus] showed potential as biomarkers of radiation injury and targets for mitigating the effects of radiation-induced hematopoietic syndrome-impaired lymphoid reconstitution. © 2019 by Radiation Research Society

INTRODUCTION

Accidental or malicious exposure to ionizing radiation can result in rapid lymphocyte cell death, inflammation, immune suppression or death. Alterations in lymphocyte subset homeostasis, reduced ratios of naïve-to-memory lymphocytes, decreased lymphocyte function, altered T-cell receptor repertoires and suppressed immunity have all been reported as acute and subacute responses to radiation (*1–5*) and as late effects in atomic bomb survivors (*6–11*). Little is known about molecular and cellular changes that occur within the primary and secondary lymphoid organs, including the thymus, spleen and lymph nodes, during acute radiation injury in primates.

Macaques are a proven animal model of radiation injury (*4, 12*), since that they are genetically closely related to humans, with similar physiology and hormonal fluctuations, allowing high translatability of data generated. The majority of non-human primate (NHP) work in the field of radiation has focused on male rhesus macaques, although some work has also been conducted in cynomolgus macaques (*1, 12, 13*). Macaques exposed to radiation experience precipitous drops in their peripheral blood lymphocyte counts, and with subsequent lymphoid reconstitution exhibit homeostatic aberrations, similar to the late effects of atomic bomb survivors (*14–17*). Despite efforts to assess the dynamics in immune cell kinetics, few studies have identified cellular and molecular changes at the tissue level in the immune system of macaques after total-body irradiation (TBI), and there is a notable lack of published studies detailing radiation effects on lymphoid organs in female cynomolgus macaques.

Previously published work by our group evaluating the effects of TBI on female cynomolgus macaques demonstrated marked alterations in targeted molecular and general histologic characteristics of thymus, spleen and lymph node

Editor's note. The online version of this article (DOI: 10.1667/RR15100.1) contains supplementary information that is available to all authorized users.

[1] Address for correspondence: Department of Pathology, Section on Comparative Medicine, Wake Forest School of Medicine, Medical Center Boulevard, Winston Salem, NC 27157-1040; email: dcaudell@wakehealth.edu or register@wakehealth.edu.

Downloaded From: https://bioone.org/journals/Radiation-Research on 27 Aug 2019
Terms of Use: https://bioone.org/terms-of-use Access provided by Wake Forest University

TABLE 1
The Top Differentially Expressed Transcripts in Lymph Nodes of Irradiated Monkeys

Gene	0 Gy	2 Gy[a]	5 Gy[a]
Increased			
CFB	1	4.69	14.20
FOS	1	3.86	15.32
MIR34A	1	6.38	8.25
TYMS	1	4.71	7.48
SFRP4	1	3.74	6.07
Decreased			
HBB	1	–35.81	–51.71
XCL1	1	–11.00	–5.04
CNR1	1	–6.16	–8.85
FCRL3	1	–4.13	–7.94
IGHG1	1	–4.09	–7.86
FCRLA	1	–3.59	–6.04
MS4A1	1	–3.01	–6.17
TLR10	1	–2.69	–6.87
SMC3	1	–9.71	–1.27

[a] Fold changes are shown relative to 0 Gy control group. The threshold was fold change > 6 and $P_{adj} < 0.05$.

(*18*). The current study extends that work through the use of transcriptional profiling and immunohistochemistry (IHC) to identify key molecular pathways in these same tissues that were altered in response to TBI, and to explore changes in cell populations, with a long-term goal of generating hypotheses for identifying potential biomarkers and/or therapeutic molecular targets that could be used to develop mitigators of radiation injury. To achieve this goal, we conducted microarray-based transcriptional profiling and IHC-based evaluation of immune cell populations in thymus, spleen and lymph node from these same animals that received 0, 2 or 5 Gy TBI. The results extend previous work in this model and provide a broad profile of the responses of lymphoid organs to single dose TBI.

MATERIALS AND METHODS

Animals and Study Design

The overall design of this study is described elsewhere (*18*). Briefly, 15 ovariectomized, adult female cynomolgus monkeys (*Macaca fascicularis*) of Indonesian origin with median age of 20 years (ranging 15–24 years) and median weight of 3.03 kg (ranging 2.56–4.59 kg) were housed at the Wake Forest School of Medicine (WFSM; Winston Salem, NC). At baseline, complete blood counts and serum chemistries performed on each NHP were within normal limits and animals tested negative for simian retroviruses. The animals were randomly assigned to one of three groups receiving either 0 (n = 3), 2 (n = 6) or 5 (n = 6) Gy irradiation. Post-mortem examinations were planned at 5, 60 and 180 days postirradiation with two animals each of the 2 and 5 Gy groups assigned to each of these time points and three animals in the 0 Gy group. All animals survived to day 5, but not all animals survived to the end points scheduled at 60 and 180 days.

In this work, gene expression data are limited to the 0 Gy control (n = 3) animals and irradiated animals [2 Gy (n = 2), 5 Gy (n = 2)], which were necropsied on day 5 postirradiation. Immunohistochemical data are reported for all monkeys (n = 15).

Complete necropsy examination was performed on all animals either at the time of their humane end point or the end of the study. Complete animal demographic information including animal survival data was published previously [see Table 1 and ref. (*18*)]. The WFSM is accredited by the Association for the Assessment and Accreditation of Laboratory Animal Care. All experimental procedures were approved by the Wake Forest University Institutional Animal Care and Use Committee and the Guide for Care and Use of Laboratory Animals (*19*).

Diet

Prior to study initiation, the animals had consumed diets formulated at WFSM, which contained milk and soy proteins with varying soy isoflavone content (*20, 21*). Animals were transitioned initially to a laboratory chow diet (Purina LabDiet® Monkey Diet 5037, Richmond, IN) for three months and then were switched to a diet mimicking the nutritional intake of a typical Western diet for a minimum of two weeks prior to irradiation. The Western diet was produced in-house and contained 34% of calories as fat, 18% of calories as protein and 48% of calories as carbohydrates, and a moderately atherogenic cholesterol content of 0.20 mg/calorie. Protein was animal-sourced (casein, lactalbumin). Fats were 40% saturated, 34% monounsaturated and 26% polyunsaturated fatty acids. The animals had unlimited access to water and for environmental enrichment they were supplemented with fresh fruits and vegetables.

Irradiation

Non-human primates were sedated with ketamine (10 mg/kg) (Vedco Inc., St. Joseph, MO) and sequentially irradiated with two opposed lateral fields of 6-MV X rays at a dose rate of 60 cGy/min using a Varian 2100C linear accelerator (Varian Medical Systems, Inc., Palo Alto, CA) for single TBI doses of 0 (sham treatment), 2 or 5 Gy to the mid-plane. The radiation source was 120 cm from the skin.

Clinical Monitoring and Husbandry

Beginning on the day of irradiation, animals were administered prophylactic antibiotics including both enrofloxacin (5 mg/kg every 12 h; Bayer HealthCare LLC, Shawnee Mission, KS) and ceftazidime (30 mg/kg every 12 h; Patterson Veterinary, Devens, MA). Antibiotics were continued daily in all animals for up to 52 days after TBI or sham TBI. All monkeys were monitored daily for signs of radiation-induced illness including vomiting, diarrhea, weight loss, hemorrhage and alopecia. Using the methods of Uckun *et al*. (*22*) as modified from the Children's Cancer Group Clinical Toxicity Criteria, monkeys were evaluated for signs of hematologic failure or infection. The animals received supportive care as needed including parenteral fluids and supplemental nutrition. If animals became moribund or reached grade 4 toxicity, as previously defined in primate trials at WFSM (*23, 24*), they were humanely euthanized by intravenous pentobarbital overdose.

Transcriptional Profiling of Lymphoid Tissue

At necropsy, sections of spleen, thymus and inguinal lymph node tissue samples were preserved in RNA_{later} (Applied Biosystems, Foster City, CA) followed by storage at –80°C. RNA was extracted from tissues using TRI Reagent® (Applied Biosystems®, Foster City, CA), RNA content and purity was determined using a NanoDrop™ 2000 (Thermo Scientific™, Waltham, MA) and RNA quality was determined by measuring the RNA integrity number (RIN) with a 2100 Bioanalyzer (Agilent Technologies, Santa Clara, CA). RNA with RIN > 8.0 was used for downstream applications. Microarray procedures were performed by Cogenics (Morrisville, NC). Briefly, 1 μg of total RNA was assayed using GeneChip™ Rhesus Macaque Genome Arrays (Affymetrix® Inc., Waltham, MA) and the GeneChip One-Cycle Target Labeling Kit (Affymetrix), according to the manufacturer's recommended protocol. This microarray included

Downloaded From: https://bioone.org/journals/Radiation-Research on 27 Aug 2019
Terms of Use: https://bioone.org/terms-of-use Access provided by Wake Forest University

52,024 probe sets for approximately 47,000 transcripts. The labeled RNA was fragmented, hybridized to arrays for 17 h, washed and scanned. Scanned images were analyzed using GeneChip Operating Software (Affymetrix) to produce transcript intensity data.

Immunohistochemistry

Sections of spleen, thymus and axillary lymph nodes were collected at the time of necropsy and fixed in 4% paraformaldehyde. After fixation for a minimum of 24 h, tissues underwent routine processing, were embedded in paraffin, sectioned at 4 μm, stained with either hematoxylin and eosin (H&E) or primary antibodies for IHC and evaluated by light microscopy by one of two veterinary pathologists (JMC and DLC) (*25*). To evaluate the effects of radiation on the immune system, tissues from affected and clinically healthy control animals were stained for T cells (anti-CD3; Dako Inc., Carpinteria, CA, A0452, clone F7.2.38, 1:300 dilution), B cells (anti-CD20cy; Dako Inc., M0755, clone L26, 1:1500) and macrophages (Sigma-Aldrich® LLC, St. Louis, MO, 279M-16, clone HAM56, 1:50). All IHC was performed using a Leica Bond RX System (Leica Biosystems Inc., Buffalo Grove, IL). Vector® Red (Burlingame, CA) was the chromogen and tissues were counterstained with Mayer's hematoxylin. Slides were imaged using a BX61VS Olympus microscope (Olympus® Inc., Waltham, MA) and IHC was quantified using the custom programmable Visiopharm Integrator System (VIS) version 6.5.0.2303 (Hoersholm, Denmark) image analysis software.

Analyses

RNA data analysis. The transcript intensity data from the microarrays were analyzed using GeneSifter® Analysis Edition software (PerkinElmer® Inc., Waltham, MA). The expression profiling data described in this article are limited to the 0 Gy control and irradiated animals that were necropsied day 5 postirradiation [see Table 1 and ref. (*18*)]. Day 5 postirradiation transcript intensity data were RMA-normalized, converted to log2 scale and screened for heterogeneity among samples and groups. Sixty- and 180 day postirradiation data were not collected as planned due to unexpected animal deaths [see Table 1 and ref. (*18*)]. For a transcript to be considered differentially expressed between treatment groups, we set the cutoff filter at a fold change greater than two. We tested the data with supervised analysis of variance (ANOVA). *P* values were corrected for multiple comparisons using the Benjamini-Hochberg method (*26, 27*) to control the false discovery rate (FDR) to $P < 0.05$. Principal components analysis (PCA), pattern navigation, cluster analysis, heat mapping and Kyoto Encyclopedia of Genes and Genomes (KEGG) pathway analysis were performed on filtered data subsets and shared genes between all tissues using Genesifter and the Database for Annotation, Visualization and Integrated Discovery (DAVID) version 6.8 (*28, 29*). Euclidean distances representing the numeric difference between treatment vectors were calculated as part of hierarchical clustering dendrograms using average linkage (Supplementary Fig. S1; http://dx.doi.org/10.1667/RR15100.1.S1).

IHC data analysis. IHC data from all animals (5, 60 and 180 days, as well as unscheduled) were included in the analyses. Customized algorithms were developed using VIS® software for quantification of the total percentage area of positive IHC signal in each lymphoid tissue section. Data were pooled from animals across all time points for each tissue in the different irradiation groups and analyzed using ANOVA with Bonferroni correction for multiple comparisons. Due to limitations in the quantity of thymic tissue available at the time of necropsy, CD3 was not quantified for thymus in one monkey that received a 5 Gy dose of radiation, CD20 was not quantified for thymus in one monkey that received a 2 Gy dose of radiation and one that received a 5 Gy dose of radiation, and HAM56 was not quantified for thymus in one animal receiving a 2 Gy dose and two animals receiving a 5 Gy dose of radiation. $P < 0.05$ was considered significant and all data were analyzed using GraphPad Prism version 7 software (La Jolla, CA).

RESULTS

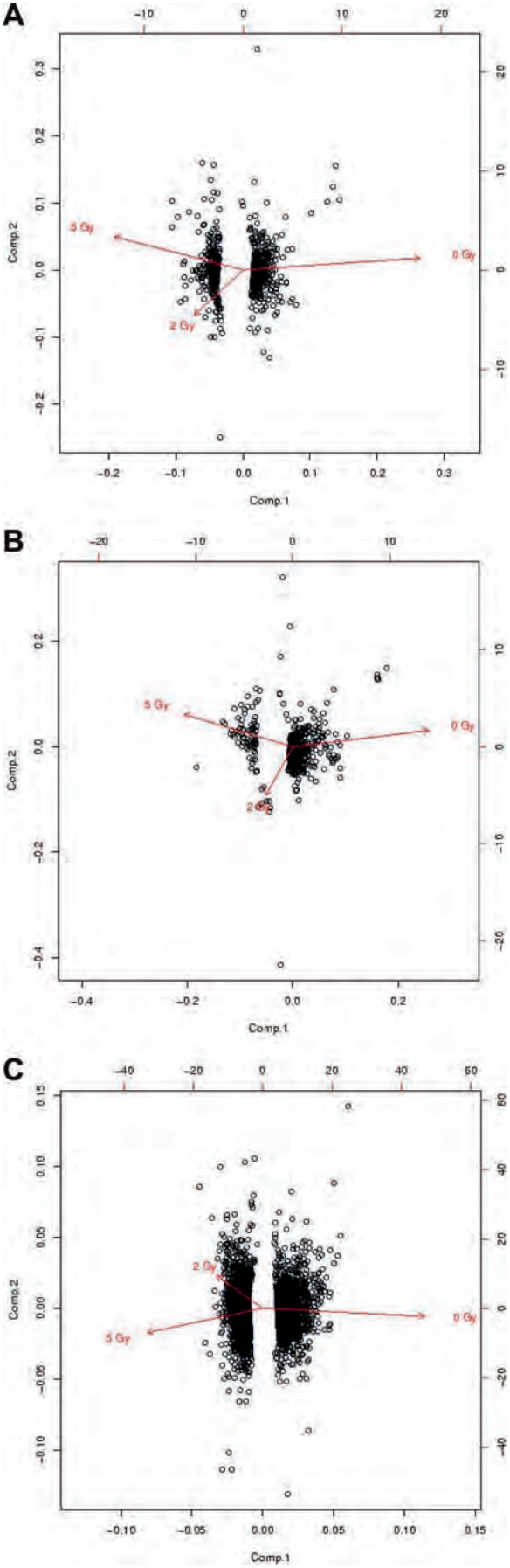
Effects of TBI on Transcriptional Profiles

Rhesus-specific gene microarrays included 52,024 probe sets for approximately 47,000 transcripts were used to evaluate gene expression signatures in the lymph node, spleen and thymus at days 0, 2 and 5 post-TBI. A total of 666 differentially expressed transcripts were identified in lymph node tissue (>2-fold change, $P_{adj} < 0.05$). The PCA of these 666 transcripts showed high clustering within treatment groups (Fig. 1A). To determine the transcripts with the greatest difference between groups, the filter was adjusted to >6-fold change (Table 1). The 666 lymph node transcripts with >2-fold change were analyzed for KEGG pathways with DAVID and ranked by fold enrichment (Table 2). The top four KEGG pathways identified were primary immunodeficiency, African trypanosomiasis and B-cell receptor signaling pathway and hematopoietic lineage.

A total of 493 differentially expressed transcripts were identified in spleen (>2-fold change, $P_{adj} < 0.05$). The PCA showed significant clustering of transcripts by exposure groups (Fig. 2B). To determine the transcripts with the greatest difference between groups the filter was adjusted to >6-fold change (Table 3). The following upregulated transcripts were identified after irradiation: *MIR34A*, *TYMS* and *DDB2*. The following downregulated transcripts were identified after irradiation: *HBB*, *MAMU-DQA1*, *TAC3*, *FCRL3*, *MS4A1*, *BCL11A*, *CD19*, *FCMR*, *IGHG1*, *AFF3*, *CXCR5*, *TLR10*, *FCRLA*, *TACSTD2*, *RFLNB*, *CD79A*, *LTB* and *WFDC21P*. The 493 splenic transcripts with >2-fold change were analyzed for KEGG pathways using DAVID and ranked by fold enrichment (Table 4). The top four KEGG pathways identified were primary immunodeficiency, intestinal immune network for IgA production, hematopoietic cell lineage and B-cell receptor signaling pathway.

A total of 3,014 differentially expressed transcripts were identified in the thymus (>2-fold change, $P_{adj} < 0.02$). Similar to spleen and lymph node, PCA showed high clustering of transcripts by exposure group (Fig. 1C). To determine the transcripts with the greatest difference between groups the filter was adjusted to >6-fold change (Table 5). The following upregulated transcripts were identified after irradiation: *KRT4*, *MIR34A*, *NEAT1*, *CEACAM5*, *SAA2*, *RNASE1*, *MGP*, *S100P*, *PTG1*, *HSPB1*, *APOD*, *FST*, *HOPX*, *TAGLN*, *RERGL*, *EPHA3*, *ANXA1*, *GSN*, *EFEMP1*, *IGHG1*, *PRELP*, *CP*, *COCH* and *KRT76*. The following downregulated transcripts were identified after irradiation: *UHRF1*, *TOP2A*, *NUSAP1*, *TMSB15A*, *CCNB2*, *E2F2*, *ARPP21*, *KIF14*, *DEPDC1B*, *COX8C*, *KIF15*, *CDK1*, *BUB1*, *CD1A*, *CD1B*, *KIF11*, *ST3GAL6*, *CKAP2*, *RAG1*, *SH2D1A*, *SLIT1*, *SCGB3A1*, *FOXM1*, *RAB11FIP4*, *CYP2U1*, *SPOCD1*, *CD1E*, *MNS1*, *ELOVL4*, *CD8A*, *CD8B*, *CHRNA3*, *CDCA7*, *HIST1H2AD*, *CYP2U1*,

Downloaded From: https://bioone.org/journals/Radiation-Research on 27 Aug 2019
Terms of Use: https://bioone.org/terms-of-use Access provided by Wake Forest University



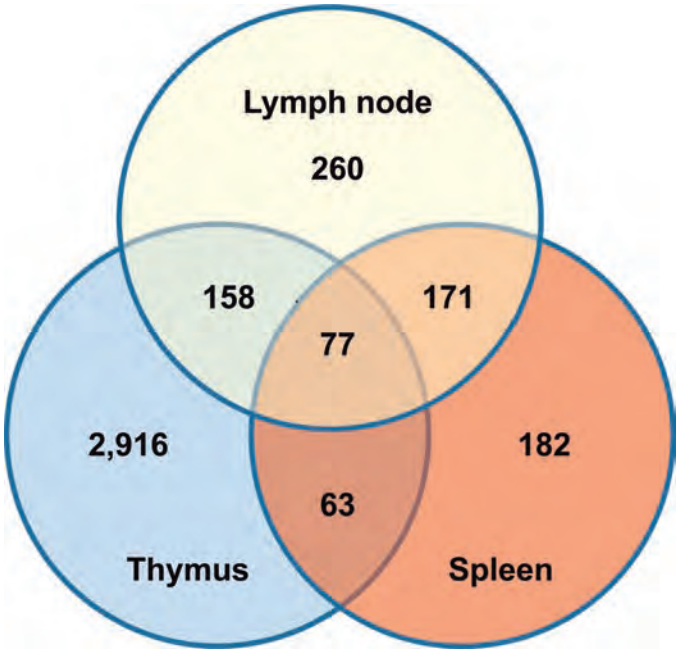


FIG. 2. Venn diagram showing shared differentially expressed transcripts among lymph node, spleen and thymus tissues. Filter was set at fold change > 2, $P_{adj} < 0.05$. A total of 77 differentially expressed transcripts were shared among the three tissue types.

RORC, *KCNJ10*, *GCSAM*, *KIF23*, *CCR9*, *ANLN*, *CD1C*, *MOB1B*, *TFDP2*, *TMEM171*, *CAMK4*, *CDK6*, *UBE2T*, *ATAD2*, *BCL2L1*, *LEF1*, *TFDP2*, *TCRB*, *BCL11B*, *DLEU2*, *PITPNM2*, *MPHOSPH9*, *ZNF711*, *SLC14A1*, *CD3G*, *THEMIS*, *AFF3* and *SMC3*. The 3,214 thymic transcripts with >2-fold change were analyzed for KEGG pathways with DAVID and ranked by fold enrichment (Table 6). The top four KEGG pathways identified were DNA replication, complement and coagulation cascades, ECM-receptor interaction and cell cycle.

A total of 77 differentially expressed transcripts were shared among the spleen, lymph node and thymus (Fig. 2). These transcripts were analyzed for KEGG pathways and ranked by fold enrichment. The three KEGG pathways identified were the p53 signaling pathway (fold enrichment: 16.2; genes: *BBC3*, *CDKN1A* and *ZMAT3*), HIF-1 signaling pathway (fold enrichment: 12.0; genes: *CDKN1A*, *ENO2* and *PRKCB*) and measles (fold enrichment: 9.8; genes: *BBC3*, *TNFRSF10B* and *PRKCQ*).

←

FIG. 1. PCA analysis of differentially expressed transcripts, obtained 5 days after 0, 2 and 5 Gy irradiation, in lymph node (panel A), spleen (panel B) and thymus (panel C). Filter was set at fold change > 2, $P_{adj} < 0.05$. These data show distinct differences between irradiated and control groups. For all tissues, the control and irradiated groups clustered separately from each other, and the vectors of the 2 and 5 Gy irradiated groups differed from each other, indicative of a dose response.

Downloaded From: https://bioone.org/journals/Radiation-Research on 27 Aug 2019
Terms of Use: https://bioone.org/terms-of-use Access provided by Wake Forest University

TABLE 2
Top Four KEGG Pathways of Differentially Expressed Transcripts in Lymph Nodes of Irradiated Monkeys

Pathway	Fold enrichment	*P*	Genes	Fold change 2 Gy[a]	Fold change 5 Gy
Primary immunodeficiency	10.6	0.0031	BLNK	–2.38	–2.23
			BTK	–1.69	–2.08
			CD19	–2.91	–5.34
			CD8A	–2.13	–2.81
			CD8B	–2.78	–3.28
African trypanosomiasis	7.5	0.015	FAS	2.01	2.47
			HBB	–35.84	–51.71
			IDO1	3.49	3.00
			PRKCB	–1.65	–2.28
B cell receptor signaling pathway	5.9	0.0011	BLNK	–2.38	–2.23
			BTK	–1.69	–2.08
			CD19	–2.91	–5.34
			CD72	–2.30	–2.75
			CR2	1.01	–2.04
			FOS	3.86	15.32
			RAC2	–1.69	–2.24
Hematopoietic cell lineage	5.7	0.00047	CD14	1.69	2.04
			CD19	–2.91	–5.34
			CD37	–2.35	–3.74
			CD8A	–2.13	–2.81
			CD8B	–2.78	–3.28
			CR2	1.01	–2.04
			FCGR1A	1.32	2.15
			MS4A1	–2.48	–5.83

[a] Fold changes relative 0 Gy control group.

Immunohistochemistry

The T- and B-lymphocyte and macrophage patterns in thymus, spleen and lymph node were evaluated by IHC. As expected, CD3 IHC resulted in staining of T cells in the periarteriolar lymphatic sheath in spleen, paracortex of lymph node and cortex and medulla of thymus. Likewise, CD20 IHC stained B cells in follicles of spleen and lymph node, and scattered throughout the medulla of thymus. Finally, HAM56 IHC staining was less intense in these tissues, but did stain scattered macrophages in follicles of spleen and lymph node and cortical sinus and medulla of lymph node. Control monkey thymus had little to no HAM56 staining.

In lymph nodes from animals that received 2 and 5 Gy TBI, a significant reduction ($P < 0.05$) of $CD3^+$ T cells was observed (Figs. 3A–C and 4B). Similarly, there was significant ($P < 0.05$) reduction in $CD20^+$ B cells in spleens from monkeys that received 2 and 5 Gy exposure and in lymph nodes of monkeys that received a 5 Gy dose (Figs. 3D–I and 4D and E). The limited number of sections available for $HAM56^+$ macrophage immunoreactivity did not allow for a useful statistical assessment of differences (Fig. 4G–I). No significant differences between groups were identified in thymus for any of the three immunomarkers (Fig. 4C, F and I), although there was a trend toward lower $CD3^+$ staining in the spleen of monkeys exposed to 5 Gy compared to 0 Gy controls (Fig. 4A, $P = 0.07$). As an alternative method of comparison, total mass of T cells within the spleen of each animal was estimated by multiplying spleen weight obtained at necropsy by percentage $CD3^+$ IHC area obtained using quantitative IHC. These estimated masses were compared using ANOVA with Bonferroni correction for multiple comparisons. There was significantly less $CD3^+$ mass in the spleen from animals that

TABLE 3
The Top Differentially Expressed Transcripts in Spleen of Irradiated Monkeys

Gene	0 Gy	2 Gy[a]	5 Gy[a]
Increased			
MIR34A	1	10.68	22.90
TYMS	1	3.05	8.04
DDB2	1	2.89	6.14
Decreased			
HBB	1	–37.55	–62.23
MAMU-DQA1	1	–17.51	–108.59
TAC3	1	–9.81	–10.46
FCRL3	1	–6.17	–14.13
MS4A1	1	–4.99	–17.23
BCL11A	1	–5.19	–14.77
CD19	1	–4.77	–13.34
FCMR	1	–4.76	–12.55
IGHG1	1	–4.23	–8.86
AFF3	1	–4.13	–8.86
CXCR5	1	–4.48	–7.46
TLR10	1	–3.19	–9.01
FCRLA	1	–4.41	–6.49
TACSTD2	1	–4.12	–6.35
RFLNB	1	–3.61	–6.23
CD79A	1	–3.57	–6.14
LTB	1	–3.11	–6.00
WFDC21P	1	–2.17	–6.43

[a] Fold changes are shown relative to 0 Gy control group. The threshold was fold change > 6 and $P_{adj} < 0.05$.

Downloaded From: https://bioone.org/journals/Radiation-Research on 27 Aug 2019
Terms of Use: https://bioone.org/terms-of-use Access provided by Wake Forest University

TABLE 4
Top Four KEGG Pathways of Differentially Expressed Transcripts in Spleens of Irradiated Monkeys

Pathway	Fold enrichment	*P*	Genes	Fold change 2 Gy[a]	Fold change 5 Gy
Primary immunodeficiency	10.6	0.0011	AICDA	–2.46	–3.79
			CD19	–4.77	–13.34
			IL2RG	–1.52	–2.14
			IL7R		
			PTPRC	–1.63	–2.61
Intestinal immune network for IgA production	9.5	0.00036	AICDA	–2.46	–3.79
			CXCR4	–1.93	–3.10
			ITGB7	–1.51	–2.54
			IL6	–3.72	–5.40
			HLA-DOB	–4.14	–4.95
			HLA-DPA1	–2.10	–1.35
Hematopoietic cell lineage	8.4	9.6E–6	CD19	–4.77	–13.34
			CD37	–2.40	–5.56
			CD5	–1.38	–2.23
			CD7	–1.87	–2.89
			CR1	–3.11	–4.12
			CR2	–6.43	–16.19
			IL6	–3.72	–5.40
			IL7R	–1.81	–3.35
			MS4A1	–4.27	–12.34
B cell receptor signaling pathway	7.7	0.00025	CARD11	–1.81	–2.22
			CD19	–4.77	–13.34
			CR2	–6.43	–16.19
			NFATC2	–1.45	–2.58
			RAC2	–1.70	–2.27
			SYK	–1.74	–2.85
			VAV2	–2.49	–2.41

[a] Fold changes relative to 0 Gy control group.

received either 2 or 5 Gy vs. 0 Gy dose ($P = 0.01$, data not shown). Similar analyses were done for CD20 and HAM56 and results were not different from data shown in Fig. 4.

Given the marked reduction in both T and B cells in secondary immune organs, we sought to determine if one population of lymphocytes was preferentially decreased over the other within the lymph node and spleen. To make this determination, the ratio of $CD3^+$ to $CD20^+$ IHC area was calculated for these tissues in each animal and compared using ANOVA with Bonferroni correction for multiple comparisons. As shown in Fig. 5A, there was a significant increase ($P < 0.05$) of the $CD3^+$:$CD20^+$ ratio in lymph node at 5 days after 5 Gy irradiation compared to 0 Gy control. This finding suggests greater loss of B cells compared to T cells at this early time point. The $CD3^+$:$CD20^+$ ratio was not significantly different from 0 Gy control animals at later times postirradiation.

DISCUSSION

The thymus, spleen and lymph nodes are primary and secondary lymphoid organs that are essential to the formation and maturation of lymphocytes necessary for acquired immunity. The effects of radiation on these organs can be both acute and long-term in individuals, manifesting as either life-threatening sepsis or impaired immunity as a result of inadequate lymphoid reconstitution.

Our study suggested a greater decrease in B cells than T cells in lymph node at 5 days postirradiation, consistent with the kinetics of relative loss of circulating $CD20^+$ B cells to $CD3^+$ T cells in male macaques after TBI reported elsewhere (*14*). Variable sensitivity of lymphocytes across immune organs was also identified. Although B- and T-cell populations had not recovered in the lymph node by 20 days after TBI (data not shown), the ratio of B to T cells at 20 days had returned to that seen in lymph node of 0 Gy control monkeys. It is possible that T-cell death was slower than B-cell death with both populations reaching approximately the same decline. Alternatively, B-cell populations may start recovering by 20 days due to repopulation of B cells in the lymph node. Regardless, these findings are consistent with several other studies in mice that demonstrated a higher sensitivity of B cells compared to T cells (*30–33*).

The highest ratio of $CD3^+$ T cells to $CD20^+$ B cells occurred at approximately 5 days in the lymph node. In general, a germinal center response to a particular antigen occurs over a seven-day period. This is a well-orchestrated process between T-follicular helper cells and B cells. Total-body irradiation is followed by a period in which the host is susceptible to death from sepsis from opportunistic infections due to bone marrow suppression and acute gastroenteritis. Our data suggest that at these doses TBI has the greatest effect on T and B cells in the lymph node during a time of great risk when early; and late initiation phases of

Downloaded From: https://bioone.org/journals/Radiation-Research on 27 Aug 2019
Terms of Use: https://bioone.org/terms-of-use Access provided by Wake Forest University

TABLE 5
The Top Differentially Expressed Transcripts in Thymus of Irradiated Monkeys

Increased				Decreased							
Gene	0 Gy	2 Gy[a]	5 Gy[a]	Gene	0 Gy	2 Gy[a]	5 Gy[a]	Gene	0 Gy	2 Gy[a]	5 Gy[a]
KRT4	1	26.92	16.08	UHRF1	1	–9.28	–53.07	CDCA7	1	–3.25	–11.22
MIR34A	1	7.26	10.32	TOP2A	1	–9.11	–36.81	HIST1H2AD	1	–6.54	–5.73
NEAT1	1	8.01	7.14	NUSAP1	1	–9.59	–27.20	CYP2U1	1	–4.09	–8.80
CEACAM5	1	8.20	6.78	TMSB15A	1	–9.52	–25.91	RORC	1	–4.34	–8.13
SAA2		8.20	5.97	CCNB2	1	–7.67	–24.53	KCNJ10	1	–5.29	–6.33
RNASE1	1	5.18	8.65	E2F2	1	–7.96	–21.63	GCSAM	1	–3.77	–8.71
MGP	1	5.38	8.00	ARPP21	1	–7.70	–20.51	KIF23	1	–4.41	–7.43
S100P	1	6.77	5.25	KIF14	1	–7.31	–20.62	CCR9	1	–3.33	–9.80
PTGE1	1	6.12	5.81	DEPDC1B	1	–7.25	–17.74	ANLN	1	–4.30	–7.46
HSPB1	1	5.56	6,20	COX8C	1	–8.12	–13.50	CD1C	1	–3.77	–8.31
APOD	1	4.46	7.44	KIF15	1	–7.00	–15.56	MOB1B	1	–3.71	–8.26
FST	1	6.54	4.95	CDK1	1	–6.20	–16.09	TFDP2	1	–3.84	–7.86
HOPX	1	6.47	5.00	BUB1	1	–4.78	–18.55	TMEM171	1	–4.08	–6.95
TAGLN	1	5.98	6.00	CD1A	1	–5.92	–14.48	CAMK4	1	–3.47	–8.06
RERGL	1	4.06	7.88	CD1B	1	–6.00	–12.26	CDK6	1	–3.51	–7.89
EPHA3	1	3.79	8.44	KIF11	1	–6.12	–10.75	UBE2T	1	–3.97	–6.92
ANXA1	1	6.23	5.10	ST3GAL6	1	–5.90	–10.52	ATAD2	1	–3.73	–7.27
GSN	1	4.77	6.55	CKAP2	1	–4.68	–13.11	BCL2L1	1	–3.60	–7.40
EFEMP1	1	4.86	6.24	RAG1	1	–6.75	–8.56	LEF1	1	–3.06	–8.60
IGHG1	1	3.20	8.75	SH2D1A	1	–4.87	–11.24	TFDP2	1	–3.76	–6.87
PRELP	1	4.01	6.83	SLIT1	1	–6.43	–8.51	TCRB	1	–3.61	–6.97
CP	1	2.10	6.83	SCGB3A1	1	–6.97	–7.50	BCL11B	1	–2.40	–10.43
COCH	1	1.35	8.18	FOXM1	1	–5.25	–9.63	DLEU2	1	–3.79	–6.55
KRT76	1	6.07	1.62	RAB11FIP4	1	–4.80	–10.12	PITPNM2	1	–3.80	–6.46
				CYP2U1	1	–4.75	–10.16	MPHOSPH9	1	–3.40	–6.54
				SPOCD1	1	–4.81	–9.62	ZNF711	1	–3.14	–6.26
				CD1E	1	–5.31	–8.64	SLC14A1	1	–2.47	–7.88
				MNS1	1	–6.03	–7.54	CD3G	1	–2.86	–6.79
				ELOVL4	1	–4.50	–9.20	THEMIS	1	–3.10	–6.18
				CD8A	1	–4.54	–8.68	AFF3	1	–2.81	–6.81
				CD8B	1	–4.27	–9.23	SMC3	1	–8.58	–1.90
				CHRNA3	1	–4.58	–8.09				

[a] Fold changes are shown relative to 0 Gy control group. The threshold was fold change > 6 and $P_{adj} < 0.05$.

germinal center formation would be helpful in battling radiation-induced gastrointestinal bacterial translocation. Our findings suggest that the cellular dynamics in lymph nodes are severely compromised at one of the most critical times necessary for mounting an immune response to pathogens.

Several transcripts from each tissue were associated with KEGG pathways related to hematopoietic cell lineage and primary immunodeficiency, most likely due to radiation-induced loss of lymphocyte populations. A number of the transcripts were dramatically downregulated, including those related to B cells including IgHG1 and MS4A1 in both spleen and lymph node, which was not surprising given the loss of B cells in these tissues, as shown by IHC.

MIR34A was one of the most highly upregulated transcripts observed in lymphoid tissues. In monkeys irradiated with 5 Gy, *MIR34a* was 22-fold higher in spleen, 8-fold higher in lymph node and 10-fold higher in thymus compared to controls. MIR34a is a highly conserved member of the mir34 family of noncoding microRNAs. In addition to its role as a tumor suppression miRNA, recently published studies have shown this miRNA represses Foxp1 activity, thus disrupting B-lymphocyte development (*34*). Furthermore, published studies of irradiated mice have shown that p53 targets *MIR34A* leading to apoptosis (*35–38*). The very high levels observed in TBI-associated lymphoid tissues here may be associated with lymphocytic p53-mediated apoptosis. Therefore, this particular miRNA may serve as a marker of dosimetry (*39, 40*) or possibly a target for mitigating the effects of radiation injury.

NEAT1, (aka Nuclear Paraspeckle Assembly Transcript 1, noncoding RNA 00084, *NCRNA00084*) is a 3.2-kb-long noncoding RNA that is a critical component of paraspeckle nuclear bodies. Thymic NEAT1 was upregulated up to 8-fold due to irradiation. It appears to be induced by DNA damage and genotoxic stress, is upregulated by p53, and may act as a transcriptional regulator of several genes associated with cell survival and cancer progression, including lymphocytic leukemias (*41, 42*).

Thymidylate synthetase (*TYMS* or TS), one of the most upregulated transcripts from spleen and lymph node, catalyzes the methylation of deoxyuridylate to deoxythymidylate and maintains the thymidine-5-prime monophosphate pool critical for DNA replication and repair (*43*).

Downloaded From: https://bioone.org/journals/Radiation-Research on 27 Aug 2019
Terms of Use: https://bioone.org/terms-of-use Access provided by Wake Forest University

TABLE 6
Top Four KEGG Pathways of Differentially Expressed Transcripts in Thymuses of Irradiated Monkeys

			Fold change					Fold change	
Fold enrichment	*P*	Genes	2 Gy[a]	5 Gy	Fold enrichment	*P*	Genes	2 Gy[a]	5 Gy
DNA replication					Cell cycle				
3.1	0.004	FEN1	–2.50	–3.61	2.9	9.7E–8	BUB1	–1.37	–18.55
		MCM2	–2.61	–3.72			BUB3	–1.07	–2.20
		MCM3	–3.04	–6.79			CCNA2	–1.23	–4.32
		MCM7	–2.72	–4.94			CCNB2	–1.41	–24.53
		POLA2	–1.75	–2.03			CCND1	2.73	2.42
		POLD1	–1.50	–2.10			CDC20	–1.36	–9.99
		POLD3	–1.57	–3.34			CDC25B	–2.04	–3.42
		RFC5	–2.60	–2.83			CDC25C	–2.71	–4.56
		RNASEH2B	–2.98	–3.20			CDC6	–1.42	–10.26
		RPA3	–2.39	–2.95			CDK1	–1.42	–16.09
Complement and coagulation cascades							CDK2	–1.16	–2.88
3.0	9.9E–5	C1R	3.24	3.40			CDK6	–1.19	–7.89
		C1S	3.30	4.91			CDKN1A	3.08	4.23
		C2	2.24	2.52			CDKN1C	3.03	4.39
		C3AR1	2.35	4.65			CHEK1	–1.40	–8.23
		C4B	2.16	2.67			ESPL1	–1.22	–3.21
		C5a	2.76	3.04			HDAC1	–1.74	–2.28
		C7	2.74	5.42			MAD1L1	–1.18	–2.24
		CFD	4.10	8.17			MAD2L1	–1.31	–6.97
		CFH	2.83	3.16			MCM2	–2.61	–3.72
		CR1	–2.18	–1.67			MCM3	–1.19	–6.79
		F3	4.49	2.89			MCM7	–1.15	–4.94
		PLAU	2.43	2.22			MYC	–2.02	–3.14
		PROS1	2.62	2.72			ORC3	–1.11	–2.31
		SERPINA1	1.94	2.71			PTTG1	–1.18	–6.86
		SERPING1	3.53	4.46			SMAD3	1.45	2.04
		TFPI	1.73	2.88			STAG2	–1.08	–2.11
		VWF	4.23	4.95			TFDP2	–1.21	–7.70
ECM-receptor interaction							TGFB3	2.64	2.50
2.9	1.7E–5	CD36	4.43	5.45			TTK	–5.86	–13.26
		COL4A1	3.70	4.07			WEE1	–1.27	–3.83
		COL4A5	3.67	4.31					
		COL4A6	3.78	5.63					
		COL5A2	2.75	2.70					
		COL6A1	4.04	4.02					
		COL6A3	4.74	4.99					
		FN1	4.83	3.95					
		ITGA3	2.63	3.60					
		ITGA4	–2.34	–3.18					
		ITGA6	–2.63	–1.75					
		ITGA8	2.31	4.53					
		ITGB5	3.27	4.26					
		LAMA2	2.70	4.18					
		LAMA5	2.99	3.19					
		LAMB1	1.96	2.48					
		LAMB2	2.69	3.15					
		LAMC1	3.25	4.52					
		SDC1	3.22	4.47					
		THBS1	3.15	3.35					
		VWF	4.23	4.95					

[a] Fold changes relative to 0 Gy controls.

Increases in *TYMS* in response to radiation suggest that cells present within these tissues were actively repairing radiation-induced DNA damage.

Toll-like receptor 10 (*TLR10*) was one of the most differentially decreased transcripts in irradiated spleen and lymph node. Studies have shown that *TLR10* may play a role in the pathogenesis of lymphoma (*44*) and is expressed by $IgM^+IgD^+CD27^+$ B cells (*45*) suggesting a role in development and maintenance of this subpopulation of B cells in humans. Marginal zone B cells are generated in the spleen and are important for early defense against bacterial pathogens such as *Streptococcus pneumoniae*, by responding to capsular polysaccharides (*46*). Published studies of mice have shown enhanced radiosensitivity of marginal

Downloaded From: https://bioone.org/journals/Radiation-Research on 27 Aug 2019
Terms of Use: https://bioone.org/terms-of-use Access provided by Wake Forest University

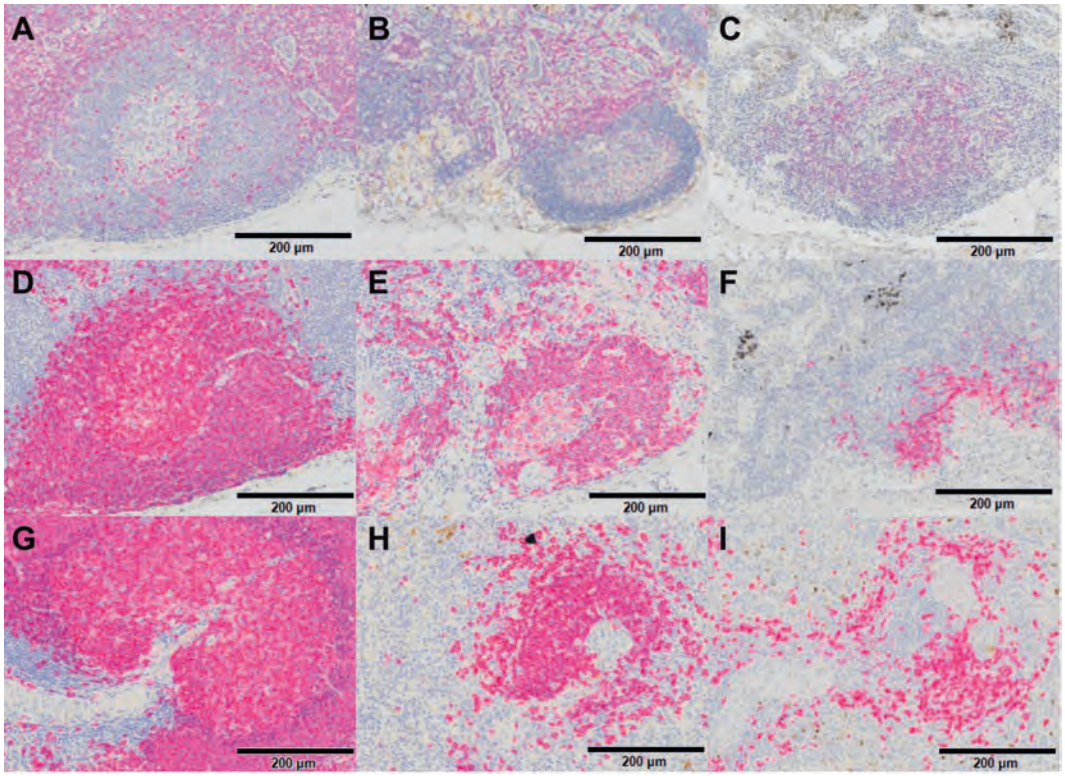


FIG. 3. Photomicrographs of IHC stains of lymphoid tissues from control and irradiated animals. Panels A–C: IHC staining for CD3 in lymph node from 0, 2 and 5 Gy irradiated animals, respectively. Panels D–F: IHC staining for CD20 in lymph node from 0, 2 and 5 Gy irradiated animals, respectively. Panels G–I: IHC staining for C20 in spleen from 0, 2 and 5 irradiated Gy animals.

zone B cells relative to other B-cell populations (*47, 48*). The TLR10 reductions in lymph node and spleen may reflect greater radiosensitivity of marginal zone B cells. Loss of this subset of B cells would place individuals exposed to radiation at increased risk of invasive infection by encapsulated bacteria. Interestingly, one 5 Gy irradiated monkey in this study succumbed to sepsis and had bacterial colonies in the lungs despite administration of prophylactic antibiotics (*18*).

Hemoglobin subunit beta (*HBB*) was the most downregulated transcript among differentially expressed genes in the spleen (by 62-fold) and lymph node (by 51-fold) in monkeys exposed to 5 Gy TBI. *HBB* encodes the beta hemoglobin subunit, which interacts with the *HBA* alpha subunit to form the hemoglobin molecule in erythrocytes. It is possible that the diminution of *HBB* expression is reflective of reduced tissue content of viable erythrocytes, since *HBB* has been used as a biomarker for blood (*49*). The potential function of this transcript in normal spleen and lymph node tissue in not clear, although expression of *HBB* in the absence of *HBA* expression occurs, and reductions in *HBB* expression in tumor cells have been associated with increased apoptotic responses to reactive oxygen species (*50*). *BCL11A*, another transcript, which was significantly decreased in spleen from irradiated monkeys, has been linked to *HBB* expression. *BCL11A* encodes a zinc finger transcription factor, which interacts with the HMG-box-containing transcription factor *SOX6* to facilitate switching of expression of fetal hemoglobin subunit gamma to *HBB* in adult human erythroid cells (*51*). Yu and colleagues describe *BCL11A* as having a binding site 85 kb upstream of the HBB gene in the mouse (*52*). They also demonstrated that *BCL11A* is essential for early B cells and common lymphoid progenitor cells to survive and proliferate. The reduced expression of *HBB* might be due to the decreased *BCL11A*, which might be downregulated due to apoptotic signaling triggered by radiation-induced DNA damage. Alternatively, reduced *HBB* and *BCL11A* may be related to diminished viable erythrocytes in irradiated tissues (*53*). Further investigation of the origin of decreases in these transcripts is warranted. It is possible that therapies aimed at enhancing *BCL11A* activity may mitigate radiation-induced lympho-depletion, particularly in B cells.

In our previously published study (*18*), we showed a decrease in thymopoiesis in irradiated monkeys as evidenced by decreased T-cell receptor excision circle (TREC) output. In this study transcriptional profiling revealed that the transcription factor *E2F2*, a target of retinoblastoma protein responsible for controlling the G_1-S phase of the cell cycle was one of the most differentially decreased transcripts in thymus (21-fold lower in the 5 Gy irradiated group). In contrast, Murga *et al.* (*54*) reported that *E2F2*$^{-/-}$ knockout mice had enhanced T-cell proliferation and accumulated autoreactive effector/memory T lymphocytes,

Downloaded From: https://bioone.org/journals/Radiation-Research on 27 Aug 2019
Terms of Use: https://bioone.org/terms-of-use Access provided by Wake Forest University

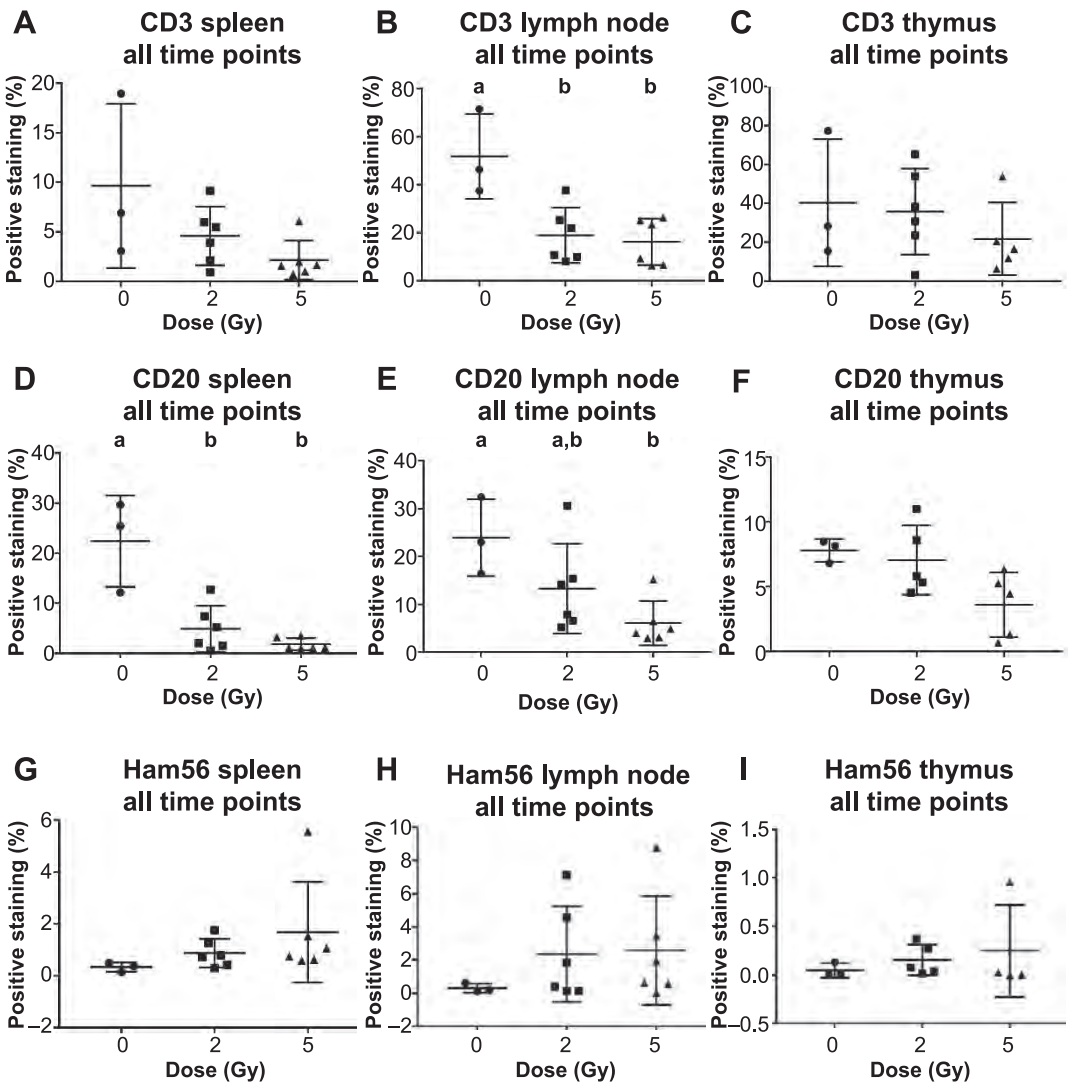


FIG. 4. Percentage area positive by IHC in tissues at 5 days after 0, 2 and 5 Gy irradiation. Panels A–C: Comparison of $CD3^+$ positive staining in spleen, lymph node and thymus, respectively. Panels D–F: Comparison of CD20 staining in spleen, lymph node and thymus, respectively. Panel G–I: Comparison of HAM56 staining in spleen, lymph node and thymus, respectively. Data were analyzed using ANOVA with Bonferroni correction for multiple comparisons. Groups with differing letters (a or b) are significantly different from one another ($P < 0.05$). Data are mean ± standard deviation (SD).

suggesting that *E2F2* represses transcriptional activity necessary for normal S-phase entry. A potential explanation for decreased E2F2 levels in thymus of irradiated monkeys is that lymphocyte progenitor cells downregulate expression of this gene as part of a proliferative response. However, the response is not enough to overcome massive loss of progenitor cells; therefore, TREC output is decreased overall despite the upregulation of proliferation by the few surviving progenitor cells.

We previously demonstrated reductions in thymus weight, thymopoiesis and bone marrow cellularity in these animals, and qRT-PCR data demonstrated alterations in T-cell markers (reduced CD3 in thymus and spleen) and macrophage markers (increased CD68), suggestive of increased macrophage/T-cell ratios in lymphoid tissues from irradiated animals (*18*). IHC immunoreactivity for the macrophage marker HAM56 also tended to be elevated in these tissues in the current study, although not significantly different from controls, perhaps due to low numbers of animals, and undersampling of tissues by IHC (single sections of tissues) versus PCR data, which represent a larger tissue sample. In addition, the exact epitope and gene product responsible for HAM56 immunoreactivity has yet to be identified.

Strengths of the current study include the use of a NHP model, the simultaneous exploration of gene expression and cellular marker IHC in multiple lymphoid organs, the use of two different radiation doses, which were carefully monitored and administered and a well-established protocol for monitoring animal health. Limitations of the study relate

Downloaded From: https://bioone.org/journals/Radiation-Research on 27 Aug 2019
Terms of Use: https://bioone.org/terms-of-use Access provided by Wake Forest University

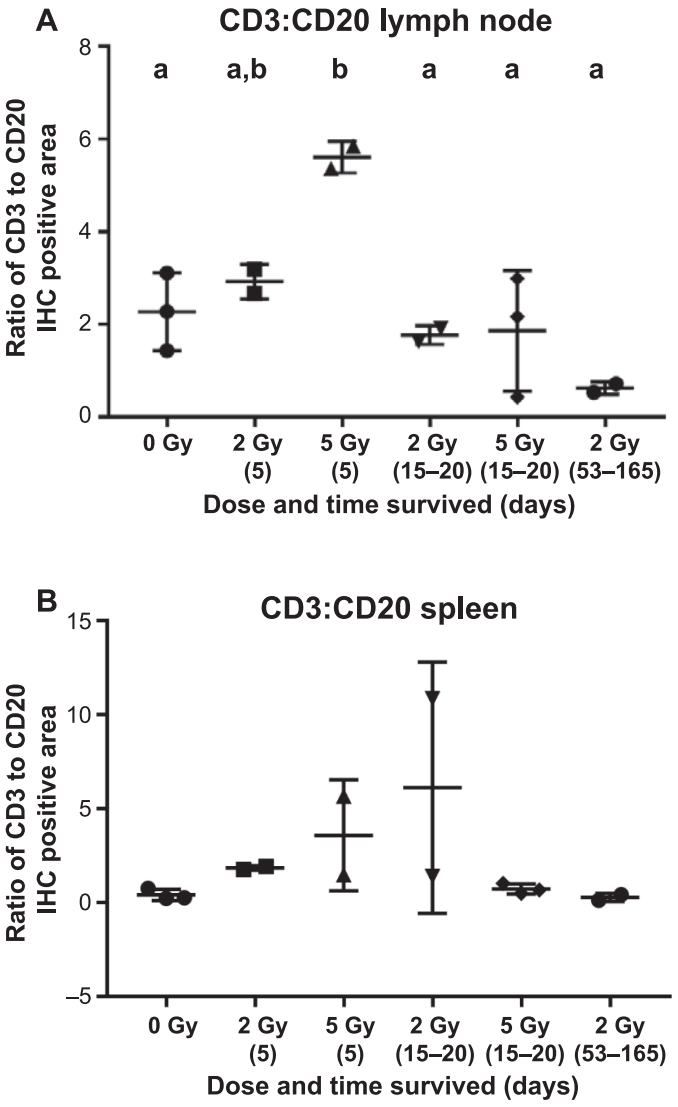


FIG. 5. Ratio of CD3 to CD20 percentage area positive by IHC in tissues at 5, 15–20 or 53-165 days after 0, 2 and 5 Gy. Panel A: Comparison of CD3:CD20 ratio in lymph node. Panel B: Comparison of CD3:CD20 ratio in spleen. Data were analyzed using ANOVA with Bonferroni correction for multiple comparisons. Groups with differing letters (a or b) are significantly different from one another ($P < 0.05$). Data are the mean ± SD.

primarily to the small number of animals and individual cells, although the strong responses of lymphoid tissues to radiation exposure allowed us to evaluate global responses for hypothesis generation. The 2 and 5 Gy radiation doses were determined to be sublethal based on previous work in male rhesus monkeys and were selected as a starting point. Assessing a broader range of doses which would be likely to occur in a malicious event was beyond the scope of this project. The use of ovariectomized female cynomolgus monkeys, as a model, is both a strength and a weakness in the current study. This paradigm has been useful in modeling surgical menopause in women, and many studies have demonstrated that monkeys respond to ovariectomy, and to exogenous hormone regimens, with remarkable similarity to that observed in women. Nevertheless, they represent a somewhat restricted population, and since we did not simultaneously study males or premenopausal females, we cannot make gender-based comparisons or draw conclusions relating to relative susceptibilities to radiation exposure.

In summary, cellular changes and unique gene expression profiles in primary and secondary lymphoid organs were identified in female cynomolgus macaques after TBI. Many of the targets identified correlated with loss of immune cells during a critical time of immune function after TBI and potential pathogen exposure. These data are useful for generating hypotheses for acute responses to radiation in lymphoid organs and for potential identification of targets for pharmacologic preservation of immunity after radiation exposure, developing strategic vaccine regimens and identifying mitigating agents for treatment after radiation exposure.

SUPPLEMENTARY INFORMATION

Fig. S1. Hierarchical clustering dendrogram of RNA microarray transcript data from thymuses of monkeys receiving 0, 2 or 5 Gy TBI. Produced using Genesifter with filter set at fold change > 2 and $P_{adj} < 0.05$.

ACKNOWLEDGMENTS

We thank the staff of the Animal Resources Program for technical support. This work was supported by a pilot grant (to T.C.R. and G.D.S.) and other funding from the Radiation Countermeasure Center for Research Excellence (grant no. NIH U19 AI067798), as well as NIH grant no. T32 OD010957, the Department of Defense (DOD grant no. W81XWH-15-1-0574), an NCI Cancer Center Support Grant (P30CA012197) to the Comprehensive Cancer Center of Wake Forest Baptist Medical Center and an equipment grant from the North Carolina Biotechnology Center (no. 2015-IDG-1006). We also acknowledge the support of the Comparative Pathology Laboratory Shared Resources of the Comprehensive Cancer Center of Wake Forest Baptist Medical Center.

Received: March 28, 2018; accepted: April 15, 2019; published online: May 6, 2019

REFERENCES

1. Chen BJ, Deoliveira D, Spasojevic I, Sempowski GD, Jiang C, Owzar K, et al. Growth hormone mitigates against lethal irradiation and enhances hematologic and immune recovery in mice and nonhuman primates. PLoS One 2010; 5:e11056.
2. Farese AM, Cohen MV, Katz BP, Smith CP, Jackson W 3rd, Cohen DM, et al. A nonhuman primate model of the hematopoietic acute radiation syndrome plus medical management. Health Phys 2012; 103:367–82.
3. Singh VK, Newman VL, Berg AN, MacVittie TJ, Animal models for acute radiation syndrome drug discovery. Expert Opin Drug Discov 2015; 10, 497–517.
4. Singh VK, Olabisi AO. Nonhuman primates as models for the discovery and development of radiation countermeasures. Expert Opin Drug Discov 2017; 12:695–709.
5. Vorobiev AI. Acute radiation disease and biological dosimetry in 1993. Stem Cells 1997; 15:269–74.
6. Akiyama M. Late effects of radiation on the human immune

Downloaded From: https://bioone.org/journals/Radiation-Research on 27 Aug 2019
Terms of Use: https://bioone.org/terms-of-use Access provided by Wake Forest University

system: an overview of immune response among the atomic-bomb survivors. Int J Radiat Biol 1995; 68:497–508.

7. Kusunoki Y, Hayashi T. Long-lasting alterations of the immune system by ionizing radiation exposure: implications for disease development among atomic bomb survivors. Int J Radiat Biol 2008; 84:1–14.
8. Kusunoki Y, Kyoizumi S, Hirai Y, Suzuki T, Nakashima E, Kodama K, et al. Flow cytometry measurements of subsets of T, B and NK cells in peripheral blood lymphocytes of atomic bomb survivors. Radiat Res 1998; 150:227–36.
9. Kusunoki Y, Yamaoka M, Kasagi F, Hayashi T, Koyama K, Kodama K, et al. T cells of atomic bomb survivors respond poorly to stimulation by Staphylococcus aureus toxins in vitro: does this stem from their peripheral lymphocyte populations having a diminished naive CD4 T-cell content? Radiat Res 2002; 158:715–24.
10. Kusunoki Y, Yamaoka M, Kasagi F, Hayashi T, MacPhee DG, Kyoizumi S. Long-lasting changes in the T-cell receptor V beta repertoires of CD4 memory T-cell populations in the peripheral blood of radiation-exposed people. Br J Haematol 2003; 122:975–84.
11. Kusunoki Y, Yamaoka M, Kubo Y, Hayashi T, Kasagi F, Douple EB, et al. T-cell immunosenescence and inflammatory response in atomic bomb survivors. Radiat Res 2010; 174:870–6.
12. Thrall KD, Love R, O'Donnell KC, Farese AM, Manning R, MacVittie TJ. An interlaboratory validation of the radiation dose response relationship (DRR) for H-ARS in the rhesus macaque. Health Phys 2015; 109:502–10.
13. Shetty G, Uthamanthil RK, Zhou W, Shao SH, Weng CC, Tailor RC, et al. Hormone suppression with GnRH antagonist promotes spermatogenic recovery from transplanted spermatogonial stem cells in irradiated cynomolgus monkeys. Andrology 2013; 1:886–98.
14. Farese AM, Hankey KG, Cohen MV, MacVittie TJ. Lymphoid and myeloid recovery in rhesus macaques following total body x-irradiation. Health Phys 2015; 109:414–26.
15. MacVittie TJ, Bennett AW, M VC, Farese AM, Higgins A, Hankey KG, Immune cell reconstitution after exposure to potentially lethal doses of radiation in the nonhuman primate. Health Phys 2014; 106:84–96.
16. MacVittie TJ, Farese AM, Jackson W 3rd, The hematopoietic syndrome of the acute radiation syndrome in rhesus macaques: A systematic review of the lethal dose response relationship. Health Phys 2015; 109:342–66.
17. Meyer C, Walker J, Dewane J, Engelmann F, Laub W, Pillai S, et al. Impact of irradiation and immunosuppressive agents on immune system homeostasis in rhesus macaques. Clin Exp Immunol 2015; 181:491–510.
18. DeBo RJ, Register TC, Caudell DL, Sempowski GD, Dugan G, Gray S, et al. Molecular and cellular profiling of acute responses to total body radiation exposure in ovariectomized female cynomolgus macaques. Int J Radiat Biol 2015; 91:510–8.
19. Council NR. Guide for the care and use of laboratory animals: 8th ed. Washington, DC: National Academies Press; 2011.
20. Adams MR, Anthony MS, Chen H, Clarkson TB. Replacement of dietary soy protein isolate with concentrates of soy 7S or 11S globulin has minimal or no effects on plasma lipoprotein profiles and biomarkers of coronary risk in monkeys. Atherosclerosis 2008; 196:76–80.
21. Wood CE, Clarkson TB, Appt SE, Franke AA, Boue SM, Burow ME, et al. Effects of soybean glyceollins and estradiol in postmenopausal female monkeys. Nutr Cancer 2006; 56:74–81.
22. Uckun FM, Yanishevski Y, Tumer N, Waurzyniak B, Messinger Y, Chelstrom LM, et al. Pharmacokinetic features, immunogenicity, and toxicity of B43(anti-CD19)-pokeweed antiviral protein immunotoxin in cynomolgus monkeys. Clin Cancer Res 1997; 3:325–37.
23. Cohen KA, Liu TF, Cline JM, Wagner JD, Hall PD, Frankel AE. Toxicology and pharmacokinetics of DT388IL3, a fusion toxin consisting of a truncated diphtheria toxin (DT388) linked to human interleukin 3 (IL3), in cynomolgus monkeys. Leuk Lymphoma 2004; 45:1647–56.
24. Hotchkiss CE, Hall PD, Cline JM, Willingham MC, Kreitman RJ, Gardin J, et al. Toxicology and pharmacokinetics of DTGM, a fusion toxin consisting of a truncated diphtheria toxin (DT388) linked to human granulocyte-macrophage colony-stimulating factor, in cynomolgus monkeys. Toxicol Appl Pharmacol 1999; 158:152–60.
25. DeBo RJ, Lees CJ, Dugan GO, Caudell DL, Michalson KT, Hanbury DB, et al. Late effects of total-body gamma irradiation on cardiac structure and function in male rhesus macaques. Radiat Res 2016; 186:55–64.
26. Benjamini Y, Hochberg Y. Controlling the false discovery rate: A practical and powerful approach to multiple testing. J R Stat Soc Series B Stat Methodol 1995; 57:289–300.
27. Reiner A, Yekutieli D, Benjamini Y. Identifying differentially expressed genes using false discovery rate controlling procedures. Bioinformatics 2003; 19:368–75.
28. Huang da W, Sherman BT, Lempicki RA. Bioinformatics enrichment tools: paths toward the comprehensive functional analysis of large gene lists. Nucleic Acids Res 2009; 37:1–13.
29. Huang da W, Sherman BT, Lempicki RA. Systematic and integrative analysis of large gene lists using DAVID bioinformatics resources. Nat Protoc 2009; 4:44–57.
30. Chambers KA, Harrington NP, Ross WM, Filion LG. Relative alterations in blood mononuclear cell populations reflect radiation injury in mice. Cytometry 1998; 31:45–52.
31. Garg S, Boerma M, Wang J, Fu Q, Loose DS, Kumar KS, et al. Influence of sublethal total-body irradiation on immune cell populations in the intestinal mucosa. Radiat Res 2010; 173:469–78.
32. Harrington NP, Chambers KA, Ross WM, Filion LG. Radiation damage and immune suppression in splenic mononuclear cell populations. Clin Exp Immunol 1997; 107:417–24.
33. Pecaut MJ, Nelson GA, Gridley DS. Dose and dose rate effects of whole-body gamma-irradiation: I. Lymphocytes and lymphoid organs. In Vivo 2001; 15:195–208.
34. Rao DS, O'Connell RM, Chaudhuri AA, Garcia-Flores Y, Geiger TL, Baltimore D. MicroRNA-34a perturbs B lymphocyte development by repressing the forkhead box transcription factor Foxp1. Immunity 2010; 33:48–59.
35. Chang TC, Wentzel EA, Kent OA, Ramachandran K, Mullendore M, Lee KH, et al. Transactivation of miR-34a by p53 broadly influences gene expression and promotes apoptosis. Mol Cell 2007; 26:745–52.
36. He L, He X, Lim LP, de Stanchina E, Xuan Z, Liang Y, et al. A microRNA component of the p53 tumour suppressor network. Nature 2007; 447:1130–4.
37. Raver-Shapira N, Marciano E, Meiri E, Spector Y, Rosenfeld N, Moskovits N, et al. Transcriptional activation of miR-34a contributes to p53-mediated apoptosis. Mol Cell 2007; 26:731–43.
38. Welch C, Chen Y, Stallings RL. MicroRNA-34a functions as a potential tumor suppressor by inducing apoptosis in neuroblastoma cells. Oncogene 2007; 26:5017–22.
39. Kato M, Paranjape T, Muller RU, Nallur S, Gillespie E, Keane K, et al. The mir-34 microRNA is required for the DNA damage response in vivo in C. elegans and in vitro in human breast cancer cells. Oncogene 2009; 28:2419–24.
40. Rana S, Kumar R, Sultana S, Sharma RK. Radiation-induced biomarkers for the detection and assessment of absorbed radiation doses. J Pharm Bioallied Sci 2010; 2:189–96.
41. Adriaens C, Standaert L, Barra J, Latil M, Verfaillie A, Kalev P, et al. p53 induces formation of NEAT1 lncRNA-containing paraspeckles that modulate replication stress response and chemosensitivity. Nat Med 2016; 22:861–8.

Downloaded From: https://bioone.org/journals/Radiation-Research on 27 Aug 2019
Terms of Use: https://bioone.org/terms-of-use Access provided by Wake Forest University

42. Blume CJ, Hotz-Wagenblatt A, Hullein J, Sellner L, Jethwa A, Stolz T, et al. p53-dependent non-coding RNA networks in chronic lymphocytic leukemia. Leukemia 2015; 29:2015–23.

43. Greenberg DM, Nath R, Humphreys GK. Purification and properties of thymidylate synthetase from calf thymus. J Biol Chem 1961; 236:2271–6.

44. Fonte E, Agathangelidis A, Reverberi D, Ntoufa S, Scarfo L, Ranghetti P, et al. Toll-like receptor stimulation in splenic marginal zone lymphoma can modulate cell signaling, activation and proliferation. Haematologica 2015; 100:1460–8.

45. Weller S, Bonnet M, Delagreverie H, Israel L, Chrabieh M, Marodi L, et al. IgM+IgD+CD27+ B cells are markedly reduced in IRAK-4-, MyD88-, and TIRAP- but not UNC-93B-deficient patients. Blood 2012; 120:4992–5001.

46. Kruetzmann S, Rosado MM, Weber H, Germing U, Tournilhac O, Peter HH, et al. Human immunoglobulin M memory B cells controlling Streptococcus pneumoniae infections are generated in the spleen. J Exp Med 2003; 197:939–45.

47. Kroese FG, Wubbena AS, Nieuwenhuis P. Germinal centre formation and follicular antigen trapping in the spleen of lethally X-irradiated and reconstituted rats. Immunology 1986; 57:99–104.

48. Riggs JE, Lussier AM, Lee SK, Appel MC, Woodland RT. Differential radiosensitivity among B cell subpopulations. J Immunol 1988; 141:1799–807.

49. Su CW, Li CY, Lee JC, Ji DD, Li SY, Daniel B, et al. A novel application of real-time RT-LAMP for body fluid identification: using HBB detection as the model. Forensic Sci Med Pathol 2015; 11:208–15.

50. Zheng Y, Miyamoto DT, Wittner BS, Sullivan JP, Aceto N, Jordan NV, et al. Expression of beta-globin by cancer cells promotes cell survival during blood-borne dissemination. Nat Commun 2017; 8:14344.

51. Xu J, Sankaran VG, Ni M, Menne TF, Puram RV, Kim W, et al. Transcriptional silencing of {gamma}-globin by BCL11A involves long-range interactions and cooperation with SOX6. Genes Dev 2010; 24:783–98.

52. Yu Y, Wang J, Khaled W, Burke S, Li P, Chen X, et al. Bcl11a is essential for lymphoid development and negatively regulates p53. J Exp Med 2012; 209:2467–83.

53. Razaq MA, Taylor S, Roberts DJ, Carpenter L. A molecular roadmap of definitive erythropoiesis from human induced pluripotent stem cells. Br J Haematol 2017; 176:971–83.

54. Murga M, Fernandez-Capetillo O, Field SJ, Moreno B, Borlado LR, Fujiwara Y, et al. Mutation of E2F2 in mice causes enhanced T lymphocyte proliferation, leading to the development of autoimmunity. Immunity 2001; 15:959–70.

Downloaded From: https://bioone.org/journals/Radiation-Research on 27 Aug 2019
Terms of Use: https://bioone.org/terms-of-use Access provided by Wake Forest University

PLOS ONE

RESEARCH ARTICLE

Late effects of total body irradiation on hematopoietic recovery and immune function in rhesus macaques

Laura P. Hale[1]*, Gowrisankar Rajam[2], George M. Carlone[2¤], Chen Jiang[3], Kouros Owzar[3,4], Greg Dugan[5], David Caudell[5], Nelson Chao[6], J. Mark Cline[5], Thomas C. Register[5], Gregory D. Sempowski[1,6]

1 Department of Pathology and Duke Human Vaccine Institute, Duke University School of Medicine, Durham, NC, United States of America, **2** Immunobiology Laboratory, Centers for Disease Control and Prevention (CDC), Atlanta, GA, United States of America, **3** Duke Cancer Institute, Duke University Medical Center, Durham, NC, United States of America, **4** Department of Biostatistics and Bioinformatics, Duke University Medical Center, Durham, NC, United States of America, **5** Department of Pathology, Section on Comparative Medicine, Wake Forest School of Medicine, Winston-Salem, NC, United States of America, **6** Department of Medicine, Duke University School of Medicine, Durham, NC, United States of America

¤ Current address: Independent Researcher, Palm Coast, FL, United States of America
* laura.hale@duke.edu

Check for updates

OPEN ACCESS

Citation: Hale LP, Rajam G, Carlone GM, Jiang C, Owzar K, Dugan G, et al. (2019) Late effects of total body irradiation on hematopoietic recovery and immune function in rhesus macaques. PLoS ONE 14(2): e0210663. https://doi.org/10.1371/journal.pone.0210663

Editor: Gayle E. Woloschak, Northwestern University Feinberg School of Medicine, UNITED STATES

Received: June 18, 2018

Accepted: December 28, 2018

Published: February 13, 2019

Copyright: This is an open access article, free of all copyright, and may be freely reproduced, distributed, transmitted, modified, built upon, or otherwise used by anyone for any lawful purpose. The work is made available under the Creative Commons CC0 public domain dedication.

Data Availability Statement: All relevant data are within the paper and its Supporting Information files.

Funding: This work was supported by National Institutes of Health/National Institute of Allergy and Infectious Diseases U19 AI67798 (NC) and by the Department of Defense/Congressionally Directed Medical Research Program grant W81XWH-15-1-0574 (JMC). The funders had no role in study

Abstract

While exposure to radiation can be lifesaving in certain settings, it can also potentially result in long-lasting adverse effects, particularly to hematopoietic and immune cells. This study investigated hematopoietic recovery and immune function in rhesus macaques Cross-sectionally (at a single time point) 2 to 5 years after exposure to a single large dose (6.5 to 8.4 Gray) of total body radiation (TBI) derived from linear accelerator-derived photons (2 MeV, 80 cGy/minute) or Cobalt 60-derived gamma irradiation (60 cGy/min). Hematopoietic recovery was assessed through measurement of complete blood counts, lymphocyte subpopulation analysis, and thymus function assessment. Capacity to mount specific antibody responses against rabies, *Streptococcus pneumoniae*, and tetanus antigens was determined 2 years after TBI. Irradiated macaques showed increased white blood cells, decreased platelets, and decreased frequencies of peripheral blood T cells. Effects of prior radiation on production and export of new T cells by the thymus was dependent on age at the time of analysis, with evidence of interaction with radiation dose for CD8+ T cells. Irradiated and control animals mounted similar mean antibody responses to proteins from tetanus and rabies and to 10 of 11 serotype-specific pneumococcal polysaccharides. However, irradiated animals uniformly failed to make antibodies against polysaccharides from serotype 5 pneumococci, in contrast to the robust responses of non-irradiated controls. Trends toward decreased serum levels of anti-tetanus IgM and slower peak antibody responses to rabies were also observed. Taken together, these data show that dose-related changes in peripheral blood cells and immune responses to both novel and recall antigens can be detected 2 to 5 years after exposure to whole body radiation. Longer term follow-up data on this cohort and independent validation will be helpful to determine whether these changes persist or whether additional changes become evident with increasing time since radiation, particularly as animals begin to develop aging-related changes in immune function.

design, data collection and analysis, decision to publish, or preparation of the manuscript.

Competing interests: The authors have declared that no competing interests exist.

Introduction

While radiation exposure can be lifesaving in the setting of cancer treatment or bone marrow transplantation for genetic or acquired disease, adverse effects may include cytopenias, abnormal immune function, delayed healing, fibrosis, and secondary malignancies, among others. The benefits of radiation are thought to outweigh the adverse effects for therapeutic radiation exposures. However, biologically significant non-beneficial radiation exposures may also potentially occur due to accidents, intentional non-therapeutic exposures (i. e. terrorist attacks), or prolonged space travel. Thus, it is important to assess the acute and long-term effects of such exposures to facilitate the development of medical countermeasures that can mitigate their harm. Abnormal function of the immune system is one of the adverse effects of radiation exposures that can potentially persist long-term (reviewed in [1]).

Immune responses depend on the presence and proper activity of both innate and adaptive immune cells. Innate immune cells include natural killer (NK) cells, dendritic cells, macrophages, and other myeloid cells that can recognize and immediately respond to a variety of markers (antigens). Adaptive immune cells include T and B cells that develop immune responses when their antigen-specific receptors bind to the corresponding antigens on potential pathogens. While B cells primarily respond to antigens by producing antibodies, T cells can respond either via producing cytokines that regulate immune responses or via direct cytotoxicity. As important regulators of both activation and resolution of immune responses, the numbers and activity of T cells are critical for proper defense against foreign invaders.

T cells develop from hematopoietic progenitor cells that migrate to the thymus, where they generate unique antigen receptors that are selected for appropriate reactivity with foreign antigens presented by other immune cells and the absence of reactivity against self-antigens. The thymus is largest and most active early in life as it establishes the initial peripheral T cell repertoire. Progressive age-related thymic involution occurs subsequently, although the thymus normally continues to produce a low number of T cells throughout the adult life [2–5]. The potentially novel antigen receptor specificities carried by these newly produced naïve T cells (thymic emigrants) have been hypothesized to be critical to maintain broad polyclonal immunity and to achieve full immune reconstitution without the development of "holes" in the immune repertoire following an insult such as chemotherapy or radiation that results in depletion of the previously established peripheral T cell repertoire [6,7]. Thymic function can be assessed non-invasively via direct detection in peripheral blood of phenotypically naïve T cells and/or extrachromosomal circles of DNA called signal joint T cell receptor excision circles (sjTRECs) that are excised during T cell receptor gene rearrangement in the thymus [8]. Since sjTRECs are not replicated during T cell proliferation in the periphery, their presence within cells provides a molecular indicator that those cells were produced *de novo* in the thymus.

The mechanisms of radiation-induced immune injury and acute recovery have been studied in a variety of small animal and primate models [9,10]. Studies that have focused on late effects of radiation (> 6 months post-radiation) have often shown incomplete hematopoietic and/or thymus recovery, especially in adults. For example, surgically post-menopausal "late-middle aged" female cynomolgus macaques (median age, 20 years; range 15–24 years) exposed to 5 Gray (Gy) radiation demonstrated acute, dose-dependent decreases in hematopoiesis that had not normalized by 6 months post-radiation. Thymus size and function were still decreased at 6 months for animals that had received either 2 or 5 Gy radiation [11]. Thymus tissues from humans exposed to up to 2.9 Gy radiation from the atomic bomb (A-bomb) in Hiroshima showed decreased thymic function at the time of their natural deaths 9–41 years later, compared to age-matched non-irradiated individuals [12]. Studies of how irradiation and thymic recovery affect immune responses to pathogens or vaccines generally have been limited by

small cohorts, short follow-up times, and/or potential immune effects of underlying disease. Changes in circulating plasmacytoid dendritic cells were recently documented in 153 Japanese female atomic bomb survivors more than 60 years after radiation exposure [13] suggesting potential effects on immune function. Unfortunately, interpretation of some findings in the human A-bomb survivor studies are often complicated due to age related effects on the immune system. For example, a recent study of the effects of prior A-bomb radiation exposure on immune responses to influenza vaccine was limited by the overall poor antibody responses of both elderly control and irradiated subjects [14]. In addition, the studies in human A-bomb survivors are limited by variable radiation doses, heterogeneous exposures, differing ages at time of exposure, complications by under-nourishment, and retrospective analysis.

The rhesus macaque non-human primate (NHP) model has been shown to be an excellent model for study of immune system homeostasis and function [15] including studies that assess radiation countermeasures [11,16–18]. We used this model to test the hypothesis that previous irradiation would impair hematopoiesis and/or humoral and cell-mediated immune responses years after irradiation, using both phenotypic and functional analyses. Hematopoietic recovery was assessed in a large cohort of rhesus macaques at a median of ~5 years post-acute radiation exposure. The capacity of a subset of these animals to mount antibody responses was determined by challenge with rabies, *Streptococcus pneumoniae*, and tetanus toxoid antigens. Individual variation in immune recovery was assessed through measurement of complete blood counts, lymphocyte subpopulation analysis, and thymus function (via signal joint T cell receptor excision circles, sjTRECs) in the larger cohort and by post-vaccine response antibody titers in the antigen-challenged subset.

Materials and methods

Subjects studied

A total of 43 male rhesus macaques (*Macaca mulatta*; 29 irradiated and 14 non-irradiated controls) were studied. All *in vivo* blood collections, immune challenges, and other post-irradiation procedures were conducted at the Wake Forest University School of Medicine with approval by the Institutional Animal Care and Use Committee of Wake Forest University. Wake Forest University is committed to provide a high-quality program of animal care in compliance with state and federal Animal Welfare Acts and the standards and policies of the US Department of Health and Human Services. Wake Forest University has an Assurance on file in the Office for Protection from Research Risks, Office of the Director, National Institutes of Health, that accepts responsibility for the humane care and use of animals (OPRR #A-3391-01). The Laboratory Animal Care Program of the Wake Forest University School of Medicine complies with the "Principles for Use of Animals", the "Guide for the Care and Use of Laboratory Animals" [19], all provisions of the Animal Welfare Act, and has been accredited by the Association for Assessment and Accreditation of Laboratory Animal Care, International (AAALAC) since April 8, 1966 (AAALAC File #8).

The control and irradiated animals used for this study were obtained from Wake Forest University, University of Maryland, University of Illinois, Armed Forces Radiobiology Research Institute, and Primate Products. Irradiated animals received 6.5 to 8.4 Gy total body radiation under IACUC oversight at their prior institution using one of two strategies: (1) linear accelerator-derived photons at a nominal mean energy of 2 MeV, delivered at 80 cGy/minute as a split dose given half anterior-posterior and half posterior-anterior; or (2) Cobalt 60-derived gamma irradiation delivered simultaneously, bilaterally at 60 cGy/min. Note that these are potentially lethal doses: the LD 10/30 for rhesus macaques is ~5.5 Gy, the LD 50/30 is ~6.7 Gy, and the LD 90/30 is 8 Gy [20]. Surviving animals were subsequently transferred to

Wake Forest School of Medicine Center for Comparative Medicine Research for long-term monitoring post-radiation. Irradiation methods, supportive care strategies, and acute effects for many animals donated to this cohort have been recently reported [17, 20, 21].

After arrival at Wake Forest, all animals were monitored twice daily by trained veterinary technical laboratory staff to assure animal well-being and social stability. Any evidence of illness was classified using a nonhuman primate-specific modification of the Children's Clinical Oncology Group toxicity criteria [22]. Sick animals were promptly evaluated by one of seven institutional veterinarians independent of the research team, two of whom are board-certified by the American College of Laboratory Animal Medicine.

Animals consumed a diet of laboratory chow (Purina LabDiet Monkey Diet 5038, Richmond, IN, USA) that was supplemented with fresh fruits and vegetables and with water *ad libitum*. They were housed socially in indoor-outdoor pens whenever possible, or in group cages if necessary for safe handling or medical care. Care was taken to ensure the animals in the groups were compatible. Environmental enrichment, including fruits/vegetables, toys, puzzles, climbing and hiding environments, was provided continuously on a rotating basis. Behavioral well-being was additionally monitored and recommendations made as needed by an independent behavioral management team. All animals were trained to cooperate in handling procedures, to minimize stress. Sampling was scheduled so that the animals were sedated the minimum number of times required for data collection.

Characteristics of the population studied are summarized in Fig 1. The median age of the animals was seven years at the time of this study, corresponding to early adulthood [15], with a range of 5.9 to 8.9 years in the non-irradiated control group and 6 to 15 years in irradiated animals (Fig 1A). The median dose received by irradiated animals was 7.2 Gy (Fig 1B). The hematologic evaluation was performed at a median of 55 months (range 44–79 months) post irradiation (Fig 1C).

Hematologic and immunologic recovery monitoring

To assess hematologic and immunologic recovery post-radiation, animals were sedated with intramuscular ketamine and blood was drawn from the femoral vein for complete blood counts (CBC) including hematocrit, red blood cells, red blood cell indices, total and differential leukocyte counts, hemoglobin, and platelet count. Lymphocyte phenotype was determined by flow cytometry on peripheral blood mononuclear cells derived by density gradient centrifugation of heparinized blood as described [15,23,24]. Analysis of sjTRECs as an indicator of thymus function was performed on bead-isolated $CD3^+$ cells derived from peripheral blood as previously described [8].

Vaccination response monitoring in a subset of the cohort

Nine young adult male rhesus macaques that had previously been irradiated (August 2006) with 7.5 to 8.5 Gy of 6 mega volt (MV) photons at the University of Maryland and four non-irradiated control animals participated in a sub-study to assess immune recovery post-irradiation. Mean age at the time of irradiation was 3.7 years (range 3.1–4.4 years). All 13 animals were immunized 2 years later on day 0 (July 2008) with a single dose of the polyvalent *Streptococcus pneumoniae* vaccine PneumoVax 23 (Merck Sharp and Dohme Corp., Kenilworth, NJ), on day 31 with the rabies vaccine Defensor 1 (Pfizer Animal Health, New York, NY), and on day 60 with a tetanus toxoid vaccine (Sanofi Pasteur, Swiftwater, PA). Age at initiation of the vaccine challenge was 5.6 years [range 5.0–6.3] in irradiated subjects and 5.2 years [range 4.2–6.2] in controls. Peripheral blood ($\leq$ 7 mL/draw) was collected at baseline and at 1, 4, 8, and 16 weeks following each respective immunization for assessment of antibody titers against the vaccines.

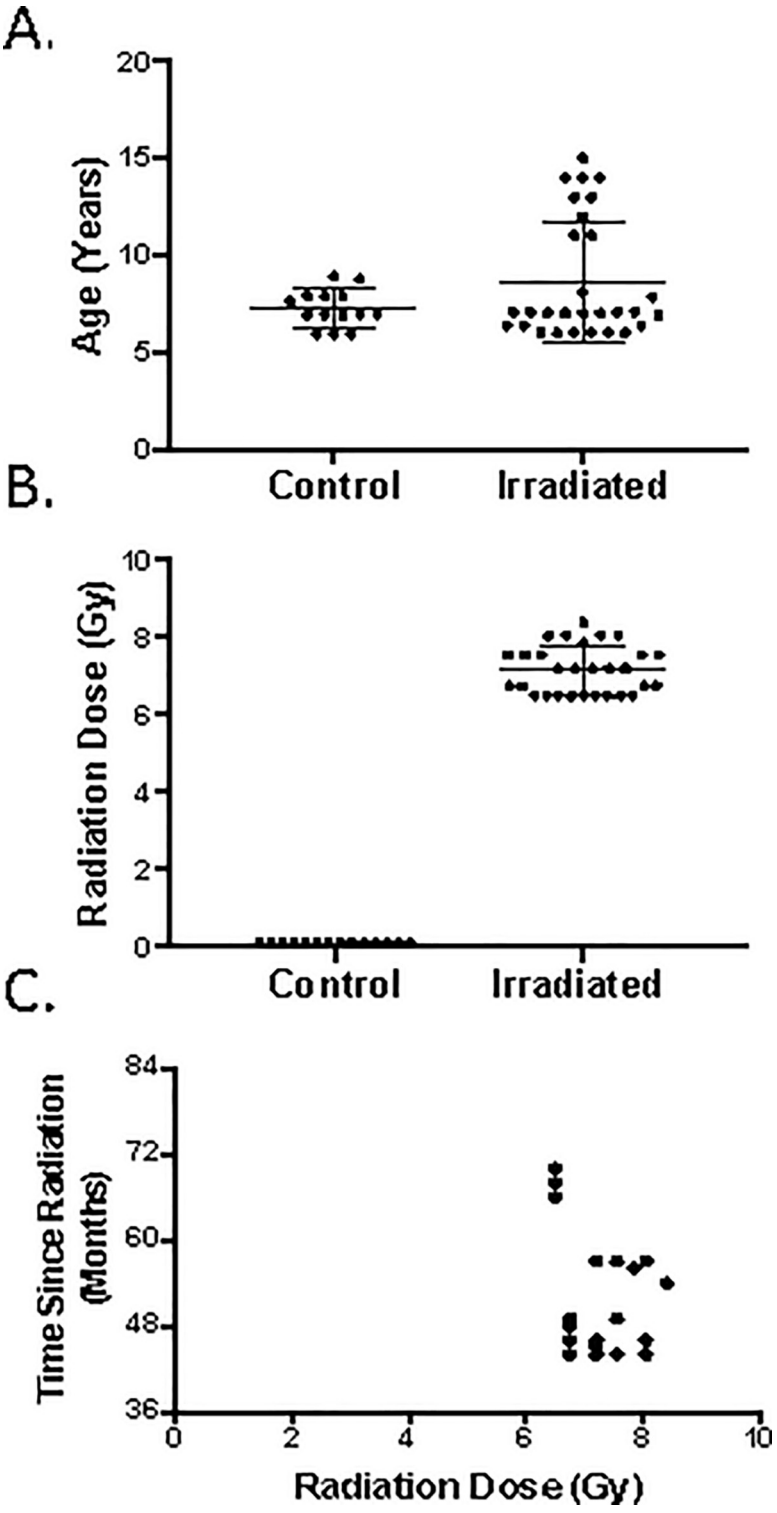


Fig 1. Demographics of the non-human primate population studied. A. The ages are shown for control (n = 14) and irradiated animals (n = 29) in the X-10-12 cohort. The median age of 7 years was similar for both groups, with a range from 5.9 to 8.9 years for the control group and a range of 6 to15 years for the irradiated group. **B**. The median dose (Gy) received by irradiated animals was 7.2 Gy, with a range of 6.5 to 8.4 Gy. **C.** The median time between radiation exposure and study/blood collection was 55 months, with a range from 44 to 70 months.

https://doi.org/10.1371/journal.pone.0210663.g001

Multiplex Luminex pneumococcal (Pnc) anti-capsular IgG capture assay

IgG antibodies directed against the capsule of pneumococcus serotypes 1, 3, 4, 5, 6B, 7F, 9V, 14, 18C, 19F, and 23F were quantitated using a customized multiplex (11-plex) pneumococcal (Pnc) anti-capsular IgG capture assay performed by the Centers for Disease Control and Prevention (CDC) based on previous methods with modifications [25]. Briefly, Pnc serotype-specific capsular polysaccharides (Ps) (American Type Culture Collection, Manassas, VA) were conjugated to poly-L-lysine (PLL, Sigma, St. Louis, MO) [26,27] and then to carboxylate-modified microspheres (Luminex Corp, Austin, TX) using a two-step carbodiimide reaction [28]. PLL-Ps beads for 11 Pnc serotypes (5,000 beads/serotype in 25 μL volume) and serum samples (25 μL /well) were transferred to a 96-well multi-screen filter plate and incubated at 37˚C for 30 minutes with 150 rpm agitation. Plates were washed three times with wash buffer (PBS containing 0.05% Tween 20 and 0.2% newborn bovine serum albumin (NBBS, Sigma, St. Louis, MO). Fifty μL/well of R-phycoerythrin (R-PE)-conjugated anti-monkey IgG (Southern Biotech, Birmingham, AL) was added and incubated at 37˚C for 30 minutes with 150 rpm agitation. Plates were washed three times in wash buffer, beads re-suspended in 130 μL wash buffer /well, and data was acquired in a Luminex reader (Luminex 200, Luminex Corp, Austin, TX) with Masterplex CT software suite (MiraiBio, South San Francisco, CA). Results reported represent the mean of three independent runs by two different operators, reported in arbitrary units relative to reference serum RS2010 as described below. A response to vaccination was defined as an increase in serotype-specific IgG from baseline (day 0) that persisted to 16 weeks post-vaccination.

Four sera (C1655, C1484, R1579 and R1580) with high signals for Pnc serotype (ST)-specific IgG were combined to generate the rhesus reference standard, RS2010. A RS2010 dilution curve was generated by plotting median fluorescence intensity (MFI) against dilution. Pnc ST-specific IgG values for each ST in RS2010 were calculated in arbitrary units (AU) = MFI × dilution factor. RS2010 was included for 8 dilutions in duplicate on each assay plate and the Pnc ST-specific IgG values in AU/mL were computed for each sample from the RS2010 standard curve using Masterplex QT software (MiraiBio, South San Francisco, CA) (S1 Fig).

Antibody responses to tetanus toxoid and rabies

Commercially available enzyme-linked immunosorbent assays (ELISAs) were used to assess IgG and IgM responses to tetanus toxoid (Monkey Anti-Tetanus Toxoid IgG and IgM ELISA Kits, Life Diagnostics, Inc.) and rabies (Platelia Rabies II Kit, BIO-RAD, Steenvoort France). Assays were run according to manufacturer's instructions.

Statistical analysis

The Jonckheere-Terpstra test [29,30] was used to test for association of hematologic parameters with prior radiation dose. The Wilcoxon test [31,32] was used to test association between pre-radiation and hematologic parameters. Kendall's test [33] was used to test the association of age with hematologic parameters. A linear regression model was to used to estimate the interaction of age and dose with respect to hematologic parameters. Differences of immune responses to vaccination between irradiated and control animals were determined using Fisher's test [34,35]. The analyses have not been adjusted for multiple testing. All statistical analyses were carried out using the R statistical enviroment [36] along with extension packages coin [37] and clinfun [38]. Packages from the tidyverse [39] ecosystem and the knitr [40] extension package were used to facilitate adherence to the principles of reproducible analysis.

Results

Total body irradiation induced persistent changes in hematologic parameters and circulating lymphocyte subsets

At a median of 55 months post- radiation, previously irradiated animals (n = 29) had similar red blood cell counts, hemoglobin, hematocrit, red blood cell indices, and percentages of whole blood neutrophils, lymphocytes, monocytes, eosinophils, and basophils as control animals (n = 14) (Fig 2A–2K). However, total white blood cell (WBC) counts in whole blood at this cross-sectional sample increased (Fig 2G; p = 0.01) and platelet counts decreased as radiation dose increased (Fig 2L; p = 0.05). A linear regression analysis indicated that these relationships were not adequately described using a linear model (p = 0.08 and 0.13, respectively). As an example of the differences observed, total WBC counts were 6.5 ± 0.6 x 10^3/μL

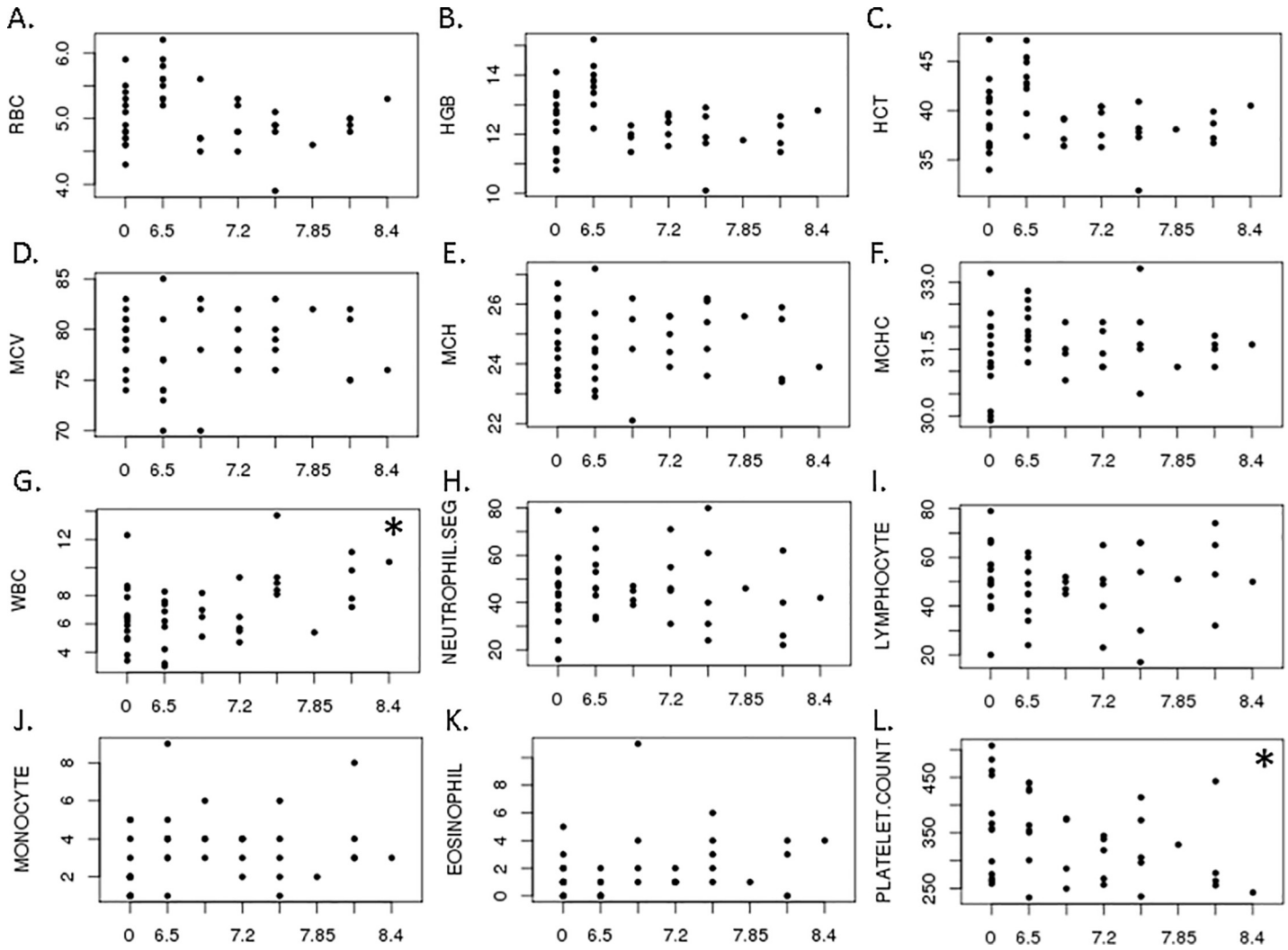


Fig 2. Hematologic parameters at a median of 55 months (~ 5 years) post-irradiation. Values of each parameter are shown as a function of radiation dose in Gy (x-axis for all plots); 0 Gy represents the control group. Each point represents a different subject (n = 43). **A**. Red blood cell (RBC) concentration, cells x 10^6/μL; **B**. Hemoglobin (Hgb), g/dL; **C**. Hematocrit (Hct), %; **D**. Mean corpuscular volume (MCV), fL; **E**. Mean cellular hemoglobin, (MCH), pg; **F**. Mean cellular hemoglobin concentration (MCHC), g/dL; **G**. White blood cells (WBC), cells x 10^3/μL; **H**. Neutrophil %; **I**. Lymphocyte %; **J**. Monocyte %; **K**. Eosinophil %; **L**. Platelet count, x 10^3/μL. Asterisk (*) indicates p = 0.01 in panel G and p = 0.05 in panel L for dose-based comparison of irradiated and control animals using the Jonckheere-Terpstra test. Raw data are provided in S1 Table.

https://doi.org/10.1371/journal.pone.0210663.g002

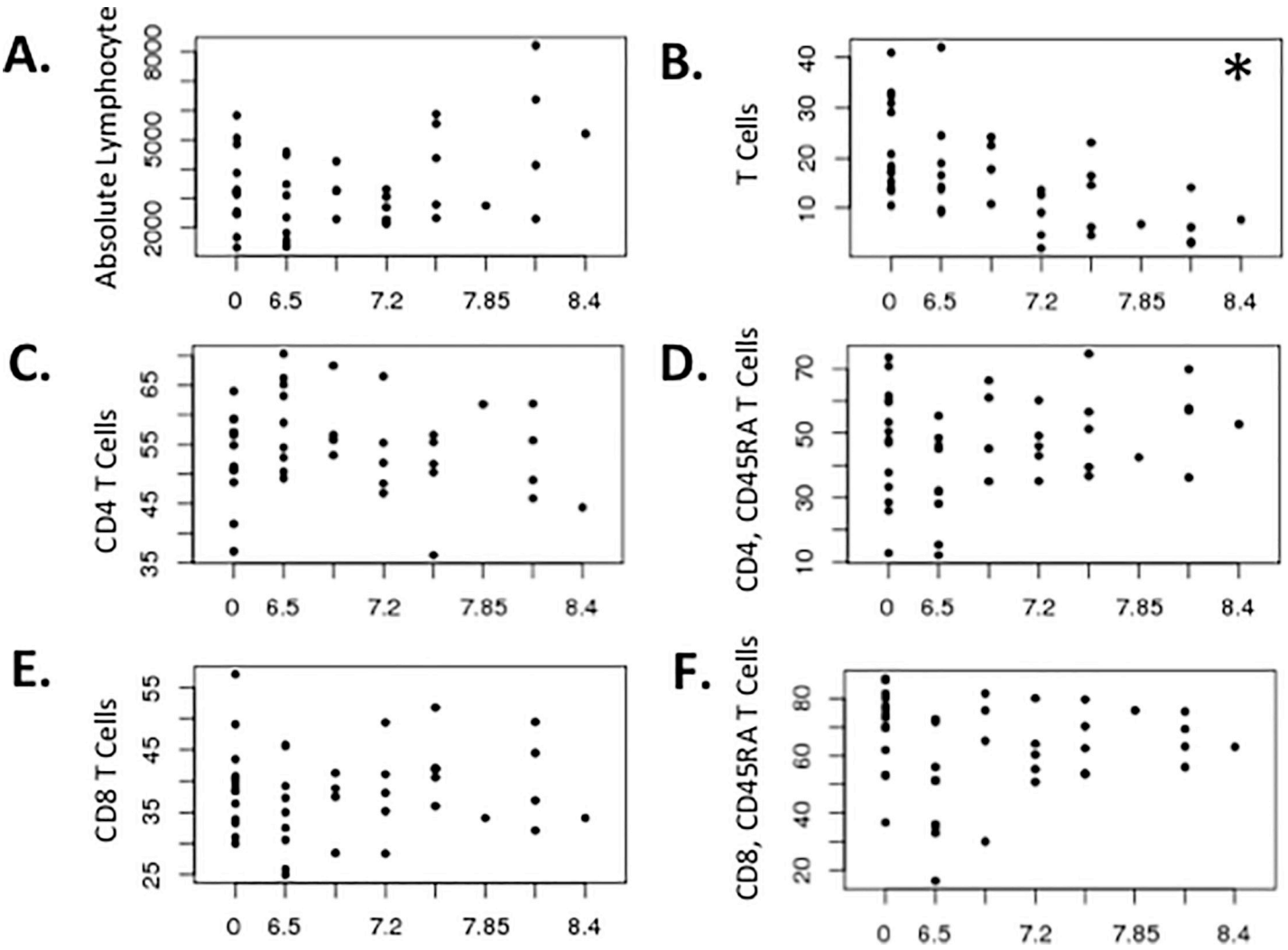


Fig 3. Lymphocyte subset recovery at a median of 55 months (~ 5 years) post-irradiation. Values of each parameter as determined by complete blood count (**A**) or flow cytometry of peripheral blood mononuclear cells isolated by density gradient centrifugation (**B–F**) are shown as a function of radiation dose in Gy as the x-axis for all plots. Each point represents a different subject (n = 43). **A**. Absolute lymphocyte counts, cells x 10^6/μL; **B**. T cell %; **C**. CD4 T cell %; **D**. CD4 CD45RA^{high} (naïve) %; **E**. CD8 T cell %; **F**. CD4 CD45RA^{high} (naïve) %. * indicates Asterisk (*) in panel B indicates p = 0.0004 for dose-based comparison of irradiated and control animals using the Jonckheere-Terpstra test. Raw data are provided in S1 Table.

https://doi.org/10.1371/journal.pone.0210663.g003

(mean ± SEM; n = 14) in control animals and 9.7 ± 1.0 x 10^3/μL (n = 5) in animals that received 7.55 Gy. Similarly, platelet counts were 357 ± 24 x 10^3/μL (mean ± SEM; n = 14) and 325 ± 31 x 10^3/μL (n = 5) in control animals versus those that received 7.55 Gy, respectively.

To further assess the effects of radiation, peripheral blood mononuclear cells isolated from heparinized blood were immunophenotyped with flow cytometry. Although absolute lymphocyte counts obtained from whole blood did not differ (Fig 3A), the percentage or frequency of T lymphocytes in the isolated peripheral blood mononuclear cells were decreased with radiation dose (Fig 3B; p = 0. 0004). A linear regression analysis showed that the decrease in T lymphocyte frequency was well-described by a linear model (p = 0.0006), with a slope of -1.3%/Gy. As expected, naïve T cells, indicated by high surface expression of the CD45RA marker (CD45RA-high), were higher in younger animals (p = 0.002 for CD4+ CD45RA-high cells and p = 0.02 for CD8+ CD45RA-high cells). Although irradiated and control animals had similar percentages of CD4+ versus CD8+ T cell subsets and fractions of these cells that were naïve

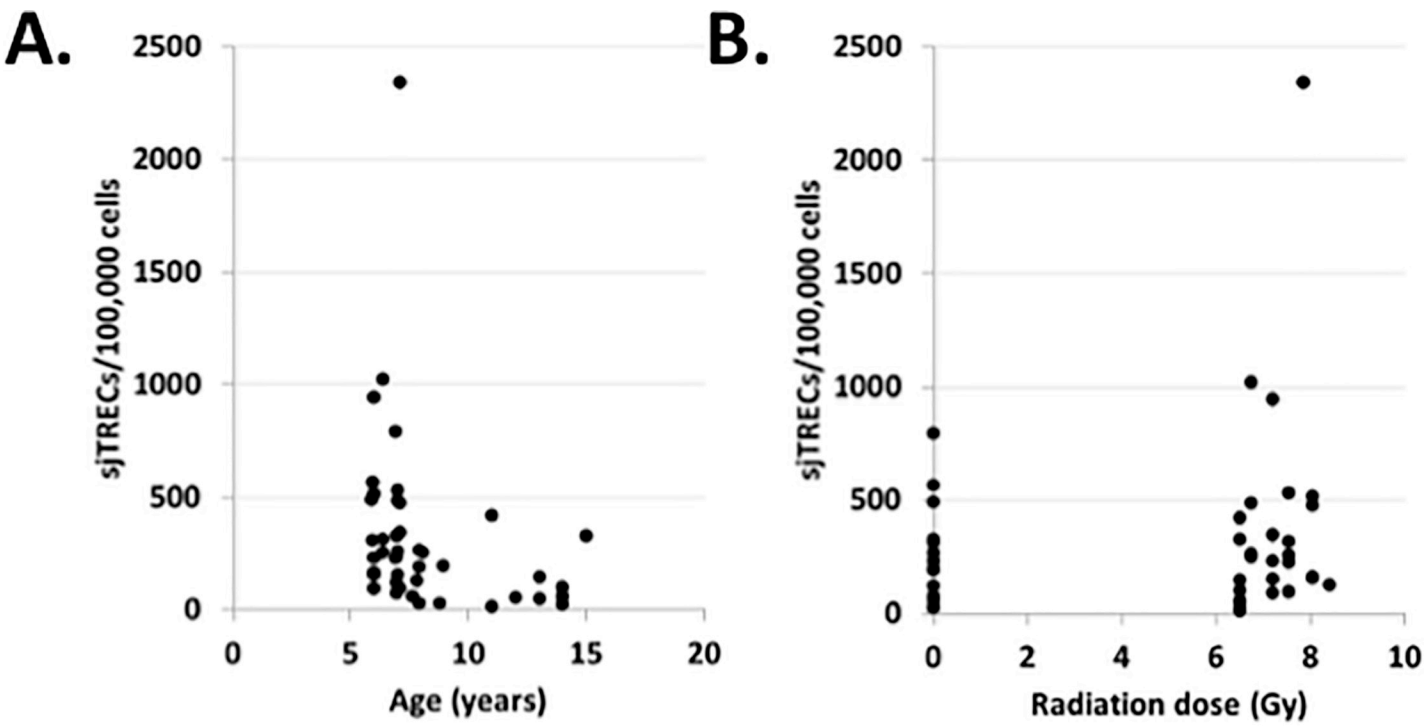


Fig 4. Thymus function ~ 5 years post-irradiation. sjTREC levels in isolated $CD3^+$ mononuclear cells from peripheral blood are plotted as a function of age (**A**) and radiation dose (**B**). Each point represents a different subject (n = 43). In panel A, the open triangles show values for control, non-irradiated animals and the solid black circles show values for irradiated animals. sjTRECs were associated with age (p = 0.002), but did not vary according to radiation dose. Raw data are provided in S1 Table.

https://doi.org/10.1371/journal.pone.0210663.g004

(CD45RA-high) (Fig 3C–3F), linear regression analysis showed that the numbers of naïve CD8+ T cells depended on age (p = 0.01) and radiation dose (p = 0.04), with suggestion of an interaction (p = 0.05) between age and prior radiation dose.

sjTREC analysis was used to further assess the late effects of prior radiation on thymus function. The number of sjTRECs, a molecular marker for T cells that recently emigrated from the thymus, were significantly higher in younger animals (Fig 4A; p = 0. 0.002) but did not differ significantly based on the radiation dose (Fig 4B).

Antibody responses to polysaccharide antigens remain compromised ~2 years post-total body irradiation

To test the hypothesis that prior irradiation leads to lasting effects on immune function, nine previously irradiated and four control macaques were immunized with commercially available vaccines against rabies, *Streptococcus pneumoniae*, and tetanus toxoid and antibody responses were determined. The proportion of animals that responded to polysaccharide antigens were similar for control and irradiated animals for 10 of the 11 pneumococcal serotypes tested (Table 1). There was also no difference in the number of serotypes to which individual macaques responded, ranging from 4 to 10 of 11 antigens tested in the control group and from 0 to 9 of 11 antigens tested in the irradiated group (p = 0.53). However, while 4/4 (100%) of control macaques mounted antibody responses to polysaccharide antigens from serotype 5 pneumococcus, 0/9 (0%) of irradiated animals responded to this serotype (p = 0. 001). Taken together, these results suggest that immune responses to certain polysaccharide antigens may be compromised in previously irradiated animals, leading to a "hole" in their immune repertoire for the serotype 5 polysaccharide and perhaps other antigens.

Table 1. Antibody responses to pneumococcal (Pnc) vaccine ~2 years post-irradiation.

	PnC Serotypes Tested											
Animal ID	**1**	**3**	**4**	**5**	**6B**	**7F**	**9V**	**14**	**18C**	**19F**	**23F**	**Total Positive**
C1	++	++	-	++	-	++	-	++	-	-	++	**6/11**
C2	++	++	++	++	++	++	++	++	++	++	-	**10/11**
C3	++	++	-	++	-	++	++	++	++	++	-	**8/11**
C4	-	++	-	++	-	-	-	-	++	++	-	**4/11**
Control (%+)	**75%**	**100%**	**25%**	**100%**	**25%**	**75%**	**50%**	**75%**	**75%**	**75%**	**25%**	
R1	++	++	++	-	++	-	-	++	++	-	++	**7/11**
R2	-	-	-	-	-	-	-	-	-	-	-	**0/11**
R3	++	++	++	-	-	++	-	++	++	++	++	**8/11**
R4	-	++	++	-	-	-	-	-	++	-	-	**3/11**
R5	-	++	++	-	-	++	++	++	++	++	++	**8/11**
R6	-	++	-	-	-	-	-	++	++	++	++	**5/11**
R7	++	++	++	-	++	-	++	++	++	++	++	**9/11**
R8	++	++	-	-	-	++	-	-	-	-	-	**3/11**
R9	-	++	-	-	-	++	++	-	++	-	++	**5/11**
Radiated (%+)	**44%**	**89%**	**56%**	**0%***	**22%**	**44%**	**33%**	**56%**	**78%**	**44%**	**67%**	

Note: A positive response (++) was classified based on a sustained increase in IgG response lasting to 16 weeks after vaccination, compared with day 0 (see S2 Fig). Lack of a positive response is indicated by (-).

* indicates a significant difference in response between control and previously irradiated animals ($p = 0.001$).

https://doi.org/10.1371/journal.pone.0210663.t001

Mean antibody responses to protein antigens have generally normalized by ~2 years post-total body irradiation

Mean IgM and IgG responses to tetanus toxoid and mean rabies combined IgM/IgG responses were statistically similar in irradiated versus control animals (Fig 5). However, irradiated animals demonstrated a strong, but non-statistically significant, trend toward decreased serum anti-tetanus IgM at all time points studied (Fig 5A). A non-significant trend toward a delay in mean peak antibody responses to rabies vaccine was also seen in irradiated animals compared with controls (Fig 5C). Larger studies with increased statistical power will be required to determine whether these trends reflect residual impairments in antibody production in irradiated animals.

Interestingly, one seven year old macaque who had received 7.85 Gy radiation prior to vaccination failed to make antibodies against 6/11 pneumococcal serotypes tested (R2 in Table 1), and had only transient responses to 5 antigens which had disappeared by 16 weeks post-vaccination. At 56 months post-irradiation, this animal had an absolute lymphocyte count of 2,754 cells/μL with 7% T cells and was an outlier with regard to sjTRECs (2,340/10^5 $CD3^+$ cells). His IgM responses to tetanus were lower than the mean for irradiated animals, IgG responses to tetanus were similar to the mean, and his combined IgG/IgM responses to rabies vaccine were similar to or above the mean, indicating that this animal had isolated deficient responses to polysaccharide but not protein antigens.

Discussion

This study of hematopoietic recovery and immune function several years after radiation exposure shows that the irradiated macaques experienced dose-related thrombocytopenia, increased total white blood cell counts, and decreased percentages of T cells in peripheral

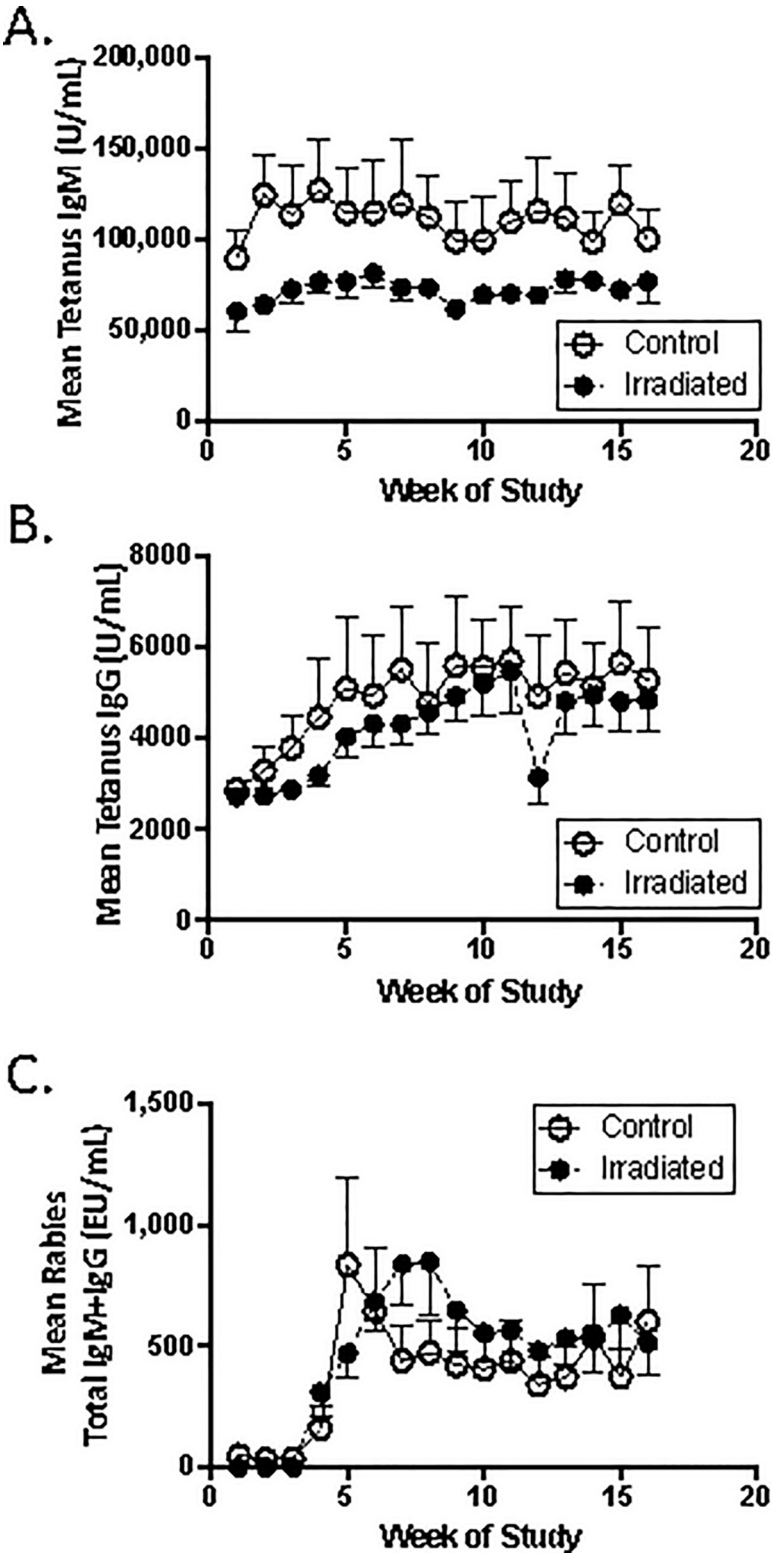


Fig 5. Antibody responses to tetanus and rabies antigens ~ 2 years post-irradiation. A. IgM responses to tetanus vaccine. **B**. IgG responses to tetanus vaccine. **C**. Combined IgM/IgG responses to rabies vaccine. Raw data are provided in S2 Table.

https://doi.org/10.1371/journal.pone.0210663.g005

blood, as a prolonged or delayed effect of radiation exposure. Effects of prior radiation on production and export of new T cells by the thymus gland was associated with age, with evidence of interaction of age and radiation exposure dose for CD8+ T cells. Irradiated and control animals generally developed similar humoral responses to protein antigens and most of the polysaccharide antigens tested, although irradiated animals uniformly failed to make antibodies against polysaccharides from serotype 5 pneumococci. Trends toward decreased serum IgM responses to tetanus and slower peak antibody responses to rabies were also observed, which need to be confirmed by larger studies with increased statistical power. Taken together, this study suggests that while irradiated animals respond to most antigens, minor impairment of immune responses persisted in these relatively young subjects despite ~ 2 years of recovery, particularly relative to polysaccharide antigens.

Irradiated macaques in the larger, broader age range cohort demonstrated long-standing decreases in platelet counts as well as dose-related increases in total peripheral blood white blood cell counts relative to control animals. Prior radiation exposure has been documented to increase peripheral white blood cell counts and chronic inflammation, as demonstrated by increased erythrocyte sedimentation rates in human survivors of atomic bomb blasts [41]. These increases in inflammation have been documented to occur via a variety of mechanisms, including direct damage to cells, cellular stress responses, endovascular injury that results in vascular leak, excessive activation of M1 pro-inflammatory macrophages, and the senescence-associated secretory phenotype (reviewed in [42]). The relative contributions of any of these specific mechanisms to the differences seen in this study are unknown. In addition, since these animals were studied cross-sectionally and were heterogeneous with respect to age, age at irradiation, time since irradiation, and radiation dose, additional follow-up studies will be required to confirm whether the observed differences are representative across populations.

Irradiated macaques demonstrated dose-related decreases in the percentages of T cells present in peripheral blood. Since T cells are generated in the thymus, we investigated several markers that can provide insight into thymus gland function (i. e., thymopoiesis). The data presented here show that levels of sjTRECs were highest in younger animals and were not associated with radiation dose. The generation of new naïve T cells in the thymus depends both on availability of precursor cells that migrate from the bone marrow and thymus-intrinsic factors that affect the output of T cells. Effects of either radiation or aging on thymopoiesis are multi-factorial and depend on survival and repopulation of bone marrow hematopoietic stem cells (HSC), potential radiation-induced skewing of functional responses with respect to cell lineage repopulation properties, migration to the thymus, appropriate seeding of thymic niches, and completion of the thymocyte/T cell maturation processes. The relative contributions of each of these factors is still poorly understood. However, the data suggest that animals irradiated early in life are more resilient for recovery of thymopoiesis, compared to those irradiated later in life.

Consistent with this, increased percentages of both CD4+ and CD8+ naïve cells detected by flow cytometric immunophenotyping were also significantly associated with younger animals. However, linear regression analysis also suggested that a significant interaction between age and prior radiation dose was limited to the CD8+ naïve T cell population. It is important to note that our analysis was based on age at the time of blood draw, and that animals were irradiated at ages of 5.9 to 15 years and their thymus function was assessed 44 to 70 months later. Also, while T cell percentages varied by dose, it is very difficult to separate variability associated with the dose range used (6.6 to 8.4 Gy) given the relatively small number of animals assessed and assay variability. The animals were exposed to radiation at different research sites that also confounds dose delivery to target sites, relative dosimetry etc. Additional studies may be necessary to fully address these issues in more controlled settings.

Previous work in ovariectomized female cynomolgus macaques showed that total body irradiation sufficient to cause acute hematopoietic syndrome (e.g. 2–5 Gy) resulted in decreased thymus weight with marked atrophy of thymic cortex and medulla and decreased sjTRECs that remained evident at least 24 weeks post-irradiation [11]. The data presented here using a broader age range of male rhesus macaques showed that age had a stronger influence on the production and export of new T cells by the thymus than total body irradiation doses when assessed ~5 years post-irradiation, although there was evidence of significant interaction with radiation dose for CD8+ T cells ($p = 0.05$). At first glance, these results may seem discordant with prior work that demonstrated significantly decreased long-term thymic function in humans exposed to atomic bomb radiation [12] and in experimentally irradiated mice [43]. However, the studies presented here differed in several ways from those previously published, including age at irradiation, radiation doses, the time elapsed between radiation and assessment relative to the lifespan of the organism, and the methods used to assess thymus function. The thymus of young mice has been shown to rapidly regenerate in weight and production of T cells following acute radiation exposure (reviewed in [43]). However, thymic regeneration is slower in older mice and humans and may not reach pre-irradiation baseline levels (reviewed in [44]). The available data in humans suggests that radiation exposure may not necessarily prevent full thymus regeneration acutely, but may accelerate age-related thymus involution [12]. Thus, the full effects of radiation on the thymus may not yet be evident in the cohort of macaques studied, where most animals were irradiated in "late adolescence" and studied as young adults, when thymic reserve is still substantial.

Although antibody responses to most of the administered vaccine antigens were statistically similar in irradiated and control animals, one exception emerged–the response to the polysaccharide antigens from pneumococcus serotype 5 –where 4 of 4 control animals produced antibodies versus 0 of 9 irradiated animals. Immune responses to polysaccharides require a more developed immune system, such that strong responses to these antigens are not typically seen in humans until about two years of age. The "hole in the immune repertoire" toward the serotype 5 polysaccharides demonstrated by irradiated animals ($p = 0.001$) may thus reflect subtle radiation-associated decreases in immune function. This interpretation is supported by the non-significant trend toward decreased IgM levels produced against tetanus toxoid, the delayed peak antibody responses to rabies that were also observed in irradiated animals, and the observation that one irradiated macaque who responded to the vaccine protein antigens had only transient responses to 5 of the polysaccharide antigens and this response had disappeared by the 16 week timepoint. Interestingly, the polysaccharide expressed by serotype 5 pneumococcus is unique among the strains contained in the 23-valent pneumococcal vaccine, by the replacement of glucose in the repeating unit of its capsular polysaccharide with galactose [45,46]. How this structural variation might influence immunogenicity in irradiated animals is unclear, and whether skewing of the recovery of thymopoiesis relative to recovery of other hematopoietic cell types contributes to this observation is unknown. It is also unknown whether the antibodies made by irradiated animals differ in their functional (opsonic) activity and thus their ability to protect against disease compared to control animals. Importantly, radiation-associated immune deficits may become more pronounced as the animals age, since aging has independently been associated with decreased thymic T cell production, frequent clonal expansion of memory T cell populations, increases in autoimmune diseases/syndromes, and diminished response to vaccinations [47–50].

In summary, the data presented show that dose-related changes in peripheral blood cells and in immune responses to antigens were detected at 2 to at least 5 years after exposure to radiation. Additional studies and longer term follow-up research is needed to determine whether these changes persist and the impact of the alterations on other systems of the body.

These data are relevant to the question of whether pathologies become more evident with increasing time since radiation, particularly as subjects begin to develop aging-related deficits in immune function.

Supporting information

S1 Table. Hematologic and immunologic parameters in peripheral blood of irradiated and control macaques (raw data). The units used for each measurement are provided in Figs 2–4.
(PDF)

S2 Table. Vaccine responses against tetanus and rabies (raw data).
(PDF)

S1 Fig. Assignment of standard values using reference serum RS2010. Reactivity of RS2010 with each pneumococcal serotype polysaccharide was used to define IgG responses to that serotype in arbitrary units (AU), defined as median fluorescence intensity in the Luminex-based immunoassay x dilution factor, as shown here for serotype 4.
(TIF)

S2 Fig. Vaccine responses against pneumococcal serotypes. The mean IgG level and standard error of the mean (n = 3 replicates) is plotted in arbitrary units for each animal relative to reference serum RS2010 for each of 11 pneumococcal serotypes, as described in the Materials and Methods. To be considered a positive reaction to vaccination, the IgG level measured at week 16 post-vaccination had to be significantly increased relative to the IgG level measured at week 0, prior to vaccination. Designation of each response as positive (+) or negative (-) is indicated for each animal and serotype combination. **A**. Serotype 1. **B**. Serotype 3. **C**. Serotype 4. **D**. Serotype 5. **E**. Serotype 6B. **F**. Serotype 7F. **G**. Serotype 9V. **H**. Serotype 14. **I.** Serotype 18C. **J**. Serotype 19F. **K**. Serotype 23F. These results were summarized in Table 1 of the manuscript.
(PDF)

Acknowledgments

The authors are grateful for contributions from RADCCORE colleagues and donations of irradiated primates from colleagues at the Armed Forces Radiobiology Research Institute, University of Maryland and University of Illinois at Chicago. The authors would like to thank Ellie Kim and Dr. Brian Plikaytis (currently and formerly of the Centers for Disease Control and Prevention, Atlanta, GA, respectively) for assistance in developing the assays used for assessing anti-pneumococcal antibody responses. Antibody responses to tetanus and rabies were performed by Mr. James Bottoms in the laboratory of Dr. Register at Wake Forest School of Medicine. Immunophenotying and sjTREC analysis were performed by Dr. Andrew Macintyre in the Immunology Unit of the Duke Regional Biocontainment Laboratory (Durham, NC). Flow Cytometry data was acquired in the Duke Human Vaccine Institute Flow Cytometry Facility, Durham NC, under the direction of Dr. Derek Cain.

Author Contributions

Conceptualization: Nelson Chao, J. Mark Cline, Thomas C. Register, Gregory D. Sempowski.

Data curation: Laura P. Hale, J. Mark Cline, Thomas C. Register, Gregory D. Sempowski.

Formal analysis: Laura P. Hale, Chen Jiang, Kouros Owzar.

Funding acquisition: Nelson Chao, J. Mark Cline, Gregory D. Sempowski.

Investigation: Gowrisankar Rajam, George M. Carlone, Greg Dugan, David Caudell, J. Mark Cline, Thomas C. Register.

Methodology: Gowrisankar Rajam, George M. Carlone, Greg Dugan, David Caudell, J. Mark Cline, Thomas C. Register.

Project administration: Gregory D. Sempowski.

Resources: Gregory D. Sempowski.

Supervision: Gregory D. Sempowski.

Visualization: Laura P. Hale, Gregory D. Sempowski.

Writing – original draft: Laura P. Hale, Gregory D. Sempowski.

Writing – review & editing: Laura P. Hale, Gowrisankar Rajam, George M. Carlone, Chen Jiang, Kouros Owzar, Greg Dugan, David Caudell, Nelson Chao, J. Mark Cline, Thomas C. Register, Gregory D. Sempowski.

References

1. Lumniczky K, Candeias SM, Gaipl US, Frey B. Editorial: Radiation and the immune system: Current knowledge and future perspectives. Front Immunol. 2017; 8: 1933. https://doi.org/10.3389/fimmu.2017.01933 PMID: 29410662
2. Douek DC, McFarland RD, Keiser PH, Gage EA, Massey JM, Haynes BF, et al. Changes in thymic function with age and during the treatment of HIV infection. Nature. 1998; 396: 690–695. https://doi.org/10.1038/25374 PMID: 9872319
3. Kong F, Chen CH, Cooper MD. Thymic function can be accurately monitored by the level of recent T cell emigrants in the circulation. Immunity. 1998; 8: 97–104. PMID: 9462515
4. Douek DC, Vescio RA, Betts MR, Brenchley JM, Hill BJ, Zhang L, et al. Assessment of thymic output in adults after haematopoietic stem-cell transplantation and prediction of T-cell reconstitution. Lancet. 2000; 355: 1875–1881. https://doi.org/10.1016/S0140-6736(00)02293-5 PMID: 10866444
5. Chinn IK, Blackburn CC, Manley NR, Sempowski GD. Changes in primary lymphoid organs with aging. Semin Immunol. 2012; 24: 309–320. https://doi.org/10.1016/j.smim.2012.04.005 PMID: 22559987
6. Gruver AL, Sempowski GD, Cytokines, leptin, and stress-induced thymic atrophy. J Leukoc Biol. 2008; 84: 915–923. https://doi.org/10.1189/jlb.0108025 PMID: 18495786
7. Lynch HE, Goldberg GL, Chidgey A, van den Brink MR, Boyd R, Sempowski GD. Thymic involution and immune reconstitution. Trends Immunol. 2009; 30: 366–373. https://doi.org/10.1016/j.it.2009.04.003 PMID: 19540807
8. Lynch HE, Sempowski GD. Molecular measurement of T cell receptor excision circles. Methods Mol. Biol. Clifton NJ. 2013; 979: 147–159.
9. Dudakov JA, van den Brink MR. Greater than the sum of their parts: Combination strategies for immune regeneration following allogeneic hematopoietic stem cell transplantation. Best Pract Res Clin Haematol. 2011; 24: 467–476. https://doi.org/10.1016/j.beha.2011.05.003 PMID: 21925100
10. Singh VK, Seed TM. A review of radiation countermeasures focusing on injury-specific medicinals and regulatory approval status: Part 1. Radiation sub-syndromes, animal models and FDA-approved countermeasures. Int J Radiat Biol. 2017; 93: 851–869. https://doi.org/10.1080/09553002.2017.1332438 PMID: 28650707
11. DeBo RJ, Register TC, Caudell DL, Sempowski GD, Dugan G, Gray S, et al. Molecular and cellular profiling of acute responses to total body radiation exposure in ovariectomized female cynomolgus macaques. Int J Radiat Biol. 2015; 91: 510–518. https://doi.org/10.3109/09553002.2015.1028597 PMID: 25786585
12. Ito R, Hale LP, Geyer SM, Li J, Sornberger A, Kajimura J, et al. Effects of age and exposure to ionizing radiation on human thymus morphology and function. Radiation Res. 2017; 187: 589–598. https://doi.org/10.1667/RR4554.1
13. Kajimura J, Lynch HE, Geyer S, French B, Yamaoka M, Shterev ID, et al. Radiation- and age-associated changes in peripheral blood dendritic cell populations among aging atomic bomb survivors in Japan. Radiat Res. 2018; 189:84–94. https://doi.org/10.1667/RR4854 PMID: 29324175

14. Hayashi T, Lynch HE, Geyer S, Yoshida K, Furudoi K, Sasaki K, et al. Impact of early life exposure to ionizing radiation on influenza vaccine response in an elderly Japanese cohort. 2018; Forthcoming.
15. Messaoudi I, Estep R, Robinson B, Wong SW. Nonhuman primate models of human immunology. Antioxid Redox Signal. 2011; 14: 261–273. https://doi.org/10.1089/ars.2010.3241 PMID: 20524846
16. Chen BJ, Deoliveira D, Spasojevic I, Sempowski GD, Jiang C, Owzar K, et al. Growth hormone mitigates against lethal irradiation and enhances hematologic and immune recovery in mice and nonhuman primates. PloS One. 2010; 5: e11056. https://doi.org/10.1371/journal.pone.0011056 PMID: 20585403
17. Farese AM, Cohen MV, Katz BP, Smith CP, Jackson W 3rd, Cohen DM, et al. A nonhuman primate model of the hematopoietic acute radiation syndrome plus medical management. Health Phys. 2012; 103: 367–382. https://doi.org/10.1097/HP.0b013e31825f75a7 PMID: 22929469
18. MacVittie TJ, Farese AM, Bennett A, Gelfond D, Shea-Donohue T, Tudor G, et al. The acute gastrointestinal subsyndrome of the acute radiation syndrome: A rhesus macaque model. Health Phys. 2012; 103: 411–426. https://doi.org/10.1097/HP.0b013e31826525f0 PMID: 22929470
19. National Research Council. 2011. Guide for the Care and Use of Laboratory Animals: Eighth Edition. Washington, DC: The National Academies Press. https://doi.org/10.17226/12910.
20. MacVittie TJ, Farese AM, Jackson W 3rd. The hematopoietic syndrome of the acute radiation syndrome in rhesus macaques: A systematic review of the lethal dose response relationship. Health Phys. 2015; 109: 342–366. https://doi.org/10.1097/HP.0000000000000352 PMID: 26425897
21. Yu JZ, Lindeblad M, Lyubimov A, Neri F, Smith B, Szilagyi E, et al. Subject-based versus population-based care after radiation exposure. Radiat Res. 2015; 184: 46–55. https://doi.org/10.1667/RR13918.1 PMID: 26121229
22. Uckun FM, Yanishevski Y, Tumer N, Waurzyniak B, Messinger Y, Chelstrom LM, et al. Pharmacokinetic features, immunogenicity, and toxicity of B43(anti-CD19)-pokeweed antiviral protein immunotoxin in cynomolgus monkeys. Clin Cancer Res. 1997; 3: 325–337. PMID: 9815689
23. Sopper S, Stahl-Hennig C, Demuth M, Johnston IC, Dorries R, ter Meulen V. Lymphocyte subsets and expression of differentiation markers in blood and lymphoid organs of rhesus monkeys. Cytometry. 1997; 29: 351–362. PMID: 9415418
24. Autissier P, Soulas C, Burdo TH, Williams KC. Immunophenotyping of lymphocyte, monocyte and dendritic cell subsets in normal rhesus macaques by 12-color flow cytometry: clarification on DC heterogeneity. J Immunol Methods. 2010; 360: 119–128. https://doi.org/10.1016/j.jim.2010.06.017 PMID: 20600075
25. Lal G, Balmer P, Stanford E, Martin S, Warrington R, Borrow R. Development and validation of a nonaplex assay for the simultaneous quantitation of antibodies to nine Streptococcus pneumoniae serotypes. J Immunol Methods. 2005; 296; 135–147. https://doi.org/10.1016/j.jim.2004.11.006 PMID: 15680158
26. Gray BM. 1979. ELISA methodology for polysaccharide antigens:protein coupling of polysaccharides for adsorption to plastic tubes. J Immunol Methods 1979; 28: 187–192. PMID: 38284
27. Pickering JW, Martins TB, Greer RW, Schroder MC, Astill ME, Litwin CM, et al. 2002. A multiplexed fluorescent microsphere immunoassay for antibodies to pneumococcal capsular polysaccharides. Am J Clin Pathol. 2002; 117: 589–596. https://doi.org/10.1309/4KEH-AGY7-UT5H-41XJ PMID: 11939734
28. Staros JV, Wright RW, Swingle DM. Enhancement by N-hydroxysulfosuccinimide of water-soluble carbodiimide mediated coupling reactions. Anal Biochem. 1986; 156: 220–222. PMID: 3740412
29. Terpstra TJ. The asymptotic normality and consistency of Kendall's test against trend, when ties are present in one ranking. Indagationes Mathematicae. 1952; 14: 327–333.
30. Jonckheere AR. A distribution-free kappa-sample test against ordered alternatives. Biometrika. 1954; 41: 133–145.
31. Wilcoxon F. Individual comparisons by ranking methods. Biometrics Bulletin. 1945; 1: 80–83.
32. Mann HB, Whitney DR. On a test of whether one of two random variables is stochastically larger than the other. Ann Math Statist. 1947; 18: 50–60.
33. Kendall M. A new measure of rank correlation. Biometrika. 1938; 30: 81–89.
34. Fisher RA. Statistical Methods for Research Workers. 14th ed. Edinburgh: Oliver and Boyd; 1970.
35. Fisher RA. The logic of inductive inference (with discussion). J Royal Statist Soc Ser A. 1935; 98: 39–82.
36. R Core Team. 2018. R: A language and environment for statistical computing. R Foundation for Statistical Computing, Available from: https://www.R-project.org/ [cited 25 May 2018].
37. Hothorn T, Hornik K, van de Wiel MA, Zeileis A (2006). A Lego system for conditional Inference. Amer Statistician. 2006; 60; 257–263.

38. Seshan VE. 2018. Clinfun: Clinical trial design and data analysis functions. R package version 1.0.15. Available from: https://CRAN.R-project.org/package [cited 25 May 2018].

39. Wickham H. 2017. Tidyverse: Easily install and load the 'Tidyverse'. R package version 1.2.1. Available from: https://CRAN.R-project.org/package [cited 25 May 2018].

40. Xie Y. 2018. Knitr: A general-purpose package for dynamic report generation in R. R package version 1.20. Available from: https://yihui.name/knitr [cited 25 May 2018].

41. Hakoda M, Kasagi F, Kusunoki Y, Matsuura S, Hayashi T, Kyoizumi S, et al. Levels of antibodies to microorganisms implicated in atherosclerosis and of C-reactive protein among atomic bomb survivors. Radiat Res. 2006; 166: 360–366. https://doi.org/10.1667/RR3589.1 PMID: 16881737

42. Citrin DE. Recent developments in radiotherapy. New Engl J Med. 2017; 377: 1065–1075. https://doi.org/10.1056/NEJMra1608986 PMID: 28902591

43. Xiao S, Shterev ID, Zhang W, Young L, Shieh J-H, Moore M, et al. Sublethal total body irradiation causes long-term deficits in thymus function by reducing lymphoid progenitors. J Immunol. 2017; 199: 2701–2712. https://doi.org/10.4049/jimmunol.1600934 PMID: 28931604

44. Lepletier A, Chidgey AP, Savino W. Perspectives for improvement of the thymic microenvironment through manipulation of thymic epithelial cells: A mini-review. Gerontol. 2015; 61: 504–514.

45. Geno KA, Gilbert GL, Song JY, Skovsted IC, Klugman KP, Jones C, et al. Clin Microbiol. Rev. 2015; 28: 871–899. https://doi.org/10.1128/CMR.00024-15 PMID: 26085553

46. Vialle S, Sepulcri P, Dubayle J, Talaga P. The teichoic acid (C-polysaccharide) synthesized by *Streptococcus pneumoniae* serotype 5 has a specific structure. Carbohydrate Res. 340;205: 91–96.

47. Fulop T, Larbi A, Pawelec G. Human T cell aging and the impact of persistent viral infections. Front Immunol. 2013; 4: 271. https://doi.org/10.3389/fimmu.2013.00271 PMID: 24062739

48. Sambhara S, McElhaney JE. Immunosenescence and influenza vaccine efficacy. Curr Top Microbiol Immunol. 2009; 333: 413–429. https://doi.org/10.1007/978-3-540-92165-3_20 PMID: 19768417

49. Haynes L, Maue AC. Effects of aging on T cell function. Curr Opin Immunol. 2009; 21: 414–417. https://doi.org/10.1016/j.coi.2009.05.009 PMID: 19500967

50. Murasko DM, Goonewardene IM. T-cell function in aging: Mechanisms of decline. Ann Rev Gerontol Geriatrics. 1990; 10: 71–96.

RADIATION RESEARCH **192**, 121–134 (2019)
0033-7587/19 $15.00
©2019 by Radiation Research Society.
All rights of reproduction in any form reserved.
DOI: 10.1667/RR15310.1

Monocyte Polarization is Altered by Total-Body Irradiation in Male Rhesus Macaques: Implications for Delayed Effects of Acute Radiation Exposure

Kristofer T. Michalson,[a,1] Andrew N. Macintyre,[d] Gregory D. Sempowski,[d] J. Daniel Bourland,[b] Timothy D. Howard,[c] Gregory A. Hawkins,[c] Gregory O. Dugan,[a] J. Mark Cline[a] and Thomas C. Register[a,2]

Departments of [a] Pathology/Comparative Medicine, [b] Radiation Oncology and [c] Biochemistry, Wake Forest University School of Medicine, Winston-Salem, North Carolina; and [d] Duke Human Vaccine Institute, Duke University School of Medicine, Durham, North Carolina

Michalson, K. T., Macintyre, A. N., Sempowski, G. D., Bourland, J. D., Howard, T. D., Hawkins, G. A., Dugan, G. O., Cline, J. M. and Register, T. C. Monocyte Polarization is Altered by Total-Body Irradiation in Male Rhesus Macaques: Implications for Delayed Effects of Acute Radiation Exposure. *Radiat. Res.* 192, 121–134 (2019).

Radiation-induced fibrosis (RIF) is a common delayed effect of acute ionizing radiation exposure (DEARE) affecting diverse tissues including the heart, lungs, liver and skin, leading to reduced tissue function and increased morbidity. Monocytes, which may be classified into classical ($CD14^{++}$, $CD16^{-}$), intermediate ($CD14^{++}$, $CD16^{+}$) and non-classical ($CD14^{+/low}$, $CD16^{++}$) subtypes in humans and non-human primates (NHPs), and monocyte-derived macrophages may play an integral role in the pathogenesis of RIF. We tested the hypothesis that moderate to high levels of total-body exposure to radiation would alter monocyte polarization and produce phenotypes that could promote multi-organ fibrosis in a well-established NHP model of DEARE. Subjects were 16 young adult male rhesus macaques, ten of which were exposed to high-energy, 4 Gy X-ray total-body irradiation (TBI) and six that received sham irradiation (control). Total monocytes assessed by complete blood counts were 89% depleted in TBI animals by day 9 postirradiation ($P < 0.05$), but recovered by day 30 postirradiation and did not differ from control levels thereafter. Monocytes were isolated from peripheral blood mononuclear cells (PBMCs) and sorted into classical, intermediate and non-classical subsets using fluorescence-activated cell sorting (FACS) prior to and at 6 months post-TBI. At 6 months postirradiation, monocyte polarization shifted towards lower classical (92% → 86%) and higher intermediate (7% → 12%) and non-classical monocyte subsets (0.6% → 2%) (all $P < 0.05$) in TBI animals compared to baseline. No change in monocyte subsets was observed in control animals. Transcriptional profiles in classical and intermediate monocyte subsets were assessed using RNAseq. Classical monocyte gene expression did not change significantly over time or differ cross-sectionally between TBI and control groups. In contrast, significant numbers of differentially expressed genes (DEGs) were detected in intermediate monocyte comparisons between the TBI animals and all animals at baseline (304 DEGs), and in the TBI versus control animals at 6 months postirradiation (67 DEGs). Intermediate monocytes also differed between baseline and 6 months in control animals (147 DEGs). Pathway analysis was used to identify genes within significant canonical pathways, yielding 52 DEGs that were specific to irradiated intermediate monocytes. These DEGs and significant canonical pathways were associated with pro-fibrotic and anti-inflammatory signaling pathways that have been noted to induce M2 macrophage polarization. These findings support the hypothesis that TBI may alter monocyte programming and polarization towards a profibrotic phenotype, providing a novel target opportunity for therapies to inhibit or prevent RIF. **© 2019 by Radiation Research Society**

INTRODUCTION

One delayed effect of acute ionizing radiation exposure (DEARE) is radiation-induced fibrosis (RIF), a debilitating condition occurring 4–12 months postirradiation in humans that has been referred to as a ''wound that fails to heal'' (*1*). Radiation-induced fibrosis has been documented in many tissues including the heart (*2*), lungs (*3*), liver (*4*) and skin (*5, 6*) and is hypothesized to involve initial injury and healing followed by a period of cellular quiescence and later progression to fibrosis (*7*). The initiation signals that lead to progression from quiescence to RIF are largely unknown, but may involve an aberrant healing response mediated by monocytes, macrophages, fibroblasts, endothelial cells and platelets (*8–10*). Ultimately, this response results in excessive deposition of extracellular matrix, which reduces tissue compliance, impairs functionality and increases morbidity. Unfortunately, there are currently no therapies that can halt or reverse RIF (*1*). In 2016, 3.05 million cancer survivors were estimated to have been treated with radiotherapy, and the number is expected to increase to

Editor's note. The online version of this article (DOI: 10.1667/RR15310.1) contains supplementary information that is available to all authorized users.

[1] Radiation Research Society Scholar-in-training.

[2] Address for correspondence: Department of Pathology, Section on Comparative Medicine, Wake Forest University School of Medicine, Medical Center Boulevard, Winston-Salem, NC 27157-1040; email: register@wakehealth.edu.

4.17 million by 2030 (*11*), representing a large at-risk population for RIF.

Monocytes are key cells of the innate immune system, constituting 5–10% of circulating white blood cells in humans and non-human primates (*12*). They respond to tissue injury and may transform into tissue-resident macrophages upon exiting the vasculature. In human and non-human primates, they are often classified based on cell surface expression of CD14 [a co-receptor with Toll-like receptor 4 and lymphocyte antigen 96 (MD2) that together function to detect LPS] and CD16 (FcγRIII) expression into classical ($CD14^{++}$, $CD16^{-}$), intermediate ($CD14^{++}$, $CD16^{+}$) and non-classical ($CD14^{+/low}$, $CD16^{++}$) monocytes (*13*). Classical monocytes represent the majority of monocytes (85–90%) with intermediate and non-classical monocytes comprising the remainder (5–10% each) (*13*). It is currently unclear whether classical monocytes differentiate over time in a linear fashion into intermediate and non-classical monocytes (*12, 14, 15*) or if they are programmed from macrophage dendritic cell progenitors (MDPs) in the bone marrow (*16*). However, it is known that these monocyte subsets have disparate phenotypes, classical monocytes being associated with inflammatory responses and anaerobic metabolism, intermediate monocytes being associated with antigen presentation and processing, and non-classical monocytes being associated with oxidative phosphorylation and protein metabolism (*17, 18*). Depending on the signals received from the local and systemic environment, monocytes may adopt pro-inflammatory (M1-like) or anti-inflammatory-tissue remodeling/profibrotic (M2-like) phenotypes as monocyte-derived macrophages (*19*).

Increased intermediate monocyte polarization and subsequent tissue infiltration has been implicated as a primary mediator of pro-fibrotic activity in pathologic fibrotic disorders including systemic sclerosis, renal fibrosis, idiopathic pulmonary fibrosis, hepatic fibrosis, cardiac fibrosis and skeletal muscle fibrosis (*13, 20, 21*) but their role in RIF is currently unclear. Groves *et al.* (*22*) recently provided clarification in this area, showing in a murine MCP-1 receptor (CCR2) knockout model of total-body irradiation (TBI) with bone marrow transplantation a significantly reduced influx of peripheral monocyte-derived macrophages and reduced radiation-induced fibrosis in the lung. Additionally, Gibbons *et al.* (*23*) demonstrated that early monocyte and macrophage depletion by clodronate in a bleomycin-induced pulmonary fibrosis model led to a reduction in fibrosis. In the current study, we sought to assess the effects of TBI on circulating monocyte polarization in rhesus macaques, a well-established model of acute and delayed effects of ionizing radiation exposure. We hypothesized that monocyte polarization would shift towards increased intermediate and non-classical subsets and that transcriptional changes would reflect increased pro-fibrotic/anti-inflammatory pathways.

MATERIALS AND METHODS

Animals

Sixteen male rhesus macaques, aged 5.8 ± 0.5 years, were obtained from World Wide Primates, Inc. (Miami, FL). Animals were pre-screened for tuberculosis and simian retroviruses and upon arrival were examined by a veterinarian, and quarantined for 60 days per standard institutional protocol. After quarantine, animals were fed a Western-like diet [typical American diet (TAD); LabDiet®, St. Louis, MO] and randomized to receive 4 Gy TBI ($n = 10$) or sham irradiation (control; $n = 6$). Irradiations were designed to mimic what might occur in a nuclear event, and were not intended to replicate radiation treatments for medical procedures, although some inferences may be made in cases where TBI is employed. The 4 Gy dose was selected to be well below the $LD_{50/60}$ of 7.5 Gy previously reported for male rhesus monkeys (*24*). Irradiations were performed on a clinical linear accelerator using two lateral fields of 6-MV X rays [174-cm source-axis-distance (SAD), 32×40 cm^2 field size at 100 cm from the source, nominal dose rate of 0.8 Gy/min at 174 cm SAD, 2.7 min irradiation time per field]. The irradiation geometry was dosimetrically confirmed prior to animal irradiation using a calibrated dosimeter system. The same dosimetry system was used for *in vivo* transit dosimetry for each radiation field delivered for each animal, with real-time analysis confirming the integrated dose received from the two fields. Each animal was sedated via an intramuscular injection of 15 mg/kg ketamine and placed in the supine position between two plastic build-up screens, knees up and arms crossed at the lower abdomen, with water-bolus compensation for thinner body regions (head and lower legs). The left side was irradiated first using 2 Gy and the animal was then rotated 180° to irradiate the right side using 2 Gy, for a total dose of 4 Gy. Dose calculations were performed for 2 Gy to mid-plane per field, based on anatomical measurements (nominal depths of 8–10 cm). Sham-irradiated animals underwent all procedural steps, including sedation, positioning and observation from outside the radiation room for the elapsed time of irradiation for each field, except that ionizing radiation was not delivered.

Monkeys were monitored daily for food consumption, defecation, urination and evidence of illness. Illness was determined using methods modified from the Children's Cancer Group Clinical Toxicity Criteria established by Uckun *et al.* (*25*). Additionally, complete blood counts and chemistry panels were conducted weekly after irradiation and intervention was guided by clinical pathologic findings as reported elsewhere by our group in DeBo *et al.* (*26*) All experimental procedures were performed in accordance with the Guide for Care and Use of Laboratory Animals and followed protocol for avoidance of pain and discomfort and conducted in compliance with the Wake Forest School of Medicine (WFSM) Institutional Animal Care and Use Committee requirements. WFSM is accredited by the Association for the Assessment and Accreditation of Laboratory Animal Care International, and operates in compliance with the Animal Welfare Act.

Total Monocyte Counts

Total monocyte and other blood cell fraction counts were obtained from complete blood counts that were collected before irradiation, then weekly after irradiation for two months and then monthly thereafter. Analyses were conducted by an external commercial veterinary laboratory (IDEXX Laboratories, North Grafton, MA).

Monocyte Isolation

Classical ($CD14^{++}$, $CD16^{-}$), intermediate ($CD14^{++}$, $CD16^{+}$) and non-classical ($CD14^{+/low}$, $CD16^{++}$) monocytes were obtained using fluorescence-activated cell sorting (FACS) on isolated peripheral blood mononuclear cells (PBMCs) before irradiation and 6 months postirradiation. PBMCs were first isolated using 50-ml Leucosep Centrifuge Tubes (Greiner Bio-One, Monroe, NC) according to

manufacturer instructions. Briefly, 15 ml of EDTA whole blood was mixed with 15 ml phosphate buffered saline (PBS) without calcium or magnesium and layered onto 15 ml of 1.077-density Ficoll-Paque® Premium (GE Healthcare Life Sciences, Marlborough, MA). Tubes were centrifuged at 800*g* for 20 min at room temperature and PBMCs were collected from the interphase layer. PBMCs were washed with PBS without calcium or magnesium and centrifuged at 300*g* for 10 min, subsequently incubated in 1:9-ratio ammonium-chloride-potassium lysing buffer for 10 min to remove residual erythrocytes, centrifuged at 300*g* for 10 min and re-washed with PBS. Washed PBMCs were counted and assessed for viability using ViaStain™ acridine orange/propidium iodide (AOPI) staining solution (Nexcelom Bioscience LLC, Lawrence, MA) on a Cellometer Vision Cell Profiler (Nexcelom Bioscience LLC, Lawrence, MA).

After isolation, PBMCs were incubated for 20 min at 4–8°C with 80 μl/1 × 10^7 cells autoMACS running buffer and 20 μl/1 × 10^7 CD14 non-human primate MicroBeads (Miltenyi Biotec, Bergisch Gladbach, Germany). PBMCs were washed with 2 ml autoMACS running buffer, centrifuged at 300*g* for 10 min, resuspended in 500 μl autoMACS running buffer and subsequently run over magnetic separation (MS) columns (Miltenyi Biotec, Bergisch Gladbach, Germany). Collected $CD14^+$ monocytes were counted and assessed for viability using AOPI staining solution on the Cellometer Vision Cell Profiler, centrifuged and resuspended in 100 μl PBS per 1 × 10^6 cells. $CD14^+$ positive monocytes were incubated with 10 μl/1 × 10^6 cells CD14-PE (Tük4 clone) conjugated and CD16-VioBlue (VEP13 clone) conjugated monoclonal antibodies and appropriate isotype controls (all from Miltenyi Biotec, Bergisch Gladbach, Germany), incubated for 1 h 30 min at 4°C during transport to the Duke Human Vaccine Institute Flow Cytometry Core (Durham, NC). Cell subset proportions and preparations were obtained by FACS through sorting into classical, intermediate and non-classical monocytes using a FACSAria™ II flow cytometer (Becton Dickinson, Franklin Lakes, NJ), then stored in 85% FBS/15% DMSO sterile freezing media within a Mr. Frosty freezing container (Thermo Fisher Scientific™, Waltham, MA) at –80°C for 24 h before transfer into a liquid nitrogen dewar.

Total RNA Isolation

Isolated classical and intermediate monocytes stored in freezing media were thawed and centrifuged at 1,000*g* for 5 min. The freezing media was drawn off, RLT buffer (QIAGEN®, Valencia, CA) was added and the sample was disrupted by passing over a QIAshredder column (QIAGEN). The disrupted samples were then extracted for total RNA using the AllPrep DNA/RNA Mini Kit according to manufacturer's protocol (QIAGEN). The extracted RNA was DNase-treated and purified using the RNA Clean & Concentrator™-5 kit (Zymo Research, Irvine, CA) and assessed for RNA quality using an Agilent 2100 Bioanalyzer and the RNA 6000 Pico Kit (Agilent Technologies, Santa Clara, CA).

cDNA Library Preparation and Sequencing Methods

Total RNA was used to prepare cDNA libraries with the SMARTer® Stranded Total RNA-Seq Kit v2 - Pico Input Mammalian (TaKaRa Bio USA Inc., Mountain View, CA). Briefly, 8 ng of total RNA was subjected to fragmentation followed by reverse-transcription. Illumina sequencing adaptors were attached during PCR amplification and the double-stranded cDNA was purified using AMPure XP magnetic beads. Finally, the cDNA was subjected to rRNA depletion and the stranded libraries were pre-amplified with PCR. The library size distribution was validated and quality inspected on an Agilent 2100 Bioanalyzer using a High Sensitivity DNA chip (Agilent Technologies). The quantity of each cDNA library was measured using a Qubit® 3.0 Fluorometer (Thermo Fisher Scientific). Libraries were sequenced to a read depth of >35*M* reads per sample using 1 × 75 bp single-end (SE) sequencing (Illumina®, San Diego, CA) on the Illumina NextSeq 500.

Data Processing and Expression Analysis

RNA sequencing quality control, alignment, read counts and differential gene expression was facilitated using Galaxy analysis platform (*27*). FASTq files were quality checked using FastQC (*28*), aligned to the rhesus macaque (rheMac3) genome using HISAT2 (*29*) and count files were generated using RefSeq genes in htseq-count using union mode (*30*). Differential gene expression was calculated via edgeR (*31, 32*) using robust settings to remove outlier genes, then filtering genes with less than 1.0 counts per million, and finally normalizing gene counts between samples using the trimmed mean of M values (TMM) method. Comparisons were made to evaluate the following: 1. differences in classical monocytes between TBI and control groups at 6 months postirradiation and changes from baseline in each group; and 2. differences between intermediate monocytes between TBI and control groups at 6 months postirradiation as well as changes in each group from baseline.

Statistics

All data were analyzed for normality and are presented as mean ± SEM. All analyses, except for gene expression analyses, were performed using Statistica™ version 13.3 (TIBCO® Software Inc., Palo Alto, CA). Difference in leukocyte counts and monocyte phenotypes were assessed using analysis of variance (ANOVA) or repeated measures ANOVA with Bonferroni post hoc tests. The level of significance was set at $P < 0.05$. Differential gene expression was calculated using edgeR with a log2 fold change threshold of 1.0 and Benjamini and Hochberg adjusted $P < 0.05$. Pathway analysis thresholds for significance are presented as an enrichment score based on a Fischer's exact test $P < 0.05$ in Ingenuity Pathway Analysis (IPA) software (QIAGEN).

Post-Statistical Analysis of Biomolecular Pathways Implicated in TBI Responses

For those genes found to meet the criteria of being differentially expressed in response to TBI, biomolecular pathway analysis was performed using IPA software.

RESULTS

Leukocyte Depletion and Recovery Postirradiation

Total white blood cells, monocyte, lymphocyte and neutrophil counts were all acutely depleted in animals receiving TBI ($P < 0.05$). Monocytes and neutrophil counts recovered by day 30 postirradiation while total white blood cells and lymphocytes were significantly decreased until days 51 and 58 postirradiation, respectively [Fig. 1 (linear scale) or Supplementary Fig. S1; http://dx.doi.org/10.1667/RR15310.1.S1 (log scale)]. Total white blood cells, monocytes and neutrophils in TBI animals did not differ from controls post-recovery, but TBI lymphocytes increased above controls by day 129 postirradiation and remained elevated to the 200-day timepoint.

Monocyte Subset Alterations in Response to TBI

Magnetic bead-selected $CD14^+$ monocytes were gated based on forward- and side-scatter parameters before final gating into classical ($CD14^{++}$, $CD16^-$), intermediate ($CD14^{++}$, $CD16^+$) and non-classical ($CD14^{+/low}$, $CD16^{++}$) subsets (Fig. 2). At 6 months postirradiation, monocyte

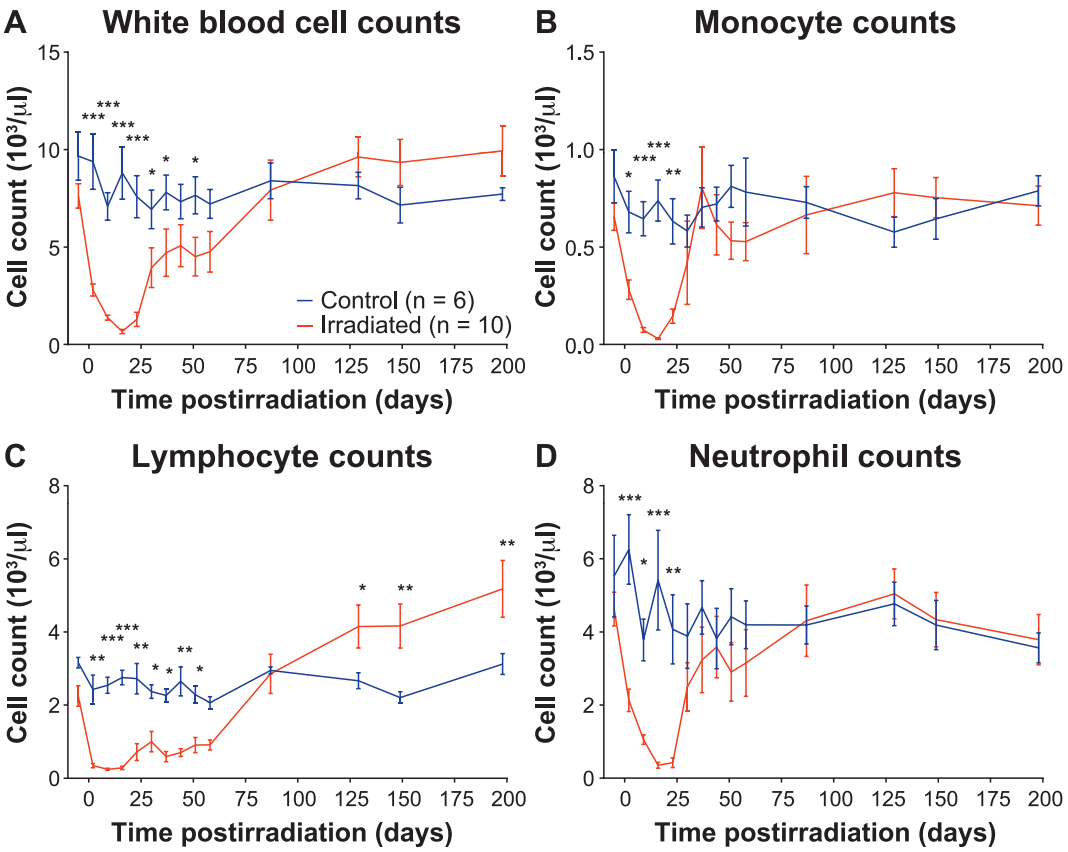


FIG. 1. Peripheral immune cell recovery after total-body irradiation. Panels A–D: Total white blood cell, monocyte, lymphocyte and neutrophil counts, respectively, were all acutely depleted by TBI. Monocytes and neutrophils recovered by dau 30 postirradiation while total white blood cells and lymphocytes remained significantly decreased until days 51 and 58 postirradiation, respectively. After recovery, total white blood cells, monocytes and neutrophils in irradiated animals did not differ from controls, but lymphocytes increased above controls animals at day 129 postirradiation and remained elevated thereafter. $*P < 0.05$, $**P < 0.01$ and $***P < 0.001$.

polarization shifted towards lower classical (92% → 86%) and higher intermediate (7% → 12%) and non-classical monocyte subsets (0.6% → 2%) (all $P < 0.05$) in TBI animals compared to baseline. No changes in monocyte subset proportions were observed in the control animals (Fig. 3).

Classical Monocyte Gene Expression Responses to TBI

Differential gene expression in classical monocytes was evaluated by comparing the following: 1. TBI at 6 months to TBI baseline; 2. control at 6 months to control baseline; and 3. TBI at 6 months to control at 6 months (Table 1). The full list of genes assessed for each comparison, including log2 fold change, raw P value and false discovery rate (FDR) P value, is provided in Supplementary Table S1A (http://dx.doi.org/10.1667/RR15310.1.S2); and an abbreviated list of genes within each comparison in which the FDR is below 0.10 is provided in Supplementary Table S1B (http://dx.doi.org/10.1667/RR15310.1.S3). For the classical subset, there were three DEGs (3 upregulated) identified when TBI at 6 months was compared to TBI at baseline;

TABLE 1
Cross-Sectional and Longitudinal Differential Gene Expression in Classical Monocytes

Classical monocyte comparisons	Total DEGs	Upregulated DEGs	Downregulated DEGs
Irradiated[a] (6 months postirradiation) vs. baseline (all animals) [b]	3	3	0
Control[c] (6 months postirradiation) vs. baseline (all animals)[b]	12[d]	12[d]	0[d]
Irradiated[a] (6 months postirradiation) vs. control[c] (6 months postirradiation)	0[d]	0[d]	0[d]

[a] Irradiated animals (n = 10).
[b] All animals (n = 16)
[c] Control animals (n = 6).
[d] Denotes potentially underpowered comparison.
Abbrevation: DEGs = differentially expressed genes.

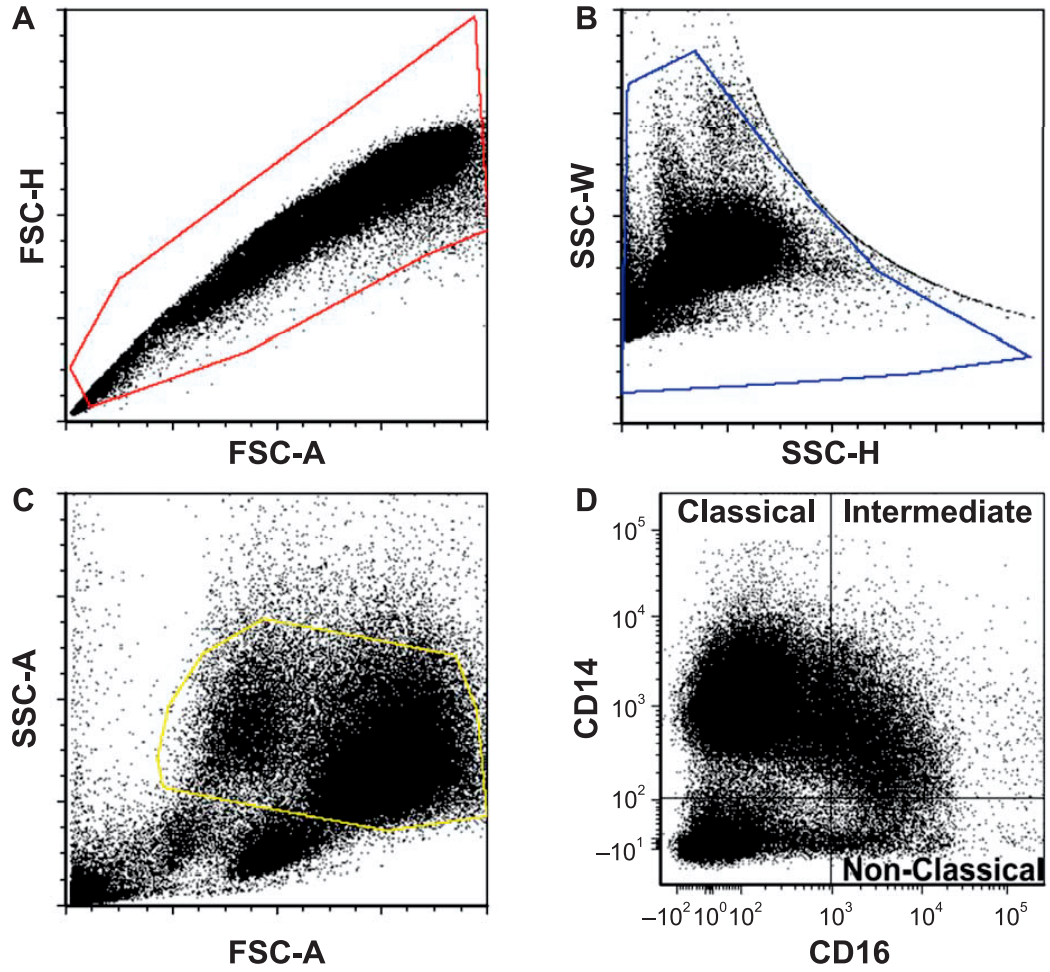


FIG. 2. Gating strategy to obtain monocyte subsets. Magnetic bead selected $CD14^+$ monocytes were gated based on forward- and side-scatter parameters before final gating into classical ($CD14^{++}$, $CD16^-$), intermediate ($CD14^{++}$, $CD16^+$) and non-classical ($CD14^{+/low}$, $CD16^{++}$) phenotypes. Panel A: Forward scatter plot. Panel B: Side scatter plot. Panel C: Forward scatter-side scatter. Panel D: Final representation of monocyte subsets by CD14 and CD16 labeling. Profiles from a representative sample from an irradiated animal at 6 months postirradiation are shown. FSC-H = forward scatter height; FSC-A = forward scatter area; SSC-W = side scatter width; SSC-H = height; SSC-A = side scatter area.

and 12 DEGs (12 upregulated) were identified when control at 6 months was compared to control at baseline. No significant DEGs were identified in a comparison between TBI at 6 months and control at 6 months. For classical monocytes, no canonical pathways were identified as being significantly influenced by TBI, using IPA.

Intermediate Monocyte Gene Expression Responses to TBI

Differences in gene expression between groups and over time in intermediate monocytes were evaluated by: 1. Comparing TBI monocytes at 6 months to baseline; 2. Comparing control monocytes at 6 months to baseline; and 3. Comparing TBI monocytes at 6 months to control at 6 months (Table 2). The full list of genes assessed for each comparison, including log2 fold change, raw *P* value and FDR *P* value are listed in Supplementary Table S2A (http://dx.doi.org/10.1667/RR15310.1.S4); and the abbreviated list of genes within each comparison, in which the FDR is below 0.10, is provided in Supplementary Table S2B(http://dx.doi.org/10.1667/RR15310.1.S5).

TABLE 2
Cross-Sectional and Longitudinal Differential Gene Expression in Intermediate Monocytes

Intermediate monocyte comparisons	Total DEGs	Upregulated DEGs	Downregulated DEGs
Irradiated (6 months postirradiation) vs. baseline	304	145	159
Control (6 months postirradiation) vs. baseline	147*	115*	32*
Irradiated (6 months postirradiation) vs. control (6 months postirradiation)	67*	25*	42*

Notes. Irradiated animals (n = 10), control animals (n = 6); *Denotes potentially underpowered comparison. DEGs = differentially expressed genes.

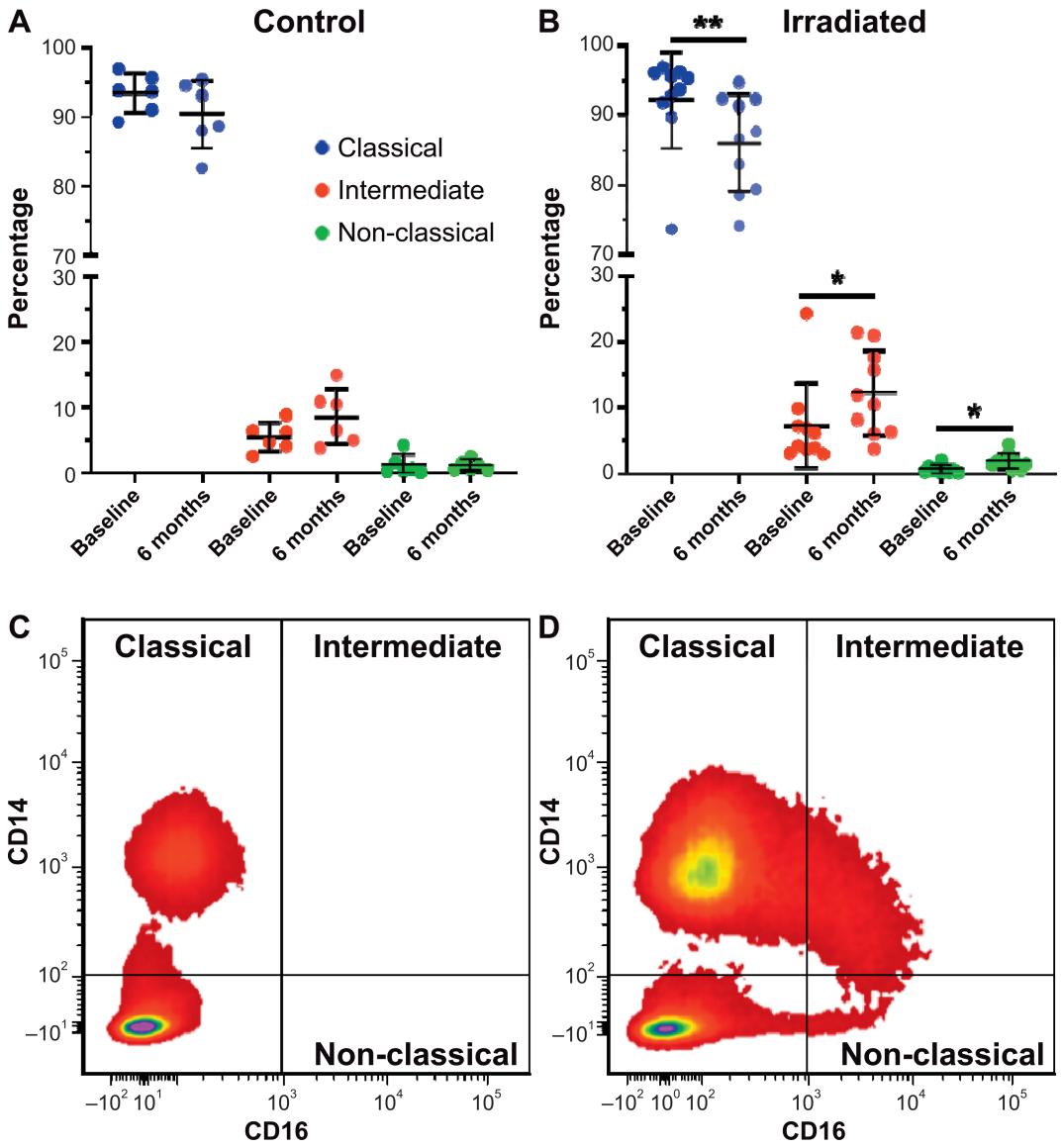


FIG. 3. Alterations in distribution of monocyte subtypes after total-body irradiation. Panel A: Monocyte polarization was unaltered in control animals at 6 months after sham irradiation. Panel B: In contrast, irradiated animals had significant shifts towards lower classical and higher intermediate and non-classical monocyte subsets compared to baseline. Panels C and D: Flow cytometry density plots from a representative control and irradiated animal, respectively, are shown at 6 months postirradiation. (*$P < 0.05$ and **$P < 0.01$).

There were 304 DEGs (145 upregulated and 159 downregulated in the TBI group) identified when the TBI group at 6 months was compared to baseline. The top five diseases and disorders associated with these DEGs were endocrine system disorders, gastrointestinal disease, inflammatory disease, inflammatory response, and organismal injury and abnormalities (all $P < 0.05$). The top 20 significant pathways (all $P < 0.05$) are shown in Fig. 4. Pathways containing a majority of upregulated genes included synaptic long-term depression, Huntington's disease signaling, cyclic AMP response element binding protein (CREB) signaling in neurons and G-protein coupled receptor signaling. Pathways containing a majority of downregulated genes included sirtuin signaling pathway, cleavage and polyadenylation of pre-mRNA, pyrimidine ribonucleotides interconversion, D-myo-inositol (1,4,5)-trisphosphate degradation, pyrimidine ribonucleotides de novo biosynthesis, alanine degradation III, alanine biosynthesis II, sperm motility, role of NFAT in cardiac hypertrophy, androgen signaling and pyrimidine deoxyribonucleotides de novo biosynthesis I. Pathways with equal number of up- and downregulated genes included antioxidant action of vitamin C, phospholipases, gustation pathway, gonadotropin-releasing hormone (GNRH) signaling and bladder cancer signaling.

There were 147 DEGs (115 upregulated and 32 downregulated) identified when control intermediate monocytes at 6 months were compared to baseline. The top five

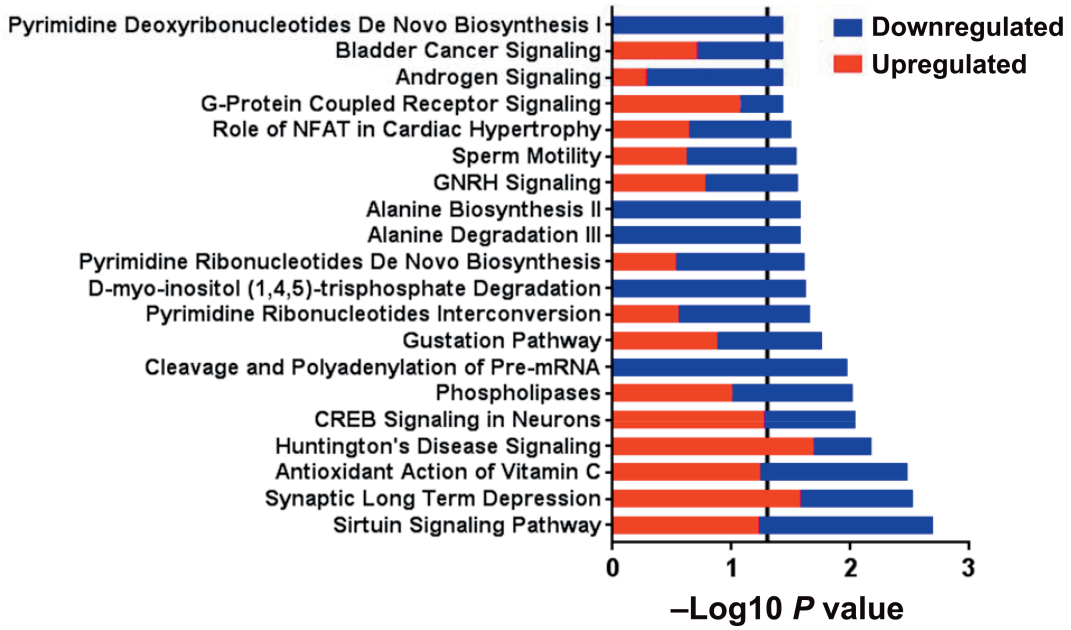


FIG. 4. Canonical pathways differentiating intermediate monocytes in irradiated subjects at 6 months (n = 10) from all subjects (n = 16) at baseline. Within each pathway red bars indicate the proportion of DEGs upregulated in irradiated subjects at 6 months, blue bars indicate the proportion of DEGs downregulated in irradiated subjects at 6 months and the overall length of the bar is the –log10 *P* value. The vertical line indicates the threshold for significance based on a –log10 *P* value of 1.3 (equal to $P < 0.05$).

diseases and disorders associated with these DEGs were neurological disease, psychological disorders, organismal injury and abnormalities, gastrointestinal disease and immunological disease (all $P < 0.05$). The top 20 significant pathways (all $P < 0.05$) are shown in Fig. 5. Pathways containing a majority of upregulated genes included triggering receptor expressed on myeloid cells (TREM1) signaling, G-protein coupled receptor signaling, gamma-aminobutyric acid (GABA) receptor signaling, cAMP-mediated signaling, polyamine regulation in colon cancer, glutamate dependent acid resistance, interleukin 12 (IL12) signaling and production in macrophages, neuroinflammation signaling pathway, thyronamine and iodothyronamine metabolism, thyroid hormone metabolism I

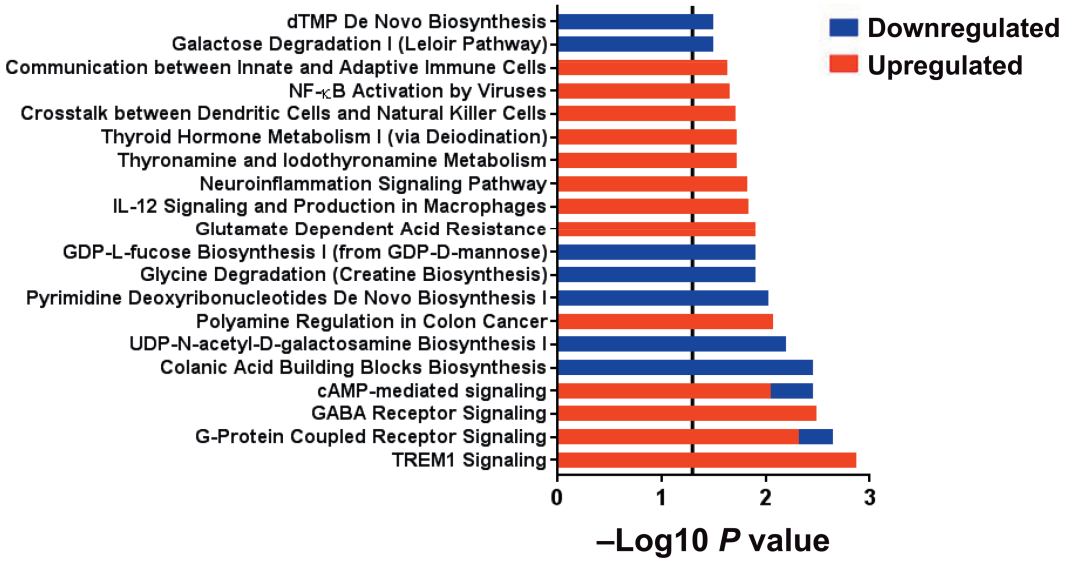


FIG. 5. Canonical pathways differentiating intermediate monocytes in control subjects at 6 months to all subjects (n = 16) at baseline. Within each pathway red bars indicate the proportion of DEGs upregulated in control subjects at 6 months, blue bars indicate the proportion of DEGs downregulated in control subjects at 6 months within the respective pathway and the overall length of the bar is the –log10 *P* value. The vertical line indicates the threshold for significance based on a –log10 *P* value of 1.3 (equal to $P < 0.05$).

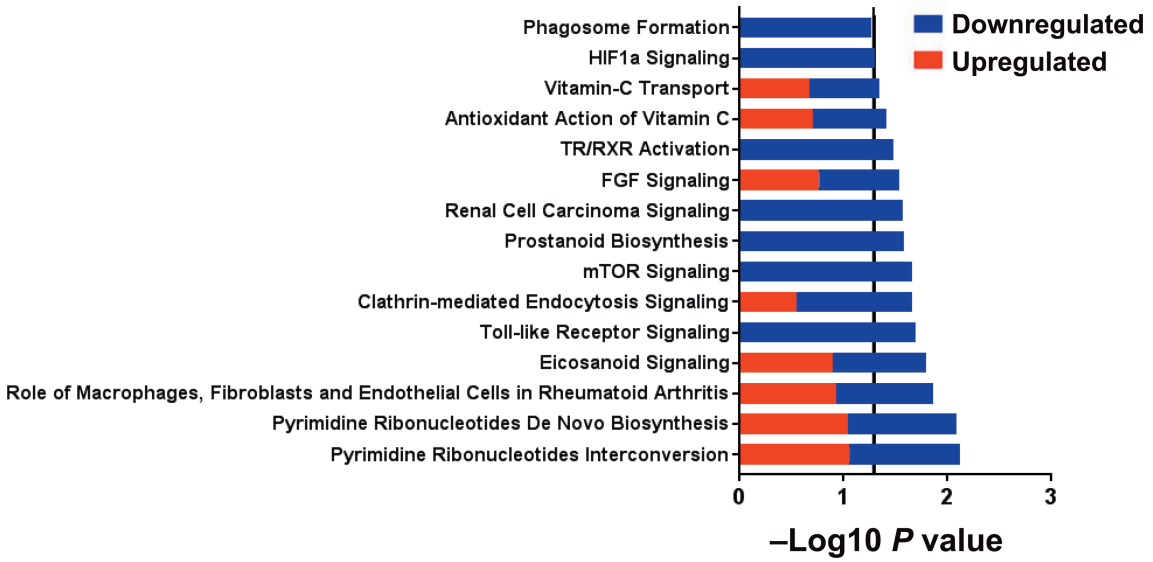


FIG. 6. Canonical pathways differentiating intermediate monocytes in irradiated subjects from control at 6 months. Within each pathway red bars indicate the proportion of DEGs upregulated in irradiated subjects, the blue bars indicate the proportion of DEGs downregulated in irradiated subjects within the respective pathway and the overall length of the bar is the –log10 *P* value. The vertical line indicates the threshold for significance based on a –log10 *P* value of 1.3 (equal to $P < 0.05$).

(via deiodination), crosstalk between dendritic cells and natural killer cells, nuclear factor kappa-light-chain-enhancer of activated B cells (NFκB) activation by viruses and communication between innate and adaptive immune cells. Pathways containing a majority of downregulated genes included colanic acid building blocks biosynthesis, UDP-N-acetyl-D-galactosamine biosynthesis I, pyrimidine deoxyribonucleotides de novo biosynthesis I, glycine degradation (creatine biosynthesis), GDP-L-fucose biosynthesis I (from GDP-D-mannose), galactose degradation I (Leloir pathway), and deoxythymidine monophosphate (dTMP) de novo biosynthesis.

We identified 67 DEGs (25 upregulated and 42 downregulated after TBI) between TBI intermediate monocytes at 6 months and controls at 6 months. The top five diseases and disorders associated with these DEGs were inflammatory response, cancer, organismal injury and abnormalities, infectious disease and neurological disease (all $P < 0.05$). The significant pathways are shown in Fig. 6 (all $P < 0.05$). For all identified pathways, at least half of the genes were downregulated in TBI. Pathways containing a majority of TBI downregulated genes included Toll-like receptor signaling, clathrin-mediated endocytosis signaling, mTOR signaling, prostanoid biosynthesis, renal cell carcinoma signaling, fibroblast growth factor (FGF) signaling, thyroid hormone receptor (TR)/retinoid X receptor (RXR) activation, hypoxia inducible factor 1 alpha (HIF1α) signaling, and phagosome. Pathways containing equal numbers of up- and downregulated genes included pyrimidine ribonucleotides interconversion, pyrimidine ribonucleotides de novo biosynthesis, role of macrophages, fibroblasts and endothelial cells in rheumatoid arthritis, eicosanoid signaling, antioxidant action of vitamin C and vitamin-C transport.

To determine DEGs that were specific to TBI intermediate monocytes at 6 months, we evaluated shared and distinct DEGs from all intermediate monocyte comparisons (TBI, 6 months vs. baseline; control, 6 months vs. baseline; and TBI, 6 months vs. control, 6 months) and removed DEGs ($n = 47$) that were found to be differentially expressed over the 6-month time period in the control group. (Fig. 7). Remaining DEGs were subsequently combined ($n = 300$) (Fig. 7) and analyzed using pathway analysis in IPA to determine canonical pathways specific to TBI, 6-month intermediate monocytes (Fig. 8). From this analysis we identified the subset of individual DEGs that were associated with significant canonical pathways. This yielded 52 DEGs (23 upregulated in TBI, 6-month monocytes compared to time-corrected control, 29 downregulated) (Table 3). The top five diseases and disorders associated with these DEGs were cancer, organismal injury and abnormalities, neurological disease, gastrointestinal disease and skeletal and muscular disorders (all $P < 0.05$). The top 10 irradiated upregulated genes by log2 fold change were: Fc fragment of IgG receptor Ia (FCGR1A), collagen type III alpha 1 chain (COL3A1), gap junction protein beta 1 (GJB1), translocase of outer mitochondrial membrane 40 like (TOMM40L), glutamate metabotropic receptor 8 (GRM8), adenylate cyclase 2 (ADCY2), glutamate metabotropic receptor 1(GRM1), gap junction protein gamma 1 (GJC1), P21 (Rac1) activated kinase 6 (PAK6), and fibroblast growth factor 7 (FGF7). The top 10 downregulated genes were taste 2 receptor member 39 (TAS2R39), cyclin dependent kinase 7 (CDK7), transforming growth factor beta 1 induced transcript 1 (TGFB1I1),

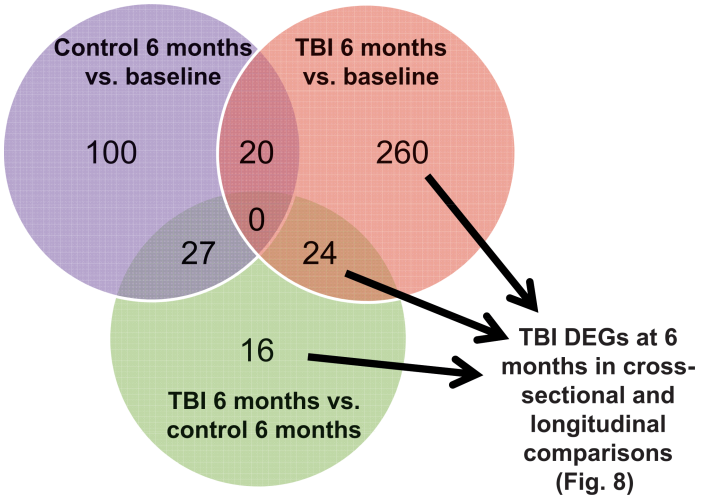


FIG. 7. Differentiating irradiated vs. control intermediate monocyte differentially expressed genes using cross-sectional and longitudinal analyses. Intermediate monocyte DEGs affected by radiation (n = 300) were determined by removing DEGs shared with longitudinal analyses of control intermediate monocytes (n = 47).

CD80 molecule (CD80), RNA polymerase II subunit G (POLR2G), G protein subunit beta 3 (GNB3), solute carrier family 25 member 42 (SLC25A42), H1 histone family, member X (H1FX), fibroblast growth factor 23 (FGF23), and phospholipase A2 group V (PLA2G5). The top 10 significant pathways (all $P < 0.05$) are shown in Fig. 8. Pathways containing a majority of upregulated genes included synaptic long-term depression and CREB signaling in neurons. Pathways containing a majority of downregulated genes included sirtuin signaling pathway, Huntington's disease signaling, cleavage and polyadenylation of pre-mRNA, dendritic cell maturation and clathrin-mediated endocytosis. Pathways indicative of the antioxidant action of vitamin C, phospholipases and gustation had equal numbers of up- and downregulated genes identified.

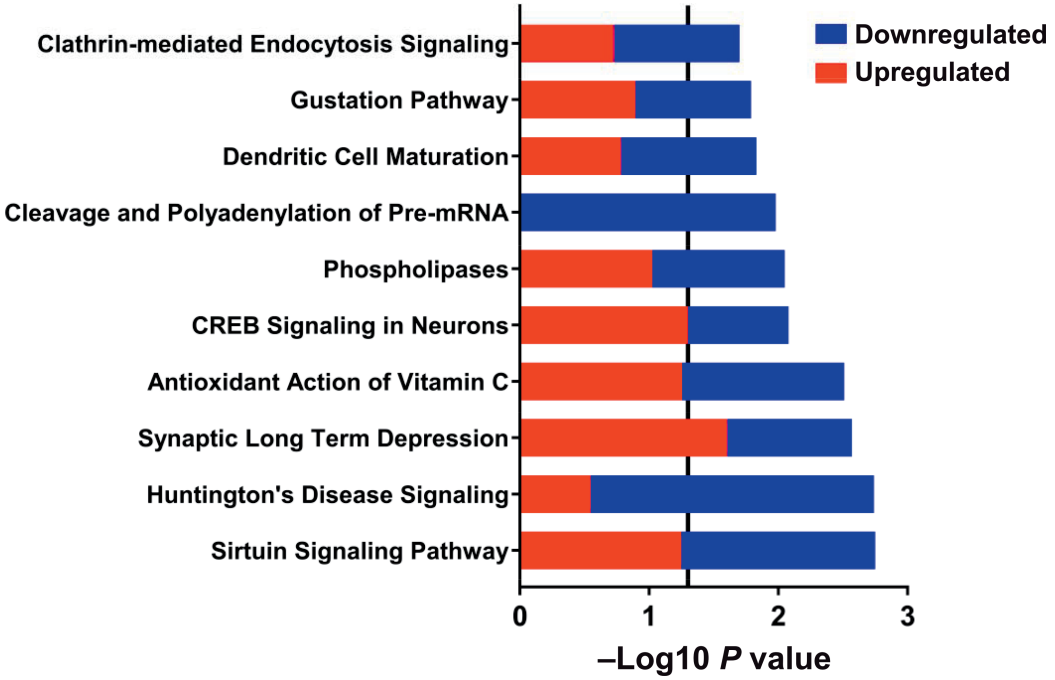


FIG. 8. Intermediate monocyte canonical pathways differentiating irradiated vs. control subjects using cross-sectional and longitudinal differentially expressed genes. Within each pathway red bars indicate the proportion of DEGs upregulated in irradiated monocytes at 6 months, blue bars indicate the proportion of DEGs downregulated in irradiated monocytes at 6, and the overall height of the bar is the –log10 *P* value. The vertical line indicates the threshold for significance based on a –log10 *P* value of 1.3 (equal to $P < 0.05$).

TABLE 3
Differentially Expressed Genes Identified in 6-Month Intermediate Monocytes from Cross Sectional and Longitudinal Comparisons

Gene	Gene ID	Log2 fold change	FDR P
Fc fragment Of IgG receptor Ia[a]	FCGR1A	5.98	0.0303
Collagen type III alpha 1 chain[b]	COL3A1	5.29	0.0001
Gap junction protein beta 1[b]	GJB1	4.95	0.0001
Translocase of outer mitochondrial membrane 40 like[a]	TOMM40L	4.79	0.0486
Glutamate metabotropic receptor 8[b]	GRM8	4.25	0.0006
Adenylate cyclase 2[b]	ADCY2	4.17	0.0005
Glutamate metabotropic receptor 1[b]	GRM1	4.13	0.0012
Gap junction protein gamma 1[b]	GJC1	4.13	0.0142
P21 (Rac1) activated kinase 6[b]	PAK6	4.04	0.0007
Fibroblast growth factor 7[c]	FGF7	3.70	0.0029
Phospholipase C like 1[b]	PLCL1	3.69	0.0087
Synaptosome associated protein 91[b]	SNAP91	3.65	0.0297
Signal transducer and activator of transcription 5A[b]	STAT5A	3.14	0.0318
Microtubule associated protein 1 light chain 3 beta[b]	MAP1LC3B	3.08	0.0297
Translocase of outer mitochondrial membrane 7[b]	TOMM7	3.06	0.0283
Matrix metallopeptidase 14[b]	MMP14	2.97	0.0244
Translocase of outer mitochondrial membrane 40[b]	TOMM40	2.95	0.0370
Nudix hydrolase 18[c]	NUDT18	2.90	0.0400
Golgi snap receptor complex member 1[b]	GOSR1	2.83	0.0147
Phospholipase A2 group XVI[c]	PLA2G16	2.80	0.0457
Calcium voltage-gated channel auxiliary subunit beta 3[b]	CACNB3	2.63	0.0401
Rab5A, member Ras oncogene family[b]	RAB5A	2.04	0.0368
Phosphodiesterase 12[b]	PDE12	1.67	0.0022
Death associated protein kinase 1[b]	DAPK1	–1.22	0.0338
Mitogen-activated protein kinase kinase kinase 1[b]	MAP3K11	–1.37	0.0297
Signal transducer and activator of transcription 2[b]	STAT2	–1.41	0.0165
Dynamin 2[b]	DNM2	–1.41	0.0359
Phospholipase C beta 2[b]	PLCB2	–1.44	0.0057
Uridine-cytidine kinase 1 like 1[b]	UCKL1	–1.50	0.0230
Autophagy related 9A[b]	ATG9A	–1.55	0.0472
Histone deacetylase 5[b]	HDAC5	–1.60	0.0297
Isocitrate dehydrogenase $NADP^+$ 2, mitochondrial[b]	IDH2	–1.63	0.0107
GA binding protein transcription factor beta subunit 1[b]	GABPB1	–1.86	0.0469
Inositol(Myo)-1(Or 4)-monophosphatase 2[b]	IMPA2	–1.97	0.0395
Inositol polyphosphate phosphatase like 1[b]	INPPL1	–2.06	0.0079
Cleavage and polyadenylation specific factor 1[b]	CPSF1	–2.07	0.0063
Intraflagellar transport 57[b]	IFT57	–2.79	0.0467
Adenylate kinase 5[c]	AK5	–3.06	0.0351
Ribosomal protein S27A[a]	RPS27A	–3.10	0.0450
Cleavage and polyadenylation specific factor 4[b]	CPSF4	–3.15	0.0394
Insulin like growth factor 1[b]	IGF1	–3.34	0.0351
Glutamic-pyruvic transaminase[b]	GPT	–3.38	0.0394
Phospholipase A2 group V[b]	PLA2G5	–3.41	0.0392
Fibroblast growth factor 23[b]	FGF23	–3.49	0.0351
H1 histone family, member X[b]	H1FX	–3.62	0.0353
Solute carrier family 25 member 42[b]	SLC25A42	–3.66	0.0297
G protein subunit beta 3[b]	GNB3	–3.73	0.0277
RNA polymerase II subunit G[b]	POLR2G	–3.75	0.0297
CD80 molecule[b]	CD80	–3.80	0.0297
Transforming growth factor beta 1 induced transcript 1[b]	TGFB1I1	–4.38	0.0109
Cyclin dependent kinase 7[b]	CDK7	–4.51	0.0097
Taste 2 receptor member 39[b]	TAS2R39	–4.99	0.0037

[a] Indicates differentially expressed genes identified only in cross-sectional comparisons.
[b] Indicates differentially expressed genes identified only in longitudinal comparisons.
[c] Indicates differentially expressed genes identified in both cross-sectional and longitudinal comparisons.

DISCUSSION

This study provides insights into the effects of ionizing radiation on circulating populations of classical, intermediate and non-classical monocytes, as defined by CD14 and CD16 surface markers, in a well-established non-human primate model, the rhesus macaque. Monocyte populations shifted from a classical phenotype towards intermediate and non-classical phenotypes at 6 months postirradiation, gene

expression changes occurred in intermediate, but not classical monocytes, and intermediate monocyte DEGs were associated with sirtuin, glutamatergic and anti-inflammatory signaling.

After radiation-induced depletion, monocyte populations returned to normal levels by approximately 30 days and remained at those levels for the study duration. A similar pattern of repopulation was observed for neutrophils, while recovery of lymphocytes was slower and actually increased above baseline in TBI compared to control animals. This apparent ''overshoot'' in circulating levels by the lymphocytes may reflect a ''ramping up'' in production after TBI and their relatively long half-life (several months) (*33*) relative to circulating lifespans of neutrophils and monocytes, which are only a few days (*34*). Despite the fact that we observed similar total monocyte numbers, monocyte phenotypic polarization was shifted 6 months postirradiation, the time frame consistent with initiation of RIF in humans, away from classical subsets towards increased intermediate and non-classical subsets. To our knowledge, this is the first time that alterations in monocyte polarization have been reported as a consequence of ionizing radiation exposure. The shift from classical to intermediate and non-classical monocyte subsets that we observed is similar to shifts observed in other pathologic fibrotic disorders (*13, 20, 21*).

We also found that TBI had differential effects on these two populations of monocytes. Interestingly, there were few DEGs detected in classical monocyte comparisons, whereas there were often hundreds of DEGs identified in intermediate monocyte comparisons. To our knowledge, this is the first time it has been shown that selected monocyte phenotypes have differentially altered gene expression after ionizing radiation exposure.

We identified DEGs that were specific to TBI 6-month intermediate monocytes by assessing shared and distinct DEGs from all intermediate monocyte comparisons (Table 3), and removing those that were found to be differentially expressed over time (perhaps due to effects of Western diet exposure) in the control group. This trimmed set of genes was subjected to further analysis to explore canonical pathways or groups of pathways that were more specific to TBI 6-month intermediate monocytes (Fig. 8). The pathways identified contained upregulated genes associated with neurologic signaling (synaptic long-term depression and CREB signaling in neurons), and the key genes driving these changes, *GRM1* and *GRM8*, have also been demonstrated as pivotal mediators of inflammatory and monocyte signaling. These metabotropic glutamate receptor genes (*GRM1*, *GRM8*) are part of family C of GPCRs comprising eight total receptors (*GRMs* 1–8) split into three groups: group I (*GRM1* and *GRM5*) receptors induce inositol 1,4,5, triphosphate (IP3) formation, whereas group II (*GRM2* and *GRM3*) and group III (*GRM4*, *GRM6*, *GRM7* and *GRM8)* receptors signal to reduce intracellular cAMP (*35*). Plasma glutamate has been noted to be increased in conditions associated with immunodeficiency, including HIV infection (*36*) and cancer (*37*), and decreased in autoimmune disorders like systemic lupus erythematosus (SLE) (*38*). The implications of these changes in glutamate concentration on monocyte/macrophage function are underexplored, but there is evidence it may lead to reduced pro-inflammatory signaling (*39*). When murine RAW 264.7 macrophages were transfected with the group I metabotropic glutamate receptor 5 (mGlu5), producing an environment with increased glutamate, they were found to have increased secretion of IL10, high mobility group box 1 protein (HMGB1), galectin 3 (Gal-3) and PPARγ (*40*). These cytokines are generally associated with anti-inflammatory signaling and IL10, HMGB1and Gal-3 specifically have been noted to induce the polarization of macrophages towards the alternatively activated-M2 macrophage state (*41–43*). Finally, the anti-inflammatory effects of PPARγ are accompanied by inhibition of sirtuin 1 (*SIRT1*) expression and activity (*44*). These associations may explain the identification of sirtuin signaling as the most significant (based on *P* value), and downregulated, pathway in our analyses of TBI intermediate monocytes 6 months postirradiation.

In monocytes and macrophages, sirtuins function as nutrient sensing proteins that respond to NAD^+ production and NAD/NADH ratios to regulate the metabolic switch from glycolysis (associated with M1-like monocyte/macrophage phenotypes) to fatty acid oxidation (associated with M2-like monocyte/macrophage phenotypes) (*45*). Downregulation of sirtuin 3 (SIRT3) signaling has been noted to promote fibroblast-myofibroblast differentiation resulting in increased pulmonary fibrosis in murine models. This effect was found to be mediated by decreased repression of TGFβ1/mothers against decapentaplegic homolog 3 (SMAD3) signaling (*46*). In contrast, sirtuin 1 (SIRT1) overexpression was observed to ameliorate renal fibrosis in partially nephrectomized rats through inhibition of the TGFβ1/SMAD3 signaling pathway, while SIRT1 knockdown produced the opposite effect (*47*). TGFβ1 is a potential ''master'' regulator of fibrosis in various fibrotic conditions including those affecting the heart (*48, 49*), lung (*50*) and kidney (*51*) via signaling through canonical (Smad-based) or non-canonical (non-Smad-based) pathways. Downregulation of sirtuin signaling in TBI intermediate monocytes could potentiate a pro-fibrotic phenotype after radiation exposure due to upregulation and signaling of metabotropic glutamate receptors in response to increased availability of systemic glutamate.

Of the remaining top 10 pathways identified (Huntington's disease signaling, antioxidant of vitamin C, phospholipases, cleavage and polyadenylation of pre-mRNA, dendritic cell maturation, gustation pathway, and clathrin-mediated endocytosis signaling) the majority contained predominately TBI downregulated genes. Several shared DEGs among these pathways encoded phospholipases, including phospholipase C beta 2 (*PLCB2*), phospholipase

A2 group XVI (*PLA2G16*), phospholipase A2 group V (*PLA2G5*) and phospholipase C like 1 (*PLCL1*). Two DEGs, insulin like growth factor 1 (*IGF1*) and NFκB inhibitor alpha (*NFKBIA)* (both downregulated) were shared between several of these pathways. IGF-1 is a 70 amino acid hormone that is predominately produced by the liver, (*52*) but also produced by skeletal myocytes, fibroblasts, endothelial cells, macrophages and monocytes (*53*). Monocyte/macrophage-derived IGF-1 has been identified as a critical regulator of normal skeletal muscle repair in mice after injury. Conditional deletion of IGF-1 in murine macrophages resulted in increased inflammation, impaired healing and dysregulated inflammatory gene expression response consisting of increased pro-inflammatory (TNFα, NOS2, IL-1β) and anti-inflammatory (IL-10) cytokines (*53*). Decreased *IGF1* expression in monocytes could result in excessive inflammation and aberrant wound healing. In human cirrhosis and non-alcoholic fatty liver disease, intermediate monocytes have been implicated in fibrosis progression (*54*) and IGF-1 deficiency may be partially responsible for progressive inflammation and matrix deposition characteristic of these diseases (*52, 55*). Downregulation of *IGF1* combined with *NFKBIA* downregulation suggests that NFκB was also downregulated, as IGF-1 has been demonstrated to activate NFκB through the PI-3 kinase pathway (*56*), which in turn activates *NFKBIA* expression, forming a self-regulating negative feedback cycle (*57*). Decreased *IGF1* and *NFKBIA* expression could suggest there is reduced NFκB activation in intermediate monocytes. These findings suggest that TBI intermediate monocytes may elicit excessive and dysregulated inflammatory responses that also result in excessive fibrogenesis, which provides some support for our findings regarding glutamatergic and sirtuin related pathways.

This study utilized a well-characterized prospective cohort of male rhesus macaques in which certain limitations were inherent and unavoidable. By design, we isolated three specific monocyte subtypes based on the relative expression of CD14 and CD16, consistent with significant literature using that method, as a practical approach to begin to answer questions related to monocyte polarization responses to radiation. Newer methodologies, such as single cell sequencing of monocytes, which would provide more detail and granularity to the spectrum of monocyte subsets and phenotype variation, which might result from radiation exposure, were beyond the scope of the current project, but will be pursued in the future. The IPA software relies on human- and animal-based data from published studies, and public and third-party databases, to provide a means to identify molecular pathways and processes associated with patterns of differential gene expression and glean insights into the overall pathobiology of the system, by its nature is dependent on available data, and may be limited in its ability to identify novel pathways to explain observed outcomes. There were also some limitations in terms of statistical power. Using the power calculator provided by Hart *et al*. (*58*), we concluded that a sample size of 10 animals per group was needed to detect a log2 fold change of 0.91 with 80% power and a false discovery rate (FDR) P value < 0.05. Therefore, while comparisons between TBI and all groups are sufficiently powered, comparisons of the control group to itself and other groups are relatively underpowered. The finding that intermediate monocyte gene expression profiles changed in control animals between baseline and 6 months postirradiation could be a result of age-related changes, or the accumulating effects of consuming a Western diet over time. There was little overlap of DEGs that changed over time in the TBI vs. control groups, which suggests that the control group changed differently from the irradiated group. Control animals consuming a Western diet gained substantial weight between baseline and 6 months post-TBI (10.8 ± 0.8 to 13.3 ± 1.1 kg, ~23% increase). Increases in fat mass and obesity have been noted to lead to increased macrophage infiltration into the expanding adipose tissue and alter monocyte polarization (*59, 60*). Animals receiving TBI lost weight afterwards, but rebounded to baseline body weights by 6 months postirradiation (10.6 ± 0.8 vs. 11.0 ± 0.9 kg).

In summary, we show that 6 months post-TBI, monocyte phenotypes were shifted towards intermediate and non-classical phenotypes, accompanied by gene expression changes in intermediate monocytes, but not classical monocytes. The pathways identified from available algorithms are associated with pro-fibrotic and anti-inflammatory signaling pathways, which could function to push intermediate monocytes towards M2 macrophage polarization upon extravasation. In particular, the 67 DEGs (25 upregulated and 42 downregulated in TBI group) between the TBI and control intermediate monocytes at 6 months postirradiation provides support for an M2 phenotype shift, as the highest-ranked disease/disorders classification included inflammatory response and organismal injury and abnormalities (Fig. 6), in which the majority of genes were downregulated in the TBI group. These findings support the notion that selective targeting of monocyte populations and programming may present a novel target opportunity for therapies to inhibit or prevent RIF. This could prove to be an exciting new area of research, but one that needs significant further and careful examination in terms of macrophage activation and other cell phenotypes in relationship to fibrosis at the tissue level in key target (and non-target) organs. These areas will be explored in future studies in the subjects described in the current study, which includes longitudinal phenotyping of cardiac structure and function by ultrasound and cardiac fibrosis via magnetic resonance imaging approaches.

SUPPLEMENTARY INFORMATION

Table S1A. Classical monocyte comparisons, full list.

Table S1B. Classical monocyte comparisons, abbreviated list.

Table S2A. Intermediate monocyte comparisons, full list.

Table S2B. Intermediate monocyte comparisons, abbreviated list.

Fig. S1. Peripheral immune cell recovery after total body irradiation (log scale).

ACKNOWLEDGMENTS

This research was supported by the National Institute of Allergy and Infectious Diseases of the National Institutes of Health (NIAID/NIH award no. U19AI067773) and by NIH grant nos. U19 AI67798, R01 HL122393, T32 OD010957 and DOD W81XWH-15-1-0574, as well as the Wake Forest Baptist Comprehensive Cancer Center's NCI Cancer Center Support Grant (no. P30CA012197-39) and Shared Instrumentation grant (no. 1S10OD023409-01). We thank the Duke Human Vaccine Institute Flow Facility for the flow cytometry work performed as well as Jean Gardin, Russell O'Donnell, Chrystal Bragg, Matt Dwyer, Michael Bennett and J. D. Bottoms for their technical assistance. The content is solely the responsibility of the authors and does not necessarily represent the official views of the NIH.

Received: December 10, 2018; accepted: May 5, 2019; published online: June 4, 2019

REFERENCES

1. Straub JM, New J, Hamilton CD, Lominska C, Shnayder Y, Thomas SM. Radiation-induced fibrosis: mechanisms and implications for therapy. J Cancer Res Clin Oncol 2015; 141:1985–94.
2. Fajardo LF, Stewart JR. Pathogenesis of radiation-induced myocardial fibrosis. Lab Invest 1973; 29:244–57.
3. Cardozo BL, Zoetelief H, van Bekkum DW, Zurcher C, Hagenbeek A. Lung damage following bone marrow transplantation: I. The contribution of irradiation. Int J Radiat Oncol Biol Phys 1985; 11:907–14.
4. Ingold JA, Reed GB, Kaplan HS, Bagshaw MA. Radiation hepatitis. Am J Roentgenol Radium Ther Nucl Med 1965; 93:200–8.
5. Bentzen SM, Thames HD, Overgaard M. Latent-time estimation for late cutaneous and subcutaneous radiation reactions in a single-follow-up clinical study. Radiother Oncol 1989; 15:267–74.
6. Brocheriou C, Verola O, Lefaix JL, Daburon F. Histopathology of cutaneous and subcutaneous irradiation-induced injuries. Br J Radiol Suppl 1986; 19:101–4.
7. Stewart JR, Fajardo LF. Radiation-induced heart disease: an update. Prog Cardiovasc Dis 1984; 27:173–94.
8. Franklin TJ. Therapeutic approaches to organ fibrosis. Int J Biochem Cell Biol 1997; 29:79–89.
9. Denham JW, Hauer-Jensen M. The radiotherapeutic injury–a complex 'wound'. Radiother Oncol 2002; 63:129–45.
10. Tak JK, Park JW. The use of ebselen for radioprotection in cultured cells and mice. Free Radic Biol Med 2009; 46:1177–85.
11. Bryant AK, Banegas MP, Martinez ME, Mell LK, Murphy JD. Trends in radiation therapy among cancer survivors in the United States, 2000–2030. Cancer Epidemiol Biomarkers Prev 2017; 26:963–70.
12. Yona S, Jung S. Monocytes: subsets, origins, fates and functions. Curr Opin Hematol 2010; 17:53–9.
13. Wong KL, Yeap WH, Tai JJ, Ong SM, Dang TM, Wong SC. The three human monocyte subsets: implications for health and disease. Immunol Res 2012; 53:41–57.
14. Geissmann F, Manz MG, Jung S, Sieweke MH, Merad M, Ley K. Development of monocytes, macrophages, and dendritic cells. Science 2010; 327:656–61.
15. Hume DA, MacDonald KP. Therapeutic applications of macrophage colony-stimulating factor-1 (CSF-1) and antagonists of CSF-1 receptor (CSF-1R) signaling. Blood 2012; 119:1810–20.
16. Hanna RN, Carlin LM, Hubbeling HG, Nackiewicz D, Green AM, Punt JA, et al. The transcription factor NR4A1 (Nur77) controls bone marrow differentiation and the survival of Ly6C- monocytes. Nat Immunol 2011; 12:778–85.
17. Zawada AM, Rogacev KS, Rotter B, Winter P, Marell RR, Fliser D, et al. SuperSAGE evidence for CD14++CD16+ monocytes as a third monocyte subset. Blood 2011; 118:e50–61.
18. Wong KL, Tai JJ-Y, Wong W-C, Han H, Sem X, Yeap W-H, et al. Gene expression profiling reveals the defining features of the classical, intermediate, and nonclassical human monocyte subsets. Blood 2011; 118:e16.
19. Shi X, Shiao SL. The role of macrophage phenotype in regulating the response to radiation therapy. Transl Res 2018; 191:64–80.
20. Westbury CB, Yarnold JR. Radiation fibrosis – current clinical and therapeutic perspectives. Clinical Oncol 2012; 24:657–72.
21. Liaskou E, Zimmermann HW, Li KK, Oo YH, Suresh S, Stamataki Z, et al. Monocyte subsets in human liver disease show distinct phenotypic and functional characteristics. Hepatology 2013; 57:385–98.
22. Groves AM, Johnston CJ, Williams JP, Finkelstein JN. Role of infiltrating monocytes in the development of radiation-induced pulmonary fibrosis. Radiat Res 2018; 189:300–11.
23. Gibbons MA, MacKinnon AC, Ramachandran P, Dhaliwal K, Duffin R, Phythian-Adams AT, et al. Ly6Chi monocytes direct alternatively activated profibrotic macrophage regulation of lung fibrosis. Am J Respir Crit Care Med 2011; 184:569–81.
24. Thrall KD, Love R, O'Donnell KC, Farese AM, Manning R, MacVittie TJ. An interlaboratory validation of the radiation dose response relationship (DRR) for H-ARS in the rhesus macaque. Health Phys 2015; 109:502–10.
25. Uckun FM, Yanishevski Y, Tumer N, Waurzyniak B, Messinger Y, Chelstrom LM, et al. Pharmacokinetic features, immunogenicity, and toxicity of B43(anti-CD19)-pokeweed antiviral protein immunotoxin in cynomolgus monkeys. Clin Cancer Res 1997; 3:325–37.
26. DeBo RJ, Lees CJ, Dugan GO, Caudell DL, Michalson KT, Hanbury DB, et al. Late effects of total-body gamma irradiation on cardiac structure and function in male rhesus macaques. Radiat Res 2016; 186:55–64.
27. Afgan E, Baker D, van den Beek M, Blankenberg D, Bouvier D, Cech M, et al. The Galaxy platform for accessible, reproducible and collaborative biomedical analyses: 2016 update. Nucleic Acids Res 2016; 44:W3–W10.
28. Andrews S. FastQC: a quality control tool for high throughput sequence data. 2010. (http://www.bioinformatics.babraham.ac.uk/projects/fastqc)
29. Kim D, Langmead B, Salzberg SL. HISAT: a fast spliced aligner with low memory requirements. Nat Methods 2015; 12:357–60.
30. Anders S, Pyl PT, Huber W. HTSeq–a Python framework to work with high-throughput sequencing data. Bioinformatics 2015; 31:166–9.
31. Robinson MD, McCarthy DJ, Smyth GK. edgeR: a Bioconductor package for differential expression analysis of digital gene expression data. Bioinformatics 2010; 26:139–40.
32. Liu R, Holik AZ, Su S, Jansz N, Chen K, Leong HS, et al. Why weight? Modelling sample and observational level variability improves power in RNA-seq analyses. Nucleic Acids Res 2015; 43:e97.
33. Salvato MS, Rater M, Pauza CD. Tracking of dye-labeled lymphocytes in rhesus macaques. J Med Primatol 1996; 25:112–21.
34. He Z, Allers C, Sugimoto C, Ahmed N, Fujioka H, Kim WK, et al. Rapid turnover and high production rate of myeloid cells in adult rhesus macaques with compensations during aging. J Immunol 2018; 200:4059–67.

35. Chiocchetti A, Miglio G, Mesturini R, Varsaldi F, Mocellin M, Orilieri E, et al. Group I mGlu receptor stimulation inhibits activation-induced cell death of human T lymphocytes. Br J Pharmacol 2006; 148:760–8.

36. Eck HP, Frey H, Droge W. Elevated plasma glutamate concentrations in HIV-1-infected patients may contribute to loss of macrophage and lymphocyte functions. Int Immunol 1989; 1:367–72.

37. Ollenschlager G, Karner J, Karner-Hanusch J, Jansen S, Schindler J, Roth E. Plasma glutamate–a prognostic marker of cancer and of other immunodeficiency syndromes? Scand J Clin Lab Invest 1989; 49:773–7.

38. Poulopoulou C, Papadopoulou-Daifoti Z, Hatzimanolis A, Fragiadaki K, Polissidis A, Anderzanova E, et al. Glutamate levels and activity of the T cell voltage-gated potassium Kv1.3 channel in patients with systemic lupus erythematosus. Arthritis Rheum 2008; 58:1445–50.

39. Eck H-P, Frey H, Droge W. Elevated plasma glutamate concentrations in HIV-1-infected patients may contribute to loss of macrophage and lymphocyte functions. Int Immunol 1989; 1:367–72.

40. Shanshiashvili L, Tsitsilashvili E, Dabrundashvili N, Kalandadze I, Mikeladze D. Metabotropic glutamate receptor 5 may be involved in macrophage plasticity. Biol Res 2017; 50:4.

41. Sinha P, Clements VK, Bunt SK, Albelda SM, Ostrand-Rosenberg S. Cross-talk between myeloid-derived suppressor cells and macrophages subverts tumor immunity toward a type 2 response. J Immunol 2007; 179:977–83.

42. MacKinnon AC, Farnworth SL, Hodkinson PS, Henderson NC, Atkinson KM, Leffler H, et al. Regulation of alternative macrophage activation by galectin-3. J Immunol 2008; 180:2650–8.

43. Novak R, Dabelic S, Dumic J. Galectin-1 and galectin-3 expression profiles in classically and alternatively activated human macrophages. Biochim Biophys Acta 2012; 1820:1383–90.

44. Han L, Zhou R, Niu J, McNutt MA, Wang P, Tong T. SIRT1 is regulated by a PPARgamma-SIRT1 negative feedback loop associated with senescence. Nucleic Acids Res 2010; 38:7458–71.

45. Vachharajani VT, Liu T, Wang X, Hoth JJ, Yoza BK, McCall CE. Sirtuins link inflammation and metabolism. J Immunol Res 2016; 2016:8167273.

46. Sosulski ML, Gongora R, Feghali-Bostwick C, Lasky JA, Sanchez CG. Sirtuin 3 deregulation promotes pulmonary fibrosis. J Gerontol A Biol Sci Med Sci 2017; 72:595–602.

47. Huang XZ, Wen D, Zhang M, Xie Q, Ma L, Guan Y, et al. Sirt1 activation ameliorates renal fibrosis by inhibiting the TGF-beta/Smad3 pathway. J Cell Biochem 2014; 115:996–1005.

48. Dobaczewski M, Chen W, Frangogiannis NG. Transforming growth factor (TGF)-beta signaling in cardiac remodeling. J Mol Cell Cardiol 2011; 51:600–6.

49. Ahamed J, Laurence J. Role of platelet-derived transforming growth factor-beta1 and reactive oxygen species in radiation-induced organ fibrosis. Antioxid Redox Signal 2017; 27:977–88.

50. Bonniaud P, Margetts PJ, Ask K, Flanders K, Gauldie J, Kolb M. TGF-beta and Smad3 Signaling Link Inflammation to Chronic Fibrogenesis. J Immunol 2005; 175:5390–5.

51. Meng XM, Nikolic-Paterson DJ, Lan HY. TGF-beta: the master regulator of fibrosis. Nat Rev Nephrol 2016; 12:325–38.

52. de la Garza RG, Morales-Garza LA, Martin-Estal I, Castilla-Cortazar I. Insulin-like growth factor-1 deficiency and cirrhosis establishment. J Clin Med Res 2017; 9:233–47.

53. Tonkin J, Temmerman L, Sampson RD, Gallego-Colon E, Barberi L, Bilbao D, et al. Monocyte/macrophage-derived IGF-1 orchestrates murine skeletal muscle regeneration and modulates autocrine polarization. Mol Ther 2015; 23:1189–200.

54. Liaskou E, Zimmermann HW, Li K-K, Oo YH, Suresh S, Stamataki Z, et al. Monocyte subsets in human liver disease show distinct phenotypic and functional characteristics. Hepatology 2013; 57:385–98.

55. Dichtel LE, Corey KE, Misdraji J, Bredella MA, Schorr M, Osganian SA, et al. The association between IGF-1 levels and the histologic severity of nonalcoholic fatty liver disease. Clin Transl Gastroenterol 2017; 8:e217.

56. Chetty A, Cao GJ, Nielsen HC. Insulin-like growth factor-I signaling mechanisms, type I collagen and alpha smooth muscle actin in human fetal lung fibroblasts. Pediatr Res 2006; 60:389–94.

57. Collins EP, Mitxitorena I, Carmody JR. The ubiquitination of NF-kappaB subunits in the control of transcription. Cells 2016; 5.

58. Hart SN, Therneau TM, Zhang Y, Poland GA, Kocher J-P. Calculating sample size estimates for RNA sequencing data. J Comput Biol 2013; 20:970–8.

59. Kraakman MJ, Murphy AJ, Jandeleit-Dahm K, Kammoun HL. Macrophage polarization in obesity and type 2 diabetes: weighing down our understanding of macrophage function? Front Immunol 2014; 5:470.

60. Lumeng CN, Bodzin JL, Saltiel AR. Obesity induces a phenotypic switch in adipose tissue macrophage polarization. J Clin Invest 2007; 117:175–84.